INFRARED MICROSCOPE STUDIES OF SURFACE TEMPERATURES PRODUCED BY FRICTION WITH GRAPHITE-EPOXY AND CARBON-PEEK COMPOSITES

by

Bhawani Sankar Tripathy

Thesis submitted to the Faculty of the
Virginia Polytechnic Institute and State University
in partial fulfillment of the requirements for the degree of

MASTER OF SCIENCE

in

Mechanical Engineering

APPROVED :

M. J. Furey, Chairman

N. S. Eiss, Jr.

B. Vick

October 1991

Blacksburg, Virginia

INFRARED MICROSCOPE STUDIES OF SURFACE TEMPERATURES PRODUCED BY FRICTION WITH GRAPHITE-EPOXY AND CARBON-PEEK COMPOSITES

by

Bhawani S. Tripathy

Michael J. Furey, Chairman

Mechanical Engineering

(ABSTRACT)

An infrared microscope system was used to measure the temperatures at the interfaces of graphite-epoxy and carbon-PEEK composites in unidirectional sliding contact with sapphire. Effects of fiber orientation and velocity on tribological parameters were examined. Oscillating contact conditions with graphite-epoxy were also examined.

Surface temperatures on the order of 100-160°C were measured at relatively low rates of frictional heat generation. The corresponding coefficients of friction were on the order of 0.45-0.65. In graphite-epoxy, fiber orientation was seen to affect coefficient of friction and wear significantly; but surface temperature was very little affected by fiber orientation. In carbon-PEEK, fiber orientation affected the coefficient of friction, wear and surface temperatures significantly. Surface temperatures in both materials initially increased with velocity, but stayed constant as the glass transition temperature of the matrix material was reached. The total wear is believed to be due to a combination of adhesive wear and fatigue wear.

Comparison of the measured surface temperatures with theoretical predictions is done. A "two-velocity-regime" tribological model is proposed to explain the tribological behavior of polymer composites.

Abstract

Acknowledgements

I am extremely grateful to Dr. M. J. Furey, my major advisor, for the invaluable help and suggestions rendered to me throughout this work. His constant encouragement and guidance has played a big role in the completion of this work.

I am also greatly thankful to Dr. N. S. Eiss, Jr., and Dr. B. Vick for their advice, help and the time to serve on the graduate committee. The numerous meetings we had proved to be extremely useful. I am also very thankful to Hamid Ghasemi and Brian Weick for their efforts in getting me acquainted with the test apparatus. I also thank Brian Weick for the surface temperature and the data acquisition programs. Besides, I would like to thank everyone else in the Tribology Lab -- Ron Rorrer, Chiunchia Kang, Rob DeTogni, Jong Yoo and Brian McCann -- for making the work all the more fun. I am also thankful to Larry Golan for his help in the theoretical temperature computations. I would also like to thank Dr. A. L. Loos and ICI Americas for supplying me with the test materials.

I am also thankful to the National Science Foundation, Tribology Program, and the Department of Mechanical Engineering, for the financial support during this study.

Finally, I am greatly indebted to my parents, brother and sisters for their love, encouragement and patience, without which my coming to U.S.A. for graduate studies would never have been possible.

Table of Contents

List of Illustrations

List of Tables

CHAPTER 1

INTRODUCTION

In the past few decades there has been a remarkable growth in the large scale industrial application of plastics and fiber reinforced - polymer matrix composites. The features that make them so promising as engineering materials are their high specific strength (strength per unit density), and specific stiffness (modulus per unit density). Further, these materials can be tailored to obtain specific material properties through the control of fiber and matrix composition and fiber orientation. In addition, these materials provide excellent ability to dampen shock and vibration, and protection against corrosion. Therefore, these have been excellent materials for a variety of applications in the aerospace, chemical, automotive and other industries. Mechanical applications of polymers and polymer composites include components such as gears, wheels, cams, impellers, brakes, clutches, seals, bushings and bearings.

All these mechanical components are subjected to different kinds of mechanical stresses. Besides, in most of these components, the material is subjected to tribological loading conditions. This introduces additional complications to the system. The tribological behavior of these composites is not well understood. Therefore, the present study has been carried out to add to the understanding of such behavior, so that

composites can be designed and utilized in such applications to their fullest extent.

1.1 RATIONALE FOR THE STUDY

The tribology of polymer composites mainly comprises the study of friction, wear, surface damage, surface temperatures and lubrication. Most of the studies carried out so far in this area have emphasized friction and wear measurements. The measurement and characterization of surface temperatures generated due to friction is also extremely important in tribology. It is even more critical for polymer composites for various reasons. First, the polymer matrices of these materials have either very low melting points, or degrade at very low temperatures compared to most other engineering materials. Most of these polymers have a glass transition temperature on the order of 100 - 250°C. At the glass transition temperature, mechanical properties such as stiffness, strength and hardness of most polymers decrease substantially. In some polymers, the decrease in stiffness could even be up to three orders of magnitude. The wear process in any material system is greatly controlled by the mechanical properties of the materials. Therefore the effect of surface temperature on wear of polymer composites, particularly for those cases in which the temperature is near the glass transition temperature of the polymer matrix, could be very important.

Second, polymers and composites have very low thermal conductivities compared to most other engineering materials. This results in a higher interfacial temperature in

a composite-composite system compared to other material systems under similar sliding conditions. Table 1 shows theoretical values of average surface temperature rise for some material systems. The values are computed using Vick's numerical technique for theoretical surface temperature calculations [14,15]. These calculations suggest that even under relatively mild sliding conditions, the surface temperature in any composite-composite system could be unexpectedly high. In most engineering materials temperature proves critical only under severe sliding conditions. But in systems involving polymer composites, surface temperatures could be critical under much less severe conditions. Further, the unrealistically high calculated temperature values in composite-composite systems suggest that the tribological behavior of polymer composites could be much more complex.

Third, surface temperature is also believed to play an important role in lubrication. High surface temperatures can adversely affect lubrication by decreasing the viscosity and eventual breakdown of the lubricant. On the other hand, high surface temperatures can be helpful in forming anti-wear films on the surface. A novel technique called "tribopolymerization", proposed by Furey [1-3], takes advantage of the high surface temperature to form protective films by reaction on the surface. Tribopolymerization is defined as *the planned or intentional formation of protective polymeric films directly and continuously on the rubbing surfaces to reduce damage and wear by the use of minor concentrations of selected monomers capable of forming polymeric films 'in situ' (e.g. by polycondensation or addition processes).* The high surface temperatures, and possibly the spontaneous emission of electrons from the freshly

Table 1. Theoretical surface temperature rise per unit coefficient of friction in some material systems. (Values computed using Vick's technique [14,15])
Load = 20 N, Sliding Velocity = 1 m/s, Coefficient of Friction = 1,

	MATERIAL SYSTEMS A -on- A	SURFACE TEMPERATURE RISE (°C) per unit coefficient of friction	
		assuming ELASTIC CONTACT AREA†	assuming PLASTIC CONTACT AREA†
Metal -on- Metal	Copper	70	70
	Steel	353	305
Polymer -on- Polymer	Polyethylene	579	1190
	Polytetrafluoroethylene (PTFE)	532	1465
Ceramic -on- Ceramic	Sapphire	750	3004
	Alumina (90% pure, opaque)	1317	5185
Composite -on- Composite	Graphite-epoxy (normal)	2260	3488
	Graphite-epoxy (parallel / anti-parallel)	8650	7510

† : Assuming a single area of contact

exposed surfaces, aid in this polymerization reaction.

Recently, there is increased interest in finding the relationships between friction, wear and surface temperature. A few attempts at finding such relationships in polymer composites have been done in the past and some interesting trends are shown (more details are discussed in the next chapter). These relationships are derived from experimental measurements. However, the measurements for surface temperatures in those studies are far from accurate as the techniques used were only capable of measuring temperatures within the bulk. These bulk temperatures are extrapolated to obtain estimates of temperature values at the surface. This study on the other hand, involves the direct measurement of the surface temperature using an infrared microscopy technique. The temperature values thus obtained are believed to be accurate.

A number of various polymer matrix composite materials are used in tribological applications. These composite materials can be classified into two broad groups -- thermoplastic polymer matrix composites and thermosetting polymer matrix composites. Thermoplasts or thermoplastic polymers are those polymers that soften and flow when heated. These could be crystalline or semi-crystalline in nature. Thermosets or thermosetting polymers do not flow when heated and are amorphous in nature. Thermosets are typically crosslinked and are dimensionally more stable under a wide variety of conditions. Because of the differences in morphology, chemical structure and response to thermal conditions, they are expected to show different tribological properties, even more so at high surface temperatures. Therefore, both types of materials are included in this study.

The properties of polymer composites depend not only on the matrix and filler materials, but also on the size, shape and orientation of the fillers. Fiber reinforced composites are most widely used in structural applications. Recently, fiber reinforced composites have also been used in tribological applications. The demand for high strength along with good friction and wear properties has necessitated the use of fiber reinforcements. Both continuous and short fiber reinforcements are used. Continuous fibers result in unidirectional composites or composites with any preferred directional combination. These composites can be designed to give specific properties in specific directions. Moreover, continuous fiber composites offer well-characterized systems with the mechanical and thermophysical properties being significantly different in the different fiber orientations.

Theoretical calculations show significant effects of fiber orientation on temperature rise. Some of the previous studies show friction and wear to be dependent on fiber orientation as well. It is believed that fiber orientation may influence the friction and wear mechanisms of polymer composites. Therefore, this study is also aimed at investigating the effect of fiber orientation on tribological properties of unidirectional fiber reinforced polymer composites.

Along with unidirectional fiber composites, short or random fiber composites are also extensively used in tribological applications. The greatest advantage of short fiber composites is their ease of fabrication. Since most tribological components have complicated geometry, random fiber orientation becomes particularly advantageous. Therefore, extensive studies on the tribological behavior of random fiber composites are

currently being carried out by Brian Weick and Dr. Furey, and Jong Yoo and Dr. Eiss.

Based on these problems and unknowns in the area of composite tribology, several objectives were chosen for this study. They are listed in the next section.

1.2 OBJECTIVES OF THE STUDY

The objectives of this research are :

1. *To experimentally determine the surface temperatures generated due to friction with selected and well characterized polymer composites.*

2. *To measure the coefficient of friction and wear along with surface temperature in these systems.*

3. *To observe the differences in the tribological behavior of thermoplast and thermoset polymer matrix composites.* As model systems, one material is chosen from each type for this study -- graphite-epoxy with a thermoset matrix and carbon-polyetheretherketone (PEEK) with a thermoplast matrix.

4. *To study the effect of velocity on friction, wear and surface temperature of polymer composites.*

5. *To study the effect of fiber orientation on friction, wear and surface temperature of polymer composites.*

6. *To examine the relationships among friction, wear and surface temperature in polymer composites.*

7. *To observe the differences in behavior between unidirectional sliding and oscillating contact.*

8. *To estimate the real area of contact and compare the experimental values of surface temperature rise with the theoretical values.*

9. *To attempt to explain the wear process using a model.*

1.3 PRESENT RESEARCH AT VPI&SU

At Virginia Polytechnic Institute and State University, continuing research is being done under the guidance of Dr. Furey on the direct measurement of surface temperatures both in oscillating/fretting and sliding conditions. The program started in 1973 using a test apparatus built around a Barnes RM-2A infrared microscope. This apparatus is capable of looking at target spots as small as 17μm diameter. A sapphire disk

transparent to infrared radiation is used as the counterface. Wiggins [4] was the first to carry out experiments under unidirectional sliding conditions. Further experiments were carried out by Omori [5], Li [6], Richardson [7], Rogers [8], Moyer [9] and Hollowell [10]. Surface temperature measurements were carried out using various metals, polymers and graphite sliding on sapphire under various loads, speeds and environments. More findings are discussed in the next chapter. A data acquisition system was also installed by Jayaram [11].

Recently, an oscillating/fretting setup was developed by Ghasemi [12,16] and used for the measurement of surface temperatures of polymer coated metal balls sliding on sapphire. Weick [13] also carried out surface temperature measurements with ceramics. Currently, a computer controlled X-Y table is being installed for automatic scanning of the contact area. A solution technique to theoretically compute surface temperatures with any arbitrary contact area has also been developed by Vick, Foo [14] and Golan [15].

This study on composites is part of the composite tribology program collectively undertaken by Dr. Furey and Dr. Eiss and sponsored by the National Science Foundation, Science and Technology Center for High Performance Polymeric Adhesives and Composites. Besides the work that will be discussed in this thesis, further research is being done by Dr. Furey and Weick on surface temperature and thermal effects on random fiber reinforced polymer composites. Dr. Eiss and Yoo [17] are investigating the behavior of polyetherimide (PEI)-PEEK blends, both unfilled and filled with short carbon fibers. In addition, tribopolymerization as a potential anti-wear mechanism for composite lubrication has also been investigated by Dr. Furey and Dr. Kempinski.

CHAPTER 2

LITERATURE REVIEW

2.1 REVIEW OF COMPOSITE TRIBOLOGY

A composite material can be defined as a heterogeneous mixture of two or more homogeneous phases which have been bonded together. Composite tribology is a relatively new area. Still it has generated a great deal of interest among researchers. Brief reviews of some of the important works in this area are discussed here. Lancaster [18] was among the first to investigate the friction and wear properties of reinforced polymers. He found that during dry sliding against steel, randomly oriented chopped fibers in a polymer matrix reduce both friction and wear to levels approximately independent of the matrix material. Fiber orientation was also seen to be important and minimum wear was obtained with fibers oriented normal to the surface. Carbon fibers were seen to be less abrasive than glass fibers. There was little evidence of carbon film formation, as is in the case of solid lubrication. He believed that fibers reduce friction and wear by preferentially supporting part of the load, and polishing the counterface.

Briscoe et al. [19] in their study with polythenes (polyethylenes), with and without

lead oxide-copper oxide fillers, had analyzed the transfer film on the steel counterface. The influence of sliding speed, load, roughness and temperature of the counterface was investigated. They believed that the wear rates in most polymers was primarily controlled by the ability of the polymer transfer film to adhere strongly to the counterface. If the polymer did not adhere strongly to the surface, repeated sliding at high loads and velocities would continuously remove and replenish the transfer film, producing a relatively high wear rate. Results showed that fillers help the polymer to strongly adhere to the steel counterface under severe sliding conditions, thus helping in reducing wear. Wear was seen to increase with an increase in counterface roughness. The fillers were ineffective in reducing wear of the polymer on a glass counterface, suggesting that some specific chemical interaction between the polymer and the steel counterface might be taking place at the temperatures generated during sliding under such severe conditions. However, the exact mechanism is unclear. Their theory was supported by the findings of Bahadur and Tabor [20]. They had performed experiments with unfilled and filled polytetrafluoroethylene (PTFE), and had observed similar transfer modes.

The wear mechanism of unidirectional oriented fiber reinforced plastics (FRP), was studied by Tsukizoe and Ohmae [21]. Various fibers (high modulus carbon, high strength carbon, E-glass, stainless steel and Kevlar-49) reinforced epoxy, polyester and PTFE matrix composites were tested in three major fiber orientations. These orientations (normal, parallel and anti-parallel) are explained in Fig. 1. On a steel counterface, best wear resistance was obtained in the normal orientation, and worst in the anti-parallel

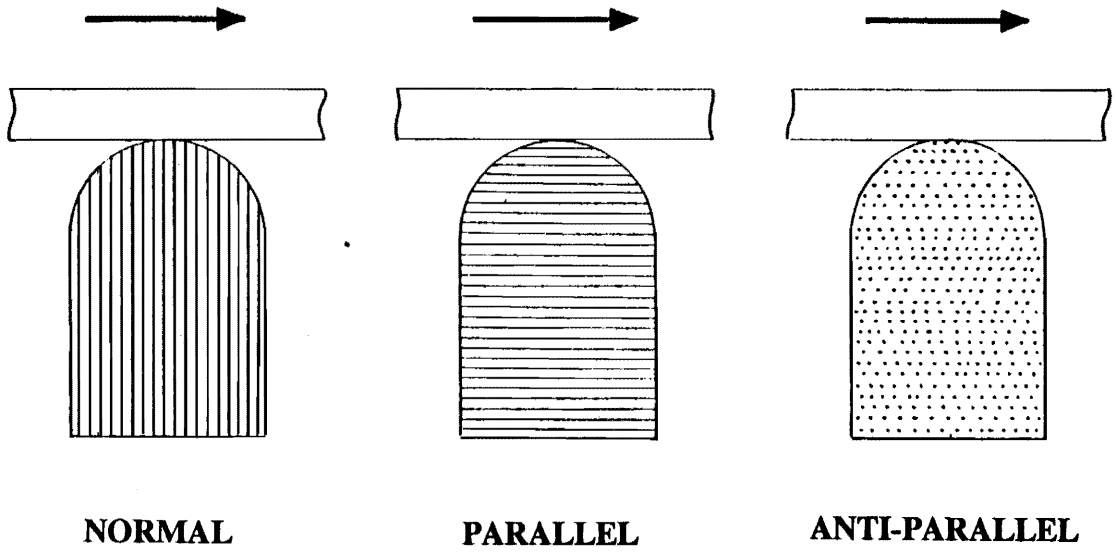

Fig. 1. The normal, parallel and anti-parallel fiber orientations.

orientation; the parallel orientation showed fairly good wear resistance. Of all the combinations of fibers and matrices examined, epoxy resin reinforced with high modulus carbon fibers showed the best wear resistance properties. In general, good wear resistance was achieved by improving the tribological properties of the fiber reinforcements, e.g., self lubricating properties and good mechanical properties as Young's modulus and interlaminar shear strength. A model was proposed that wear of FRP proceeds by wear thinning of fiber reinforcements, with subsequent "breakdown and pull off" from the matrix.

Fusaro and Sliney [22] found that addition-type highly crosslinked polyimides, with low elastic strength and low modulus graphite fiber reinforcements show lower friction and wear rates compared to condensation-type polyimides with high modulus fiber reinforcements at room temperature, but the difference becomes less at higher temperatures. They thought that the wear behavior is due more to the interaction between the fiber and matrix, rather than being dominated by the fiber or the matrix properties individually.

Tanaka [23], in his measurements with PTFE and polyacetals incorporating glass and carbon fibers and sliding on glass and steel counterfaces, observed that carbon fibers reduced the coefficient of friction and wear of both materials; glass fibers increased the wear of polyacetals. At high speeds, the wear-reducing action of both the fibers was remarkably good on the glass counterface. The fiber-rich surfaces resulting from sliding and the flash temperatures at the fiber-matrix interface were believed to influence wear.

Sung and Suh [24] proposed the "delamination wear theory" as being one of the wear mechanisms for polymer composites. It says that debonding occurs at the fiber matrix interface, starting from the surface. In the normal orientation, due to the lateral constraints, cracks do not propagate to greater depths. On the other hand, in parallel and anti-parallel orientations, cracks are less constrained to grow along the fiber matrix interface. This results in higher wear in parallel and anti-parallel orientations. A schematic representation of the failure modes is shown in Fig. 2. This theory was supported by Clerico and Patierno [25]. In their studies with "Ultramid A3WG5" and "Ultramid ASR" (glass fiber filled nylon 6/6 composites) sliding on steel, subsurfaces of both polymers showed plastic deformation and sub-surface cracks. The cracks were seen to nucleate at the matrix-glass fiber interface and propagate parallel to the surface at a depth which depends on the normal load and sliding velocity. After reaching a critical length, the cracks shear to the surface, thus producing wear sheets.

Chang [26] studied the effect of fiber orientation of continuous fiber graphite-epoxy composite on wear. Specimen rings were slid against steel blocks at various fiber orientation angles (0°, 30°, 45°, 60°, 75° and 90° between the parallel and anti-parallel orientations). Surface temperature was also estimated using an infrared fiber optic probe which was focussed on the block near the sliding interface. The temperatures measured were thus apparent interfacial temperatures. Minimum wear was found to occur when the fibers were oriented at 30° to the sliding interface. A good correlation was observed between the apparent interfacial temperature and the wear rate, with a sharp increase near the glass transition temperature of the matrix material. Fig. 3. shows some of his

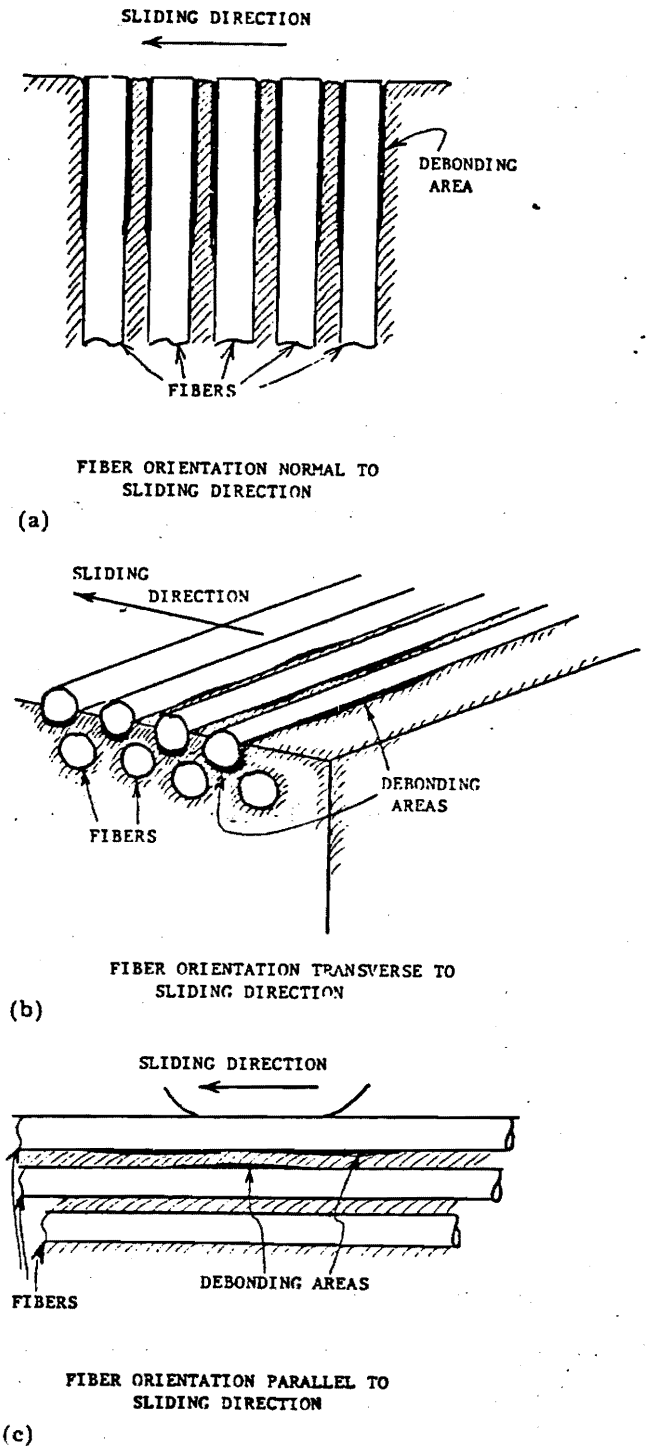

Fig. 2. Schematic representation of failure modes in uniaxial continuous fiber reinforced composites under sliding surface; fiber orientation normal (a), transverse (b), and longitudinal (c) to the sliding direction [24].

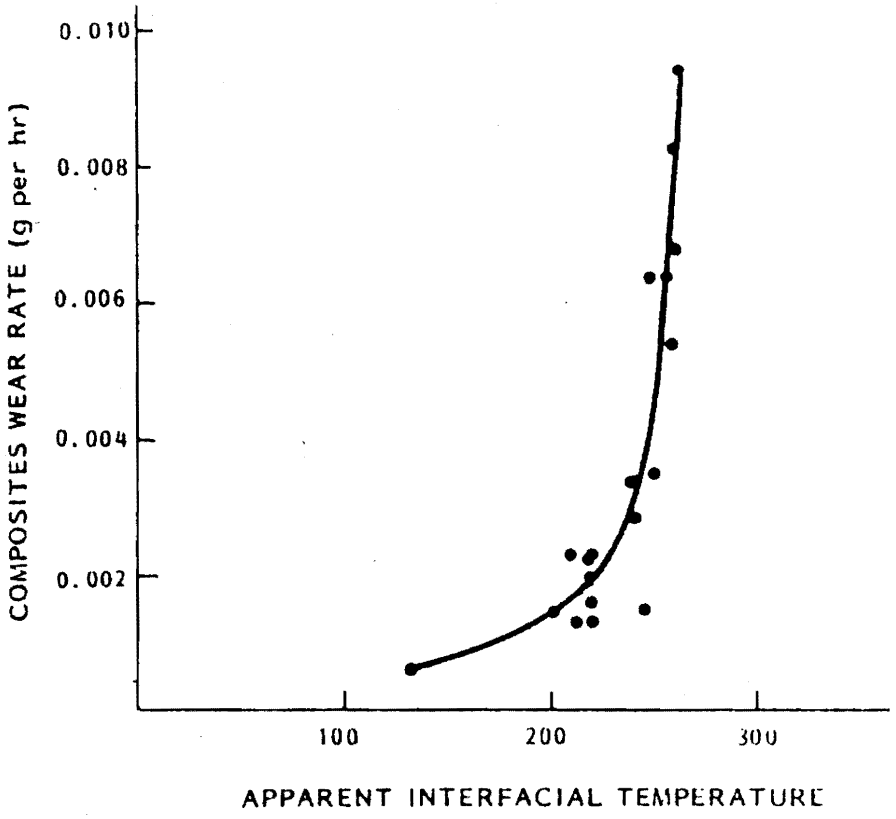

Fig. 3. Wear as a function of interfacial temperature [26].

results. He believed that due to more fiber breakage in the anti-parallel orientation, more mechanical energy is used up, producing a lower temperature rise. This results in a lower wear rate in the anti-parallel orientation.

Roberts et al.[27] investigated the use of continuous fiber/particulate composites as total surface hip replacements. Continuous fiber E-glass/epoxy composite femoral shells, having the same elastic properties as bone, were fabricated and coated with Al_2O_3+Cu and stainless steel+Al_2O_3 particulate filled epoxy coatings. The objective behind using the coating was to make the surface harder and more wear resistant, and to improve the thermal characteristics of the epoxy composites. They were tested against ultra high molecular weight polyethylene (UHMWPE) acetabular cups. The experiments were conducted in a total hip simulator at 30 walking cycles per minute and a programmed load simulating walking. Wear test weight measurement results showed an increase in wear of the acetabular cups by a factor of 25, over standard Vitallium balls.

In other experiments with UHMWPE and polycarbonate pins, sliding against graphite-epoxy plates, Roberts [28,29] observed minimum wear to occur at two different fiber orientations in the two material systems. In oscillating wear with the same materials [30], surface roughness seemed to be controlling wear more than fiber orientation. However Fusaro [31] did not observe any correlation between counterface roughness and wear.

Abarou et al.[32] showed the effect of mutual overlap coefficient (MOC), on wear of composites used in dry oscillating applications. MOC is defined as the ratio of the area of contact of the pin to the area of the wear track. A significant increase in wear

rate was observed at an MOC equal to about 0.6. The data, along with the materials examined, are shown in Fig. 4. Further, at higher MOCs, the wear rate was very sensitive to the bulk temperature.

Counterface wear due to abrasiveness of composites was studied by Anderson and Davies [33]. It is shown that a suitable composite-counterface couple should be an important consideration in bearing designs.

Abrasive wear of graphite fiber-reinforced polyimide, nylon and polyphenylene sulphide, rubbing against steel, was investigated by McGee et al.[34]. Abrasive wear of composites was found to be significantly higher than that of aluminum and steel. The fiber-matrix adhesion and the ductility of the matrix were believed to be important in determining the abrasive wear response of chopped fiber-polymer composites. Composites with fibers oriented normal to the surface showed the least amount of wear, possibly because in this configuration, the weak fiber-matrix interface is least exposed to the abrading surface directly. The wear in the transverse (anti-parallel) orientation was the highest, as the fibers were subjected to shear, bending and torsion loading by the abrading particles.

Voss and Friedrich [35] showed that addition of short glass or carbon fibers to polyetheretherketone (PEEK) can improve the wear resistance of PEEK, with carbon fibers being more effective. A higher degree of crystallinity of the PEEK matrix, due to an annealing process, was seen to reduce the wear rate slightly. When rubbed against abrasive paper, the fiber reinforcement seemed to be ineffective in reducing wear.

Hanmin et al. [36] have investigated the friction and wear behavior of

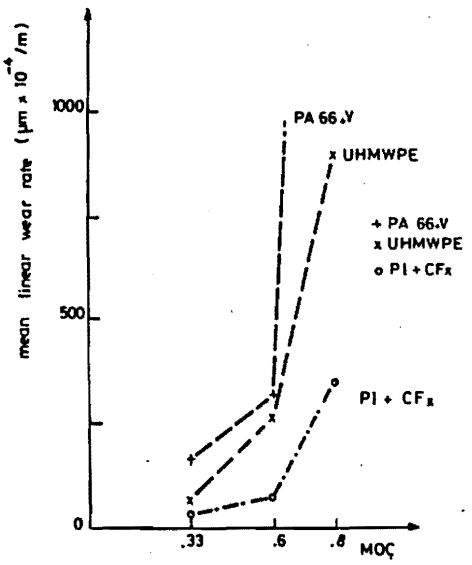

—Linear wear rate variation as function of MOC for PI + CFx, PA66 + V, and UHMWPE (Configuration GI; θ = 50°C, W = 40 N).

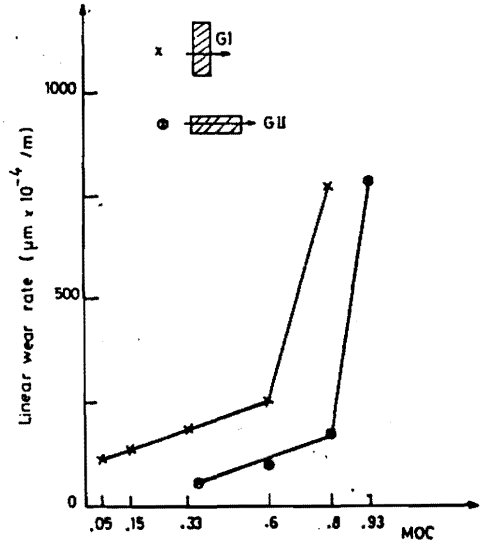

—Linear wear rate variation for UHMWPE as function of MOC with two pin geometric configurations GI and GII. (θ = 50°C; W = 40 N).

Fig. 4. Linear wear rate variation as a function of Mutual Overlap Coefficient [32].

polyphenylene sulphide (PPS) and its chopped carbon fiber composites, sliding against steel. Average contact temperature was also measured using a "natural thermocouple", which was composed of the counterface steel and the carbon fiber incorporated in the pins as reinforcement. The temperature was determined by comparison of the measured thermo-emf with the thermo-emf of a special thermocouple made out of a strand of carbon fiber and a similar wire of carbon steel and calibrated in an oil thermostat. The average contact temperature, coefficient of friction and wear rate were seen to increase with load. Contact temperatures as high as 250°C were detected under severe sliding conditions (600 N load and 0.4 m/s sliding velocity). The average contact temperature and coefficient of friction showed a minimum at a fiber content of 20-30% .

There have been some attempts at mathematical modelling of composite wear. Friedrich [37] used the "rule of mixtures", to predict the wear rate of a composite from the wear rates of its constituents. This is given as :

$$\frac{1}{W_c} = \frac{1}{W_f} + \frac{1}{W_m}$$

where : W_c = Wear rate of the composite material

W_f = Wear rate of the fiber material

W_m = Wear rate of the matrix material

This theory however could not be applied successfully to many composite systems as the wear characteristics not only depend on the fiber and matrix materials, but also on the fiber-matrix interaction.

Kar and Bahadur [38] derived a wear equation using dimensional analysis for

adhesive wear. Another attempt at mathematical modelling of wear was made by Bohner and Gardos [39] using least square regression of experimental data. They pointed out that wear volume varies non-linearly with, a) load, due to a combination of reinforcement phase interacting with the characteristic creep of the polymer matrix and load sharing; b) velocity, due to viscoelastic effects on polymer shear and the degree of fiber matrix debonding; and c) sliding duration, due to run-in effects.

An empirical wear equation to show the effect of fiber orientation on abrasive wear behavior of polymer composites was developed by Cirino et al. [40]. Two composite systems, continuous fiber reinforced carbon-PEEK and Aramid-epoxy sliding on abrasive SiC paper, were used to determine wear as a function of fiber orientation. Optimum wear resistance occurred when the fibers were oriented normal to the surface in both cases. The idea of a "wear tensor" (suggested by Hornbogen) was used to represent wear rates in the basic directions.

A wear model, based on fracture mechanics concepts and observed wear-induced microstructure, was developed by Lhymn [41-43]. It was seen that microcracks can initiate at the fiber-matrix interface, or from a defective site in the matrix phase. Such discrete microcracks can then grow under the influence of normal and frictional loads. The model, however, requires a certain statistical parameter to be determined from experiments in order to be implemented.

In another study, Lhymn and Light [44], derived an equation for the wear rate as a function of sliding velocity. It is based on the physics of crack propagation, and the "thermally activated process" concept. The equation is interpreted as follows :

- When the temperature rise at the contact spot is not significantly high, such that the frictional stress is not "thermally activated", the specific wear rate is inversely proportional to the sliding velocity. This is the case in which velocity is relatively low.
- When the temperature rise is significant, so that a "deformation-frictional" wear process can be "thermally activated", the wear rate increases exponentially with velocity. In this range, the exponential increase in wear rate out-weighs the linear decreasing term mentioned above.

A theoretical curve of the specific wear rate vs sliding velocity is shown in Fig. 5. The effect of normal load has also been explained using the concept of crack propagation and classical fracture mechanics [45]. The effect of fiber orientation on friction-wear properties of uniaxial PPS-carbon fiber composites has also been explained by the variation of elastic modulus, fracture strain and interlaminar shear strength.

Lhymn [46,47] has further shown the effect of environment on the two-body abrasion of PEEK-carbon fiber composites, sliding against emery paper. It was seen that the presence of liquid lubricants as water and oil generally increases the wear rate as compared to wear in an air environment. The wear rates for dry as well as lubricated sliding was seen to decrease with an increase in normal load and sliding velocity. A fatigue wear mechanism based on microstructural observations was employed to explain the measured data. Damage accumulation via crack initiation /propagation along the weak path was evident from the microstructural features.

Some of the initial studies on the tribological behavior of polymer composites at high bulk and surface temperatures were made with brake materials. Tanaka et al. [48]

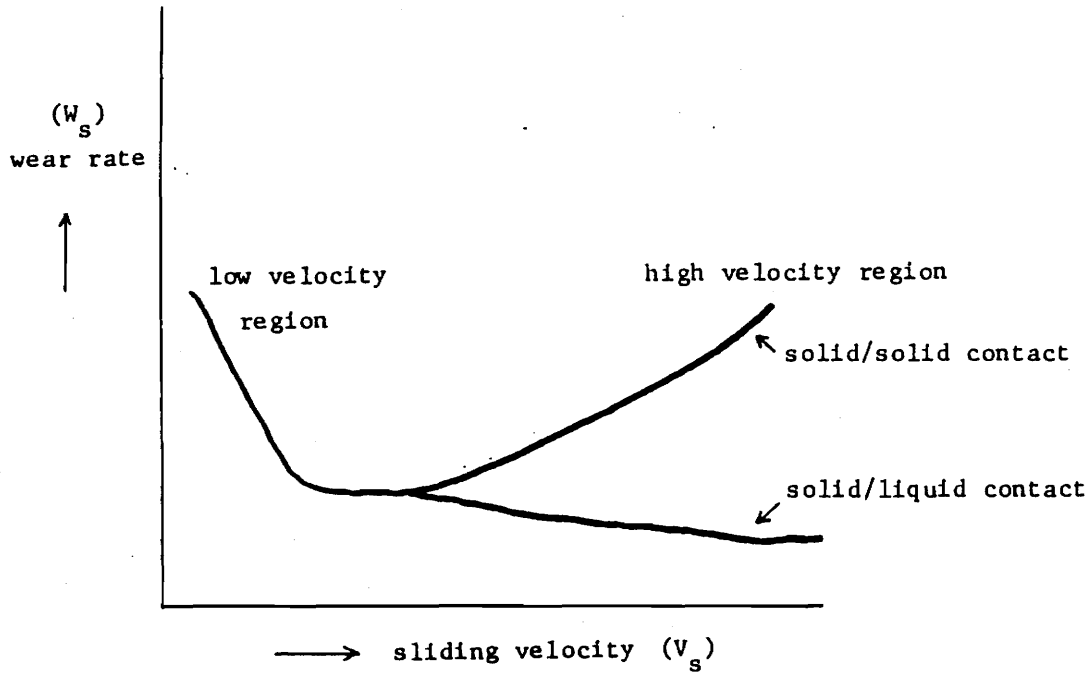

Fig. 5. Theoretical curve of the specific wear rate vs. sliding velocity [44].

studied the behavior of phenolic resins and resin-asbestos composites at elevated temperatures. Friction was seen to decrease with an increase in temperature, but wear increased sharply at temperatures above 150° - 200°C. Further, minimum wear was observed with 60% filler composition. It was believed that low friction at high temperatures could be due to the lubricating action of liquid and gaseous products of resin decomposition in the neighborhood of fillers that act as hot spots due to frictional heating.

In another study by Gong et al. [49] on polymer brake composites, in an environmental temperature range of 100° to 600°C, it was seen that friction stability at high temperature depends not only on thermo-oxidation resistance of the composites, but also on the properties of the surface layer during sliding. Addition of a "friction stabilizer" (a nitrogen containing organic compound) helped keep friction at a higher value and reduce wear. An "equilibrious" temperature was defined beyond which an increase in velocity did not result in any further increase in the temperature.

Evans [50], among many others, studied the tribological behavior of PTFE with various fillers at bulk temperatures ranging from 20° to 300°C. The wear rate was seen to increase with temperature, almost exponentially in the case of inorganic fillers and fibers. With organic fillers and fibers, the wear rate remained almost constant up to about 150°C, but increased rapidly beyond this temperature. The wear rate was one order of magnitude lower in the case of organic fillers compared to inorganic fillers at 150°C.

The effect of carbon and glass fillers on transfer films of PTFE was studied by

Briscoe and Steward [51]. Addition of fillers reduced the wear rate by three orders of magnitude, and relatively harder fillers were more beneficial. They hypothesized that adhesive wear was the dominant wear mechanism. Details of their theory have been reviewed before in this chapter. They believed that the fillers provide intense local conditions at the interface, producing intense stresses and temperatures, which could provide suitable mechanical and chemical conditions for the polymer to adhere well to the counterface. The wear rate was seen to decrease with a decrease in counterface roughness and finer filler particles. Although the results were in general agreement with the argument, the mechanism of enhanced adhesion was not clear.

West and Senior [52] showed that in bearing applications, PPS composites could offer significant improvements over epoxy composites at temperatures above 120°C. Baranovskii et al. [53] investigated the temperature dependence of thermo-physical properties of PTFE-bronze anti-friction material. Thermal conductivity was seen to increase, and thermal diffusivity decrease, with increasing temperature. However, due to the low thermal conductivity of the matrix material, thermal conductivity of the composite is dominated primarily by that of the matrix material, until very large filler concentrations are reached.

Some attempts at theoretically predicting surface temperatures generated during sliding of polymer composites have also been made. Ling and Yang [54] found an analytical solution for the interfacial temperature in moving layered composites. Roberts and Griffin [55] combined experimental and analytical techniques to determine surface temperature and heat distribution at the interface. They measured the temperatures at a

large number of points inside stationary composite specimens (nylon 6/6 + 20% PTFE, polycarbonate + 10% PTFE, and two powdered graphite-filled phenolics) sliding on steel, using an infrared fiber optics thermal monitor. Using finite element analysis, they calculated the temperature and heat flux at the interface. This was an indirect approach, since the temperature at the surface was extrapolated from the temperature distribution in the sub-surface region. Day [56], in his work on thermal analysis of automotive drum brakes, also used finite element analysis to predict the temperature at the interface of composite brakes.

Besides the studies on the tribological behavior of polymer composites, there are a number of studies on such behavior of pure polymers. Most of those studies have not been reviewed here. However, since the present research is primarily on the measurement of surface temperature and the effects of surface temperature on friction and wear of polymer composites, it is thought relevant to review such studies involving pure polymers. Effects of bulk temperature on friction and wear of polymers are also included in this section.

Tabor and McLaren [57] observed lower coefficients of friction at higher bulk temperatures for PTFE sliding on steel. Vinogradov et al. [58] experimentally determined the effect of bulk temperature on shear strength, adhesion tear-off strength, and coefficient of friction for "high pressure" polyethylene and isotactic polypropylene sliding on steel. They found that by reducing the temperature from 100°C to -20°C the adhesion shear strength could reduce 35-fold. But friction coefficients for both polymers were generally found to be higher at lower bulk temperatures.

Price and Burks [59] attempted to measure surface temperatures of sliding polyimides and pyrones on steel using imbedded thermocouples. Similar attempts were made by Kar and Bahadur [60] for high density polyethylene, polyoxymethylene, PTFE and polypropylene using iron-constantan thermocouples. Temperature rises on the order of 100°C to 200°C were measured for rather severe conditions. Failure of polyethylene and polyoxymethylene occurred due to thermal softening.

Ettles [61] proposed that under severe dry sliding contact, a regime could eventually be initiated where friction is governed by the heat flow. His theory is based on the argument that under such conditions, a maximum allowable surface temperature is defined, from which closed-form results for coefficient of friction can be obtained. This allowable temperature is characteristically the softening temperature of the polymer; this, however, may not be very clearly defined for some polymers. Moreover, only a very thin interfacial layer is thought to have reached the softening point, with the bulk still capable of supporting the load. The coefficient of friction is then back-calculated from the maximum allowable temperature rise, using Archard's theory. He showed reasonable agreement of his theory with experimental results from various polymer systems (data collected from literature). He also presented experimental data using a glass sphere sliding on soft and hard rubber plates [62]. Agreement with the theory was better at high loads, suggesting that the theory applies to severe conditions only.

Tanaka and Yamada [63] found relatively low steady state coefficients of friction at bulk temperatures above 200°C for polyimide (PI), polyamide-imide (PAI) and PEEK sliding against steel. PPS (filled with glass fibers) and polyether sulphone (PES) sliding

against steel showed relatively high coefficients of friction at temperatures above 150°C. Besides, PI and PAI showed wear peaks at temperatures between 150° - 200°C, and PES, PPS and PEEK showed sharp increases in the wear rates at certain critical temperatures ranging between 100° - 300°C. These critical temperatures varied with the system. These results are shown in Fig. 6. Such behavior was believed to be due to chemical reactions occurring in the unreacted portion of the polymer chains at the high temperatures generated during sliding.

Transitions in friction and wear near the glass transition temperature of nylon 6/6 sliding on steel were also observed by Vroegop et al.[64]. The coefficient of friction was seen to increase rather sharply beyond this critical temperature. But the wear rate showed a minimum at this temperature. These results are shown in Fig. 7. Below this critical temperature, friction was seen to be almost independent of counterface roughness. But Anderson and Robbins [65] observed very little effect of bulk temperature on wear of UHMWPE and polyacetals sliding on steel under less severe conditions.

Table 2. summarizes some of the important theories developed so far in the area of composite tribology.

A)

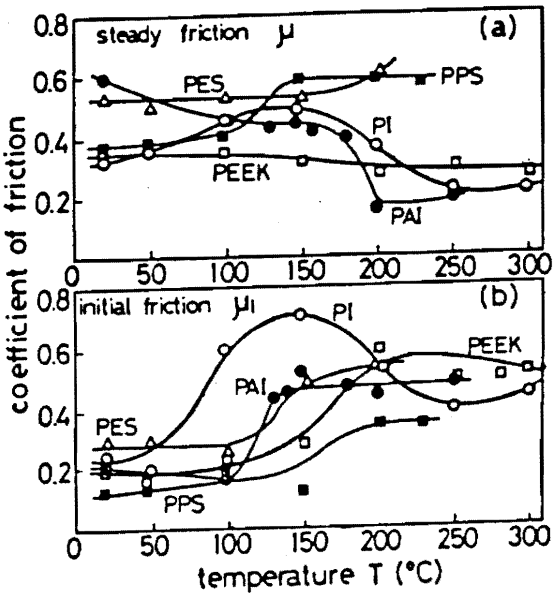

B)

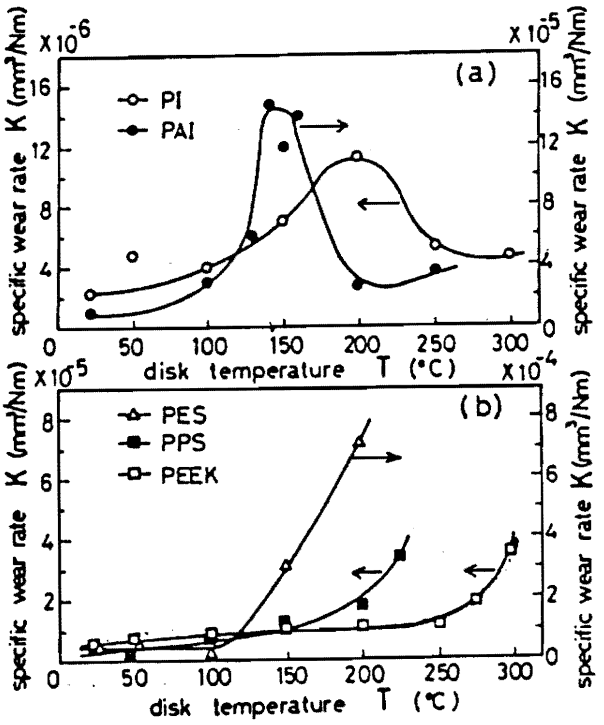

Fig. 6. A) Variations in the coefficients of friction of various polymers with disk temperature; a) steady state friction, b) initial friction.
B) Variations of the specific wear rates with disk temperature [63].

A)

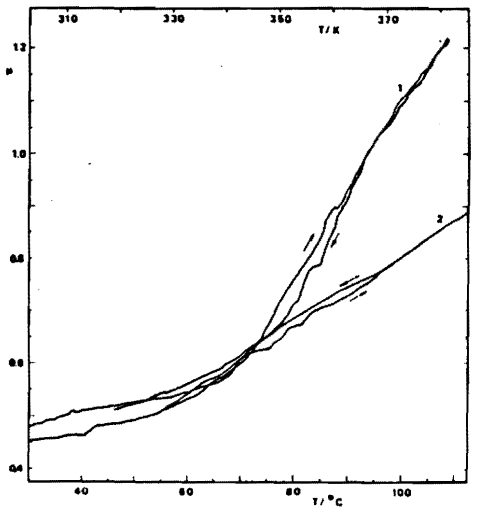

B)

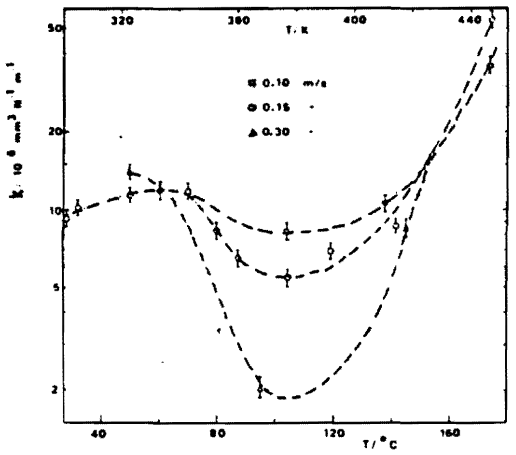

Fig. 7. A) Friction -- Temperature recordings of Nylon 6/6 on steel.
B) Wear coefficient of Nylon 6/6 as a function of steel substrate temperature [64].

Table 2. Major theories in composite tribology.

THEORY	RESEARCHERS
Fibers reduce friction by preferentially supporting part of the load.	Lancaster [18]
Fillers help the polymer transfer film to strongly adhere to the counterface, thus preventing continuous removal of material.	Briscoe, Pogasian and Tabor [19], Bahadur and Tabor [20]
Wear proceeds by wear thinning of fiber reinforcements and subsequent break down of the fibers and pull off from the matrix.	Tsukizoe and Ohmae [21]
Fiber-matrix interaction.	Fusaro and Sliney [22], McGee [34]
Delamination wear theory.	Sung and Suh [24], Clerino and Patierno [25]
Flash temperatures at the fiber-matrix interface result in resin decomposition. The liquid and gaseous products act as lubricating agents.	Tanaka [23]
Fatigue wear.	Lhymn [41-47]
Fiber breakage dissipates mechanical energy; hence surface temperature stays lower resulting in less wear.	Chang [26]

2.2 REVIEW OF SURFACE TEMPERATURE MEASUREMENT

2.2.1 Experimental Techniques

Some of the early attempts by Santini and Kennedy [66], Spurr [67], and Ling and Simkins [68] were based on the use of embedded thermocouples. However, they were able to measure only the bulk temperature, away from the surface. Besides, these thermocouples give inaccurate results, as they interrupt the flow of heat. Dynamic or Herbert-Gotwein thermocouples were used by Shore [69], and Furey [70]. Furey used a fixed constantan ball loaded against a rotating steel cylinder. He found that the mean surface temperature was fairly independent of running time and gross wear of the constantan ball, but was markedly affected by load and speed. Comparison of the experimental data with the existing theories showed that the experimental mean surface temperature rise was much less than that predicted by theory.

Kannel et al. [71] used a bisignal transducer which could be used to simultaneously measure pressure and temperature at any point at the interface. This transducer consisted of a titanium thin film temperature transducer deposited on top of a manganin thin film pressure transducer. Quinn and Winer [72] used photographic methods to record visible hot spots on the surface. Quinn [73] also used X-ray diffraction techniques to attempt to correlate the formation of iron oxide with surface temperature.

The use of infrared devices is perhaps the most appropriate and direct technique

for the measurement of surface temperatures at the interface. In the work by Parker and Thomas [74], an infrared sensitive photoconductive cell was used to measure temperature at the interface of a brake shoe and drum. Bowden and Thomas [75] used a lead sulfide cell to measure the surface temperature of a pin sliding against a quartz disk. Temperatures during metal cutting operations have also been measured using lead sulfide cells by Chao et al.[76].

A Barnes Infrared Radiometric Microscope was used by Winer et al.[77-79] for measurement of surface temperatures for elastohydrodynamic (EHD) lubrication conditions. Winer et al. [80] also carried out an investigation that included mapping of fluid temperatures and ball surface temperatures for EHD contact. Griffioen et al.[81] have used an infrared scanning camera to determine the temperatures at the asperities in an unlubricated contact between a silicon nitride pin and a sapphire disk. Temperatures as high as 2700°C have been detected concentrated in areas of about 100μm in diameter.

At Virginia Polytechnic Institute and State University, a research program was started in 1973 for the measurement of surface temperatures using a Barnes RM-2A infrared microscope. A sapphire disk transparent to infrared radiation is used as the counterface. This apparatus, being capable of looking at target spots as small as 17 micrometer in diameter, gives transient temperature values over very small contact areas. The results of the initial research may be found in the theses by Wiggins [4], Omori [5], Li [6] and Richardson [7]. An overall review of this research including the major results and possible sources of error has been discussed by Furey [82,83]. Temperature measurements for several metals, graphite, and polymers have been carried out at various

loads, speeds and environments. Relationships between friction, the real area of contact, and surface temperatures have been investigated. The effect of macroscopic subdivision of the contact area on surface temperature of copper sliding on sapphire was studied by Rogers [8]. Moyer [9] studied the effect of environment on oxide formation and its relation to surface temperature for the system of iron on sapphire. The effect of load, velocity and environment on surface temperature of silver sliding on sapphire was studied by Hollowell [10]. An advanced computerized data acquisition system was installed by Jayaram [11] and area mapping of the surface temperature distribution was also done.

Recently, an oscillating/fretting set-up was developed by Ghasemi [16] to measure the temperatures in oscillating/fretting contacts. The effect of surface temperature on the life of polymeric films on metal substrates in fretting motion against sapphire is being investigated. Further, a technique has been developed to video record the contact area during the experiment using a photomacroscope. Using the oscillating setup, surface temperatures in ceramic-on-sapphire systems have been measured by Weick [13]. The experimental results have been compared with the newly developed theory by Vick et al.[84]. At present, a computer-controlled precision X-Y table is being installed that would enable automatic scanning of the contact area for temperature profile mapping.

2.2.2 Theoretical Techniques

The theoretical prediction of surface temperatures resulting from frictional heating was initiated with the pioneering works of Blok [85,86] and Jaeger [88]. Both employed

an analytical solution for the temperature distribution due to a point source to construct the solution for a uniformly distributed heat source over a single contact patch on the surface of a semi-infinite medium. Blok calculated the temperature distribution for stationary and moving sources subject to a uniform heat flux. The total heat flux was then partitioned such that the maximum temperatures on the two sources were the same. Jaeger, instead, matched the average temperatures of the two surfaces to determine the frictional heat distribution between the two surfaces. Later, Archard [89] suggested that the average interfacial temperature rise is the harmonic mean of the average rises if each surface received all the heat flux. In a more recent paper [90], Archard extended his formulation to allow to estimate the temperature distribution in the sub-surface regions as well.

Ling [91,92] eliminated the need to approximate the division of frictional heat by evoking the condition that all points of mating elements in intimate contact must have the same surface temperature. This leads to a singular integral equation for the heat partition function and shows that the correct partitioning function varies with both the position within the real area of contact and velocity. The effect of multiple contact area was also investigated by Ling [93,94]. A large number of contact spots were generated within the nominal contact area in a random manner; the resulting flash temperatures at the contact spots were found to be much higher than elsewhere on the surface.

The analytical treatment of surface temperatures has also been extended to include the effect of lubricant and third-body layers between the sliding surfaces. Lai and Cheng [95] considered lubricated sliding with rough contact where the surface roughness was

generated numerically. The results showed that scuffing is associated with high temperature asperities which are above the material softening point.

Numerical methods have also been used for the analysis of surface temperature, especially for sliding bodies of complex shapes. Both finite difference and finite elements have been employed. In order to accurately calculate the large temperature gradients in the vicinity of the contact areas, the finite difference technique requires an excessively fine grid, resulting in long computing times and storage. As a result the finite element technique seems more suited to these types of problems using a fine mesh in the region of the contact and a coarser mesh elsewhere. However, in cases of high Peclet number this technique may result in numerical oscillations and inaccuracies.

The finite element technique was applied by Kennedy [96] to analyze temperatures in various systems as disk brakes, bearings and gas seals. Kennedy et al. [97] also used the technique to predict temperatures in oscillating contacts with low frequency and high amplitude. Colon and Floquet [98] used a hybrid technique, which employed a finite element method only in the component that was complex in geometry and integral transfer technique in the simpler component.

The boundary integral equation method (BIEM) is a relatively new numerical technique for analysis of thermal problems. The BIEM was first applied by Rizzo and Shippy [99] for the solution of transient heat conduction problems. They used Laplace transform in a time variable. More details about other works in this area are reviewed by Furey et al.[84] and Vick et al.[100].

A recent improvement in the BIEM technique has been done at Virginia

Polytechnic Institute and State University under the guidance of Dr. Vick. A moving, full-space Green's function is used as the fundamental solution [14]. The numerical characteristics and limitations of the solution method as well as the physical parameters that affect the solution method are presented. Since the real area of contact is extremely important, the theoretical analysis has the flexibility to handle any size, shape and distribution of contact area. The technique has also been modified to compute surface temperatures in the presence of a film [15].

CHAPTER 3

EXPERIMENTAL TECHNIQUE

3.1 OVERVIEW OF TEST APPARATUS

This study was carried out on an infrared microscope system developed at Virginia Polytechnic Institute and State University. Surface temperatures at the contact area, generated during sliding, are measured using an infrared technique. Besides the measurement of surface temperatures, this study also includes the measurement of friction, wear, and observation of surface damage. Two composite materials sliding against sapphire are examined. Both unidirectional sliding and oscillating contact conditions are investigated. A brief description of the test apparatus and the techniques used is given in this chapter.

The basic contact geometry, as shown in Fig. 8., consists of a spherical-ended cylindrical pin rubbing against a sapphire disk in oscillating or sliding motion. Such a geometry of the specimen was chosen over spherical balls, because of the relative ease of fabrication. The various types of specimens and their configurations used are shown in section 3.2. Sapphire is used as the counterface, as it is transparent to infrared

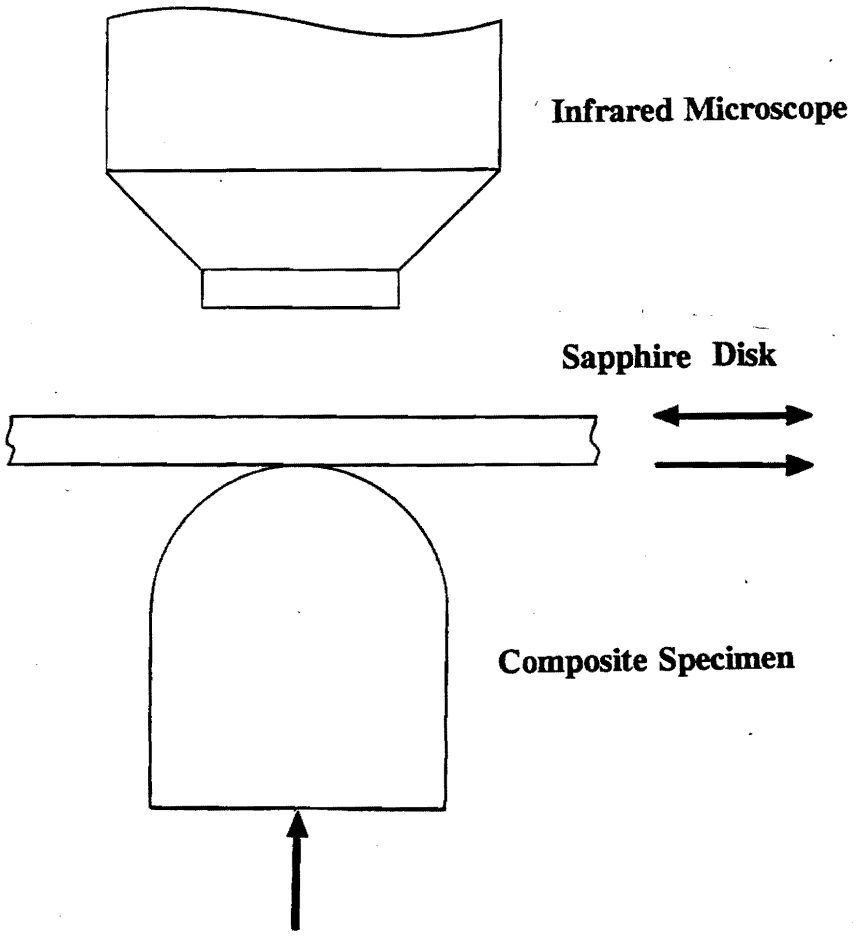

Fig. 8. Basic Contact Geometry.

radiation in the frequency band in which the microscope operates. Sapphire is transparent to visible light as well. The optical flatness of the sapphire disks keeps the target spot in the focal plane of the microscope. In addition, sapphire, being very hard, is less susceptible to surface damage.

Figures 9 and 10 show schematically the main components of the system in the sliding and oscillating set-ups, respectively. It consists of an infrared microscope that looks at the contact region and picks up the radiance signals, a drive system that rotates or oscillates the sapphire disk, a loading system that applies the normal load, transducers that pick up friction, velocity and acceleration signals, and thermistors that measure the ambient temperatures. Photographs of the unidirectional sliding and oscillating set-ups are shown in Figs. 11 and 12. The position of the microscope is monitored with the help of linear variable differential transducers (LVDT). A more detailed description of the various units is covered in the following sections. In addition, techniques used to measure emissivity, glass transition temperature, and estimated contact area are discussed in the following sections. The outputs from the instruments -- including the microscope, transducers, LVDTs, and thermistors -- in the form of electrical signals, are stored using a Frequency Modulation (FM) tape recorder. The signals are processed using an analog-to-digital converter connected to an IBM PC.

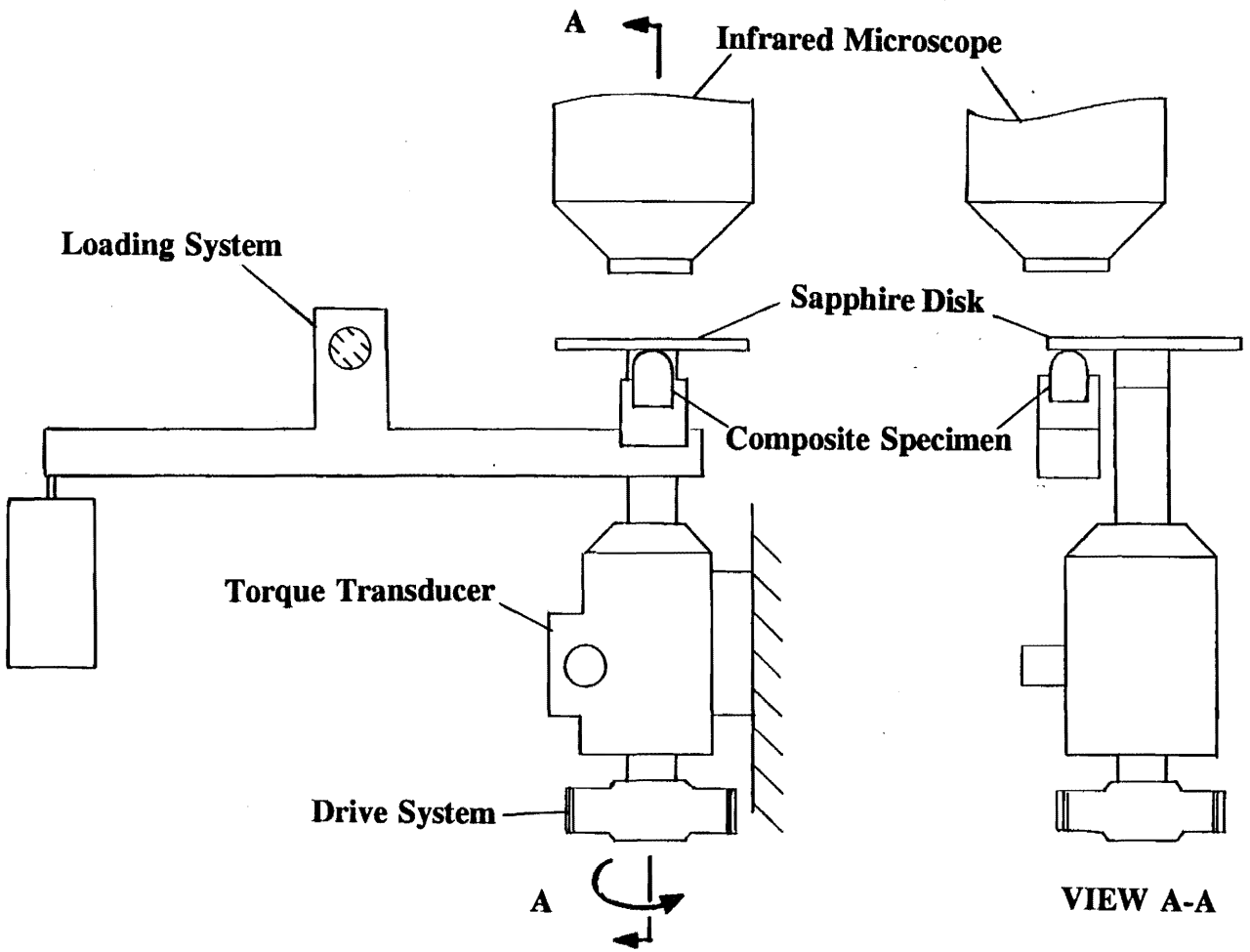

Fig. 9. Schematic diagram of the unidirectional sliding contact system using a rotating sapphire disk.

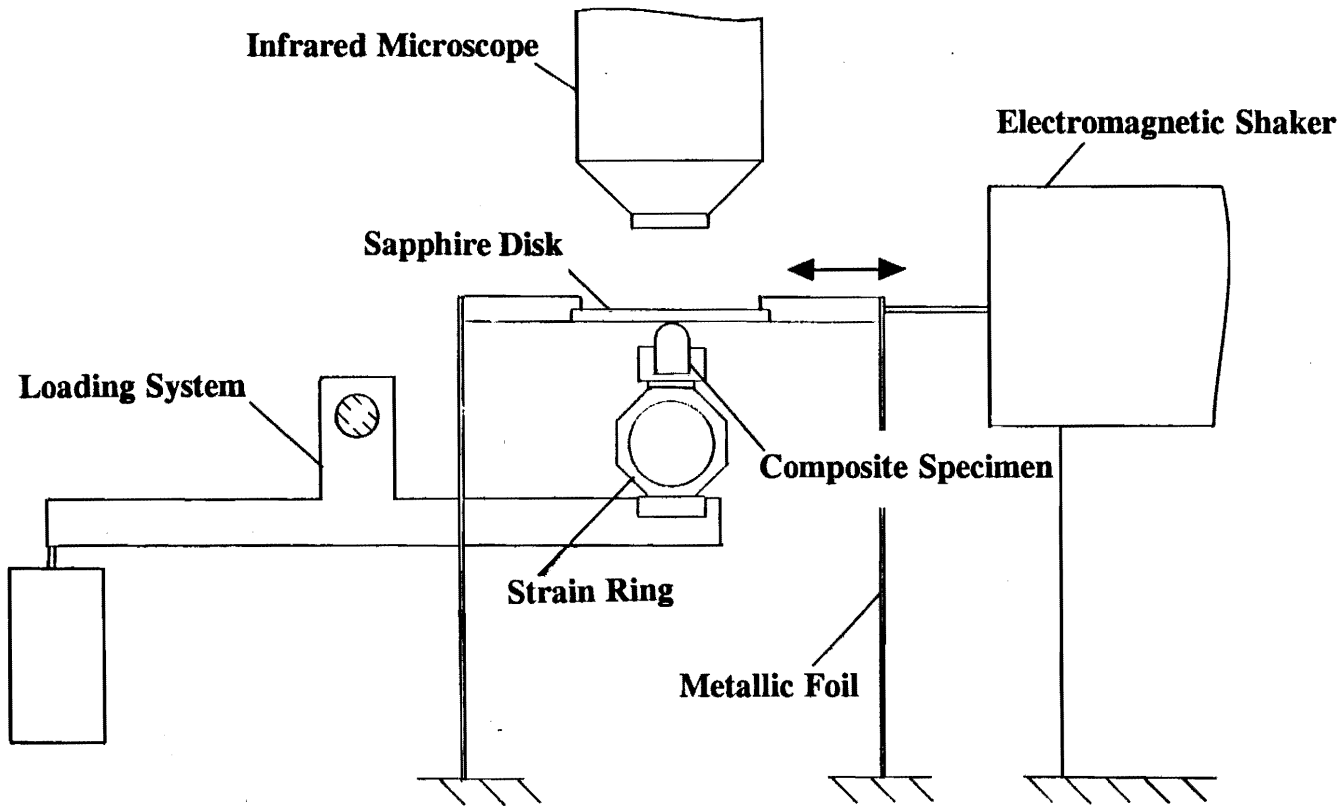

Fig. 10. Schematic diagram of the oscillating/fretting contact system using an oscillating sapphire disk.

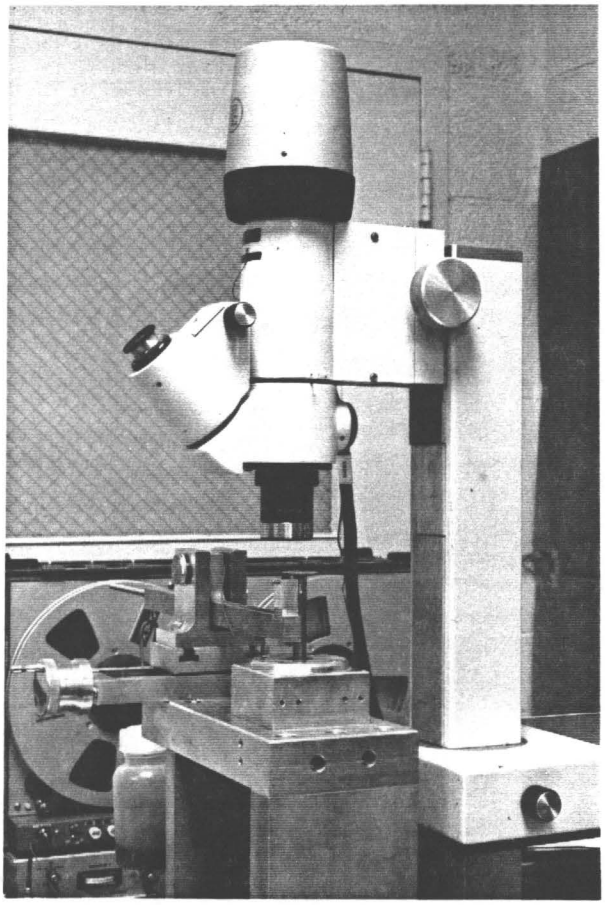

Fig. 11. View of the unidirectional sliding contact test apparatus.

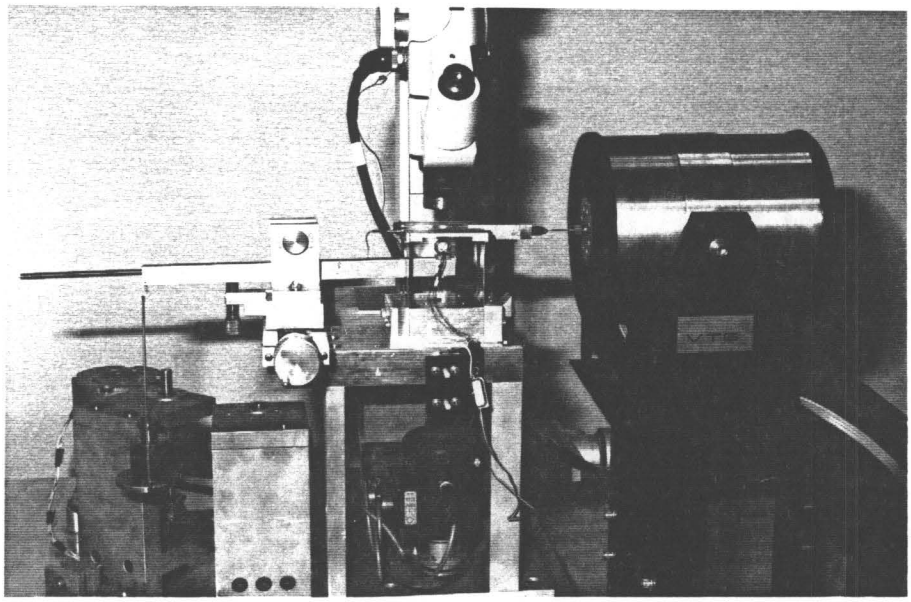

Fig. 12. View of the oscillating/fretting contact test apparatus.

Further details on this experimental apparatus can be found in the theses by Wiggins [4], Omori [5], Li [6], Richardson [7], Rogers [8], Moyer [9], Hollowell [10], and Weick [13], as well as in the summary review papers by Furey [80], Furey, Vick, Foo and Weick [81], Furey and Ghasemi [12], and Furey and Jayaram [102].

3.1.1 Drive Systems

Two different drive systems are used for the two types of motions. The oscillatory motion of the sapphire disk is created by shaking a platform mounted on thin metal foils of very low stiffness. The sapphire disk is mounted on this platform. The vibratory motion is generated by an electromagnetic shaker, driven by a wave generator through a high power amplifier. The frequency and form of the wave is controlled by the wave generator, and the amplitude is controlled by the power amplifier. Figure 13a shows a view of the drive system.

The drive system in the sliding set-up consists of a hysteresis synchronous constant speed motor rotating at 3600 revolutions per minute. The desired speed of rotation of the disk is achieved through gears and belts. Only stepped increases or decreases in rotary speed can be obtained with this system. But it does not allow any slippage, ensuring a constant rpm throughout the experiment. The drive system is shown in Fig. 13b. More details of the system are discussed in references [4].

Rotational motion from the motor is transmitted to the torque transducer shaft

a)

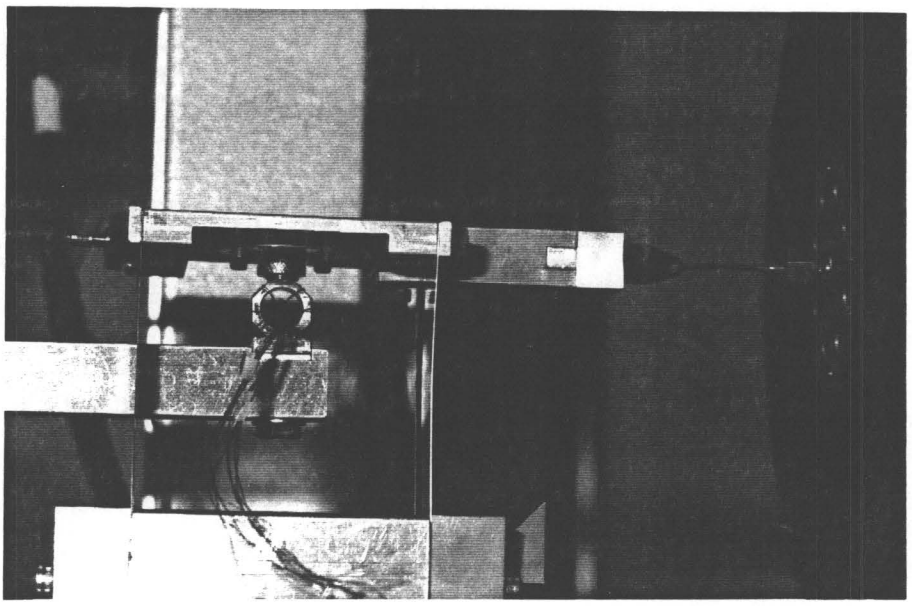

b)

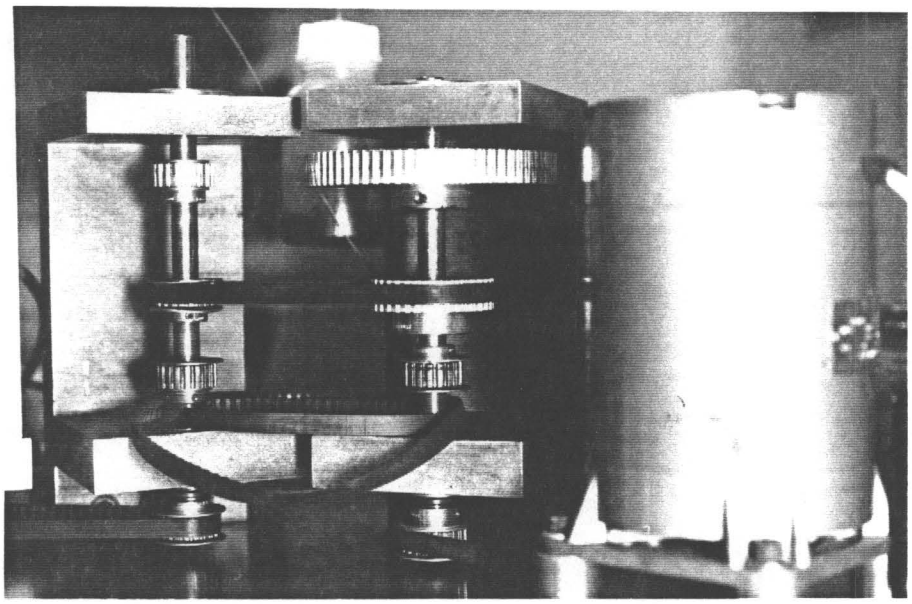

Fig. 13. Drive system for, a) oscillatory motion, b) unidirectional motion.

through the gears and belts. An intermediate shaft supported on bearings is fixed to the other end of the torque transducer shaft through a flexible coupling. The sapphire disk is bonded to the end of a steel pin using Hysol 1-C white epoxy cement. To ensure proper alignment of the disk, a special fixture is used for bonding. The pin is screwed on to the intermediate shaft. A view of the mounted sapphire disk is shown in Fig. 14, along with the specimen. Figure 15 shows a view of the disk mounting fixture.

3.1.2 Surface Temperature Measurement

As mentioned earlier, a Barnes RM-2A infrared radiometric microscope is used for the measurement of surface temperature. It operates in the wave length range of 1.8 to 5.5 micrometers. A schematic functional diagram and a three-dimensional schematic view of the microscope are shown in Figs. 16 and 17. Infrared and visible energy from the target spot enter the microscope through a reflective objective lens. Either a 15X objective lens with a target spot diameter of 35.4 micrometers and visual magnification of 150X, or a 36X objective lens with a target spot diameter of 17.8 micrometers and visual magnification of 360X can be used. The visible part of the radiation is reflected by a germanium dichroic optical element into the visible channel, which helps in positioning and focussing of the microscope and continual observation of the contact area during an experiment. The infrared radiation on the other hand, passes through the germanium element and impinges on the liquid nitrogen cooled indium antimonide photovoltaic detector. A vibrating tuning fork chopper alternately allows the

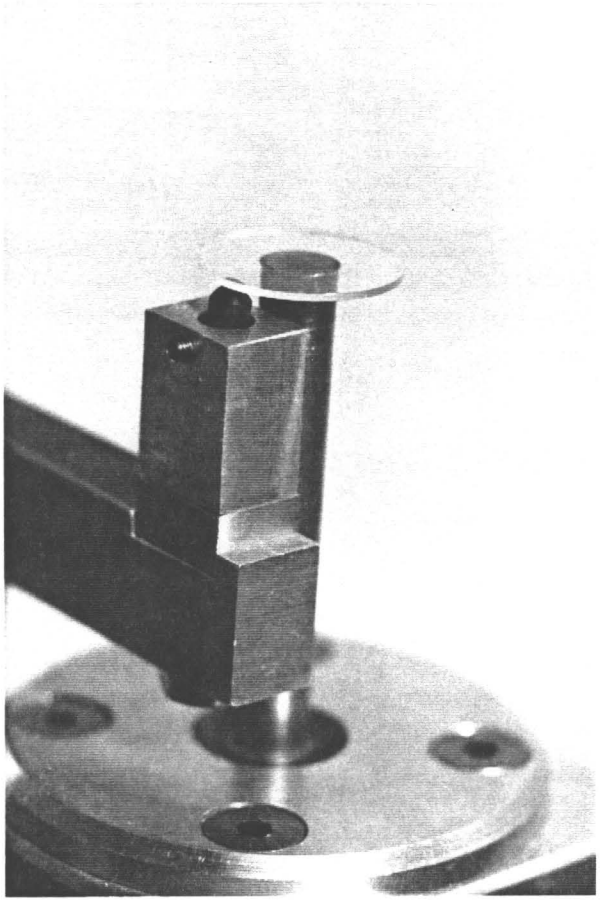

Fig. 14. View of the mounted sapphire disk and specimen.

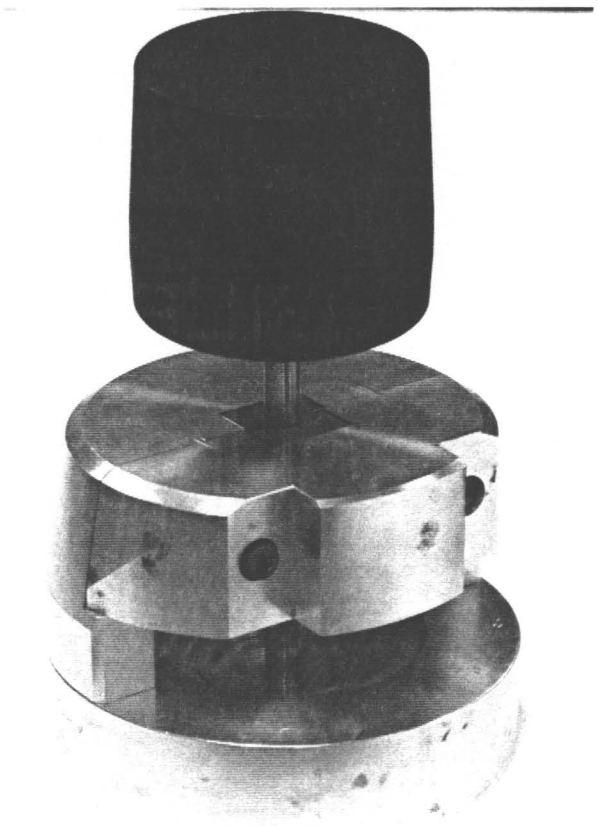

Fig. 15. View of the disk mounting fixture.

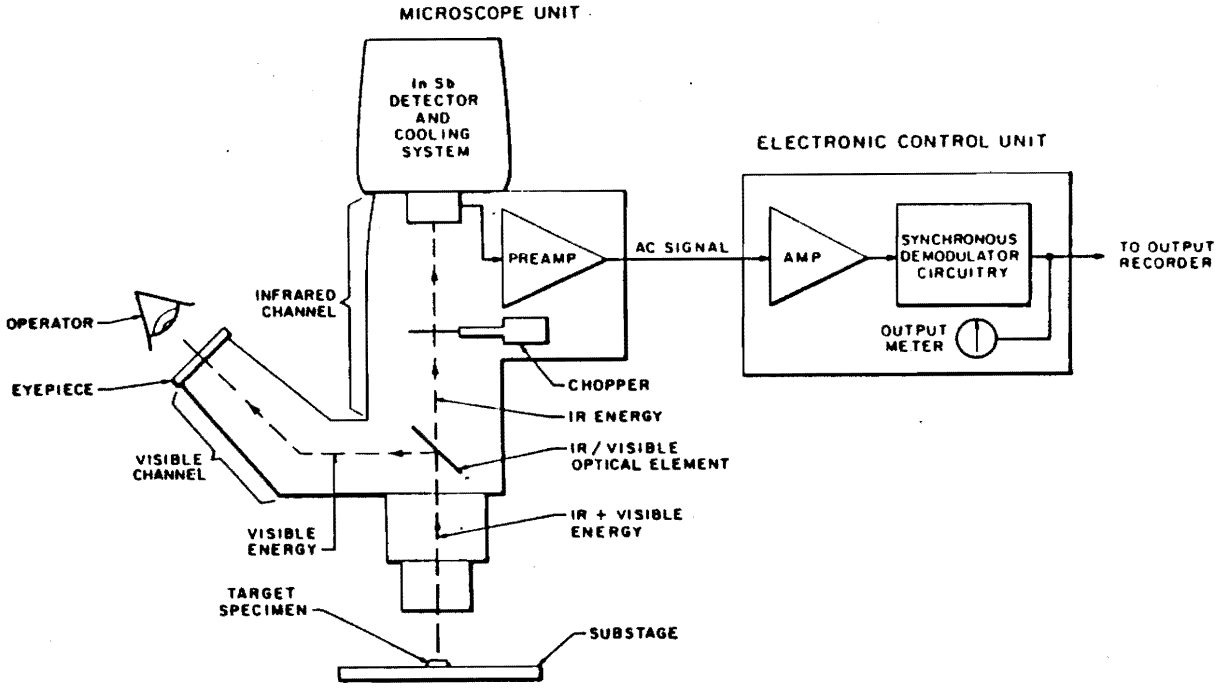

Fig. 16. Schematic functional diagram of the Barnes-2A Infrared Microscope [103].

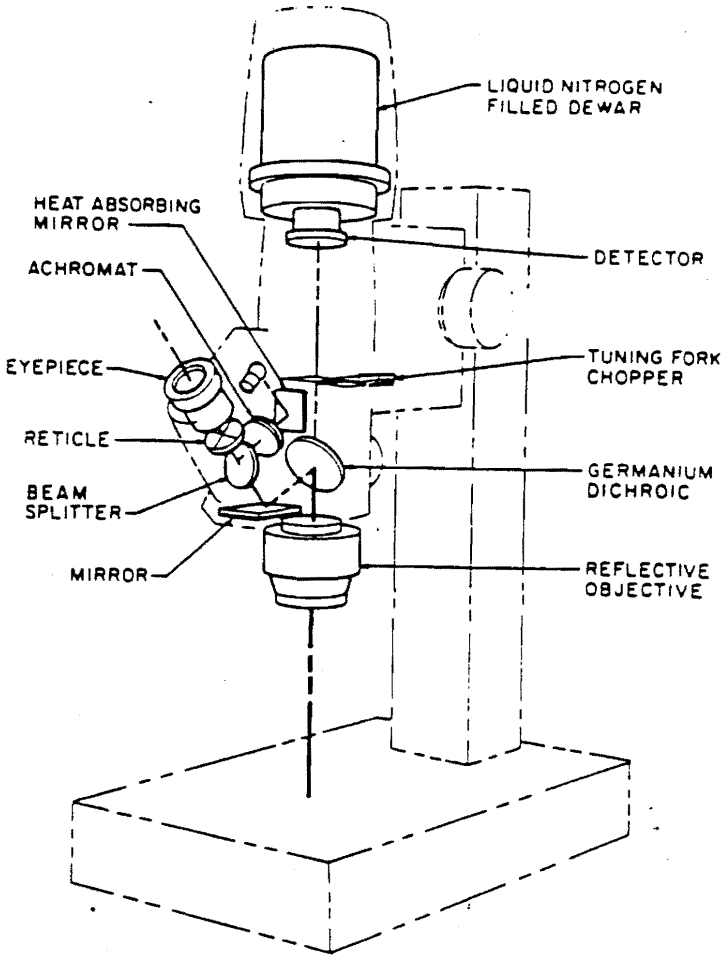

Fig. 17. Schematic 3-dimensional view of the Barnes RM-2A Infrared Microscope [98].

infrared radiation and a reference radiation from the tuning fork blades to impinge on the detector. Thus it converts the DC radiance signal to an AC signal used for fast thermal transients. A third mode of signal output called the AC/DC channel bypasses the final stage of DC filter and gives higher voltage output, still keeping some of the transient response. DC and AC/DC outputs were used in this study. Further details on the operational theory of the microscope can be found in references [4 - 13]. A Barnes RM 121-1 Black-body calibration source is used in accordance with the procedure in Appendix A to calibrate the microscope.

3.1.3 Velocity Measurement

The velocity data in the oscillating set-up is obtained with the help of an accelerometer. The accelerometer is mounted on the platform in the direction of oscillation. Figure 13a shows the position of the accelerometer. It measures the acceleration of the platform directly, and hence that of the sapphire disk. The acceleration signal is integrated to obtain velocity. In these experiments, sine wave oscillation is used. The velocity therefore is in the form of a sine wave, but 90° out of phase with the acceleration. The displacement is also obtained by integrating the velocity signal.

Velocity in the sliding set-up is obtained by measuring the speed of rotation and the distance between the center of rotation and the contact region. A magnetic speed sensor is used to measure the speed of rotation. The magnetic speed sensor records a

spike for each revolution of the disk, and by counting the number of spikes over a certain time period, the rotational speed is obtained. Figure 18 shows the position of the magnetic speed sensor.

3.1.4 Friction Measurement

Two different friction measuring devices are used for the two contact systems. In the oscillating set-up, an octagonal strain ring designed by Weick [13] is used. It consists of eight strain gages mounted on an octagonal ring at positions of maximum strain, four each for the tangential and normal loads, and arranged on separate Wheatstone bridge circuits. The tangential friction force induces strain on the octagonal ring, the magnitude of which is proportional to that of the friction force. The strain is converted to electrical signal by the strain gages. A view of the strain ring is shown in Fig. 13a. Friction force is then derived from the strain ring signal using the calibration curve. The calibration method and the curves can be found in Appendix B. The normal channel also works in the same way.

The friction force measurement in the sliding set up is done using a Lebow model 1102-50 rotary torque transducer as shown in Fig. 18. It consists of temperature-compensated strain gages mounted at 45° to the axis on a square shaft. The signal from the gages is fed through silver-graphite slip rings to an output jack. This transducer measures the frictional torque. Friction force is obtained from the torque by dividing the torque by the distance between the center of rotation and the position of the apparent

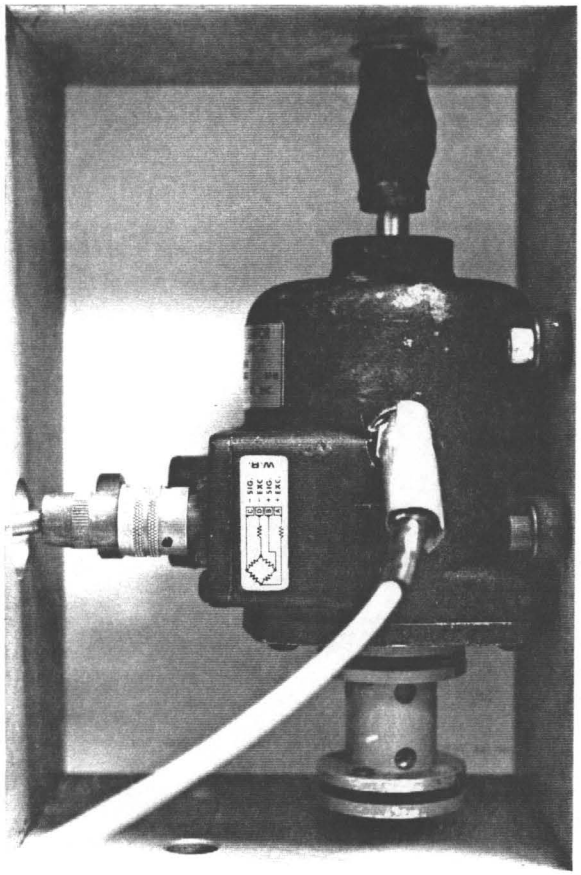

Fig. 18. View of the torque transducer and speed sensor used in unidirectional sliding experiments.

contact area. Knowing the normal load, the coefficient of friction is calculated from the friction force. This transducer has a torque sensing capacity of 0.706 N-cm (1.0 in.-oz) to 35.3 N-cm (50.0 in.-oz) and a speed range of up to 20,000 rpm.

For situations in which the normal load varies, the variation naturally needs to be taken into account for computation of coefficient of friction. Of the two types of experiments conducted in this study -- unidirectional sliding and oscillating, the variation in the normal load was significant in the unidirectional sliding experiments. This will be discussed later. The method used to compute the coefficient of friction, taking this load variation into account, is described in Appendix E.

3.1.5 Surface Damage and Wear Measurement

In this study, wear was measured in terms of volume loss. As the specimen ends are spherical, the wear scars are typically circular. The scars are viewed through a Leitz-Wild photomacroscope and the diameters are measured after projecting the pictures on to a calibrated television screen using a video camera. The wear volumes are then computed from the diameters of the wear scars.

Surface damage is also studied using the photomacroscope and scanning electron microscope (SEM). Figure 19 shows a view of the photomacroscope.

3.1.6 Estimation of Contact Area

Temperature rise and distribution at the interface and the subsurface is

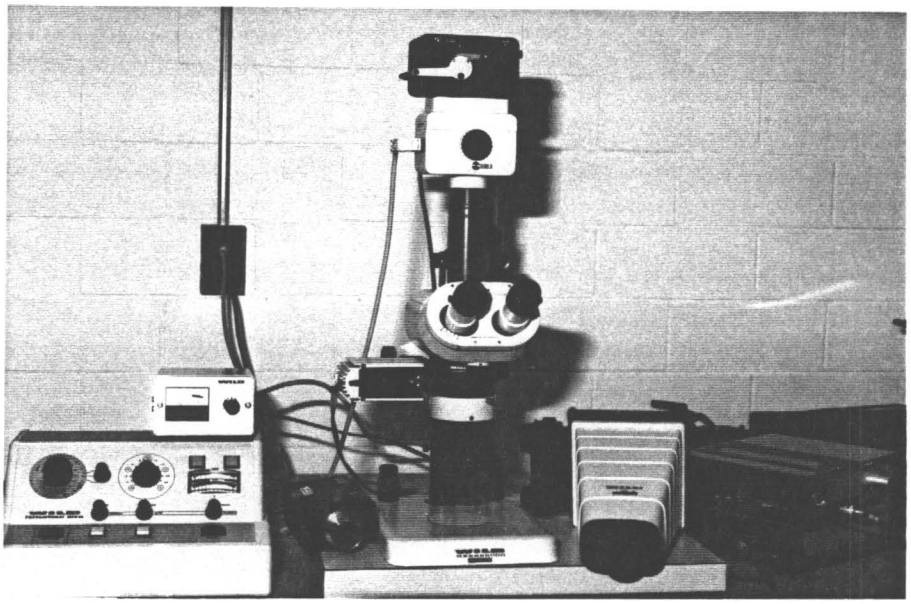

Fig. 19. View of Leitz-Wild Photomacroscope.

significantly controlled by the real area of contact. Attempts at estimating the size, shape and distribution of the real area of contact are made using photomacro/video techniques. One of the methods involves the estimation of the size and distribution of peaks and valleys on the contact region from photomacrographs and Scanning Electron Micrographs (SEM), at the end of an experiment.

Another technique used involves mounting the photomacroscope on the experimental set-up and looking directly at the contact region through the sapphire disk during the experiment. A view of the mounted photomacroscope on the experimental set-up is shown in Fig. 20. Due to different optical properties (light absorptivity, to be more specific) of the composite specimen and air, the regions of contact within the apparent contact area at the interface, are seen as darker patches compared to regions of no-contact. Photographs and video pictures of the apparent contact area, both when unloaded and loaded are taken. The central illumination of the photomacroscope is used. A set of such pictures, to illustrate this idea, is shown in Fig. 21. Figure 21 a) shows the total wear scar, viewed through the sapphire disk but not in contact with the disk. The scar appears bright as the scar surface is fairly smooth after sliding. The same scar in contact with the sapphire disk is shown in Fig. 21 b). Certain dark patches within the wear scar are seen in Fig. 21 b), which correspond to the real area of contact. The real area of contact can thus be distinguished from the macroscopic contact area (the total wear scar).

Attempts were also made at video recording the changes in contact area during the experiment. However, the pictures did not come out very clear. The vibration of

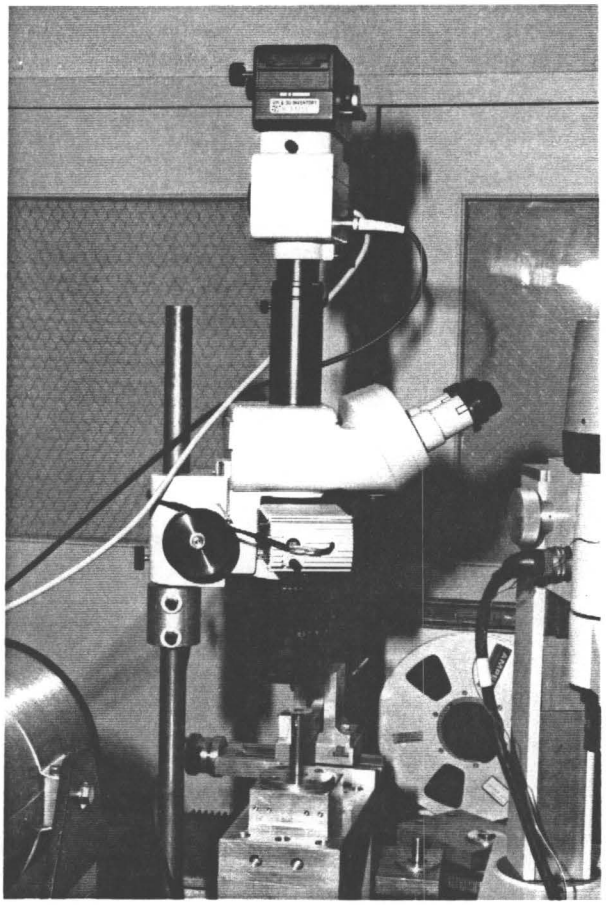

Fig. 20. View of the mounted photomacroscope on the experimental set-up.

a)

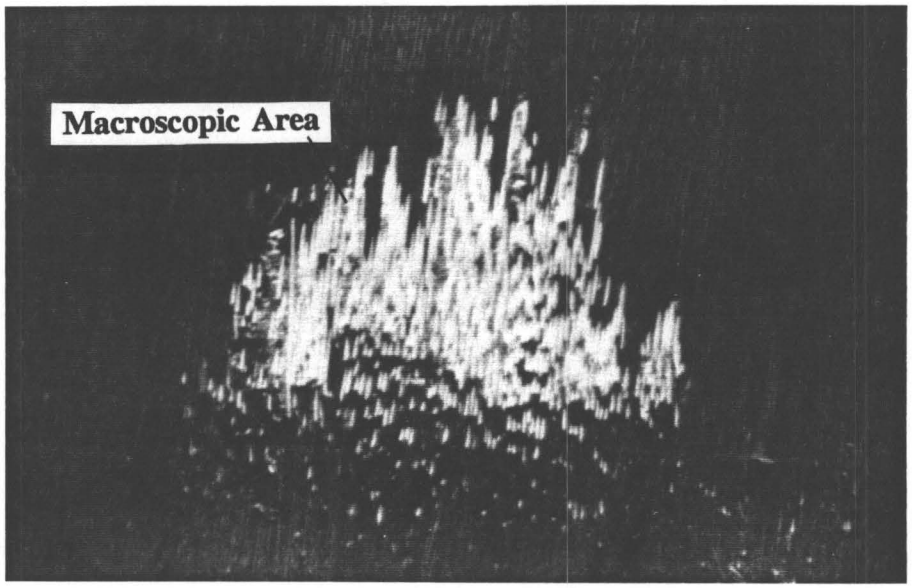

b)

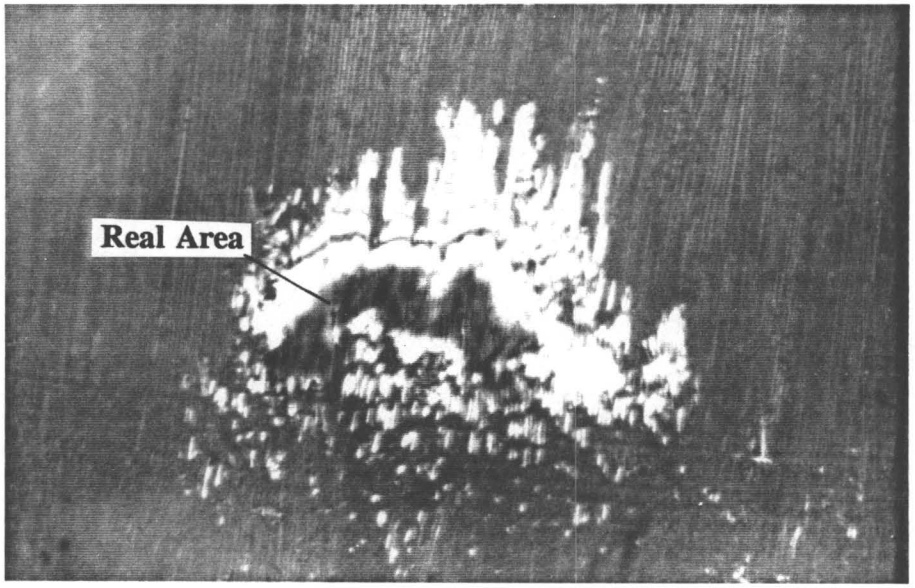

Fig. 21. Photomacrographs showing macroscopic and the real areas of contact. a) View of the macroscopic contact area (wear scar on the composite) when not in contact with sapphire. b) View of the same area when in contact with sapphire. The dark patches within the scar (in b)) represent the real area of contact.

the camera, due to the vibration transmitted from the motor/shaker, made the pictures fuzzy. Therefore, estimations were done only under static conditions. Sliding was stopped at different times during the experiment and static photographs were taken, both under loaded and unloaded conditions. When unloaded, the complete wear scar is seen and is used as a reference and for the computation of wear volume.

This technique is limited by the optical properties of the specimens and the resolution of the microscope. In these experiments, the maximum available magnification of the microscope, 80X, was used. However, it is possible that this might have failed to identify any finer distribution of the real area of contact. It is therefore possible that the real areas of contact could be smaller and more distributed than that measured here. Nevertheless, this technique gives a much better estimation than the apparent or macroscopic contact area.

3.1.7 Emissivity Measurement

Emissivity of the radiating surface is a necessary parameter to convert the radiance data measured by the infrared microscope into temperatures. To measure the emissivity, a small region of the specimen is painted with a thin black paint, having a known emissivity of 0.90 - 0.95 and placed inside an enclosed heater with a small opening at the top. The radiance level (in volts) of the unpainted region very close to the painted region is compared with that of the painted region. The ratio of the two radiances gives the emissivity. A view of the heater used for emissivity measurement

is shown in Fig. 22. Emissivity is measured over a wide range of temperatures (e.g., 20° - 110°C). In case of unidirectional composites, because of the anisotropy, emissivity is expected to be different for different fiber orientations. Therefore, measurements were carried out for all fiber orientations examined.

3.1.8 Glass Transition Temperature Measurement

Glass transition temperatures of the polymer composites were measured using Differential Scanning Calorimetry (DSC). This technique plots the change in specific heat with temperature. From the plot, the glass transition temperature is derived.

In any polymer, a change in specific heat may occur at three transformation temperatures, namely (a) the glass transition temperature, where the glassy solid transforms into a rubbery solid, (b) the crystallization temperature, and (c) the melting point. A 100% amorphous polymer would not show any crystallization temperature, whereas a 100% crystalline polymer would show no glass transition temperature. However, since most polymers are semi-crystalline, with both amorphous and crystalline phases being present, all three temperatures are expected to be seen.

The technique involves constantly increasing the temperature of a sample at a steady rate. The heat absorbed or given out is plotted by the calorimeter against temperature. The first transition, which shows up as an upward shift of the base line, is the glass transition temperature.

Although the term "glass transition temperature" may suggest a discrete

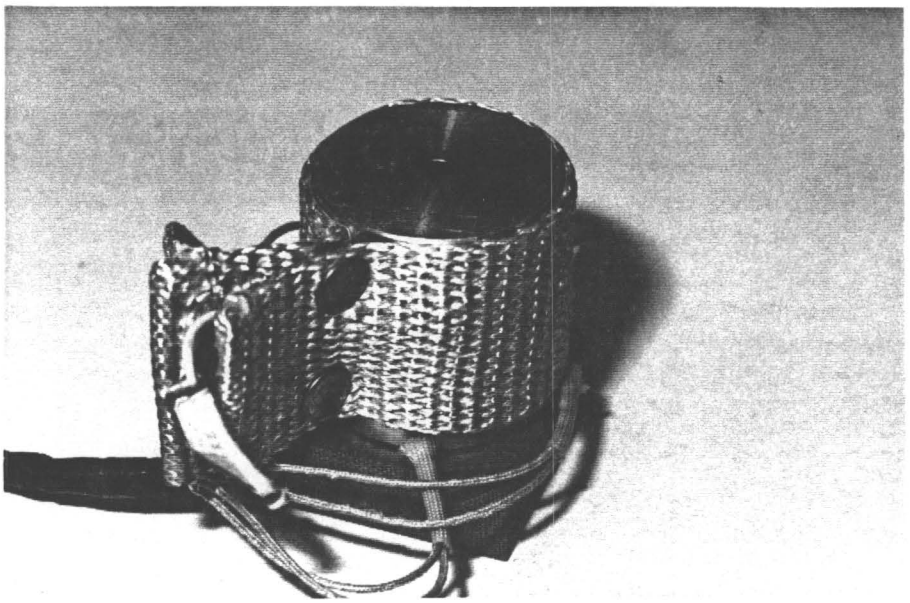

Fig. 22. View of the heater for emissivity measurement.

temperature value, it actually occurs over a range of temperature. Typically, the range may be 10-20°C. Some report the onset of transition as the glass transition temperature, whereas others report the mid-point of the range. In this study, the mid-point of the transition range is reported as the glass transition temperature.

A Perkin-Elmer DSC-II Differential Scanning Calorimeter was used in this study. Because of the presence of high percentage of fibers, a relatively large mass of sample (20 mg) was used for the tests to obtain a good signal-to-noise ratio.

3.1.9 Data Recording and Analysis

The output signals from the infrared microscope, LVDTs, torque transducer or strain ring, magnetic speed sensor, and accelerometer are stored in a FM tape using a Honeywell model 5600E portable tape recorder/reproducer. Seven of the eight available channels were used for data recording. Figure 23 shows a view of the FM tape recorder.

The signals are analyzed using a Data Translation 2801 data acquisition board connected to an IBM personal computer. The data are sampled with the help of a computer program written by Sankar [11] and later modified by Weick [13]. A sampling rate of 8000 Hz was used. The program also allows for sampling of several channels simultaneously. The sampled data in ASCII format is then written to a floppy disk.

The outputs thus obtained, in terms of volts, are then processed using the calibration curves to get real values for frictional torque, microscope position, radiance, and acceleration. Some data were further analyzed using a Global Lab software package

Fig. 23. View of the FM tape recorder/reproducer along with other instrumentation used.

to obtain the frequency content of the signals.

3.2 PREPARATION OF TEST SPECIMENS

Two different materials were tested in this study: graphite-epoxy and carbon-PEEK (polyetheretherketone). The material composition and properties are listed in Table 3. The test specimens were prepared from unidirectional fiber reinforced laminates. Graphite-epoxy specimens were prepared from 1/4 in. thick plates. Cylinders of 3/8 in. length and 1/4 in. diameter were machined out of the laminates on a lathe. One end was cut to a hemispherical shape of 1/4 in. diameter, using a form tool. The surface was polished with 600 grade emery paper while closely maintaining the specified geometry.

Carbon-PEEK samples, on the other hand, were made out of 1/8 in. thick plates due to unavailability of 1/4 in. thick plates. They were cut into square rods of 3/8 in. long and 1/8 in. each side. One end was machined to a hemispherical surface of 1/4 in. diameter, in the same way as the graphite-epoxy. A special holder attachment was made to hold these specimens.

The composite samples were tested in three fiber orientations -- normal, parallel and anti-parallel. These orientations are already shown in Fig. 1. These orientations are defined only for unidirectional composites. In normal orientation, the fibers are perpendicular to the sliding surface. In parallel orientation, the fibers are oriented along

Table 3. Properties of the materials examined.

PROPERTIES	MATERIALS				
	SAPPHIRE††	GRAPHITE-EPOXY †		CARBON-PEEK ‡	
		LONGITUDINAL	TRANSVERSE	LONGITUDINAL	TRANSVERSE
Modulus of Elasticity (N/m^2)	3.65 E 11	2.06 E 11	5.15 E 10	_	_
Hardness (N/m^2)	1.77 E 10	2.06 E 09	3.50 E 08	_	_
Poisson's Ratio	.20	.25	.00625	_	_
Density (kg/m^3)	3.98 E 03	1.56 E 03	1.56 E 03	_	_
Thermal Conductivity (J/s.m.C)	41.8	5.012	.1122	6.03	.624
Specific Heat (J/kg.C)	420.0	1342.0	1342.0	1482.0	1482.0

† : Composition of graphite-epoxy -- 62% volume fraction of AS4 fibers.
Property data collected from reference [104,105].

‡ : Composition of carbon-PEEK -- 60% volume fraction of AS4 fibers and APC-2 matrix.
Property data supplied by ICI America. Only the thermal property data were available.

†† : Data supplied by General Ruby and Sapphire Corporation.

NOTES : ◦ LONGITUDINAL direction corresponds to NORMAL orientation.
◦ TRANSVERSE direction corresponds to PARALLEL / ANTI-PARALLEL orientation.

the plane of the sliding surface and parallel to the direction of sliding. In anti-parallel orientation, the fibers are also oriented along the plane of the sliding surface, but perpendicular to the direction of sliding.

Before each experiment, the specimens are cleaned in a methanol bath in an ultrasonic vibrator for about 20 minutes to remove any loose particles and inorganic deposits. That is followed by cleaning in a hexane bath in the vibrator for another 20 minutes to remove organic deposits. All the specimens are air dried.

The sapphire disks are cleaned with hydrochloric acid (HCl) followed by methanol and hexane in separate baths in the vibrator for 5 minutes each. They are thoroughly rinsed with distilled water and allowed to air dry. Often the same disk is used for more than one experiment. Cleaning with HCl of such disks is done carefully using cotton swabs, such that the acid does not touch and react with the epoxy cement used to bond the disk to the pin.

Specimens examined under SEM had to be specially gold coated with a film of approximately 14 nm thickness using a sputter coater.

3.3 EXPERIMENTAL PROCEDURE

The experimental procedure used to obtain surface temperatures is quite complex. A systematic procedure was therefore developed to minimize experimental error as much as possible. The following section outlines the procedure.

Before performing any experiment, all the instruments are calibrated. The calibration procedures are described in Appendices A - D. The infrared microscope is calibrated at three different "range" settings, i.e., the X1, X10 and X100 settings. The torque transducer, strain ring, and LVDTs are also calibrated prior to the experiments.

After the specimen and the sapphire disk are thoroughly cleaned, they are properly mounted in their respective holders. The specimen is positioned at the proper radius for the correct sliding velocity. All the instrumentation is turned on and allowed about 30 minutes to stabilize. The room temperature, measured by the thermistor, is kept at the same value for all the experiments (21°C (70°F)). The Dewar of the microscope is then filled with liquid nitrogen, and some time is allowed for the temperature inside the microscope to stabilize. The microscope is then turned on.

For the oscillating experiments, the frequency of the wave generator is set at the desired value. The accelerometer reading to give the desired amplitude is computed prior to the start of the experiment. The strain ring output is zeroed using the potentiometers connected to the strain ring. For the sliding experiments the rotational speed of the disk is checked using a Strobotac stroboscope.

Load is then applied by unscrewing the load support screw. Looking through the optical channel of the microscope, the contact area is located and the microscope is focussed on the center of the contact area. The internal light source of the microscope was found to be very useful in this task. The LVDTs are then zeroed using the threaded rods. All this is done prior to each experiment.

The FM tape recorder is switched on to record the ambient radiance for about 10

seconds, prior to switching on the motor in unidirectional sliding experiments, or increasing the amplitude in oscillating experiments. All the sliding experiments were run for the same sliding distance. Therefore, the duration of each experiment was different depending on the velocity. Outputs from all the channels are recorded on FM tapes and analyzed later.

Surfaces of all the specimens are examined under the photomacroscope after each experiment. The diameter of the wear scar is measured and the wear volume is computed. Some of the specimens are examined under SEM. Emissivity values of the unworn and worn surfaces of the specimens are also measured.

After completion of each experiment, the data recorded in the FM tapes are replayed back and analyzed using a IBM personal computer. The surface temperatures are calculated using computer programs given elsewhere (reference [13]).

Three experiments, one for each of the three fiber orientations of graphite-epoxy were also conducted to estimate the contact area change during an experiment. For this, the photomacroscope was mounted on the infrared set-up. The experiments were stopped at different time intervals (1-2 min) and the wear scars were photographed, both when loaded and unloaded. The actual contacts could be seen as only a part of the total wear scar.

The test conditions are listed in Table 4. One repeat experiment (two in a few cases) was done under each test condition.

Table 4. Test Conditions.

	UNIDIRECTIONAL SLIDING	OSCILLATING
Load (N)	4	40
Sliding Velocity (m/s)	2.17 (1800 RPM at 11.5 mm Radius)	.066 (220 μm p-p Amplitude at 150 Hz Frequency)
	3.5 (2900 RPM at 11.5 mm Radius)	.128 (320 μm p-p Amplitude at 200 Hz Frequency)
	7.0 (5800 RPM at 11.5 mm Radius)	
Sliding Distance (m)	520	28
Ambient Temperature (°C)	21	21

CHAPTER 4

RESULTS

It has been mentioned earlier that the measurement of friction, surface temperature, wear, and observation of surface damage of unidirectional fiber-reinforced graphite-epoxy and carbon-PEEK composites sliding on sapphire are the main objectives of this study. Besides, for conversion of radiance data into temperatures, emissivities of the materials needed to be determined. All these measured results are presented in this chapter. Emissivity results are presented in section 4.1. Results of the sliding experiments of graphite-epoxy are presented in section 4.2. It may be mentioned here that more extensive studies have been carried out with graphite-epoxy compared to carbon-PEEK. This includes experiments in oscillatory motion and estimation of contact area. Hence the results section on graphite-epoxy has three sub-sections -- unidirectional sliding motion, oscillating motion, and contact area estimation. Since only unidirectional sliding experiments have been done with carbon-PEEK, those results are presented in section 4.3.

In this chapter, a general format has been adopted for the presentation of the results. Friction, surface temperature, and wear results from all the three fiber

orientations are presented collectively; the purpose is to get some insight into the differences in the tribological behavior of various fiber orientations. For each material and sliding type, friction, radiance and temperature, as well as wear and surface damage results, are presented in separate sections. In friction and temperature sections, typical changes over the length of the experiment, as well as cycle-to-cycle fluctuations, are shown. Typical scanning results showing the variation of temperature over the contact region are also presented. Along with wear results, photomacrographs and scanning electron micrographs of some of the wear scars are also presented.

Results of some of the oscillating experiments have been analyzed using Fourier analysis techniques to estimate the frequency contents in the friction and temperature signals. These results are presented in the corresponding sections.

4.1 EMISSIVITY MEASUREMENTS

The technique used to measure emissivity has been explained in section 3.1.7. The results are presented here. Table F1 in Appendix F lists the values of emissivity of graphite-epoxy in both normal and parallel/anti-parallel orientations. Figure 24 shows this variation as a function of temperature. Similar results for carbon-PEEK are shown in Table F2 of Appendix F and Fig. 25. The general trend shows an increase in emissivity when the temperature is increased from room temperature to about 50°C. Beyond 50°C it is seen to remain unchanged. Also, very little difference in the emissivity values of the worn and unworn surfaces of both the materials was detected.

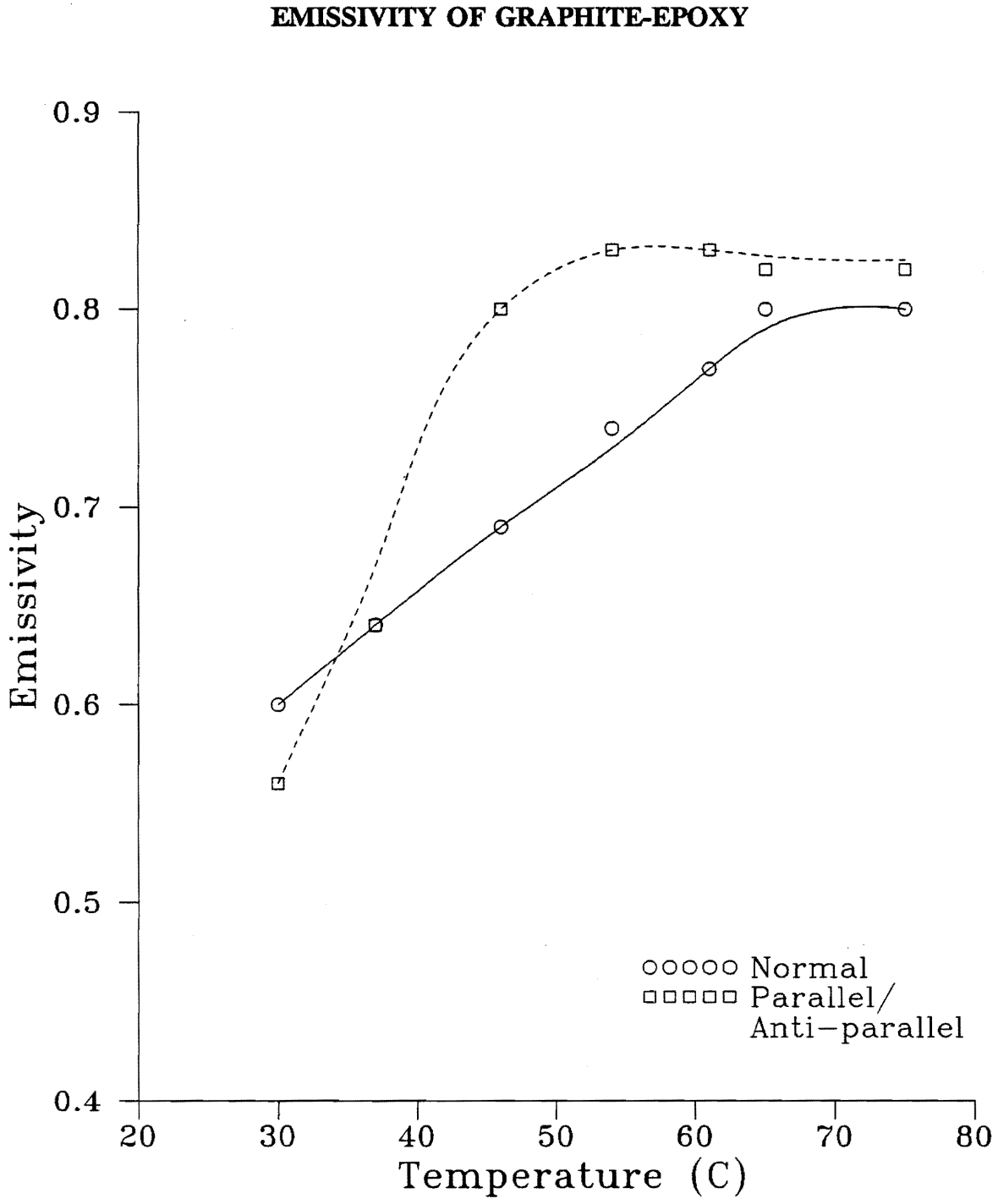

Fig. 24. Emissivity of the worn surface of graphite-epoxy in the normal and parallel/anti-parallel orientations as a function of temperature.

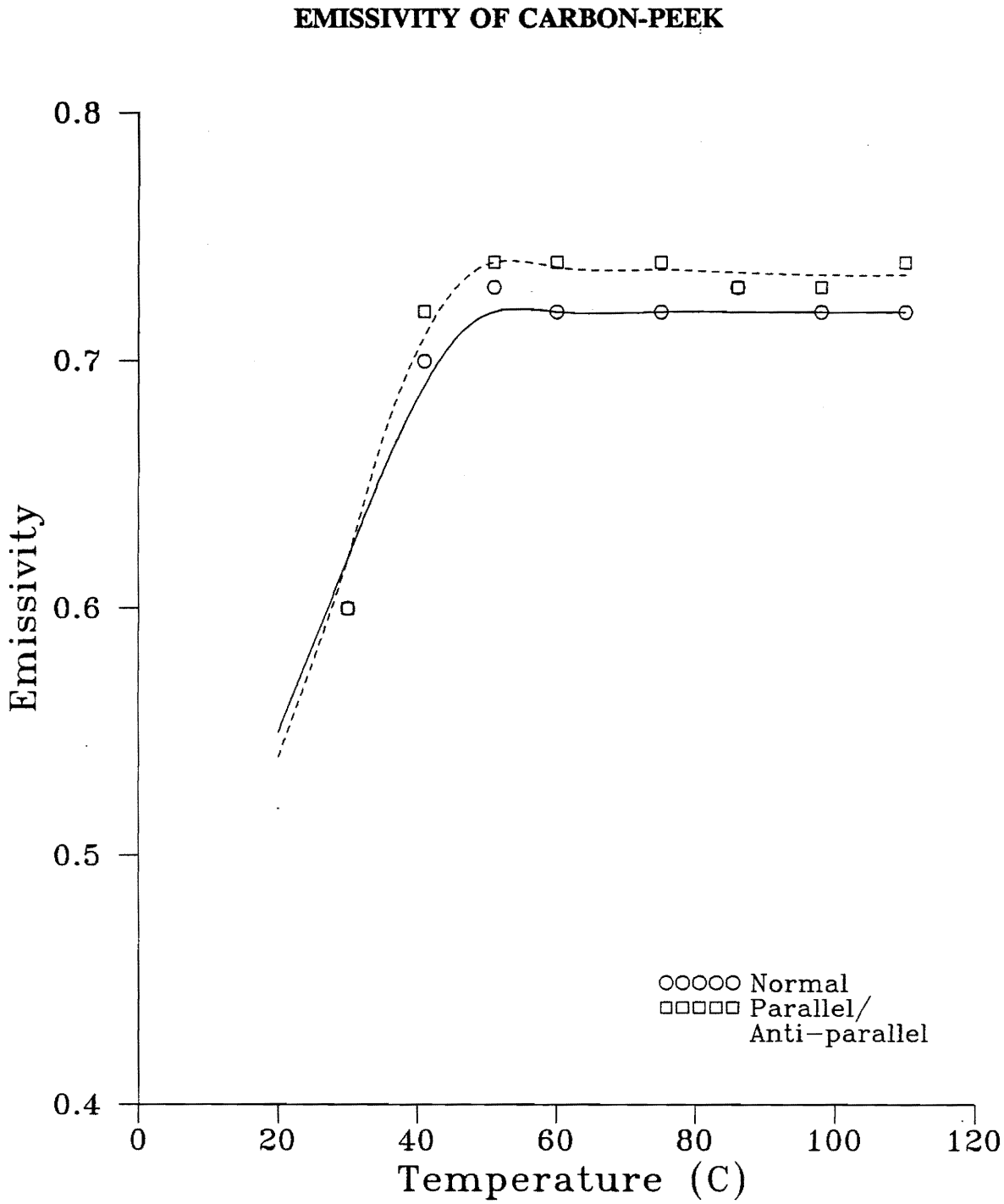

Fig. 25. Emissivity of the worn surface of carbon-PEEK in the normal and parallel/anti-parallel orientations as a function of temperature.

4.2 GRAPHITE-EPOXY RESULTS

A typical friction trace and the corresponding radiance traces of a unidirectional sliding experiment of graphite-epoxy are shown in Fig. 26. The frictional torque signal has been filtered with a 10 Hz. filter to show the mean friction level. Along with the unfiltered radiance, a filtered radiance signal (filtered with a 10 Hz. filter) representing the DC level is also shown. These figures are referred to later on in this section.

4.2.1 Graphite-Epoxy : Unidirectional Sliding Motion

4.2.1.1 Friction results

The typical frictional torque signal shown in Fig. 26, represents the frictional force as well, since the distance between the axis of rotation and the contact area was the same at all times. In all the experiments, friction force increases from zero almost instantaneously with the start of sliding and stays fairly constant for the whole duration of the experiment. In some cases, particularly for the normal and anti-parallel orientations, friction force is seen to increase gradually for the first 100 - 200 m of sliding before steadying out.

The friction signal over a very short time is shown in Fig. 27. It shows the variation in friction force with time on a cycle-to-cycle scale. This variation is primarily due to the fluctuation in normal load. It has been mentioned before that the wobble of the sapphire disk is responsible for this fluctuation in normal load. Due to the wobble, the load arm along with the dead weight vibrates at a frequency equal to the frequency

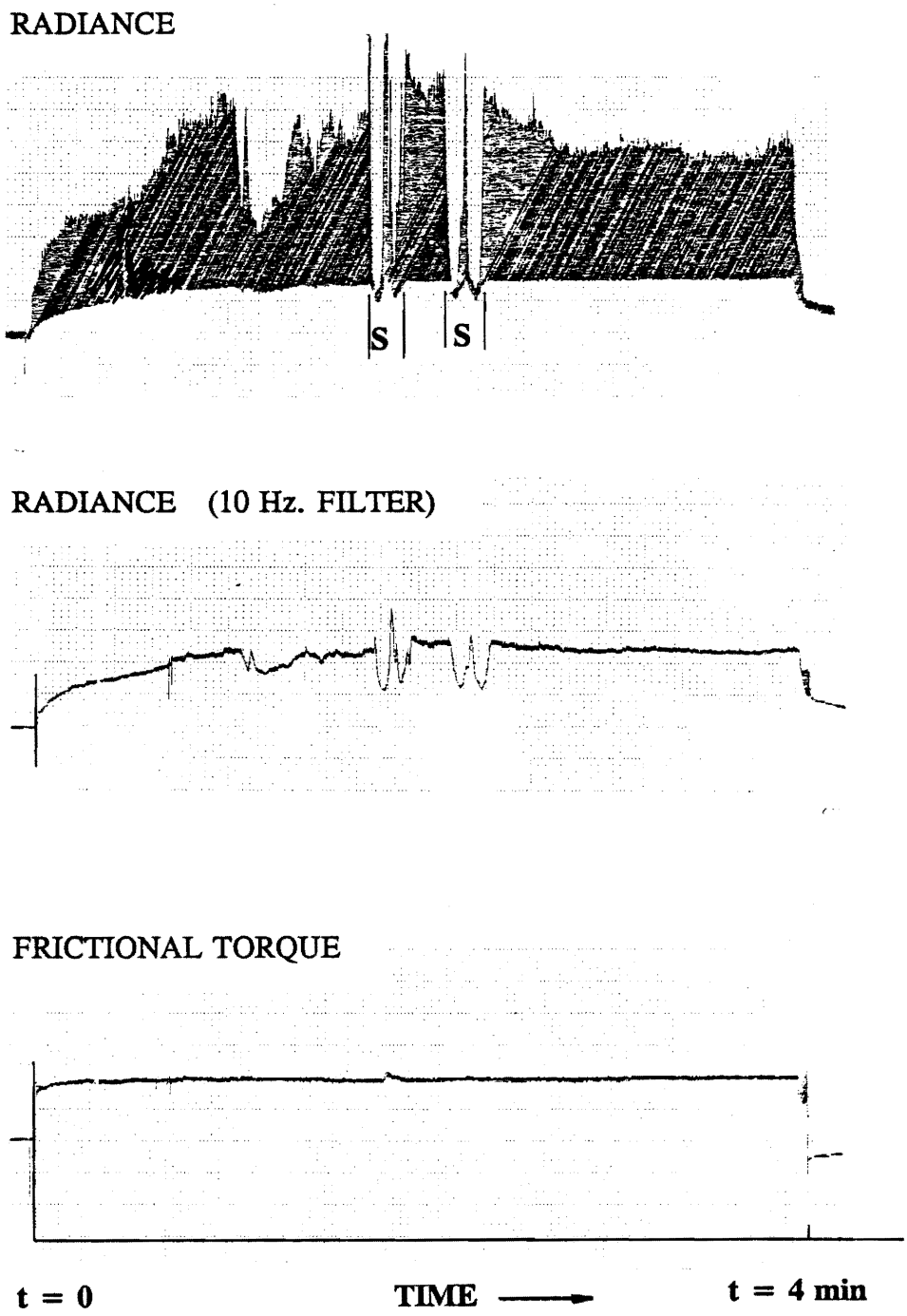

Fig. 26. Radiance and frictional torque traces of a typical unidirectional sliding experiment.

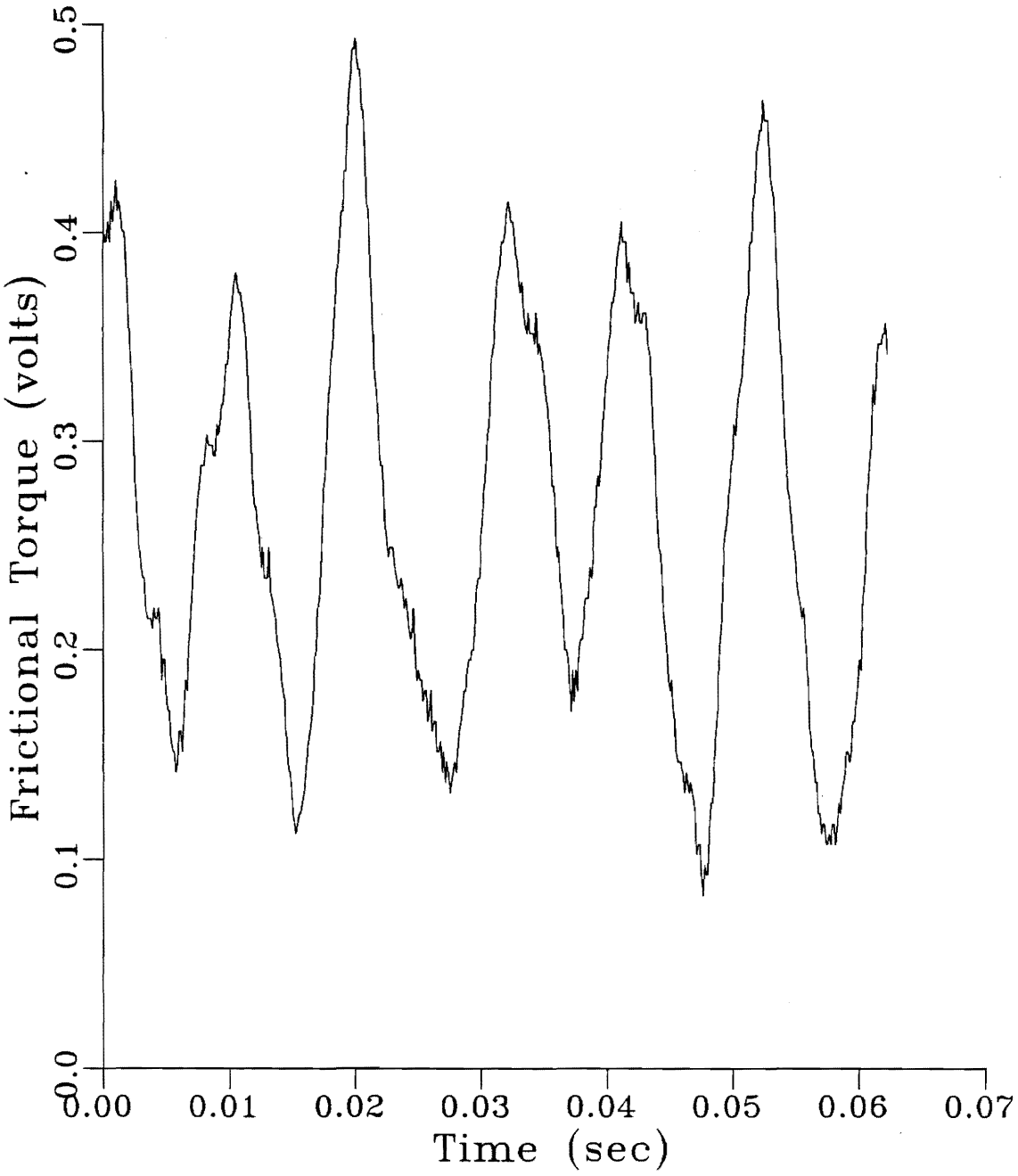

Fig. 27. Cycle-to-cycle variation of frictional torque in graphite-epoxy (normal).

of rotation of the disk, with the peak-to-peak amplitude being almost equal to the magnitude of the wobble. This is revealed in the Fast Fourier Transform (FFT) of the friction and loading arm vibration signals. FFT plots of the friction force and the arm vibration signals are shown in Figs. 28 and 29, respectively. It can be observed that peaks in both the signals exist at the frequency corresponding to the rotational frequency of the disk.

The difference in friction coefficients among the three fiber orientations as a function of velocity is shown in Fig. 30. The actual values are listed in Table 5. The coefficient of friction in the normal and parallel orientations is seen to decrease with an increase in velocity within the velocity range tested. In the anti-parallel orientation, friction increases initially and then starts to decrease. There is a marked difference in the coefficient of friction among the three fiber orientations at lower velocities, with the normal orientation showing the highest and the anti-parallel orientation showing lowest values. At higher velocities, the coefficient of friction is found to be highest in the anti-parallel orientation and lowest in the normal orientation. The difference is found to be less at higher velocities.

Results from the analysis of variance (ANOVA) show a significant effect of velocity on coefficient of friction. A significant effect of fiber orientation can also be observed through the interaction term. The ANOVA table is given in Appendix G.

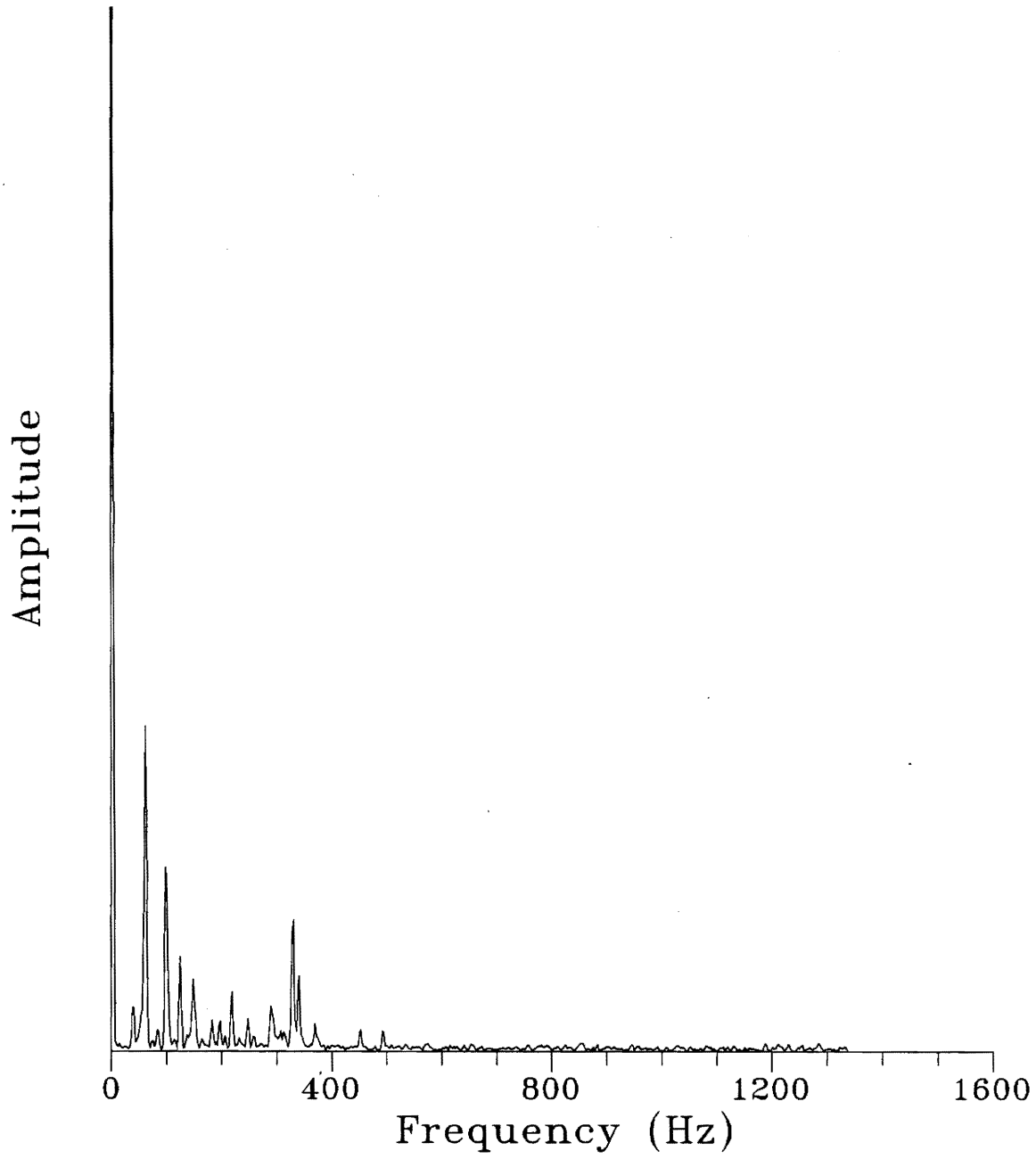

Fig. 28. Fast Fourier Transform (FFT) of friction signal.
Experiment was run at 5900 rpm (rotational frequency = 98.3 Hz.)

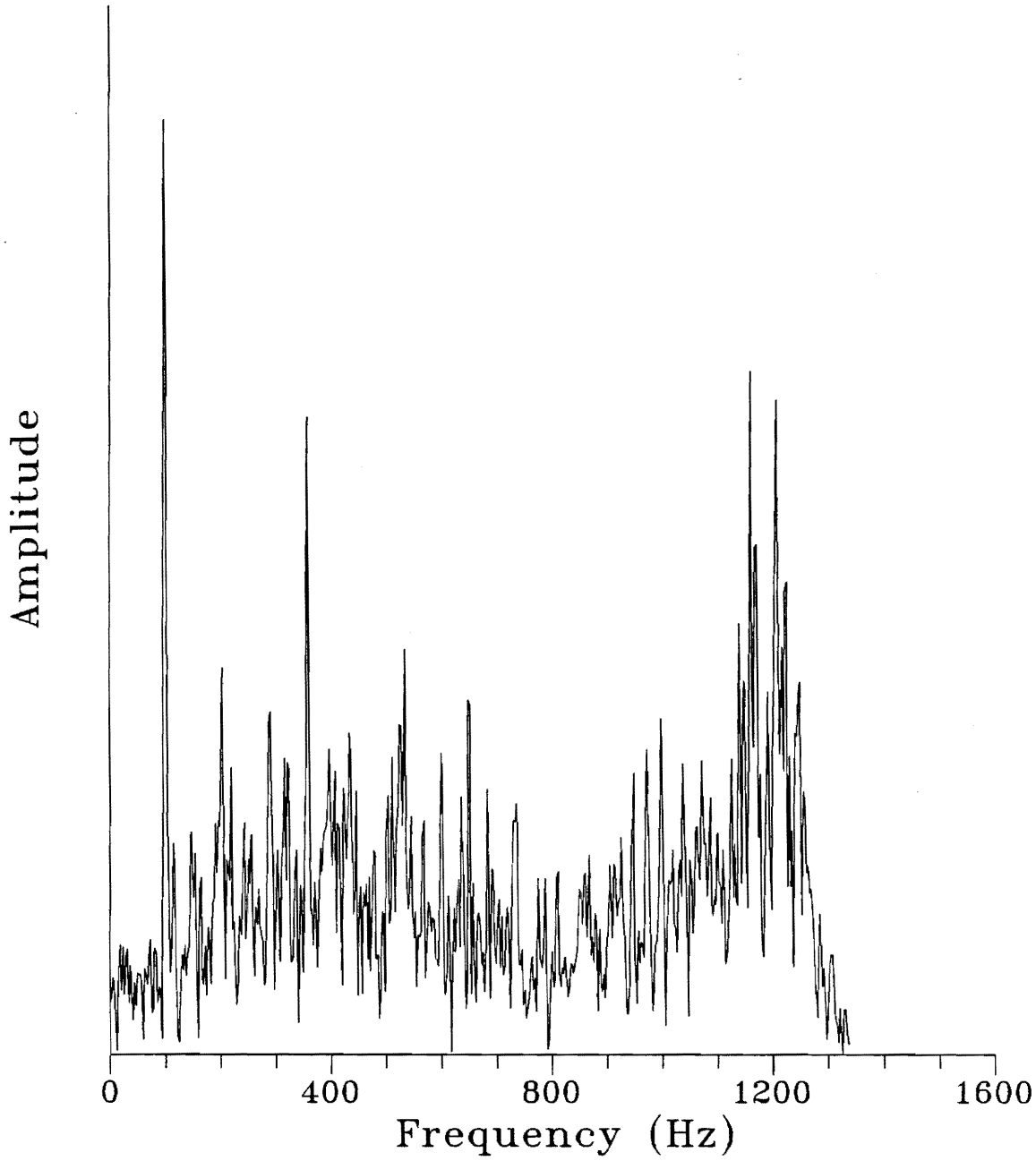

Fig. 29. FFT of loading arm vibration signal.
Experiment was at 5900 rpm (rotational frequency = 98.3 Hz.)

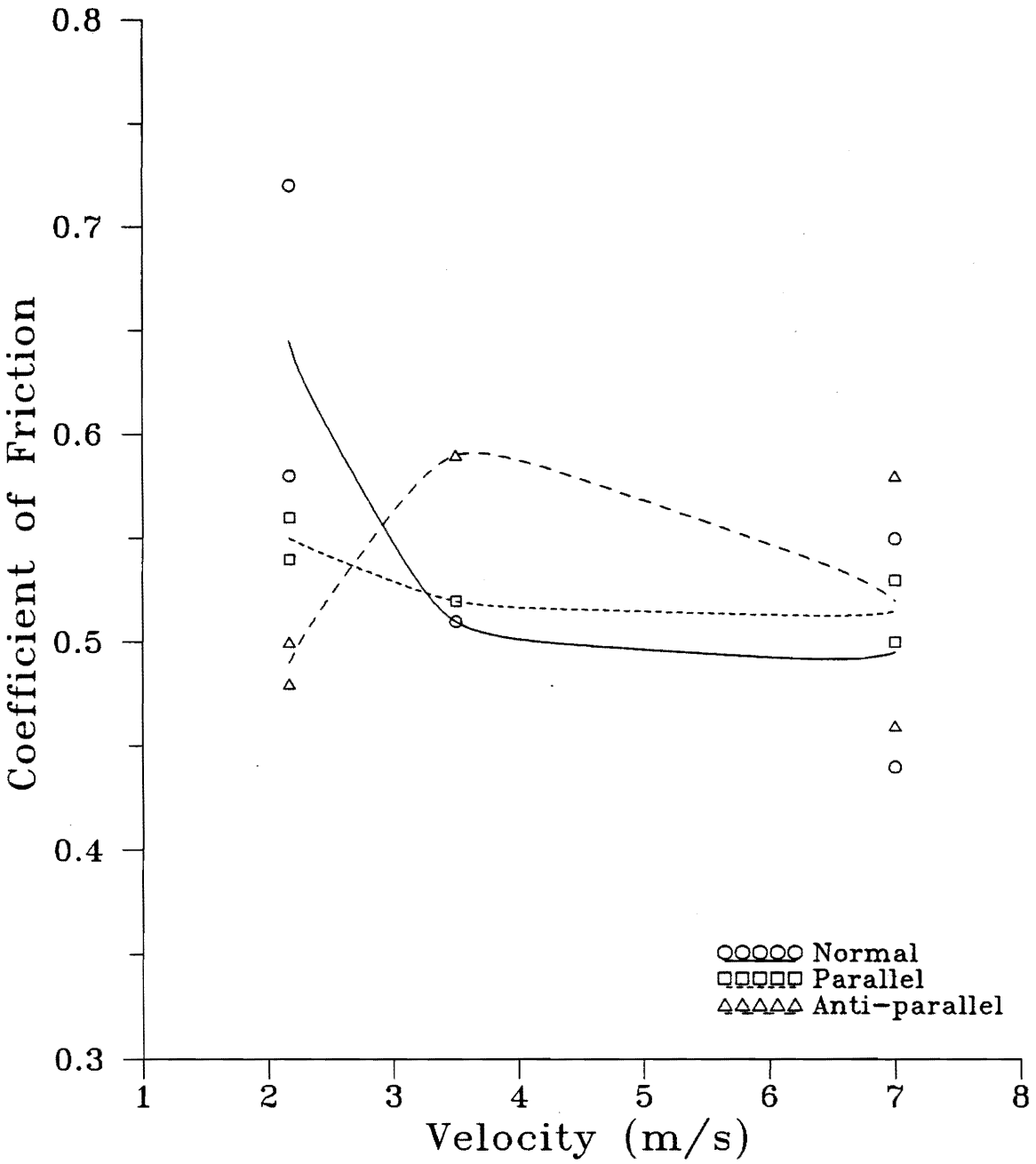

Fig. 30. Coefficient of friction of graphite-epoxy as a function of velocity.

Table 5. Test results of coefficient of friction of graphite-epoxy.

VELOCITY	FIBER ORIENTATION					
	NORMAL		PARALLEL		ANTI-PARALLEL	
	Exp. 1	Exp. 2	Exp. 1	Exp. 2	Exp. 1	Exp. 2
2.17 m/s	.72	.58	.56	.54	.50	.48
3.5 m/s	.51	.51	.52	.52	.59	.59
7.0 m/s	.44	.55	.50	.53	.46	.58

4.2.1.2 Radiance and Temperature Results

A radiance trace of graphite-epoxy has also been shown in Fig. 26. Typically, the radiance increases from the ambient radiance to a maximum value in about 50 to 100 m of sliding, after which it remains fairly constant. In certain cases, radiance is seen to increase continuously during the experiment.

The scanning results can also be observed on this radiance trace. The scanning regions are marked as 'S'. It can be seen that radiance decreases drastically as one moves out of the contact region. This tells us that, as expected, the temperature at the contact region is much higher than the adjacent "no-contact" region. In addition, the temperature may not be uniform all through the contact area. Figures 31 and 32 show the temperature distribution on the contact area along two scan directions. It can be observed that the maximum temperature rise does not necessarily occur at the geometric center of the contact area. It is seen to be more skewed towards the trailing edge. Further, more than one peak in radiance can also be observed over the contact region suggesting that more than one discrete real area of contact may be present within the macroscopic contact region.

Figure 33 shows the variation in radiance over a very short time period. It can be observed that the radiance fluctuates between a maximum and a minimum value corresponding to two different temperature levels. Therefore, two different temperature values are presented -- the maximum temperature rise and the mean temperature rise. These radiance levels are shown in Fig. 33. It can also be seen that radiance fluctuates at a frequency equal to the rotational frequency of the disk (98.3 Hz). A Fast Fourier

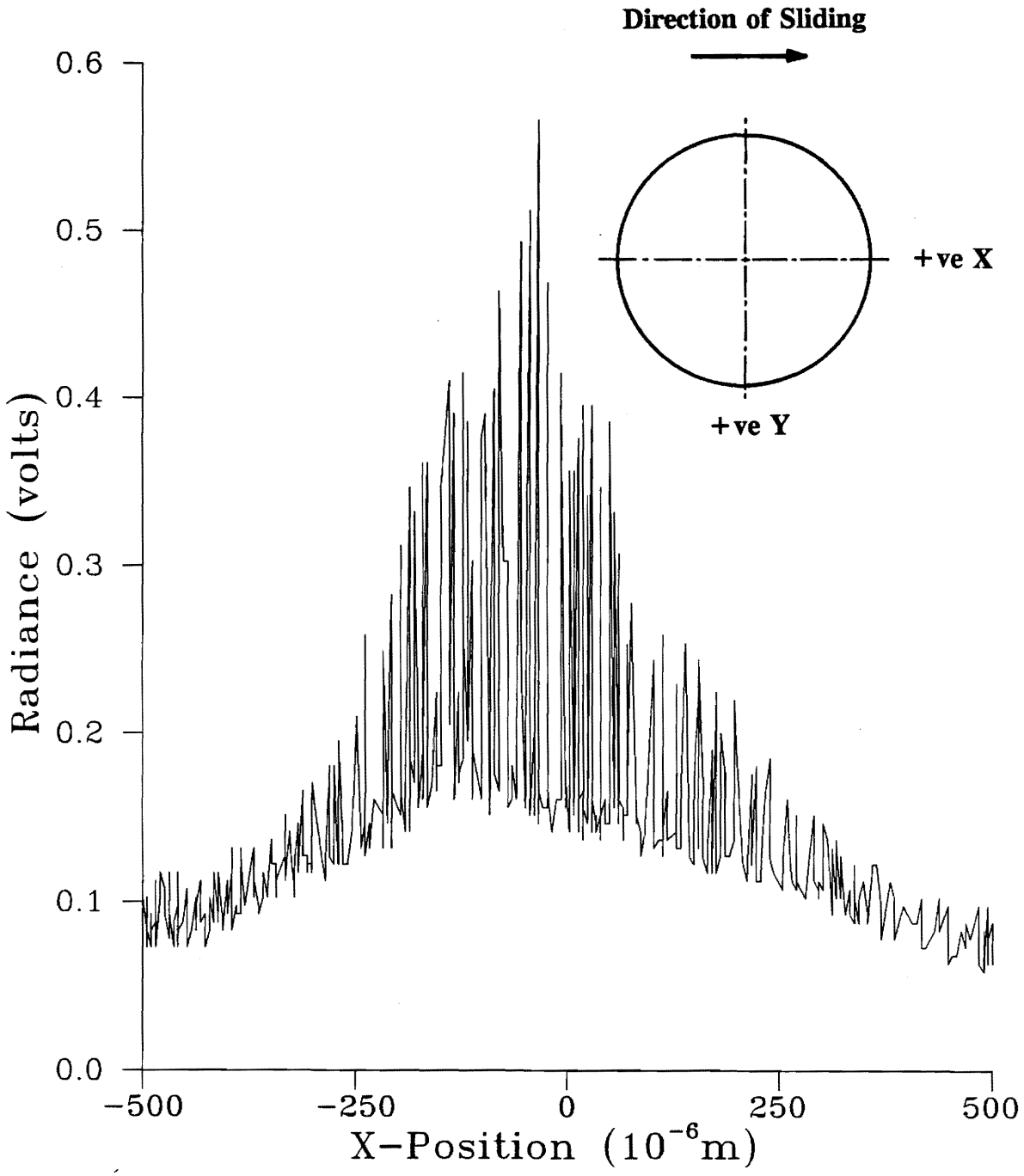

Fig. 31. Typical radiance distribution along X-direction of the contact area.

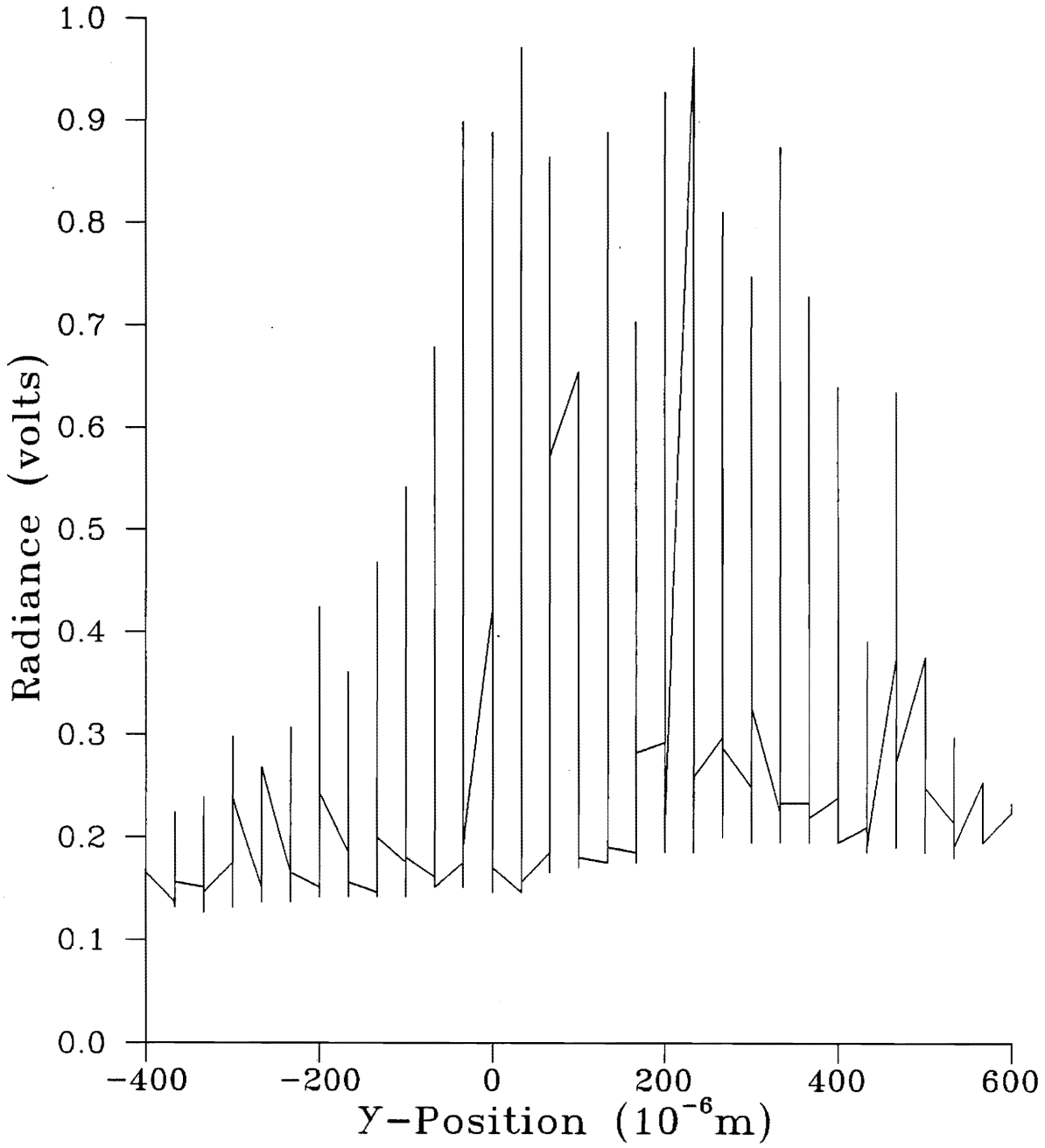

Fig. 32. Typical radiance distribution along Y-direction of the contact area.

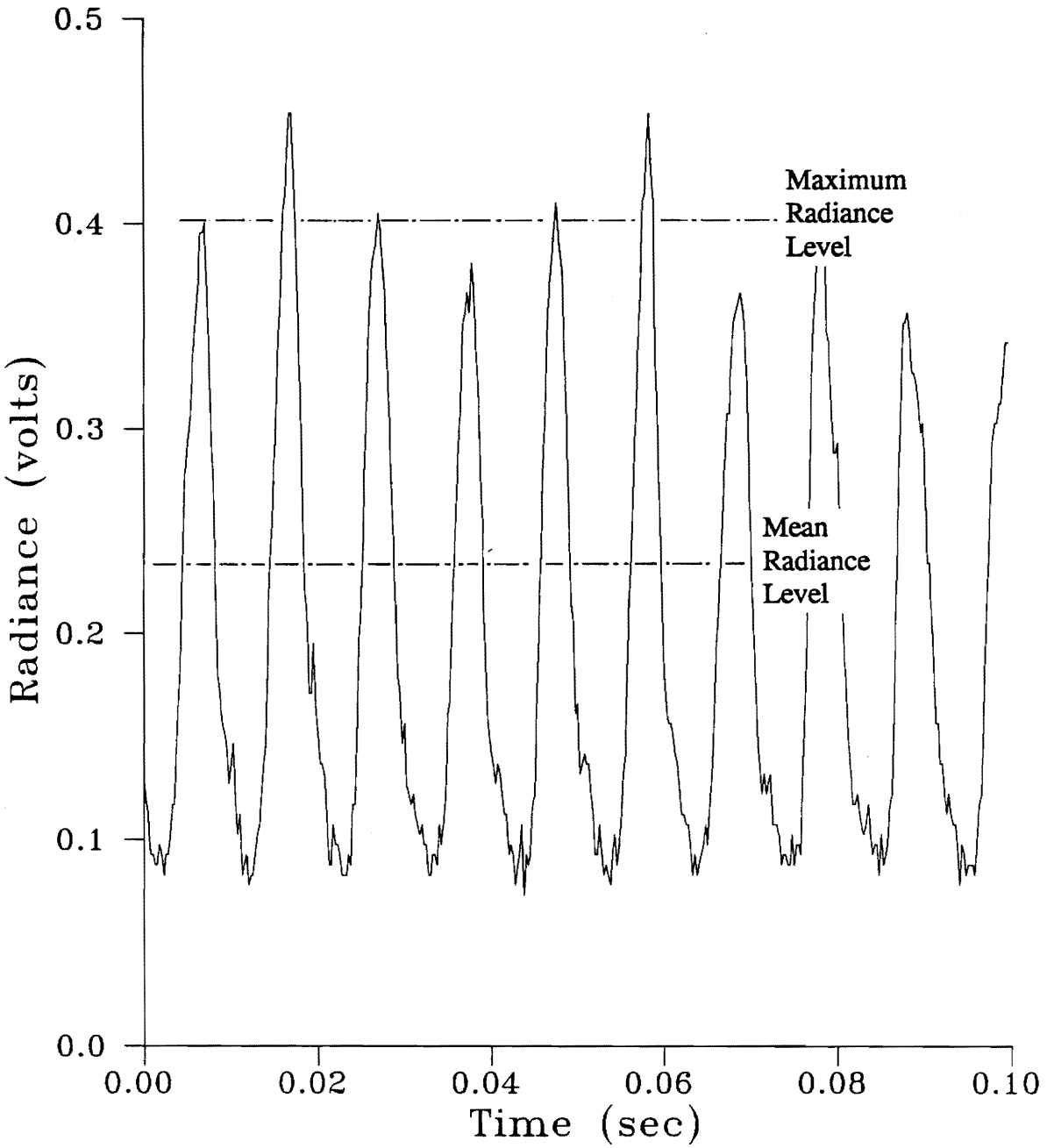

Fig. 33. Cycle-to-cycle variation of radiance in graphite-epoxy (normal). Rotational frequency = 98.3 Hz. The frequency of this radiance signal is also equal to 98.3 Hz.

Transform plot of a typical radiance signal is shown in Fig. 34.

Using the measured emissivities, the radiance data is converted to temperatures. These maximum and mean interfacial surface temperature rises are listed in Table 6. The variation of maximum and mean temperature rises with velocity are plotted for all the three fiber orientations in Figs. 35 and 36 respectively. It can be observed that with increasing velocity, the mean surface temperature initially increases up to a certain value and then levels off. An increase in velocity results in an increased rate of frictional heat generation. In spite of higher rates of heat generation at higher velocities, the mean surface temperature remains unchanged. Figures 37 and 38 show the variation of surface temperature rise with frictional heat generation. The highest levels of the mean surface temperature (which are found at velocities greater than 3.5 - 4 m/s) are in the same range of the glass transition temperature of the matrix material (i.e., about 120°C). Various factors that may be responsible for such a behavior are discussed in the next chapter.

Among the three fiber orientations, maximum temperature rise is found to be the highest in the normal orientation and lowest in the parallel orientation. However, the difference in the mean temperature rises among the three fiber orientations is very small.

The ANOVA results (given in Appendix G) show that velocity has significant effect on mean surface temperature rise. On the other hand, fiber orientation does not have a significant effect on surface temperature rise.

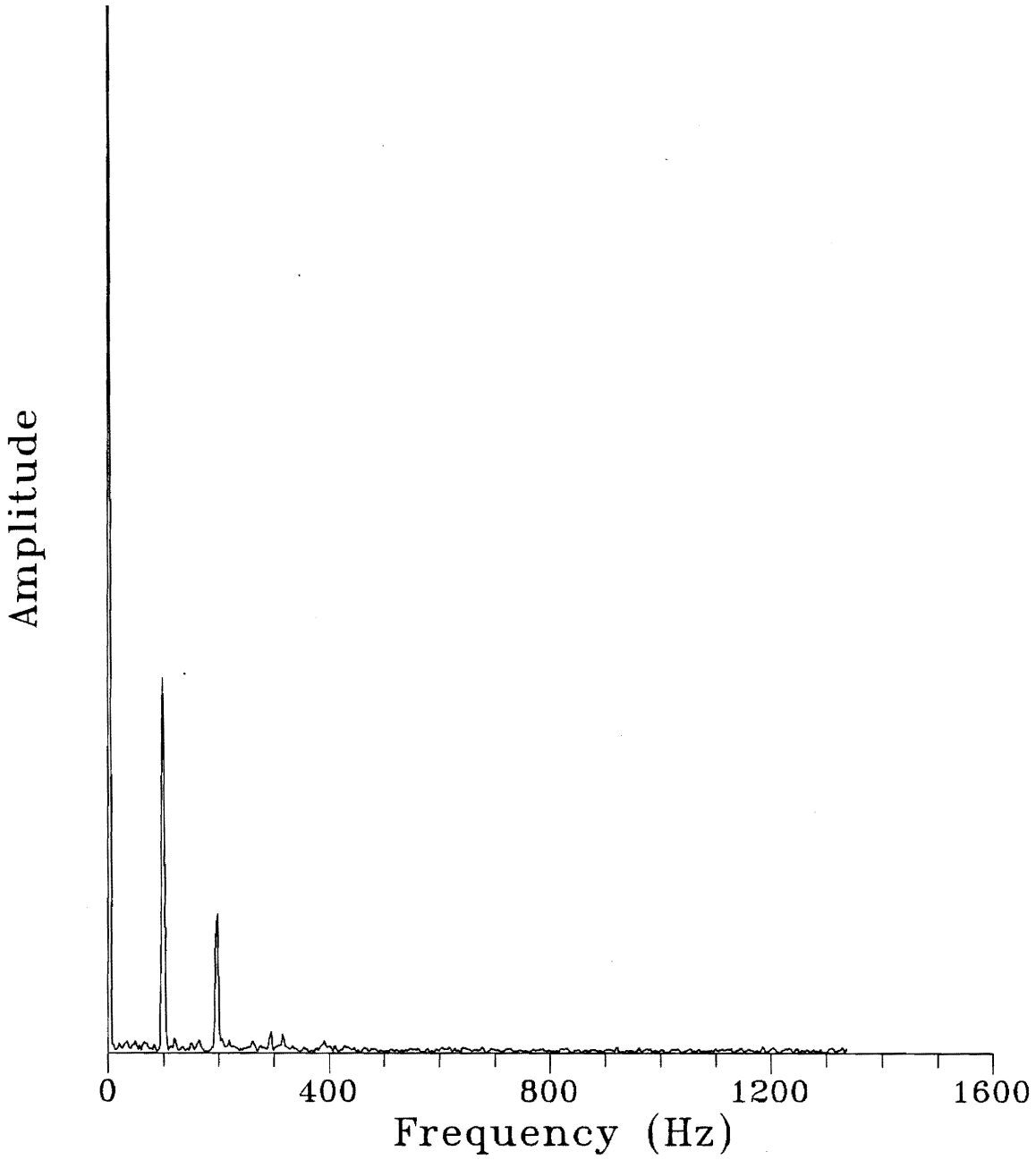

Fig. 34. Fast Fourier Transform of radiance signal. (Rotational frequency = 98.3 Hz.)

Table 6. Test results of maximum and mean surface temperature rises of graphite-epoxy.

MAXIMUM TEMPERATURE RISE (°C)

VELOCITY	FIBER ORIENTATION					
	NORMAL		PARALLEL		ANTI-PARALLEL	
	Exp. 1	Exp. 2	Exp. 1	Exp. 2	Exp. 1	Exp. 2
2.17 m/s		143.1	86.4	149.7	80.2	141.7
3.5 m/s	162.9	141.7	106.8	143.8	107.9	163.6
7.0 m/s		156.6	137.5	171.8	121.1	180.0

MEAN TEMPERATURE RISE (°C)

VELOCITY	FIBER ORIENTATION					
	NORMAL		PARALLEL		ANTI-PARALLEL	
	Exp. 1	Exp. 2	Exp. 1	Exp. 2	Exp. 1	Exp. 2
2.17 m/s		58.0	38.1	71.2	38.5	68.2
3.5 m/s	104.3	122.5	82.8	119.8	87.2	141.5
7.0 m/s		92.5	83.4	139.7	76.0	129.0

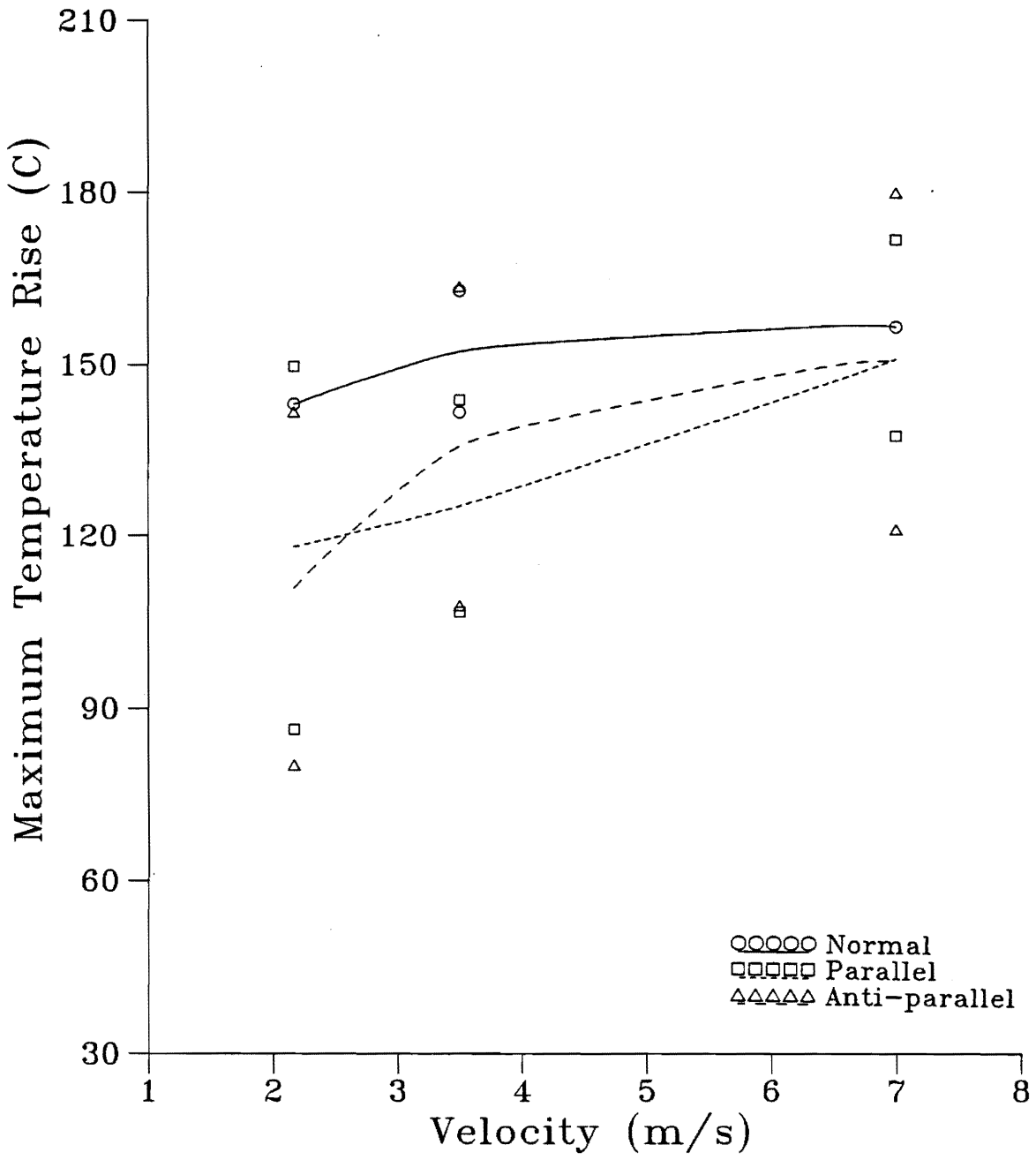

Fig. 35. Maximum surface temperature rise -vs- sliding velocity for various fiber orientations of graphite-epoxy.

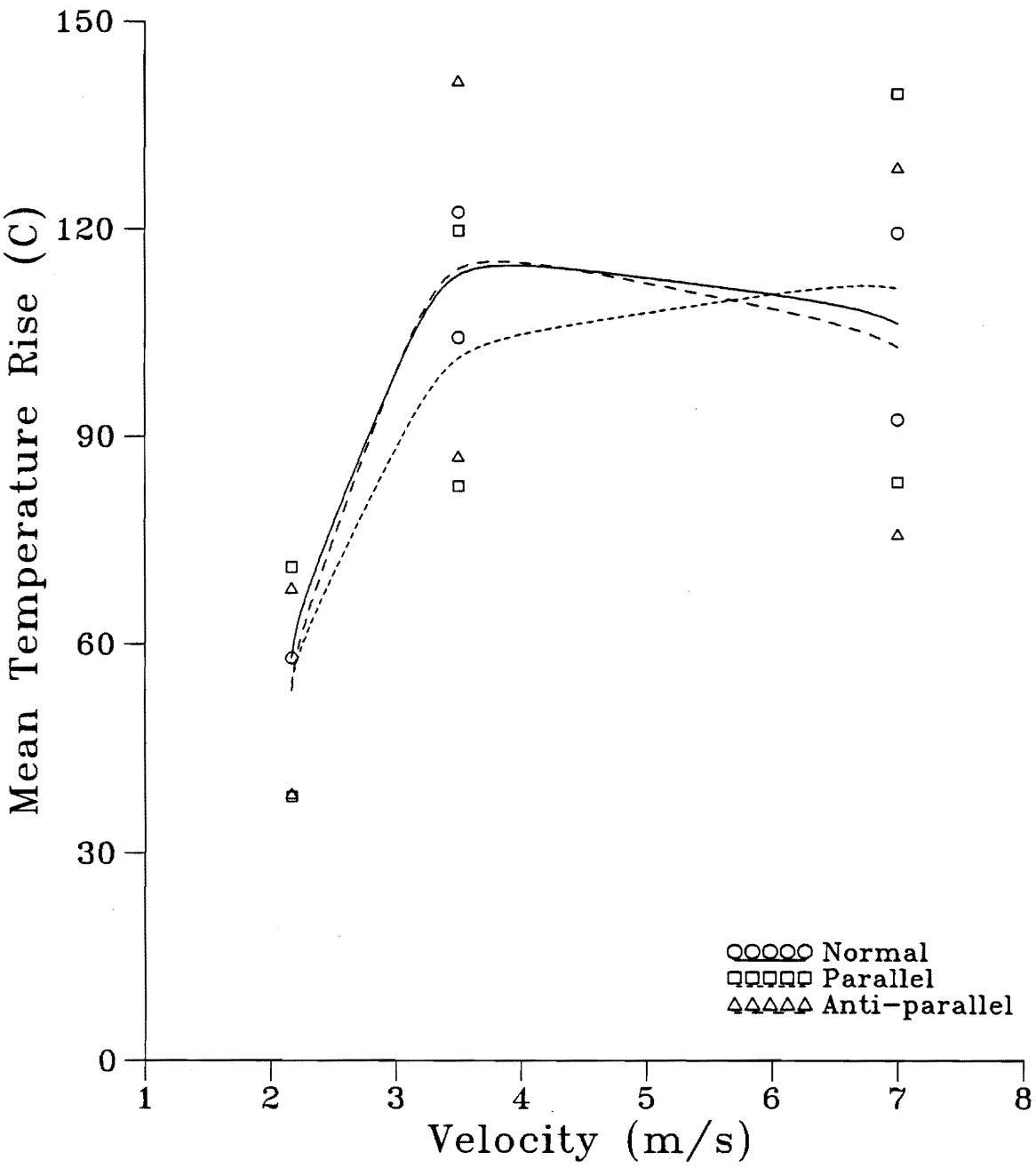

Fig. 36. Mean surface temperature rise -vs- sliding velocity for various fiber orientations of graphite-epoxy.

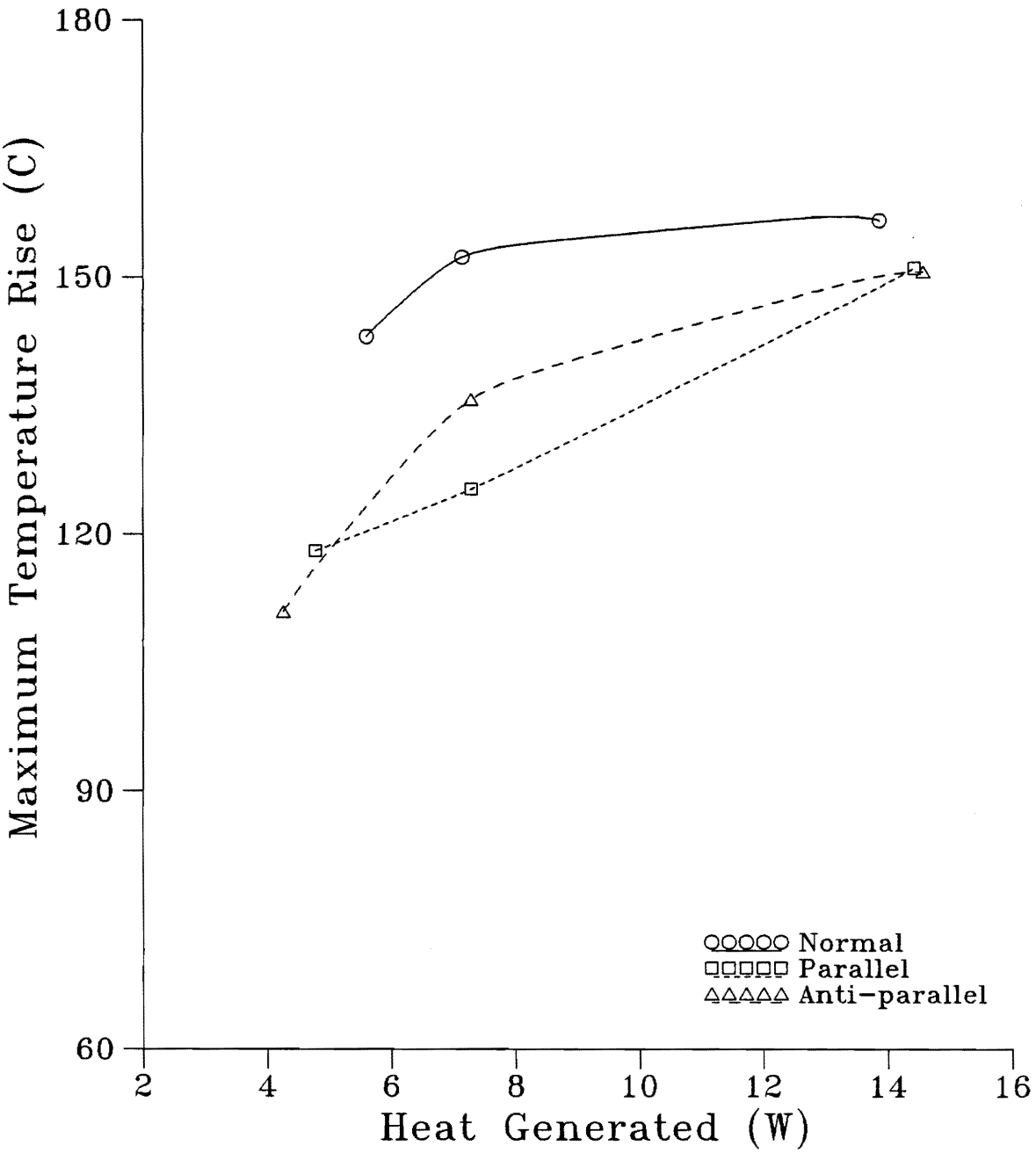

Fig. 37. Maximum surface temperature rise -vs- frictional heat generation for various fiber orientations of graphite-epoxy.

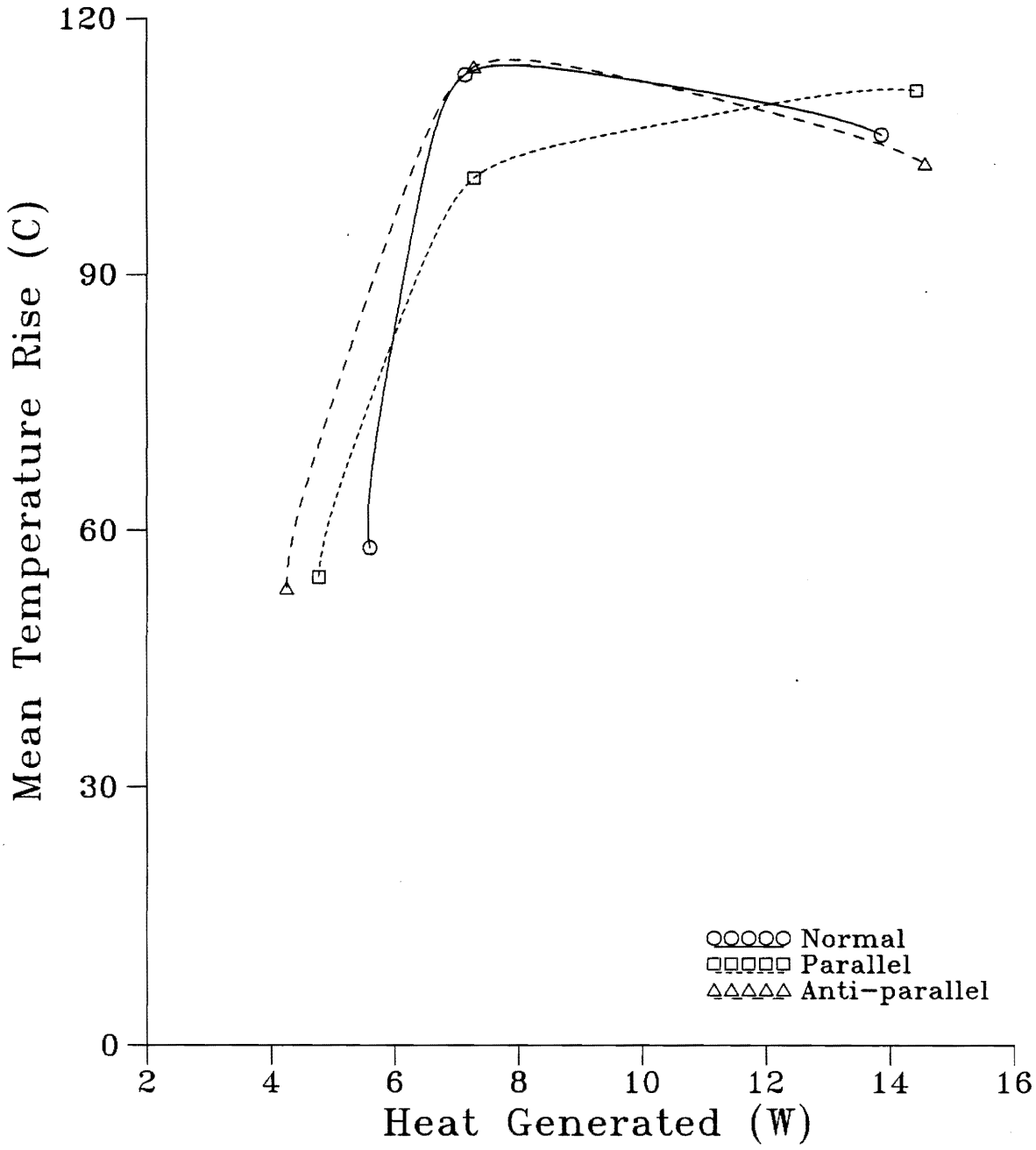

Fig. 38. Mean surface temperature rise -vs- frictional heat generation for various fiber orientations of graphite-epoxy.

4.2.1.3 Wear Results

The wear results are presented here in terms of volume of wear at the end of a fixed distance of sliding. In much of the literature, wear parameters as "wear rate" (defined as wear volume per unit sliding distance) and "specific wear rate" (defined as wear volume per unit sliding distance per unit load) are presented. This definition normalizes wear volume with respect to applied load and sliding distance and could be appropriately used where experiments are performed at different loads and for different sliding distances. However, such a definition is meaningful only when wear varies linearly with sliding distance and load, which may or may not be true for all tribological systems. In this study, all the experiments were run at the same load (4 N), and for the same sliding distance (520 m). Hence, the end-of-the-experiment wear volumes are reported. This is a fair representation of wear for comparison among fiber orientations.

The wear results for all the fiber orientations are listed in Table 7. The variation of wear with velocity is shown in Fig. 39. It can be observed that wear decreases with an increase in velocity up to a certain minimum value, beyond which it increases. The same trend can be seen for all three fiber orientations. It can also be seen that wear is highest in the normal orientation and lowest in the anti-parallel orientation. At the velocity for which wear volume is the minimum, fiber orientation has no effect on wear. Analysis of variance also shows the effects of velocity and fiber orientation on wear to be significant. The ANOVA table for wear is shown in Appendix G.

A photomacrograph of a typical wear scar showing the circular shape of the scar is shown in Fig. 40. SEM pictures of the wear scars, shown in Figures 41 - 43, reveal

Table 7. Test results of wear volume of graphite-epoxy after 520m of sliding.

WEAR VOLUME (10^{-12} m^3)

VELOCITY	FIBER ORIENTATION					
	NORMAL		PARALLEL		ANTI-PARALLEL	
	Exp. 1	Exp. 2	Exp. 1	Exp. 2	Exp. 1	Exp. 2
2.17 m/s	9.0	14.0	12.3	6.3	7.9	2.3
3.5 m/s	2.2	0.15	1.47	0.28	1.53	0.95
7.0 m/s	11.7	13.5	5.32	0.89	3.62	1.58

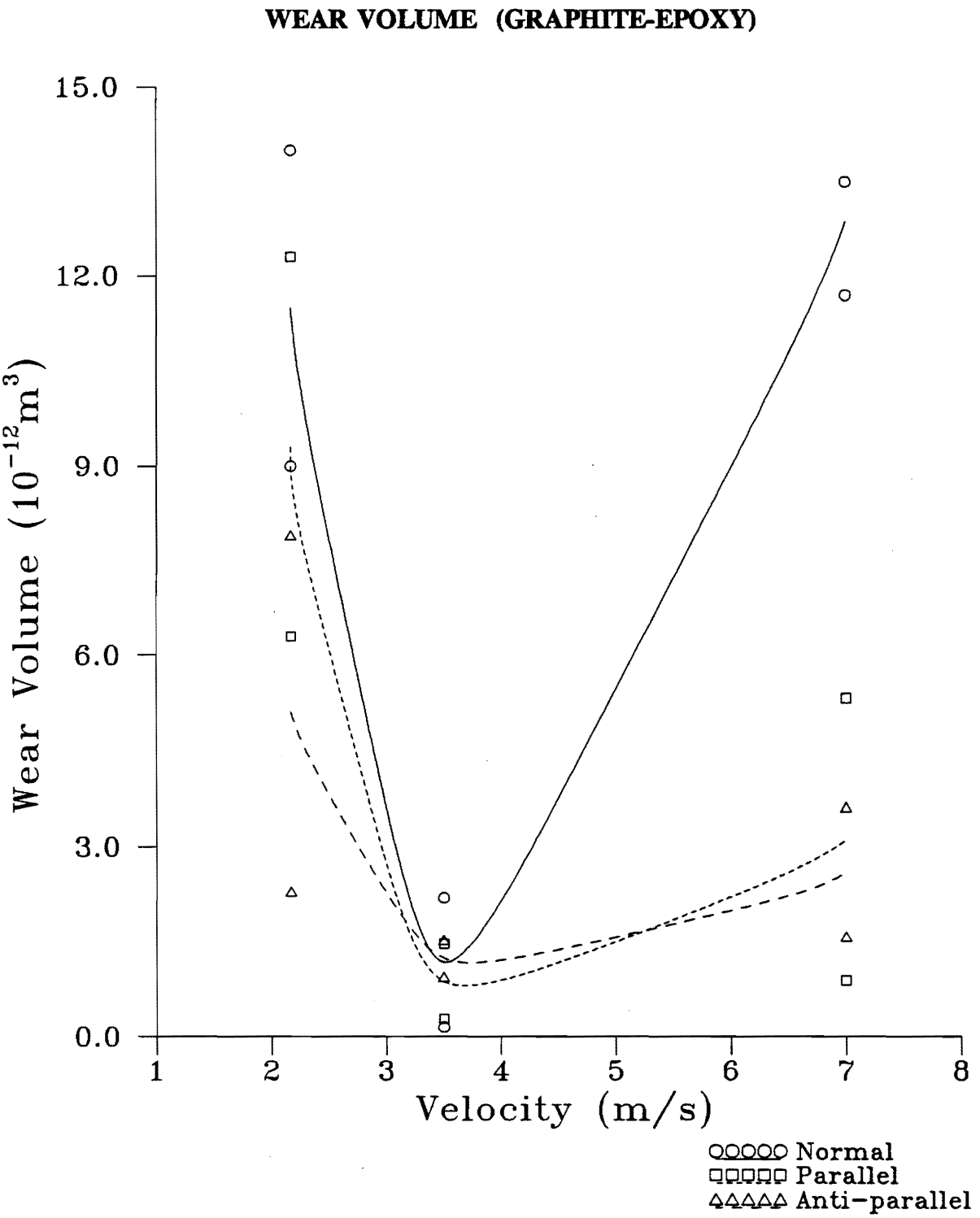

Fig. 39. Wear volume -vs- sliding velocity of graphite-epoxy for various fiber orientations. Sliding distance is the same for all data points (520 m). The load used was 4 N.

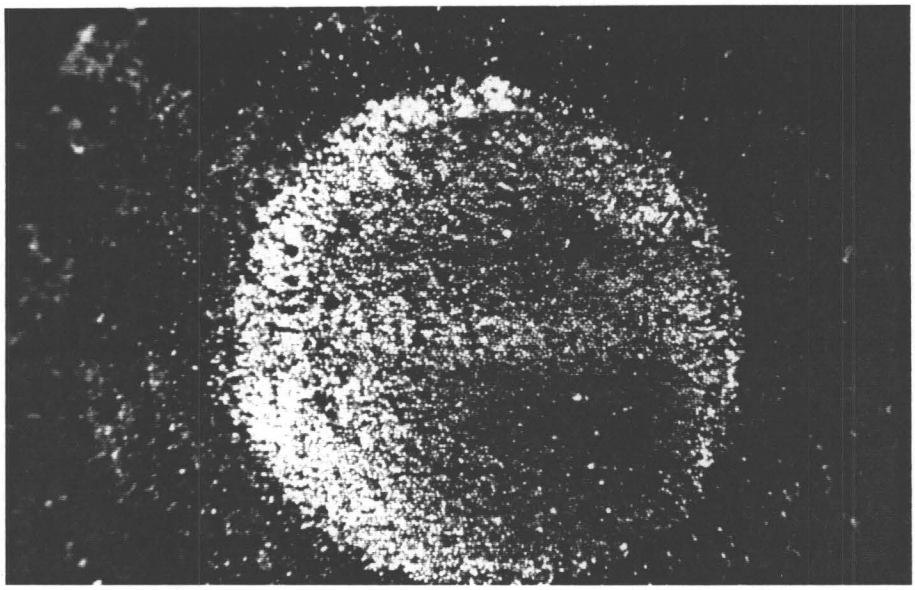

Fig. 40. Photomacrograph of a typical wear scar in the normal orientation.

a)

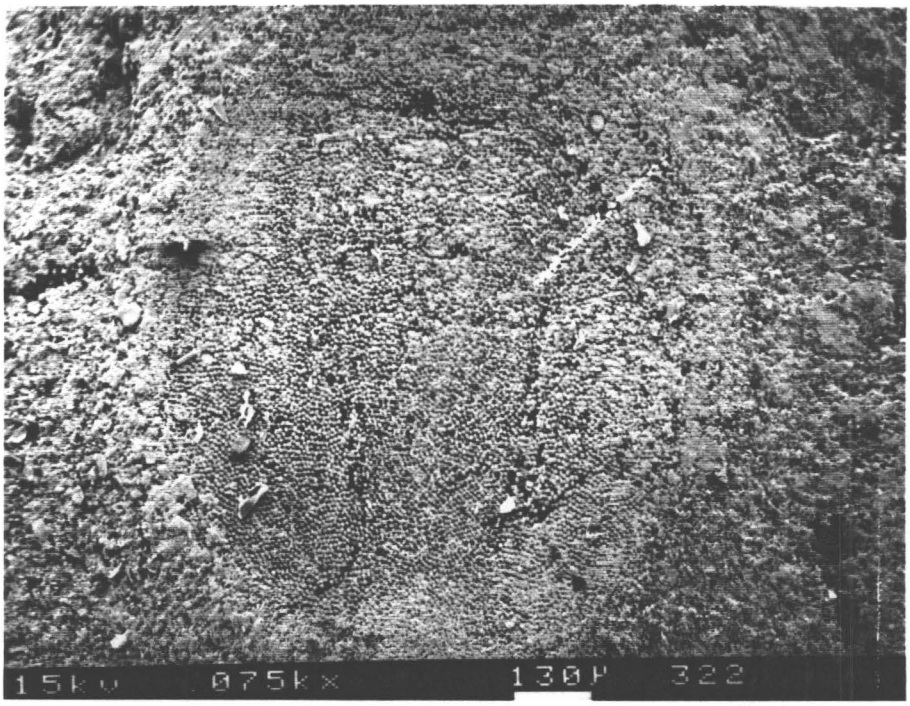

b)

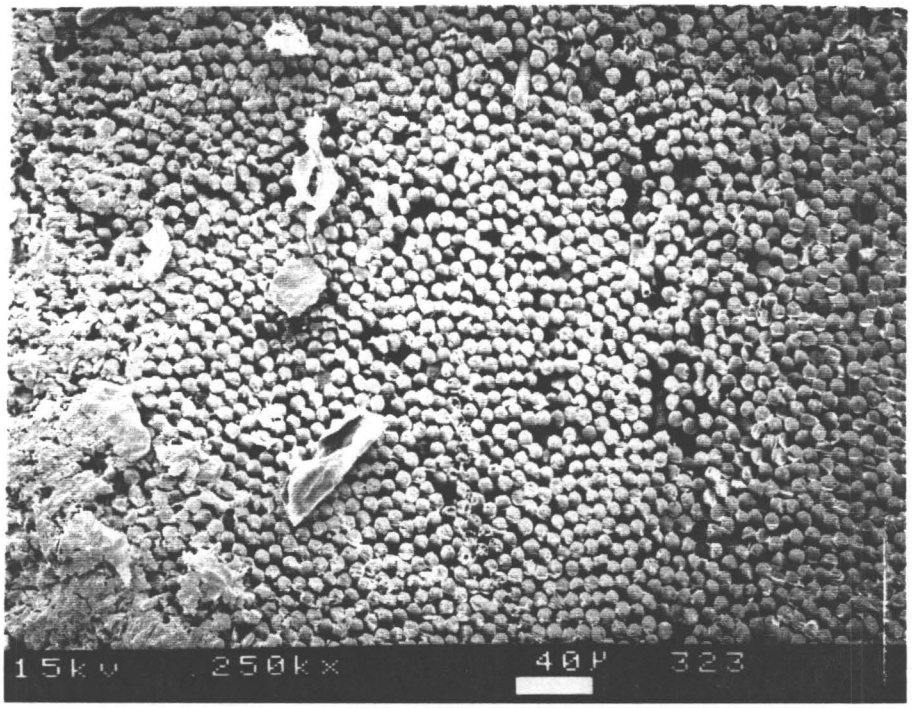

Fig. 41. SEM's of wear scar in the normal orientation of graphite-epoxy.
a) complete wear scar, **b)** portion of the scar showing wear debris.

c)

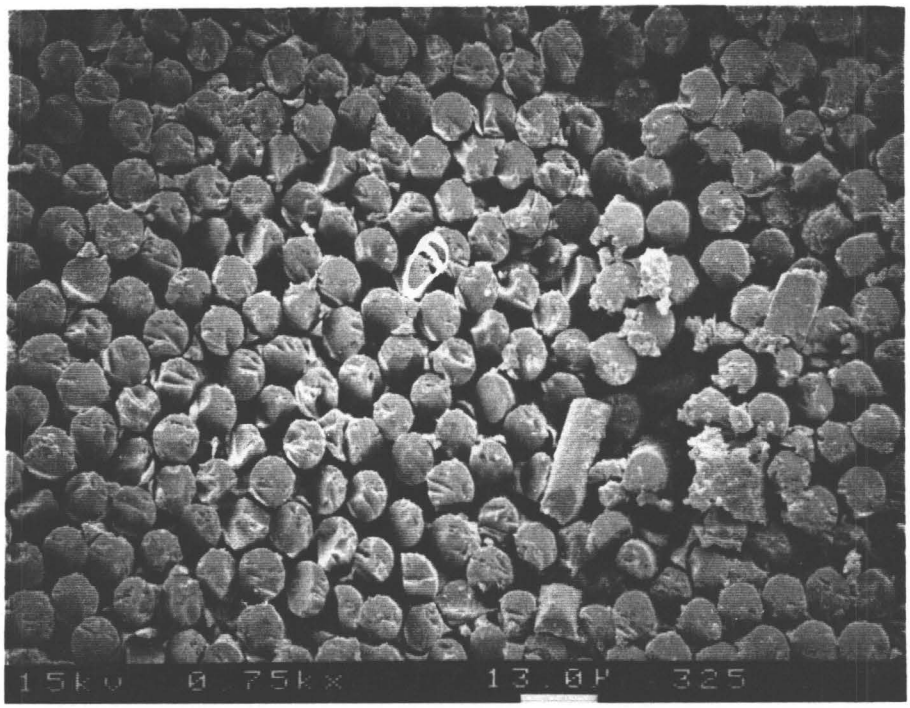

d)

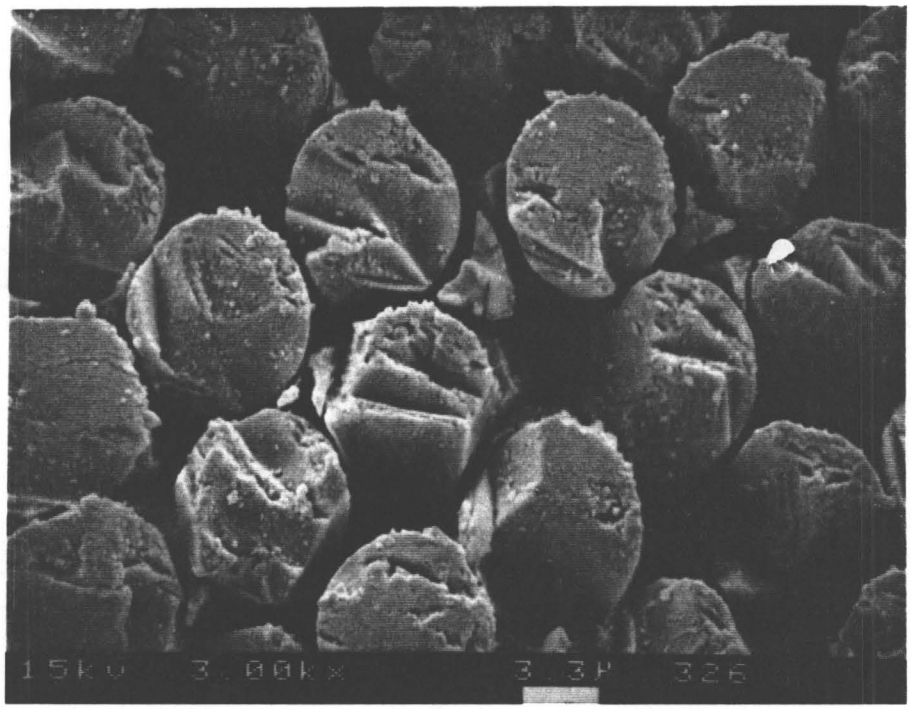

Fig. 41. (cont.) SEM's of wear scar in the normal orientation of graphite-epoxy. **c)** matrix removed at the surface, **d)** fibers chipped at the ends.

e)

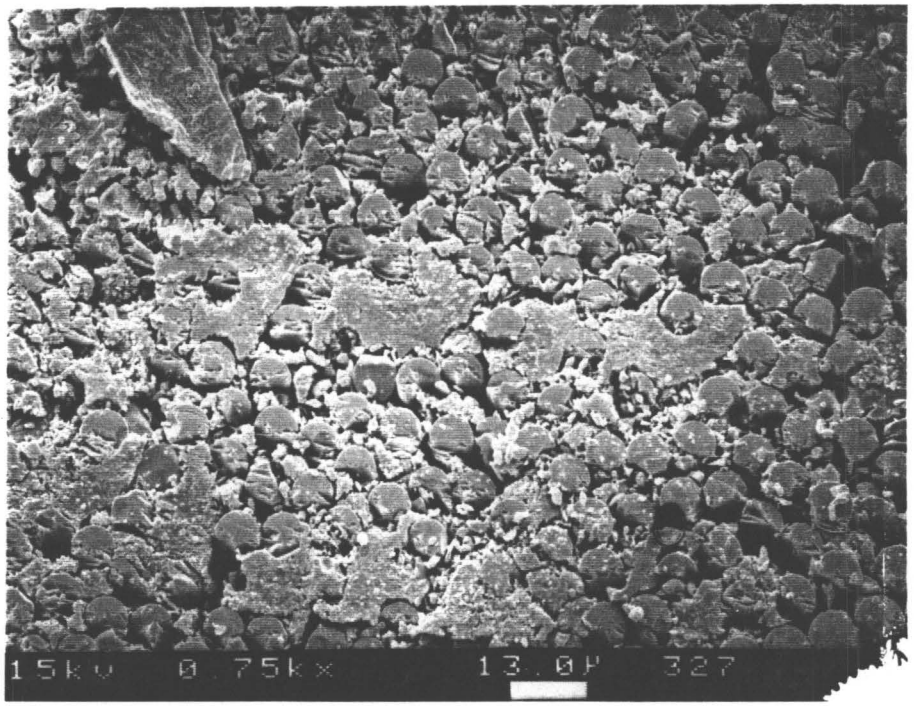

f)

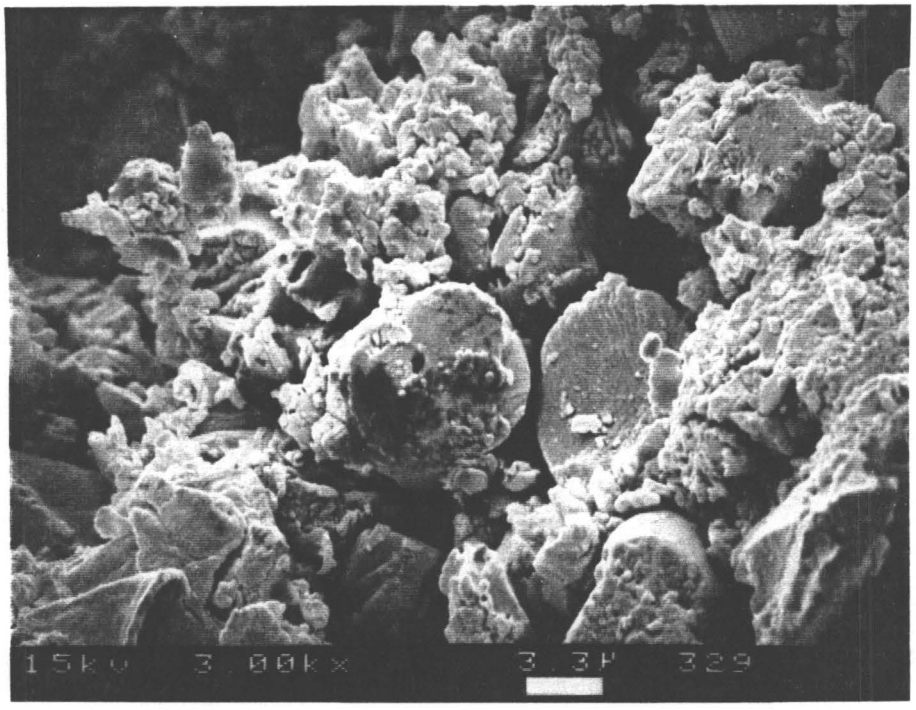

Fig. 41. (cont.) SEM's of wear scar in the normal orientation of graphite-epoxy.
e) and **f)** matrix removed and deposited around the edges of the wear scar.

g)

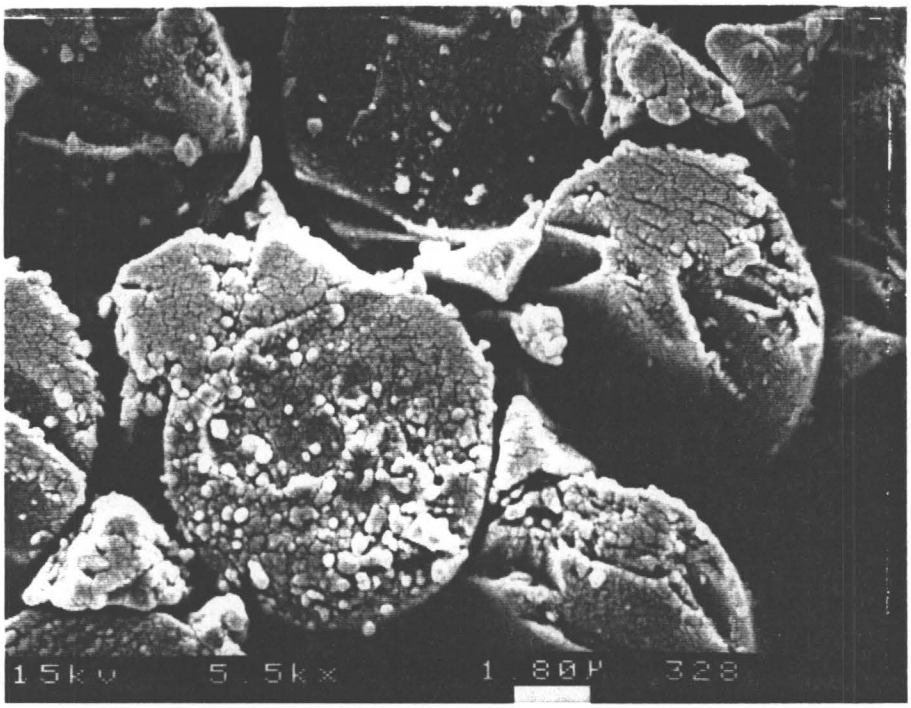

Fig. 41. (cont.) SEM's of wear scar in the normal orientation of graphite-epoxy.
g) fine wear debris deposited on ends of fibers.

a)

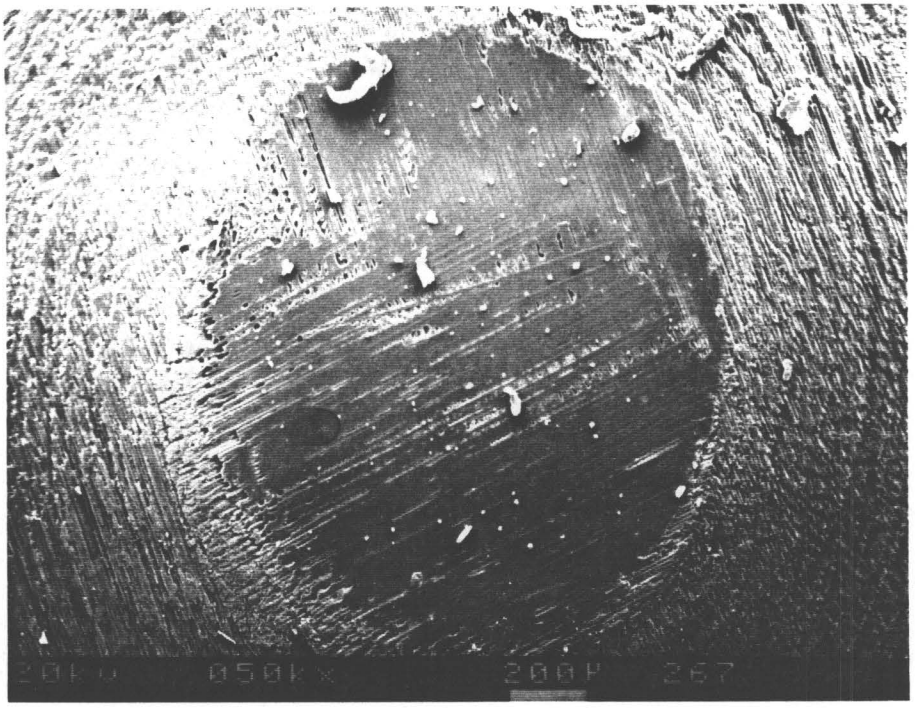

b)

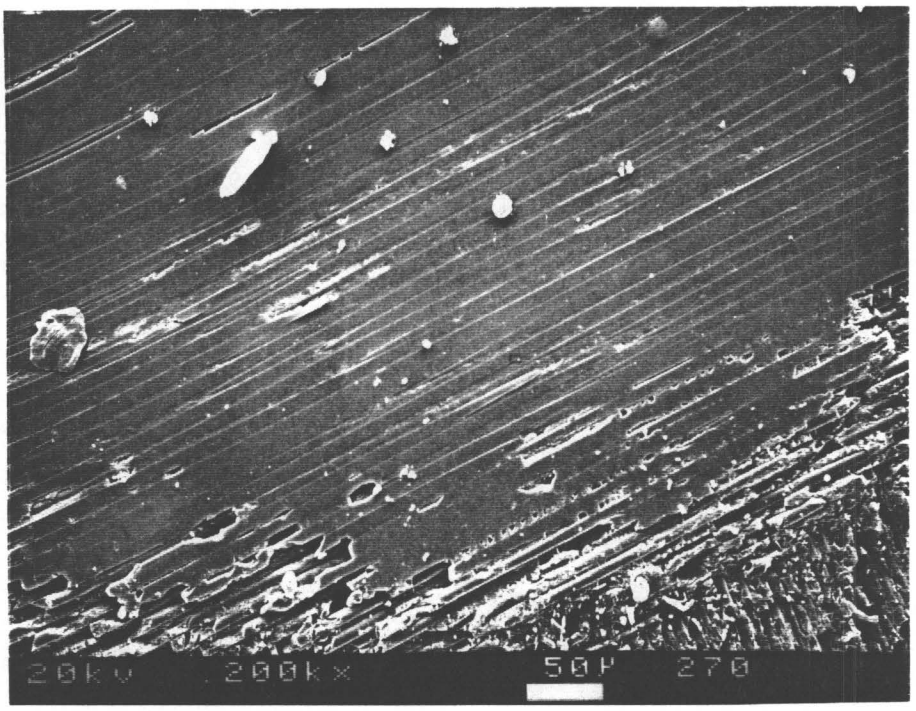

Fig. 42. SEM's of wear scar in the parallel orientation of graphite-epoxy. **a)** complete wear scar, **b)** edge of the wear scar.

c)

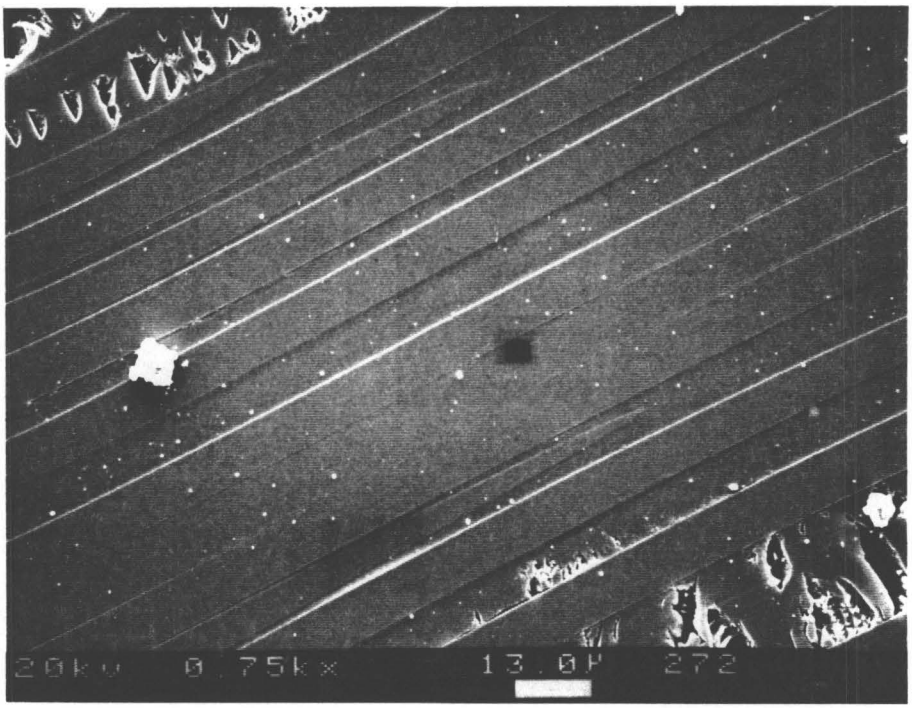

d)

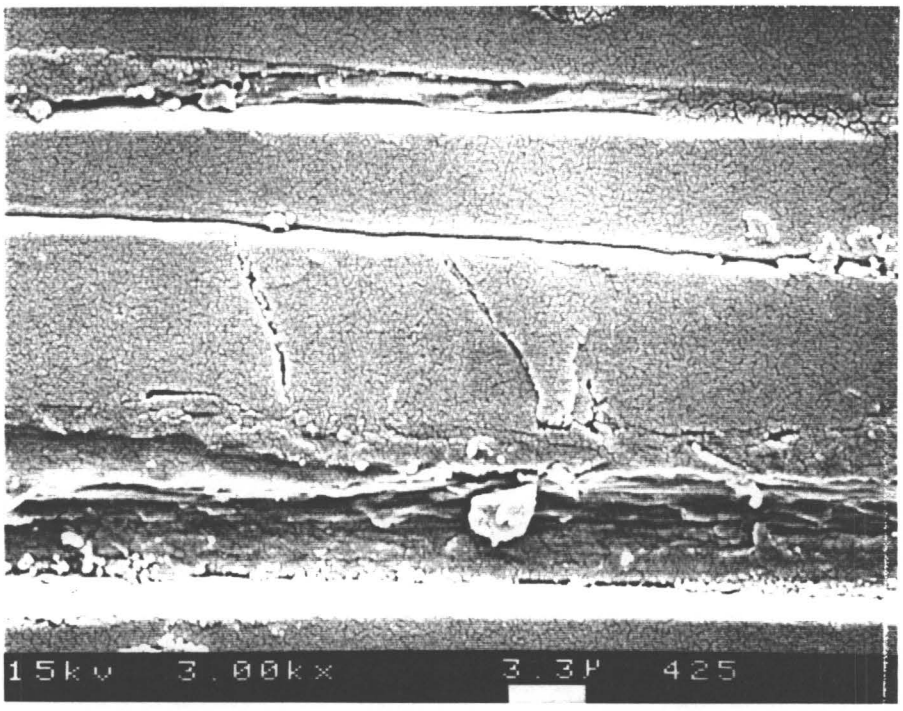

Fig. 42. (cont.) SEM's of wear scar in the parallel orientation of graphite-epoxy. **c)** smooth surface of the wear scar shows that fibers and matrix are removed uniformly. **d)** transverse cracks in the fibers.

a)

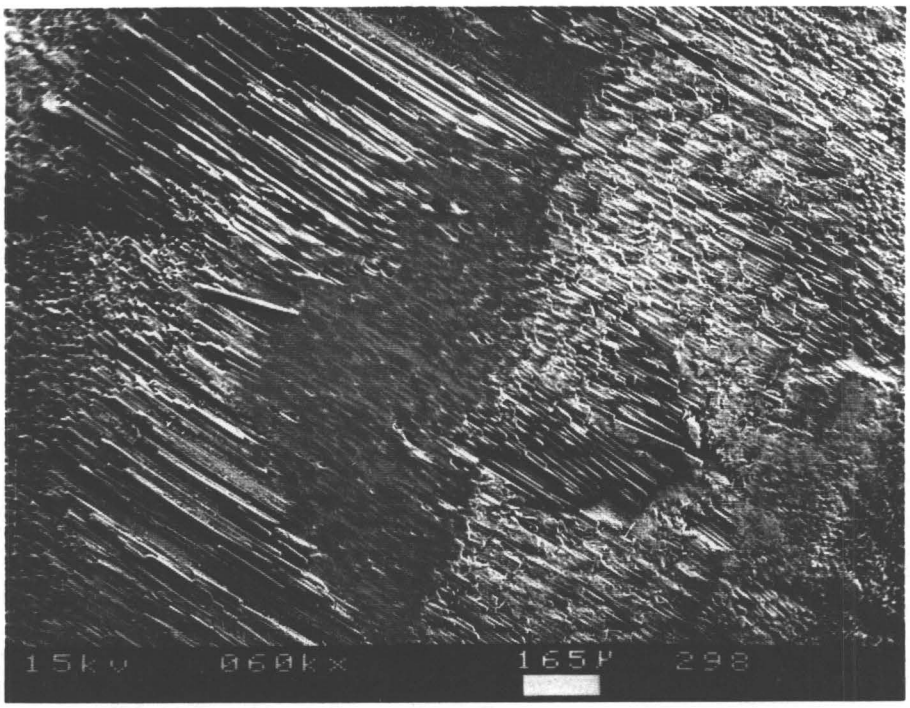

b)

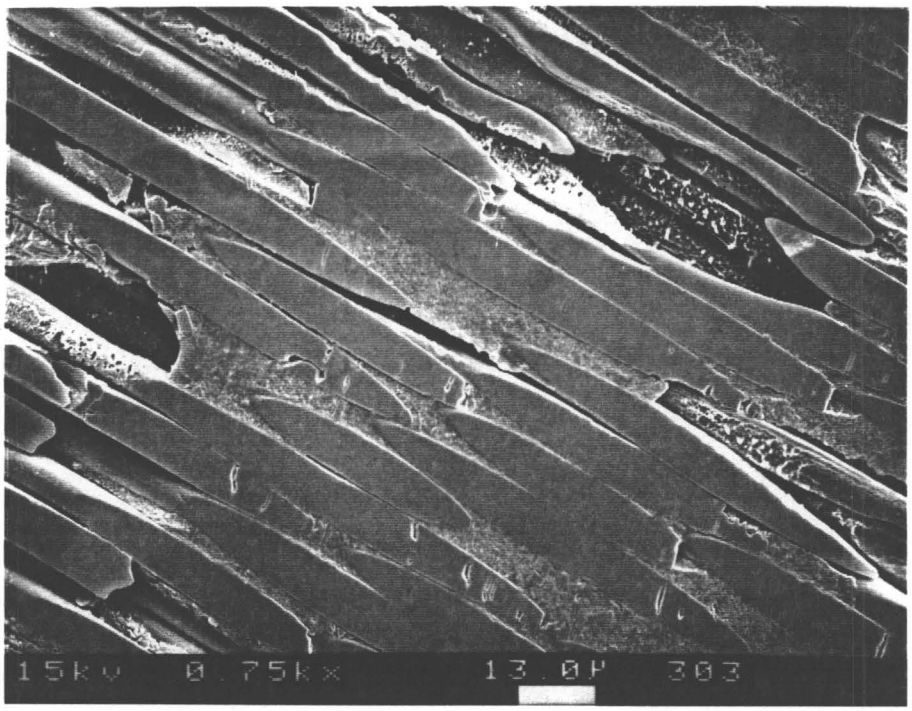

Fig. 43. SEM's of wear scar in the anti-parallel orientation of graphite-epoxy. **a)** complete wear scar, **b)** fiber cross-sections on the wear scar.

c)

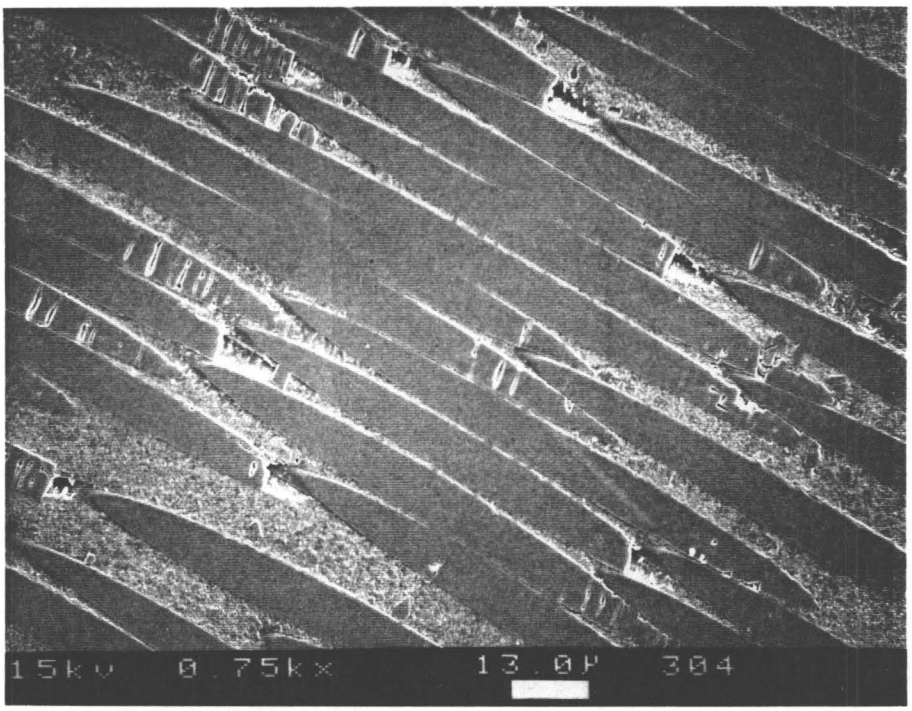

d)

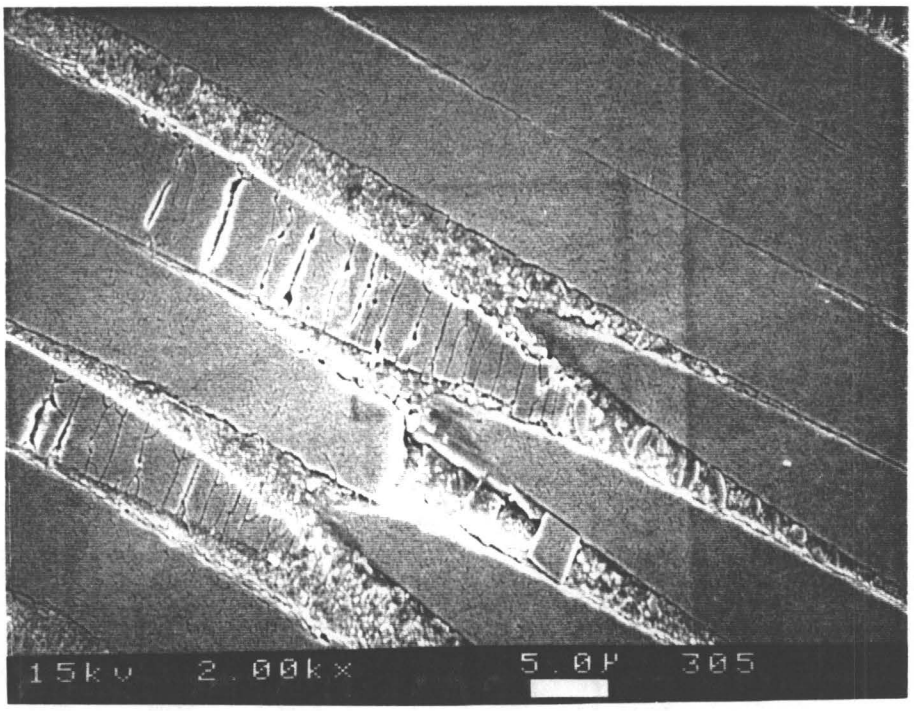

Fig. 43. (cont.) SEM's of wear scar in the anti-parallel orientation of graphite-epoxy.
c) cracks in the fibers, fibers and matrix are seen to wear uniformly,
d) transverse cracking and subsequent removal of the fibers.

e)

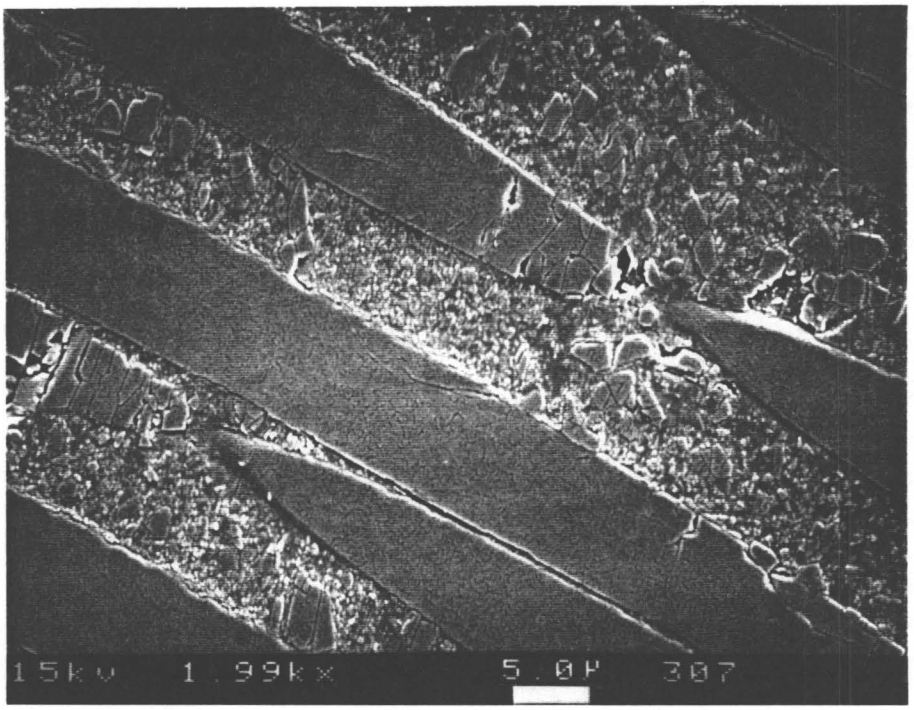

f)

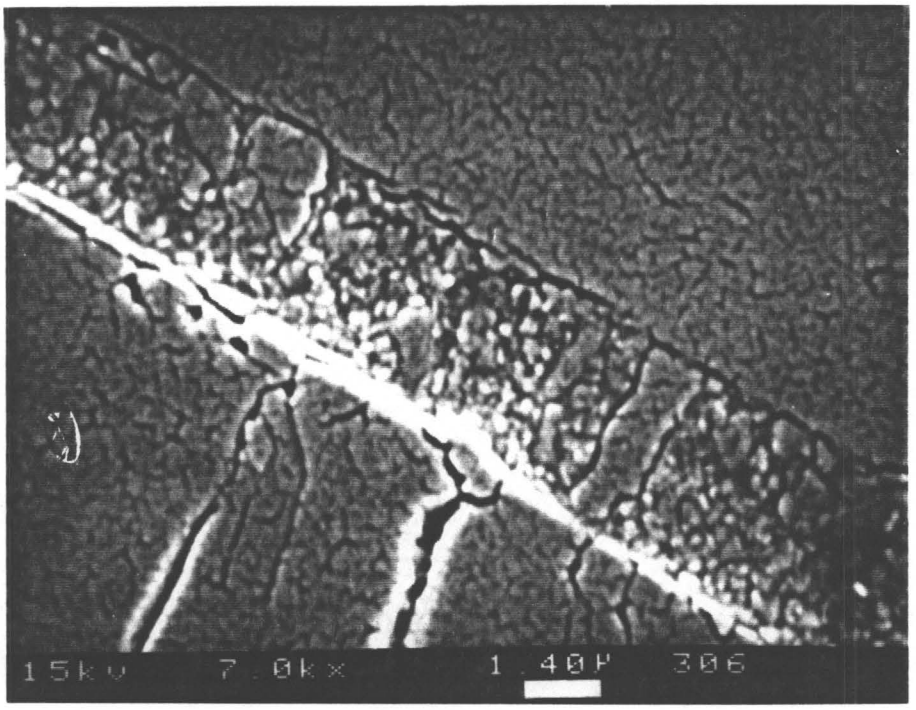

Fig. 43. (cont.) SEM's of wear scar in the anti-parallel orientation of graphite-epoxy. **e)** cracks in matrix, **f)** cracks under high magnification.

a great deal about the nature of the wear mechanism. Some of the observations and inferences from these micrographs are listed below.

1. The fibers and the matrix of graphite-epoxy composite are worn simultaneously, with the height reducing equally in both phases for the parallel and anti-parallel orientations. Some deviation is observed in the normal orientation, where gaps seem to be present between fibers, possibly due to faster removal of matrix compared to the fibers. This can be observed in Figs. 41 c) and 41 d).
2. In the normal orientation, there is very little evidence of fiber shearing and fibers being pulled out of the matrix. Although in much of the literature it has been shown that fiber removal occurs through "transverse shear" of the fibers, it is not observed here.
3. In the normal orientation, small pieces of the fibers are seen to have been broken at the ends. This can be seen in Fig. 41 d). This results in fiber removal as very fine debris. The debris has dimensions much less than the fiber diameter -- mostly in the order of a few hundred nanometers. Much fine debris is also seen deposited on the ends of fibers (as seen in Fig. 41 g)). These could be brittle fractured fragments of fiber and matrix. This could be resulting in "three-body abrasive wear" as well. However, this debris is seen to have deposited only on the ends of the fibers in the normal orientation, and not on the sides of the fibers in the other two orientations.
5. In the parallel and anti-parallel orientations, the fibers and matrix are worn to a very smooth and flat surface. There is no evidence of fiber pull-out from the

matrix. Wear proceeds by gradual and continual removal of fiber and matrix, simultaneously and at the same rate (Figs. 42 c) and 43 c)).

6. In the micrographs of the scar in the anti-parallel orientation (Fig. 43 b)), the cross sections of the fibers cut along the plane of the wear scar are seen to be elliptical. Perfectly anti-parallel orientation should have resulted in long rectangular sections. Such elliptical sections are only possible if the fibers are oriented at an angle to the sliding interface. From the dimensions of the ellipse, this angle can be computed to be 6.4° in these specimens. Observation of the SEM pictures, as in Fig. 43 c), reveals a large number of transverse cracks on the fibers at the thinner end, running across the whole width of the fiber. At places, pieces of these broken fibers are seen to have been removed.

4.2.2 Graphite-Epoxy : Oscillatory Motion

Figure 44 shows the radiance and friction force traces from one of the oscillating experiments with graphite-epoxy. The results are discussed below separately.

4.2.2.1 Friction Results

As can be seen from the traces (Fig. 44.), friction force increases to a certain level very sharply after the start of the experiment. In the normal and anti-parallel orientations, friction force is seen to stay fairly constant throughout the experiment, whereas in the parallel orientation, it is seen to be increase gradually during the experiment.

The cycle-to-cycle variation in friction force is shown in Fig. 45. In each cycle, the friction force changes direction twice because of the change in direction of velocity. Therefore, it looks like a harmonic signal with the frequency equal to the frequency of the velocity. It is expected to look like a perfect square wave, if there were no difference between static and kinetic friction forces, no change in friction force with velocity, and instantaneous system response. Typically, the friction force shows a peak every time the velocity increases from zero, which follows immediately after the sliding direction is reversed. This is due to a higher static coefficient of friction compared to the kinetic coefficient of friction. Throughout the rest of the half cycle, until sliding velocity is reversed again, the friction force stays fairly constant even though some minor fluctuations are present. Traces from all the three fiber orientations show this general trend.

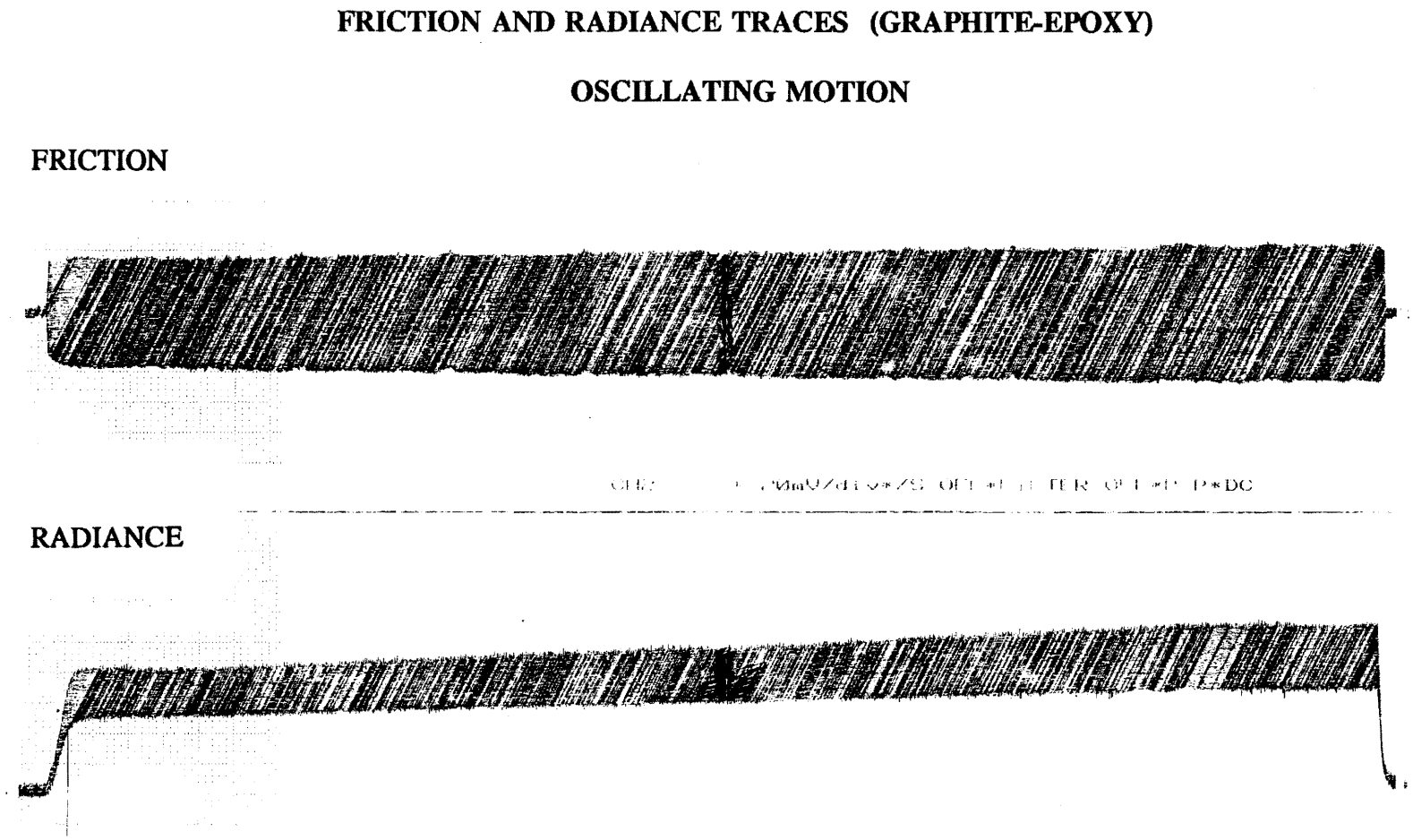

Fig. 44. Friction and radiance traces of a typical oscillating experiment with graphite-epoxy.

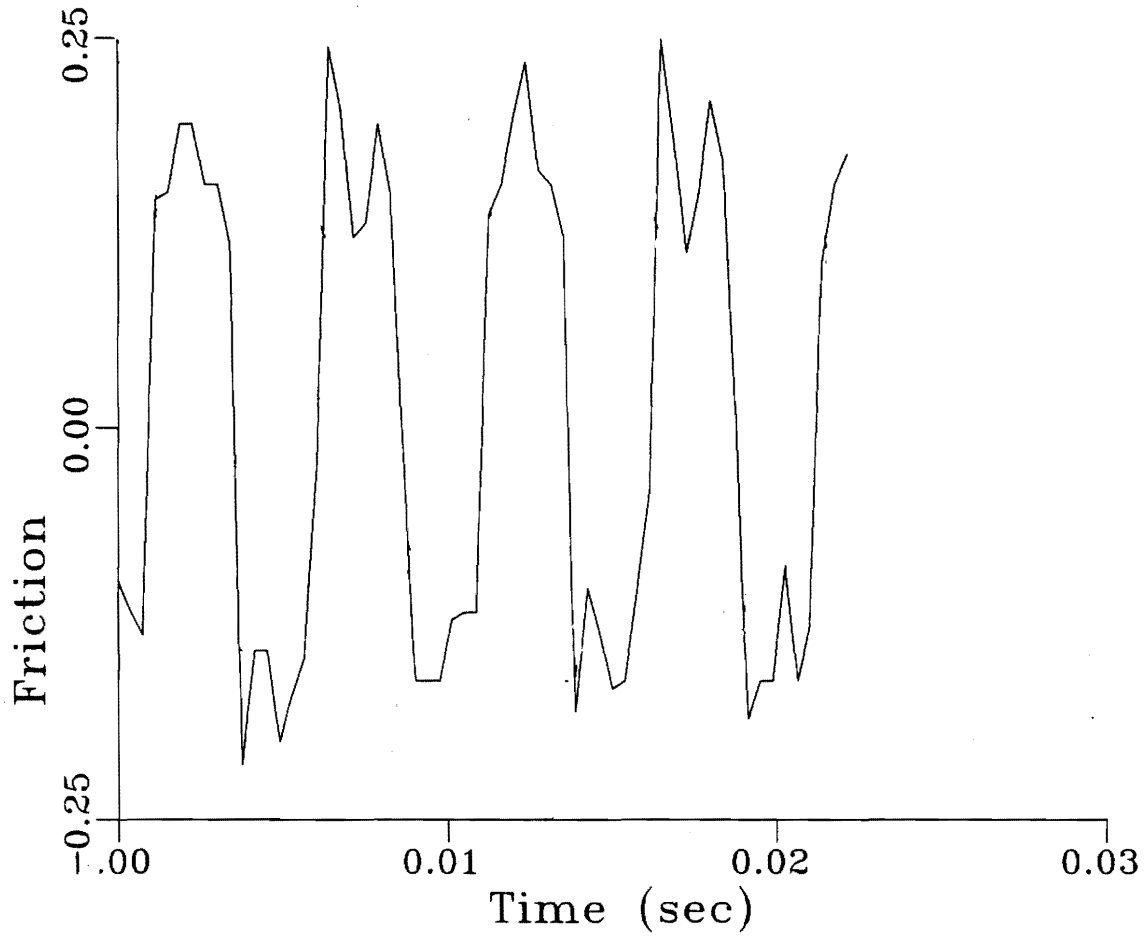

Fig. 45. Cycle-to-cycle variation of friction force signal in oscillating motion of graphite-epoxy.

The measured values of coefficient of friction are listed in Table 8. Figure 46 shows the coefficients of friction for the three fiber orientations at the two mean oscillating velocities. With an increase in mean oscillating velocity, there is a small increase in the coefficient of friction in the normal and parallel orientations. The coefficient of friction in the anti-parallel orientation seems to be fairly constant over the velocity range. The coefficient of friction is found to be highest in the parallel orientation, and lowest in the normal orientation.

4.2.2.2 Radiance and Temperature Results

The radiance is also seen to increase fairly quickly, immediately after the start of the experiment (Fig. 44.). After this sharp initial increase, it is seen to change in three general fashions, which seems to be the characteristic behavior of the three fiber orientations. In the normal orientation, after the increase, it is seen to decrease gradually as the experiment proceeds. In the parallel orientation, however, it is seen to increase gradually during the experiment. No major change is observed in the anti-parallel orientation. Comparison of the radiance traces with friction traces show some good correlation.

A cycle-to-cycle variation in the radiance for a typical experiment with graphite-epoxy is shown in Fig. 47. All experiments show similar behavior. The fluctuation is seen to be harmonic, as in the case of friction force. However, the frequency of radiance fluctuation is twice that of the friction force or velocity. This can be seen from the Fast Fourier Transform (FFT) of the radiance, friction force and acceleration signals,

Table 8. Test results of oscillating experiments of graphite-epoxy.

COEFFICIENT OF FRICTION

MEAN VELOCITY	FIBER ORIENTATION					
	NORMAL		PARALLEL		ANTI-PARALLEL	
	Exp. 1	Exp. 2	Exp. 1	Exp. 2	Exp. 1	Exp. 2
.066 m/s	.38	.37	.45	.45	.38	.50
.128 m/s	.28	.52	.45	.52	.40	.47

MEAN TEMPERATURE RISE (°C)

MEAN VELOCITY	FIBER ORIENTATION					
	NORMAL		PARALLEL		ANTI-PARALLEL	
	Exp. 1	Exp. 2	Exp. 1	Exp. 2	Exp. 1	Exp. 2
.066 m/s		19.7	19.7	15.5	15.1	18.1
.128 m/s	31.0	44.5	29.4	43.6	52.8	46.7

WEAR VOLUME (10^{-12} m^3)

MEAN VELOCITY	FIBER ORIENTATION					
	NORMAL		PARALLEL		ANTI-PARALLEL	
	Exp. 1	Exp. 2	Exp. 1	Exp. 2	Exp. 1	Exp. 2
.066 m/s		5.9	1.86	0.61	0.77	1.15
.128 m/s	4.6	2.2	2.8	1.2	0.71	1.15

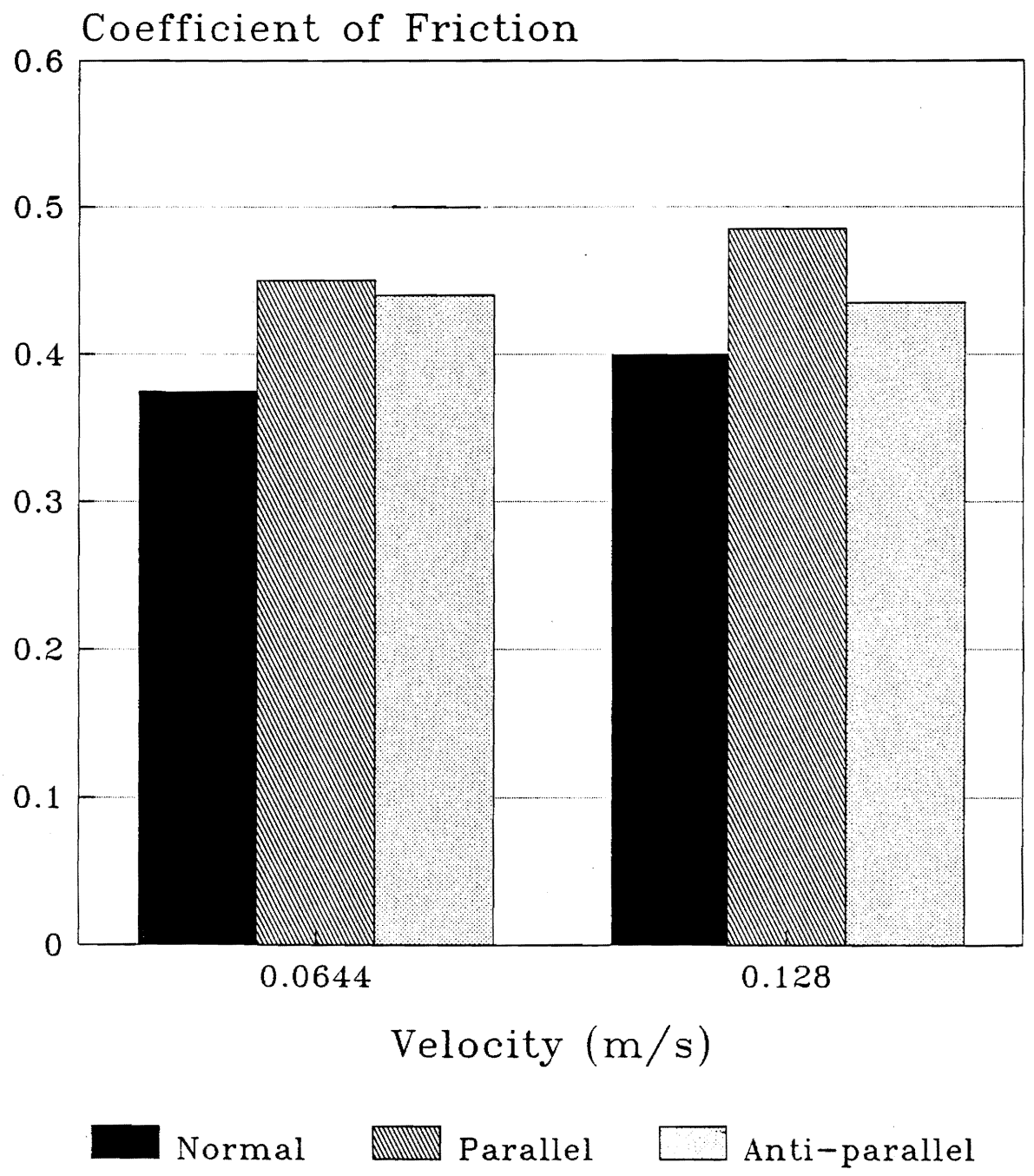

Fig. 46. Coefficient of friction in oscillating contact of graphite-epoxy. The values shown here are the averages of two experiments.

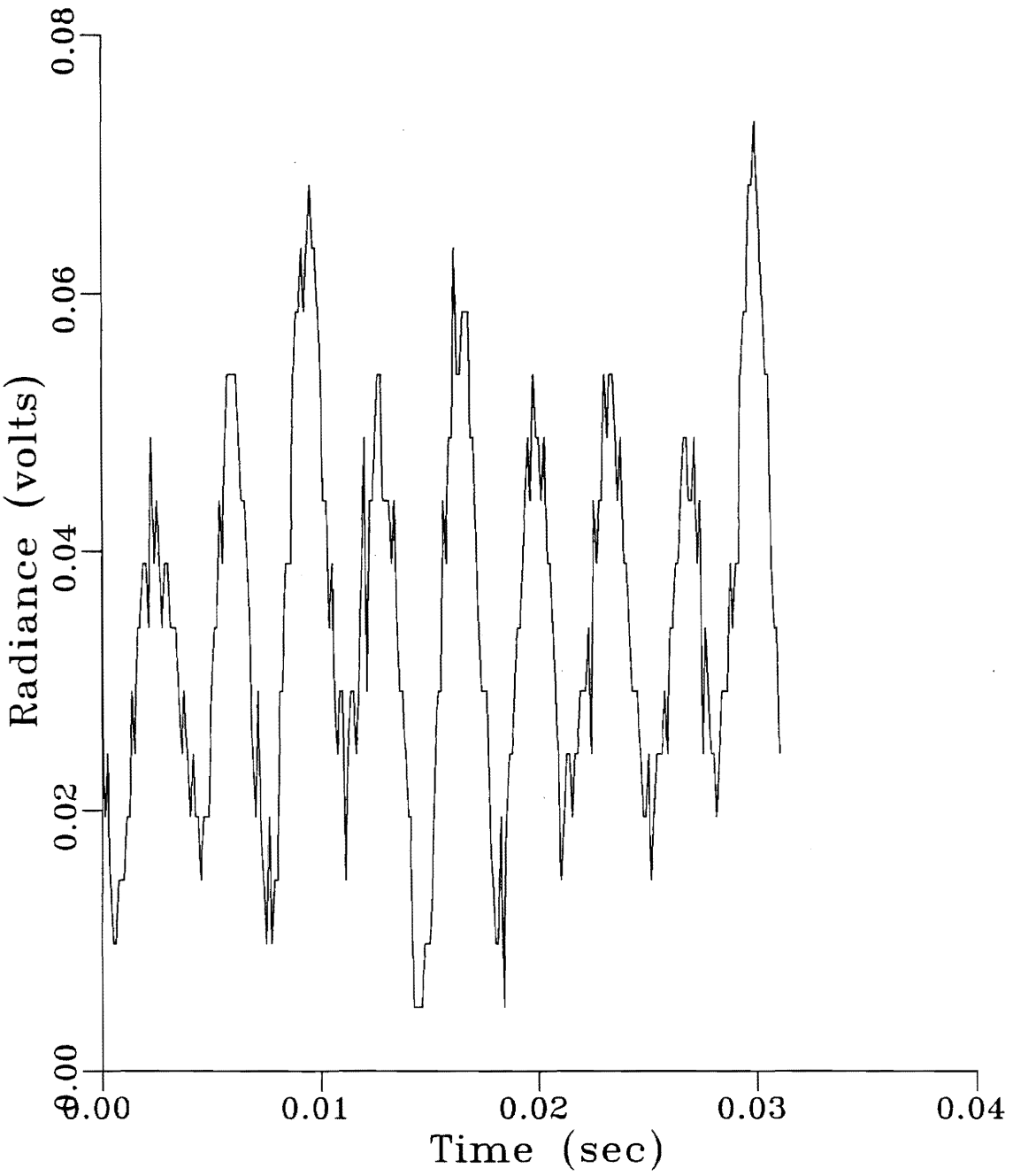

Fig. 47. Cycle-to-cycle variation in the radiance signal of graphite-epoxy.

as shown in Figs. 48 - 50. Typically, the temperature reaches a maximum as the velocity reaches a maximum, although there may be some phase difference depending on the mean velocity of oscillation, and position of the target spot. Since the velocity reaches its maximum magnitude twice in a cycle, the frequency of the radiance signal is therefore twice the oscillating frequency.

The mean temperatures at the two sliding velocities, computed from the radiance data are shown in Fig. 51. Temperature values for the three fiber orientations examined are also shown. It can be observed that at the lower velocity, the difference in temperature rise among the three fiber orientations is small and probably not significant. With an increase in velocity, the temperature rise is seen to increase in all three fiber orientations. In addition, the anti-parallel orientation shows higher temperature rise at the higher velocity.

In Fig. 52, the temperature rises of both the unidirectional sliding and oscillatory motions are plotted as a function of frictional heat generated. It is interesting to note that in spite of two completely different velocity modes, the temperature rise increases almost linearly with increase in frictional heat generated, up to the aforementioned maximum temperature value. After that, the temperature rise levels off for each of the three fiber orientations. The effect of fiber orientation on surface temperature rise is relatively small.

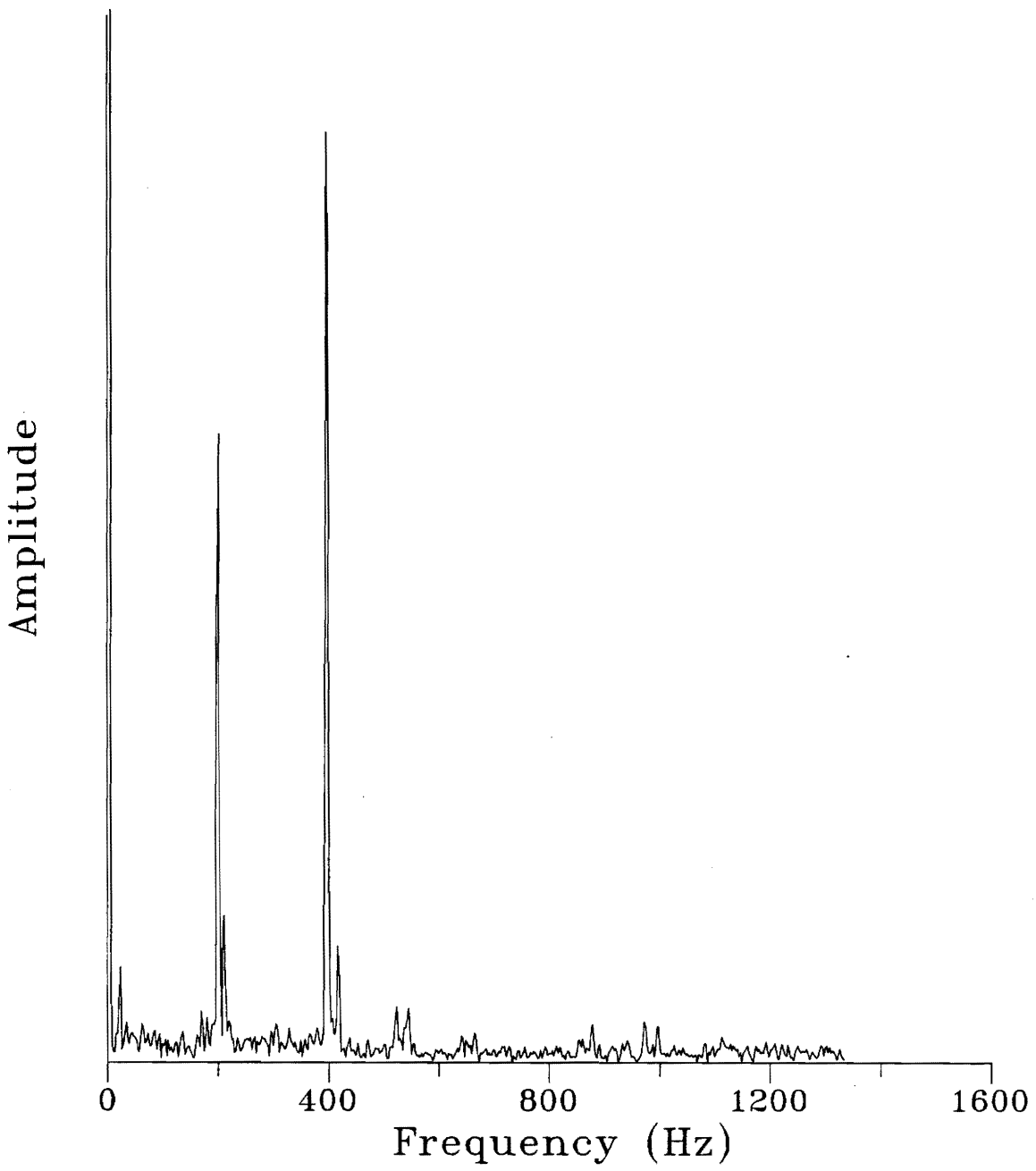

Fig. 48. Fast Fourier Transform of the radiance signal of graphite-epoxy in oscillating contact.

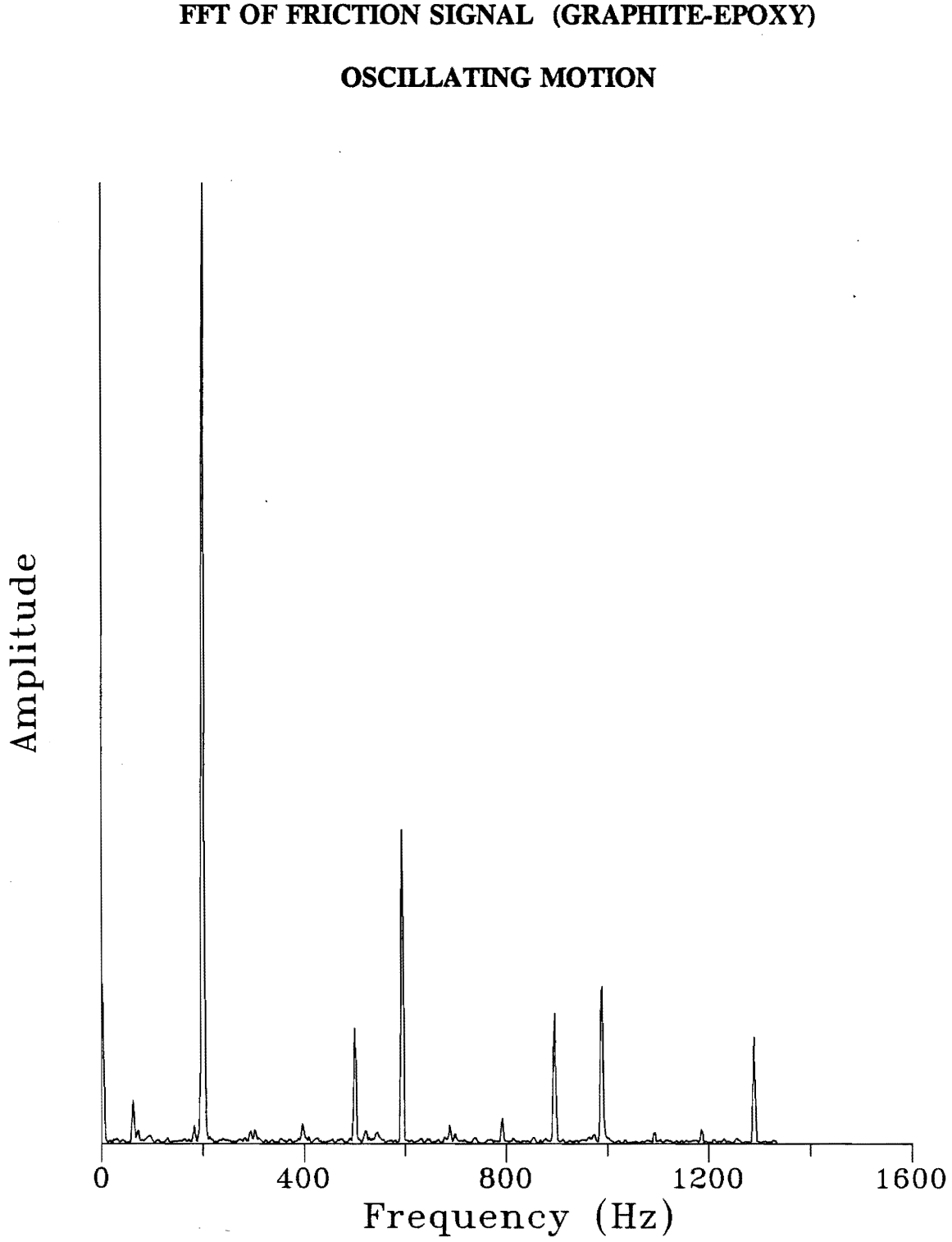

Fig. 49. Fast Fourier Transform of the friction signal of graphite-epoxy in oscillating contact.

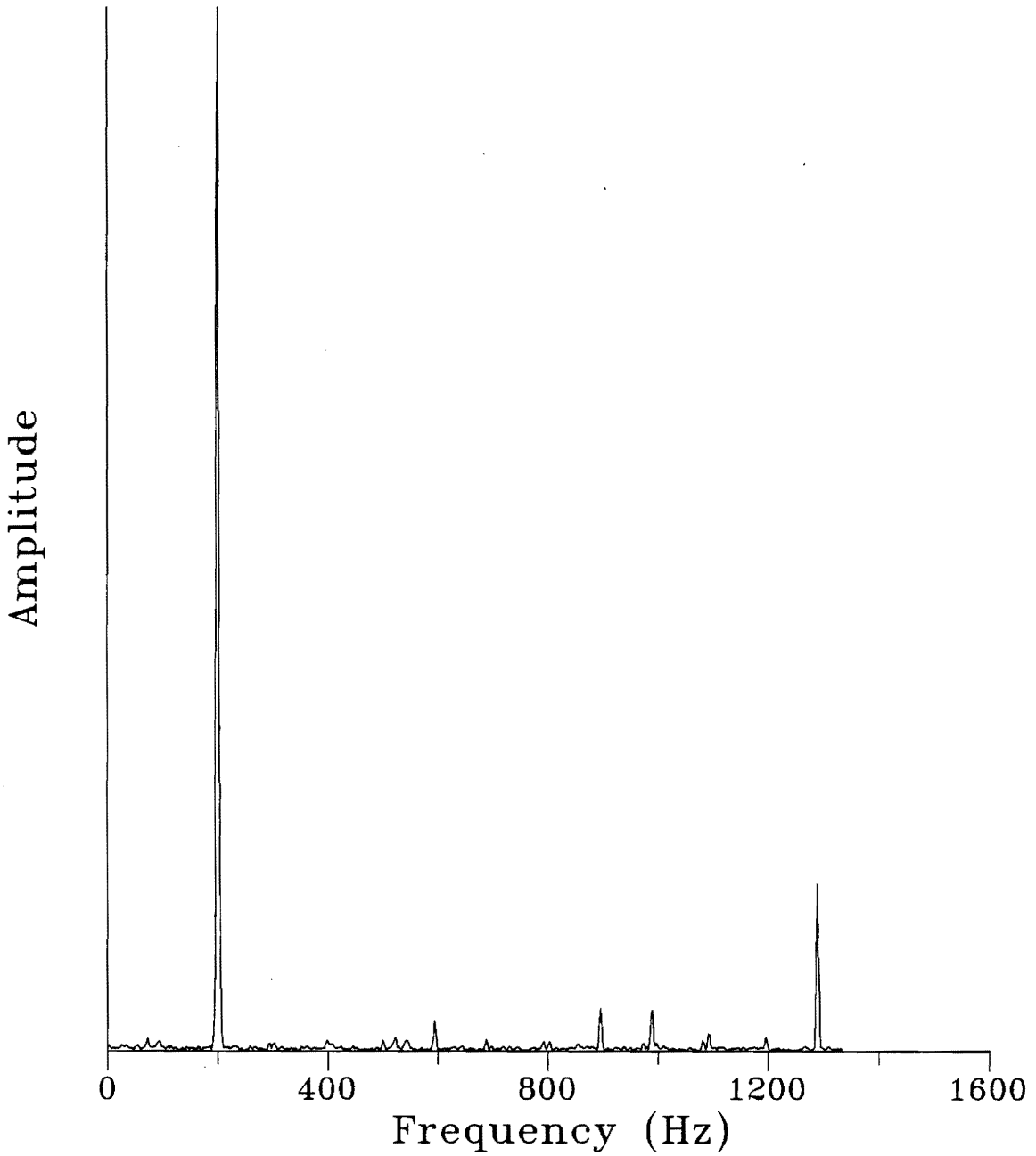

Fig. 50. Fast Fourier Transform of the velocity signal of graphite-epoxy in oscillating contact.

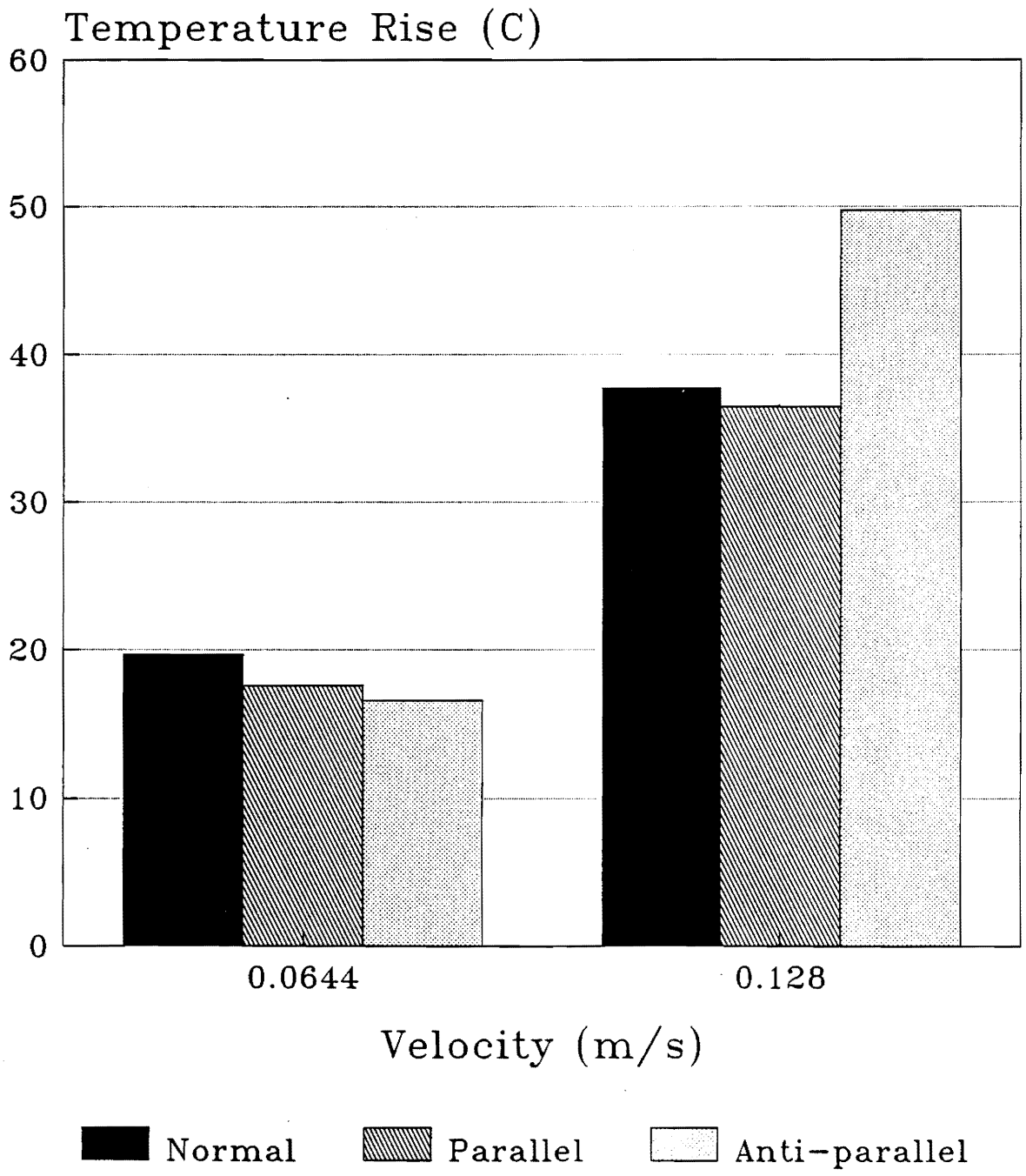

Fig. 51. Mean surface temperature rise of graphite-epoxy in oscillating contact. The values shown are the averages of two experiments.

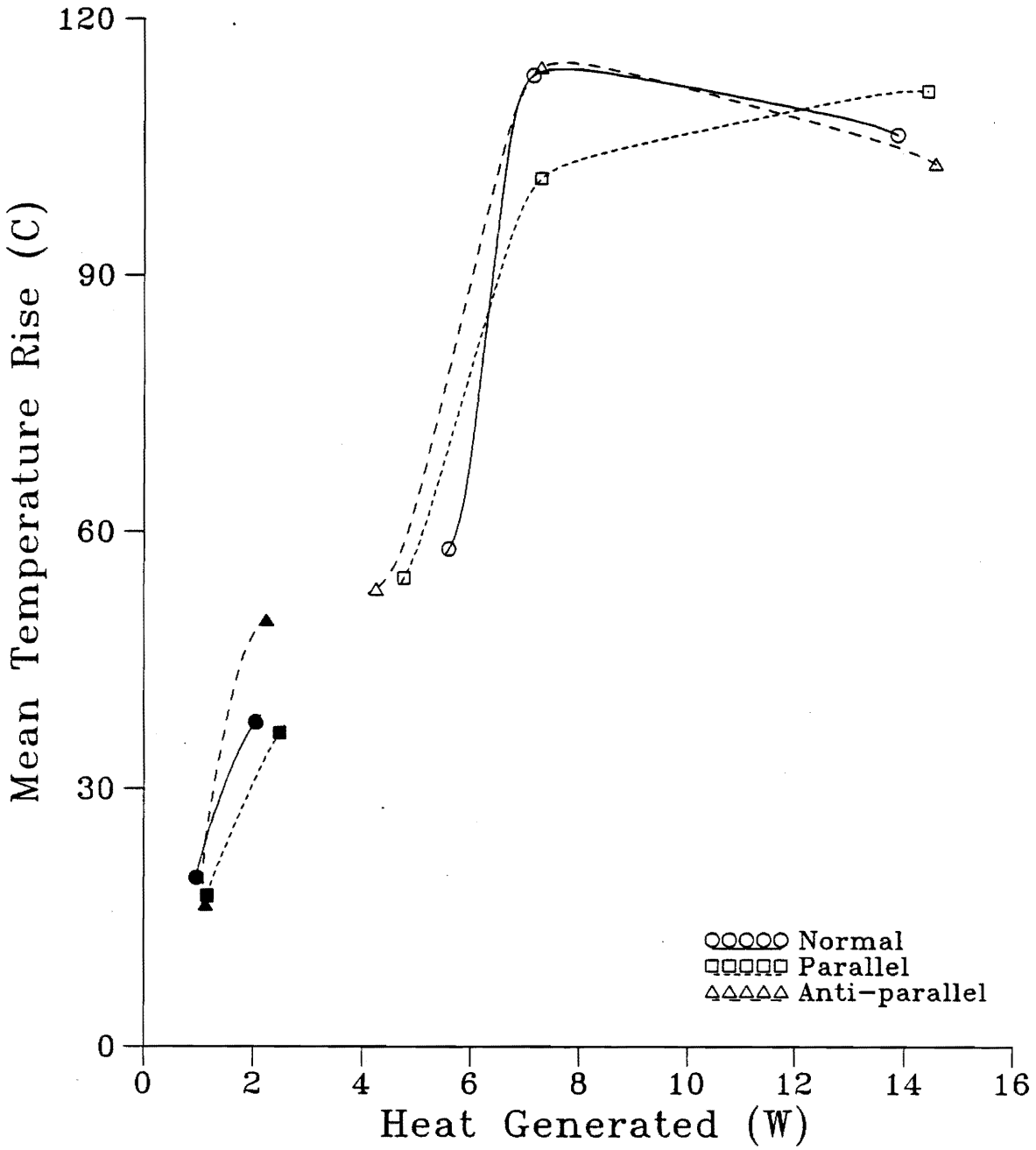

Fig. 52. Mean surface temperature rise -vs- frictional heat generation of graphite-epoxy. The data from the unidirectional sliding experiments are plotted along side the data from the oscillating experiments. Results from oscillating experiments are represented by solid symbols. The almost linear increase in temperature at low velocity range may be observed.

4.2.2.3 Wear Results

As before, the wear results are presented in terms of volume of wear after a fixed sliding distance. The results for the two mean oscillating velocities are summarized in Fig. 53. The three fiber orientations are seen to show different wear behaviors. With an increase in velocity, wear decreases for the normal orientation, increases for the parallel orientation, and stays unaffected for the anti-parallel orientation. Moreover, highest wear is observed in the normal orientation and lowest in the anti-parallel orientation.

4.2.3 Graphite-epoxy : Contact Area Estimation

Three experiments, one for each of the three fiber orientations, at 4 N load and unidirectional sliding velocity of 7 m/s, were conducted to estimate the contact area change during the experiment. The second technique (as described in section 3.1.6), in which the contact and no-contact photomacrographs are compared was used here. Thus the contact area was estimated under static conditions, but after different sliding distances. Results could be obtained in the parallel and anti-parallel orientations only. In the normal orientation, no clearly distinguishable contact area could be observed. This might have been due to very fine distribution of the real area of contact in the normal orientation, which was beyond the resolution capability of the macroscope. It could also have been due to different light absoptivity of the fibers along the ends compared to the sides (as in parallel and anti-parallel orientations).

The results of contact area variation as a function of sliding distance in the

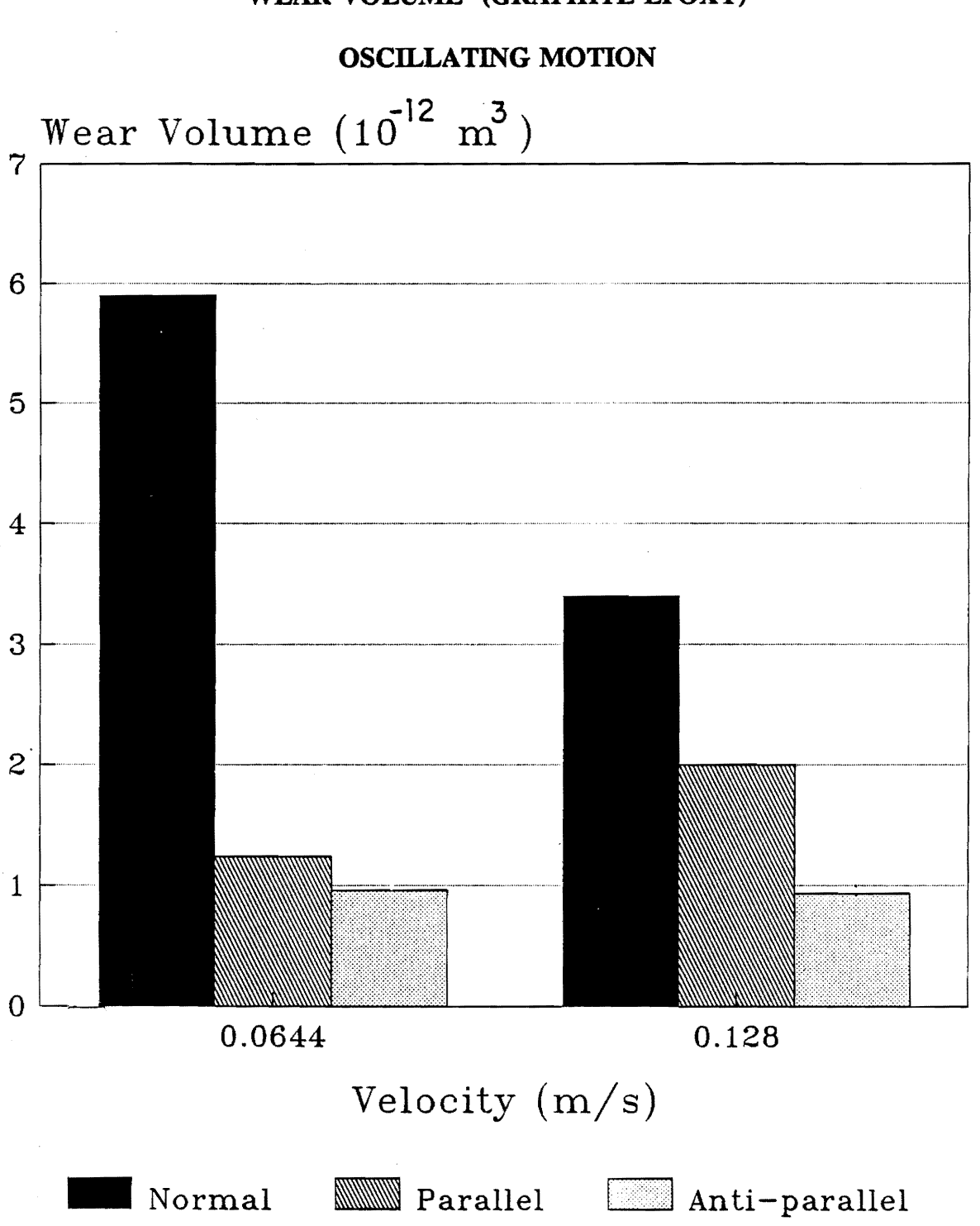

Fig. 53. Wear volume of graphite-epoxy after 28 m of sliding in oscillatory motion. The load was 40 N for all the experiments. The values shown are the averages of two experiments.

parallel and anti-parallel orientations are plotted in Fig. 54. It can be seen that in the parallel orientation, the estimated real area of contact increases sharply from the elastic contact area, up to a maximum and then remains constant. On the other hand, the increase in estimated real area of contact in the anti-parallel orientation is more gradual.

Figures 55 - 57 show the variation in static contact area, coefficient of friction, surface temperature rise and wear volume as a function of sliding distance in the three fiber orientations. In the normal orientation, as previously mentioned, no data on the contact area were obtained. Experiments were conducted for a much larger sliding distance (up to 7 km.) to observe long term changes in the tribological parameters. The following observations can be made from these data.

1. The coefficient of friction is seen to increase initially and then decrease with increasing sliding distance. The variation is more random in the normal orientation. The coefficient of friction in the normal orientation is seen to vary between 0.8 to 1.1. It should be mentioned here that these values obtained from this experiment are much higher than the values obtained for this orientation under similar sliding conditions; the reasons for these high values are not known. There is not much difference in the coefficients of friction between the parallel and the anti-parallel orientations, which vary within 0.4 - 0.55.
2. The increase in wear volume with sliding distance is seen to be fairly linear initially, but the rate increases after some distance. The difference in wear rates among the three fiber orientations is also evident from these graphs. It is found to be highest in the normal orientation (.006 mm^3/km), fairly high in the parallel

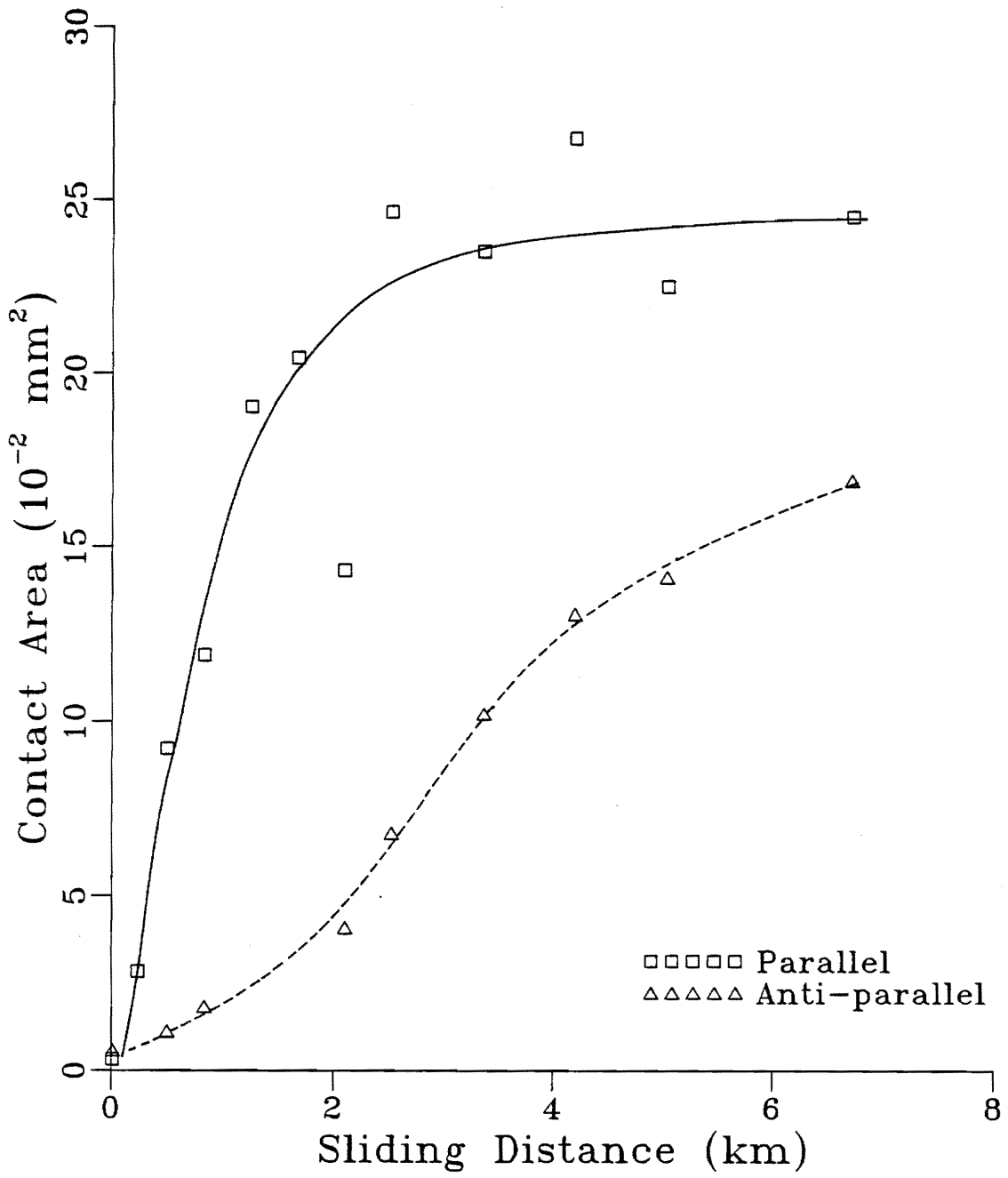

Fig. 54. Contact area variation with sliding distance of graphite-epoxy in the parallel and anti-parallel orientations. Calculated elastic area = .0111 mm^2 and calculated plastic area = .0114 mm^2.

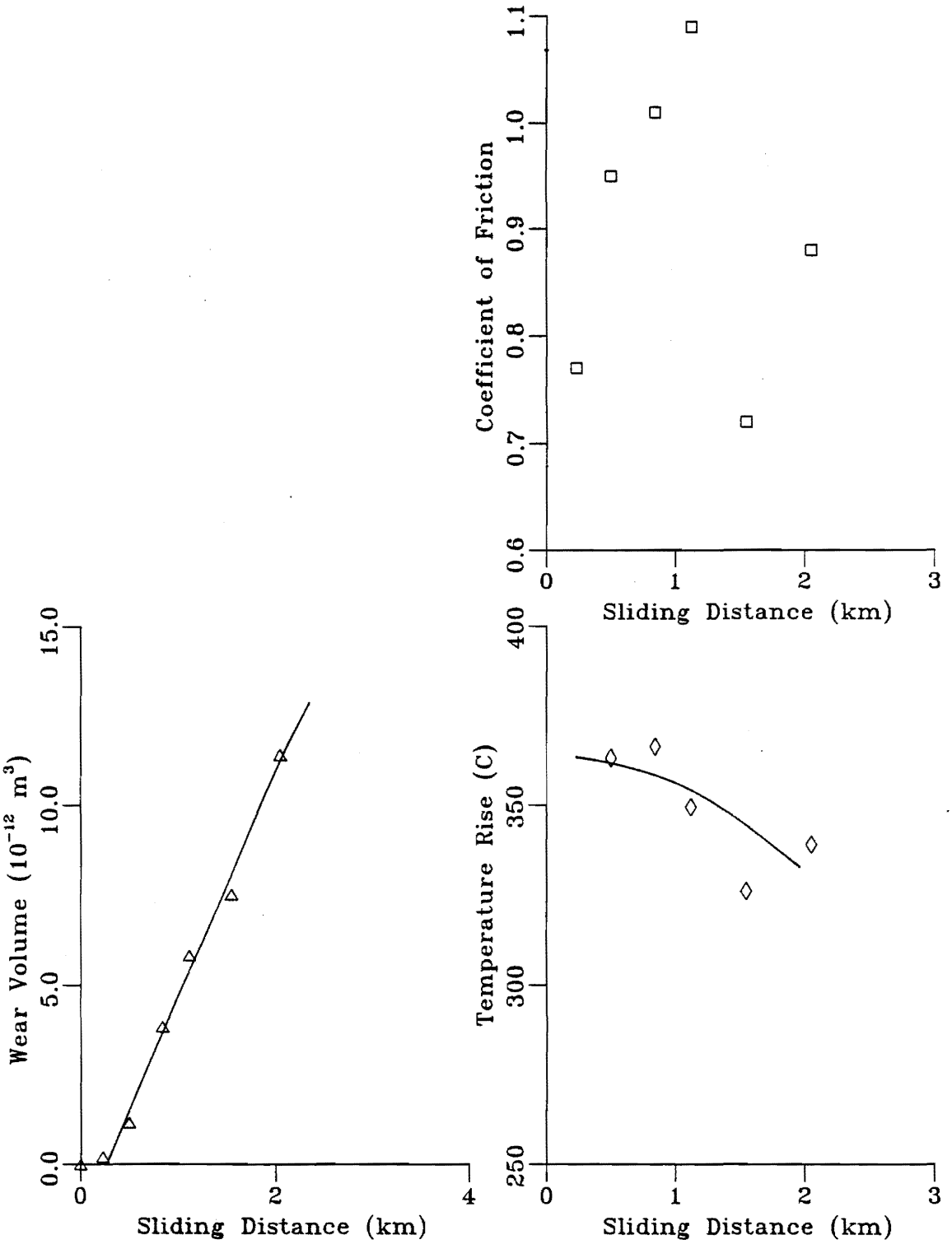

Fig. 55. Variation of coefficient of friction, wear and temperature rise for the normal orientation of graphite-epoxy in unidirectional sliding.

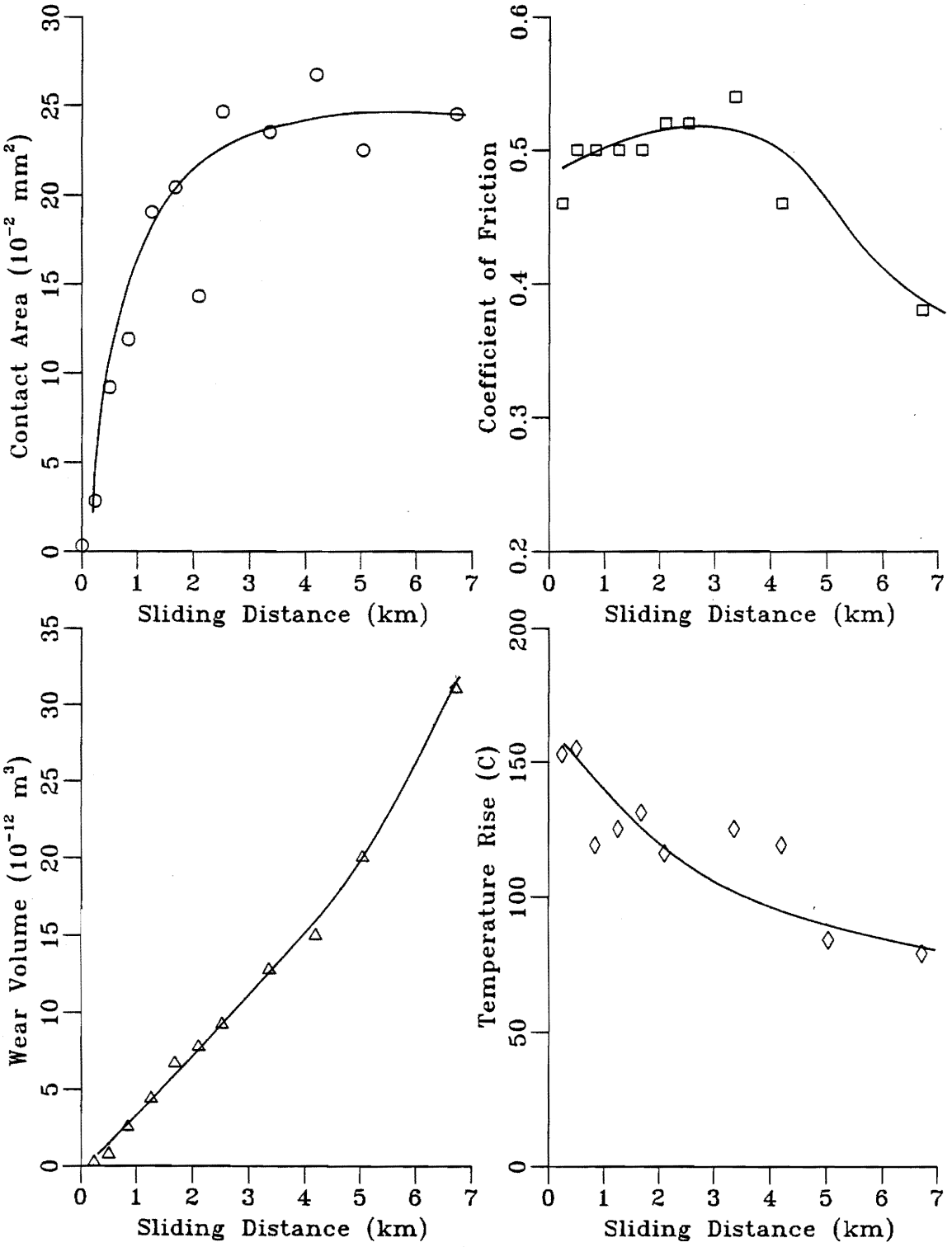

Fig. 56. Variation of contact area, coefficient of friction, wear and temperature rise for the parallel orientation of graphite-epoxy in unidirectional sliding.

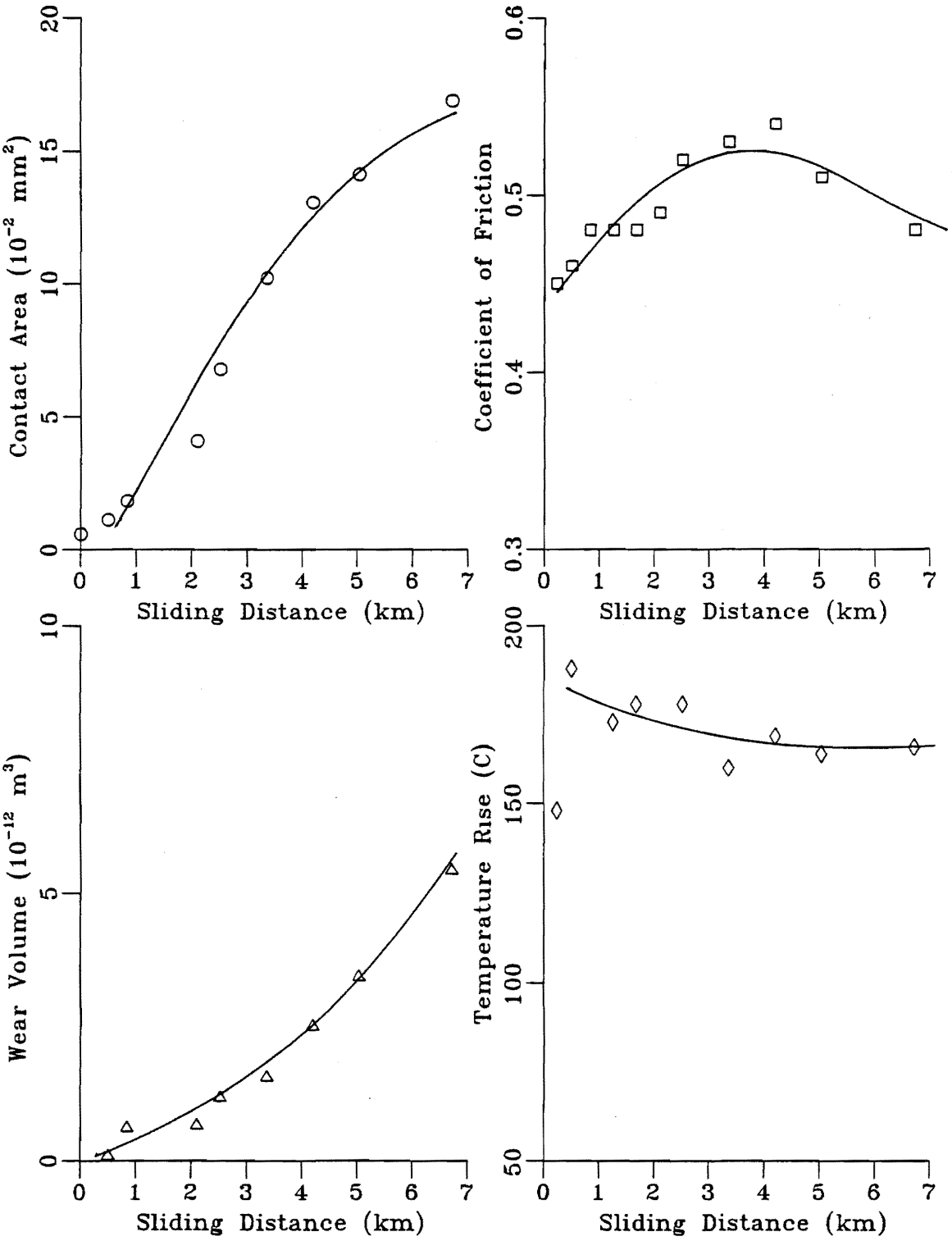

Fig. 57. Variation of contact area, coefficient of friction, wear and temperature rise for the anti-parallel orientation of graphite-epoxy in unidirectional sliding.

orientation (.0043 mm^3/km) and lowest in the anti-parallel orientation (.0007 mm^3/km).

3. The data on surface temperature rise appears to be more scattered. The general observation for all three fiber orientations is that the temperature rise is higher at the start of the experiment, but falls to a fairly steady value after some distance of sliding. These steady maximum temperature values are on the order of 350°C in the normal orientation, 80°C in the parallel orientation and 160°C in the anti-parallel orientation.

4.3 CARBON-PEEK : *Unidirectional Sliding*

4.3.1 Friction Results

The friction torque traces of the unidirectional sliding experiments of carbon-PEEK are very much like the ones shown by graphite-epoxy. As in the case of graphite-epoxy, friction force increases almost instantaneously from zero to a certain value at the start of the experiment. Thereafter, it is seen to increase rather gradually for some sliding distance before levelling out. In some of the experiments with the anti-parallel orientation, the signal is seen to increase continuously during the experiment.

The coefficients of friction for the carbon-PEEK sliding on sapphire are listed in Table 9. The variation of coefficient of friction with velocity for the three fiber orientations is plotted in Fig. 58. The coefficients of friction are seen to be highest in the anti-parallel orientation and lowest in the normal orientation. At low velocities, the

Table 9. Test results of coefficient of friction of carbon-PEEK.
The values within brackets are the results obtained from a third test.

COEFFICIENT OF FRICTION

VELOCITY	FIBER ORIENTATION					
	NORMAL		PARALLEL		ANTI-PARALLEL	
	Exp. 1	Exp. 2	Exp. 1	Exp. 2	Exp. 1	Exp. 2
2.17 m/s	.62	.75	.54	.56	.55	.57
3.5 m/s	.39	.51	.41	.57(.6)	.74(.67)	.57
7.0 m/s	.40	.43	.44	.42	.49	.44

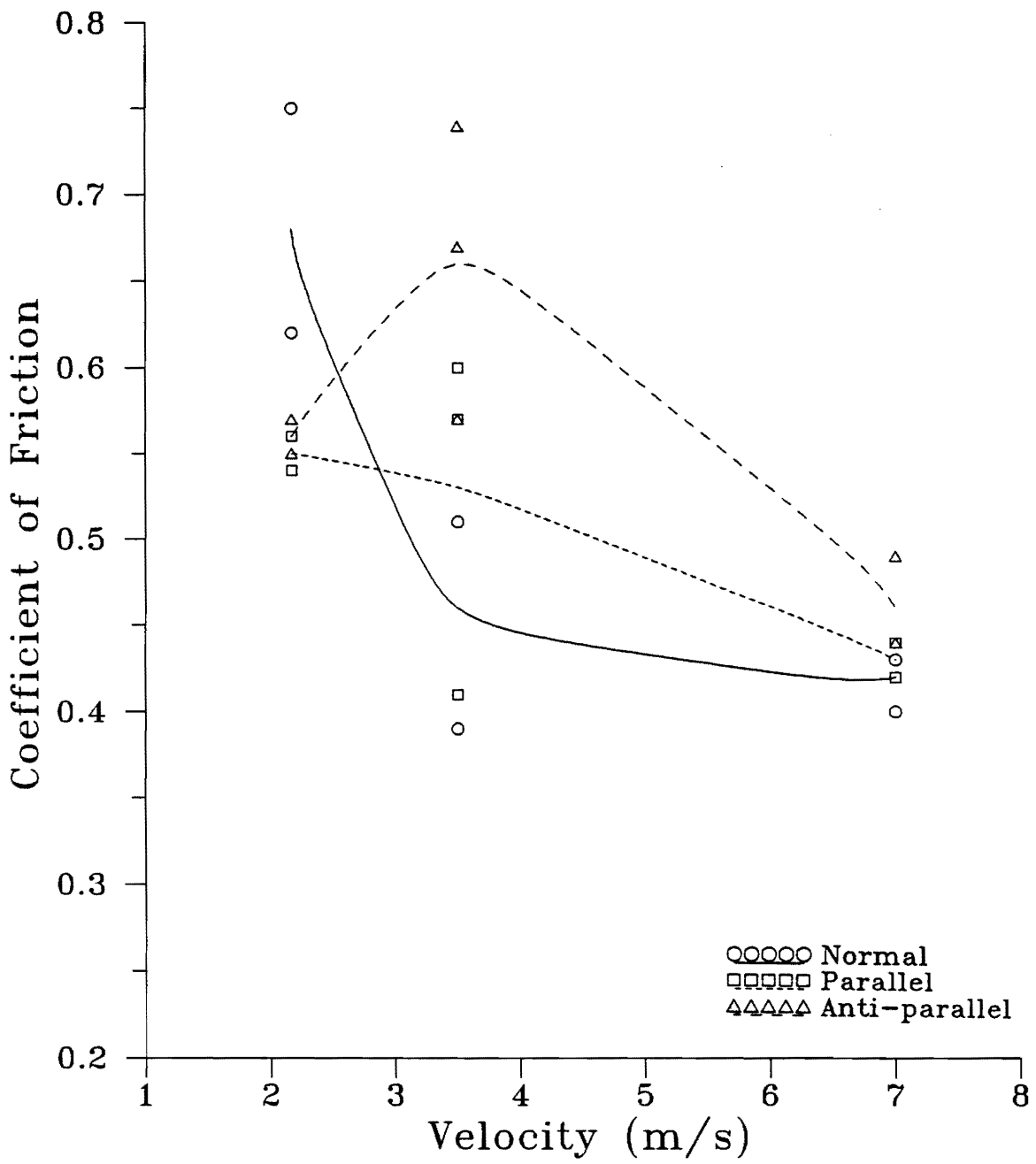

Fig. 58. Variation in coefficient of friction of carbon-PEEK with velocity.

coefficient of friction is found to be highest in the normal orientation. As in the case of graphite-epoxy, coefficients of friction in the normal and parallel orientations show a decreasing trend with increasing velocity, with the slope tending to level off at higher velocities. In the anti-parallel orientation, the coefficient of friction is seen to increase initially, but then decrease at higher velocities. Analysis of variance shows that the dependence of coefficient of friction on fiber orientation and velocity is highly significant. The ANOVA results are tabulated in Appendix G.

4.3.2 Radiance and Temperature Results

The nature in which the radiance in carbon-PEEK changes with time during the experiment is very similar to the behavior exhibited by graphite-epoxy. The radiance typically increases from the ambient radiance to a certain maximum value in each experiment within the first 100 - 200 m of sliding. In certain cases, a further increase in radiance could also be observed at a later stage in the experiment.

Temperatures for each experiment (converted from the radiance using the emissivity data) are listed in Table 10. Maximum and mean temperature rises as a function of sliding velocity are shown in Figs. 59 and 60, respectively. Both values are reported since the temperature fluctuated significantly over a cycle. The average temperature rise represents the temperature rise averaged over a cycle of rotation.

The variation of surface temperature rise with velocity shows the same kind of trend which is observed in case of graphite-epoxy. The mean surface temperature rise increases with velocity initially until it reaches a maximum value. After this value is

Table 10. Test results of maximum and mean surface temperature rises of carbon-PEEK.

MAXIMUM TEMPERATURE RISE (°C)

VELOCITY	FIBER ORIENTATION					
	NORMAL		PARALLEL		ANTI-PARALLEL	
	Exp. 1	Exp. 2	Exp. 1	Exp. 2	Exp. 1	Exp. 2
2.17 m/s	142.3	117.4	80.8	94.4	95.9	119.3
3.5 m/s	206.7	180.1	123.3	129.9 (159.4)	161.3	191.3 (180.8)
7.0 m/s	179.6	188.7	192.6	146.0	197.6	184.6

MEAN TEMPERATURE RISE (°C)

VELOCITY	FIBER ORIENTATION					
	NORMAL		PARALLEL		ANTI-PARALLEL	
	Exp. 1	Exp. 2	Exp. 1	Exp. 2	Exp. 1	Exp. 2
2.17 m/s	106.7	62.1	58.2	68.5	72.0	87.3
3.5 m/s	182.2	158.8	91.1	115.4 (135.6)	127.1	168.2 (158.8)
7.0 m/s	153.8	153.1	153.7	129.7	167.5	137.4

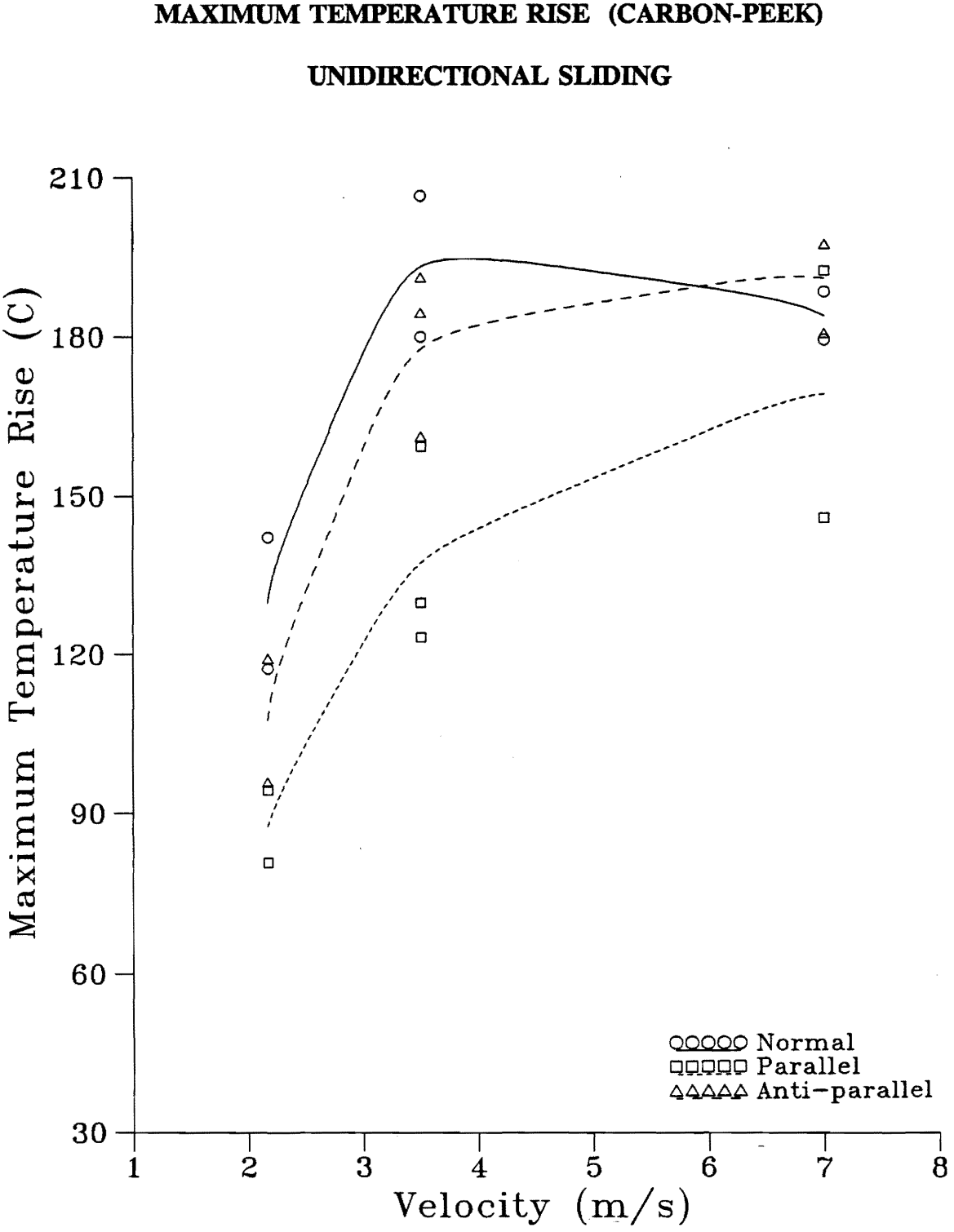

Fig. 59. Variation of maximum temperature rise of carbon-PEEK with velocity.

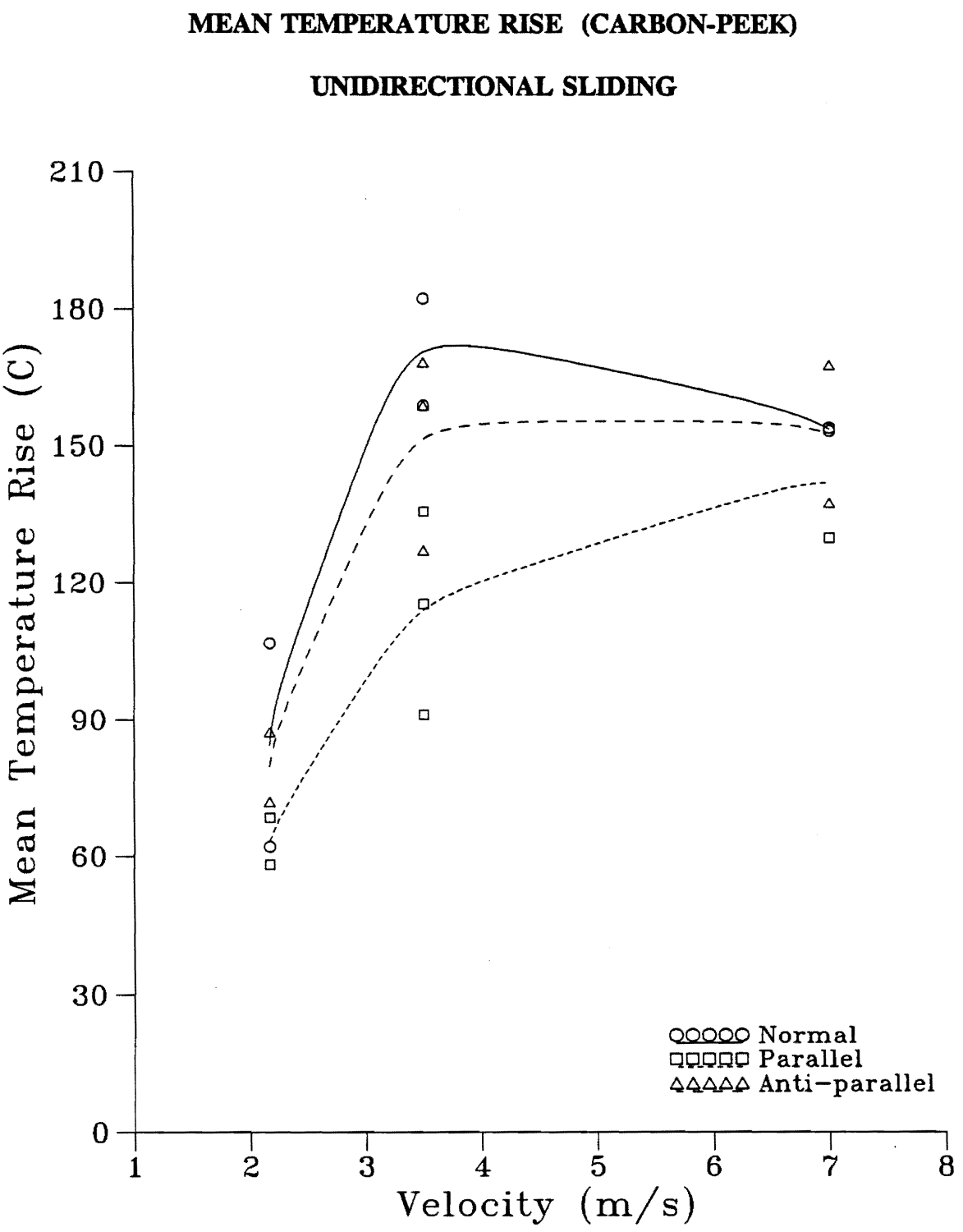

Fig. 60. Variation of mean temperature rise of carbon-PEEK with velocity.

reached, there is not much change in temperature rise with a further increase in sliding velocity, even though there is an increase in the amount of heat generated. This value is different from that reached in case of graphite-epoxy. In the parallel orientation, this temperature was not yet reached within the velocity range studied, but the trend indicates that it would ultimately reach this value at a higher velocity. Some possible reasons for such behavior are discussed in the next chapter.

The temperature values are found to be highest in the normal orientation and lowest in the parallel orientation, except at high velocities where the normal orientation resulted in the lowest temperature rise. However, the maximum levels of the mean surface temperatures in the three fiber orientations are fairly close. Even though the general behavior shown by carbon-PEEK is very similar to the behavior of graphite-epoxy, the measured temperature levels are found to be higher with carbon-PEEK.

The ANOVA results of mean surface temperature rise of carbon-PEEK are given in Appendix G. The effects of fiber orientation and velocity on mean surface temperature are found to be highly significant.

4.3.3 Wear Results

The wear volumes for all three fiber orientations at different velocities are reported in Table 11. The variation of wear with sliding velocity is plotted in Fig. 61.

It can be seen that in the normal and anti-parallel orientations, wear initially increases up to a certain maximum and then decreases with an increase in velocity. In the parallel orientation, there is very little effect of sliding velocity on wear. Wear is

Table 11. Test results of wear volume of carbon-PEEK after 520m of sliding.

WEAR VOLUME (10^{-12} m^3)

VELOCITY	FIBER ORIENTATION					
	NORMAL		PARALLEL		ANTI-PARALLEL	
	Exp. 1	Exp. 2	Exp. 1	Exp. 2	Exp. 1	Exp. 2
2.17 m/s	2.6	5.9	2.5	2.1	1.2	.85
3.5 m/s	7.4	2.8	4.5	1.4 (.93)	5.1	.38 (1.33)
7.0 m/s	4.3	1.9	2.8	1.6	1.45	1.3

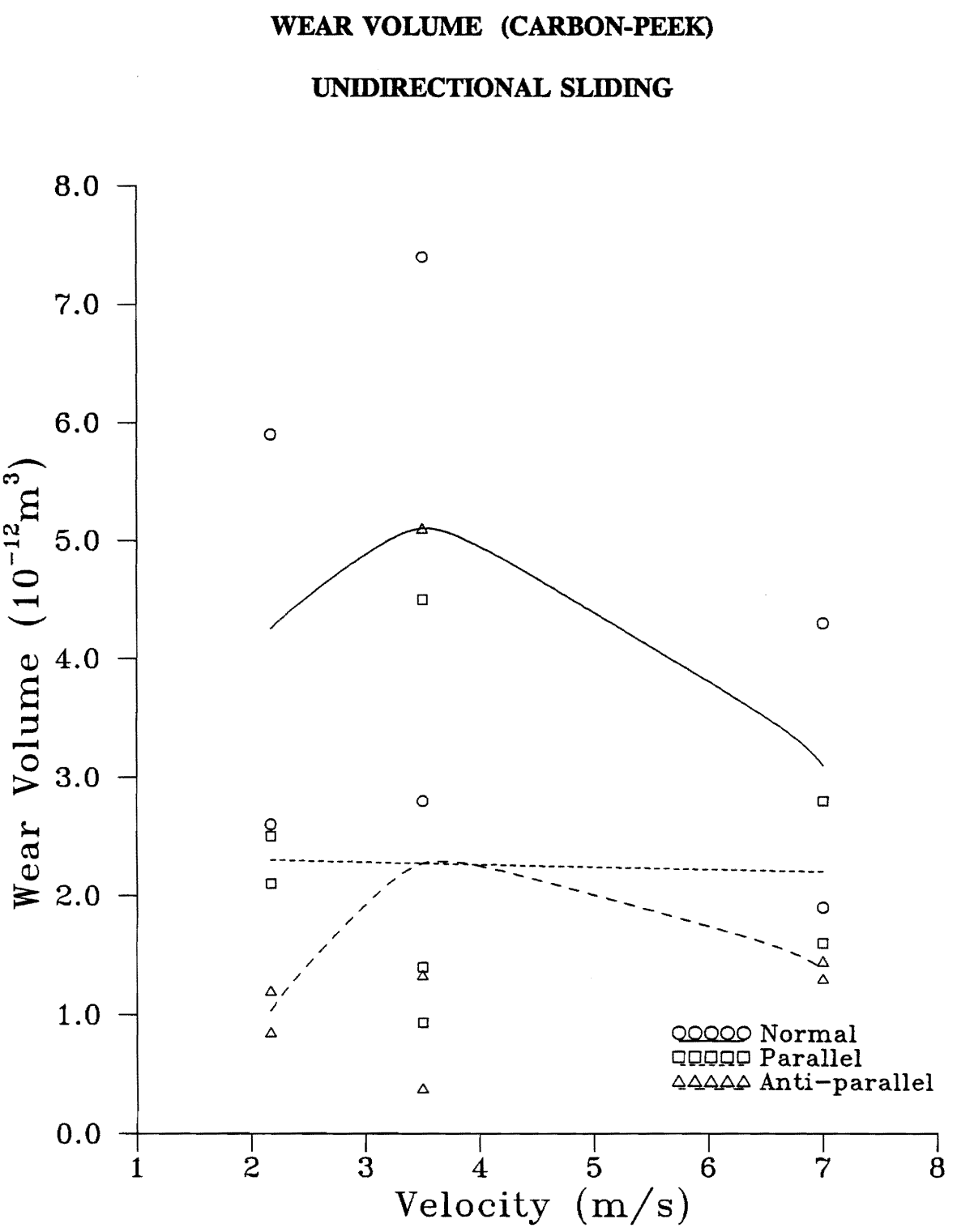

Fig. 61. Variation of wear volume of carbon-PEEK with velocity. The sliding distance was 520 m in each experiment.

found to be highest in the normal orientation, and lowest in the anti-parallel orientation. The ANOVA results (shown in Appendix G) also show that fiber orientation as well as velocity have significant effects on wear rate. Some possible reasons for this type of behavior are discussed in the next chapter.

Besides the measurement of wear, photomacrographs and scanning electron micrographs of the wear scars have also been analyzed. SEM pictures of some of the wear scars are shown in Figs. 62 - 64. These throw some light on the mechanisms of material removal. Some important observations from these micrographs are listed below.

1. The scar surfaces are not as smooth as they are with graphite-epoxy. Most of the SEM pictures show rough wear scars.
2. In all three fiber orientations, there is evidence of fiber breakage and pull-out from the matrix. These fiber pieces can be seen scattered all over the wear scar. The sizes of these broken fiber pieces varied, being very small (a fraction of the fiber diameter) in the normal orientation, and quite large (up to 6 - 8 times the fiber diameter) in the parallel orientation. This can be observed in Figs. 62 c), 62 d), 65 b) and 66 c).
3. The size of the wear debris is seen to vary from a few hundred nanometers to tens of micrometers.
4. There is some evidence of debonding at the fiber-matrix interphase in all the three fiber orientations. This can be observed in Figs. 63 b) and 64 b). It may be mentioned here that the DSC of the sample has shown some exothermic reactions in the temperature ranges attained during these experiments, this may be due to

a)

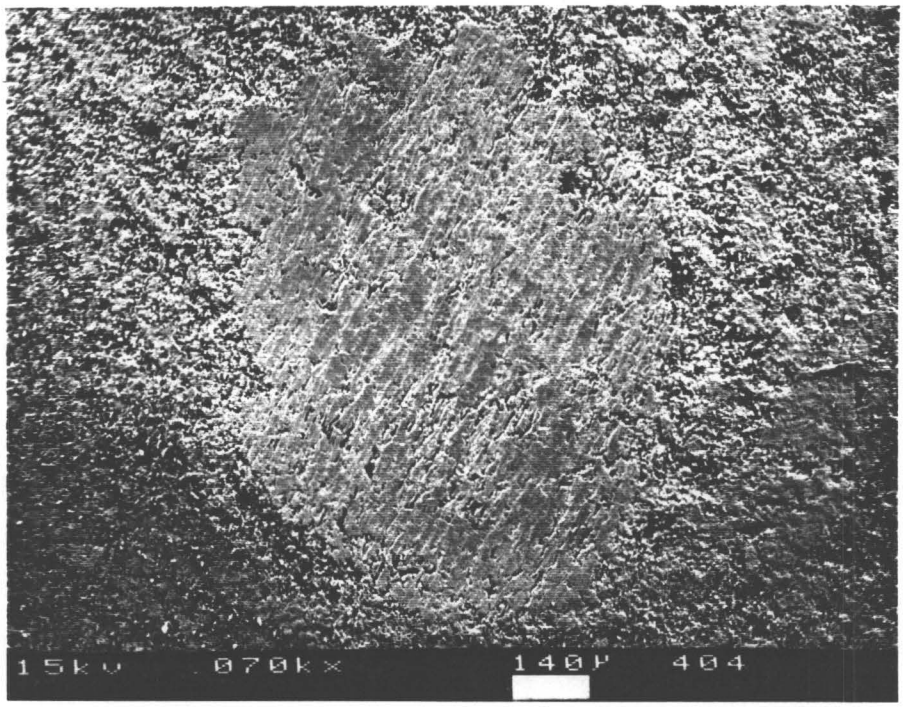

b)

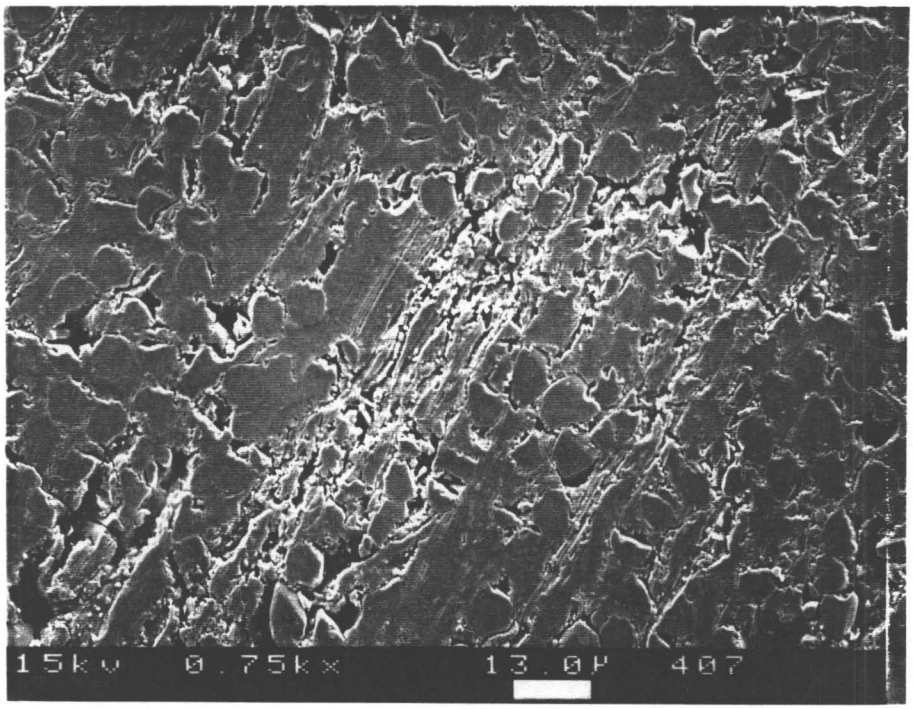

Fig. 62. SEM's of wear scar in the normal orientation of carbon-PEEK.
a) complete wear scar, **b)** portion of the scar at a higher magnification.

c)

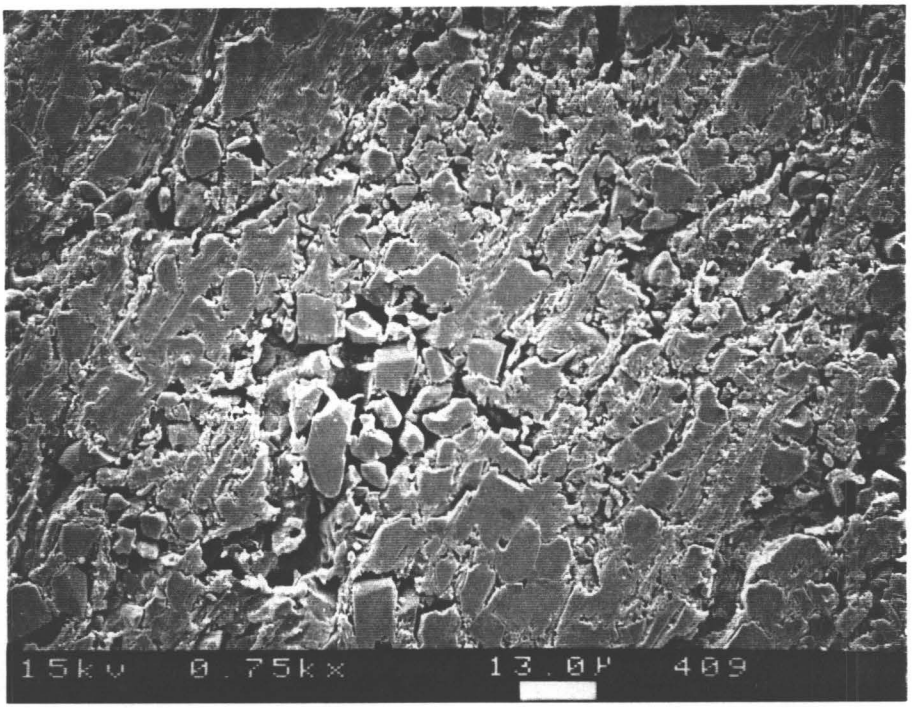

d)

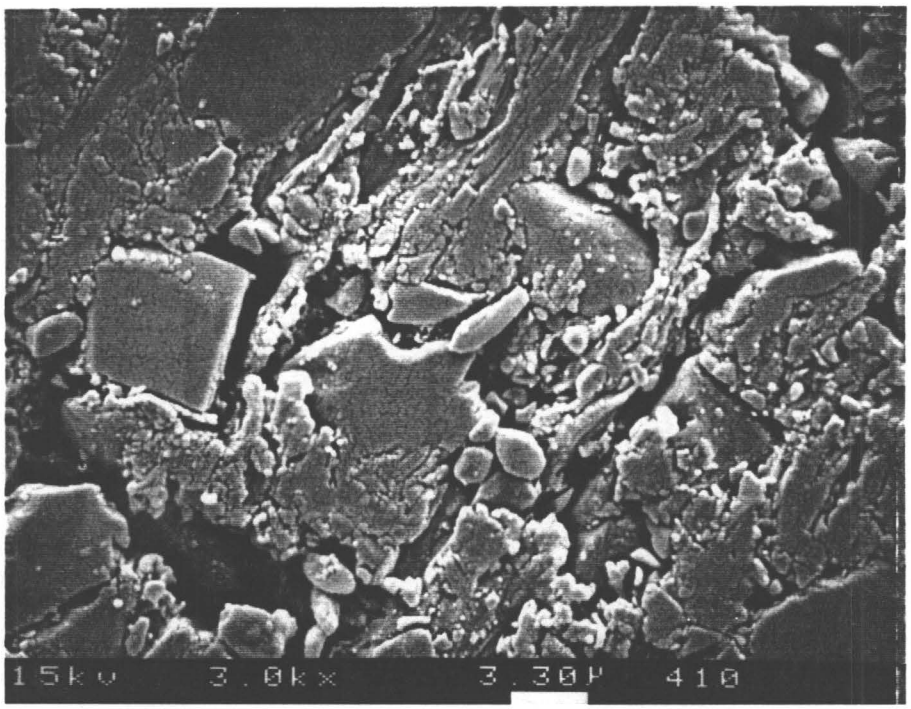

Fig. 62. (cont.) SEM's of wear scar in the normal orientation of carbon-PEEK. **c)** pieces of broken fibers in the wear debris, **d)** various sizes of wear debris.

e)

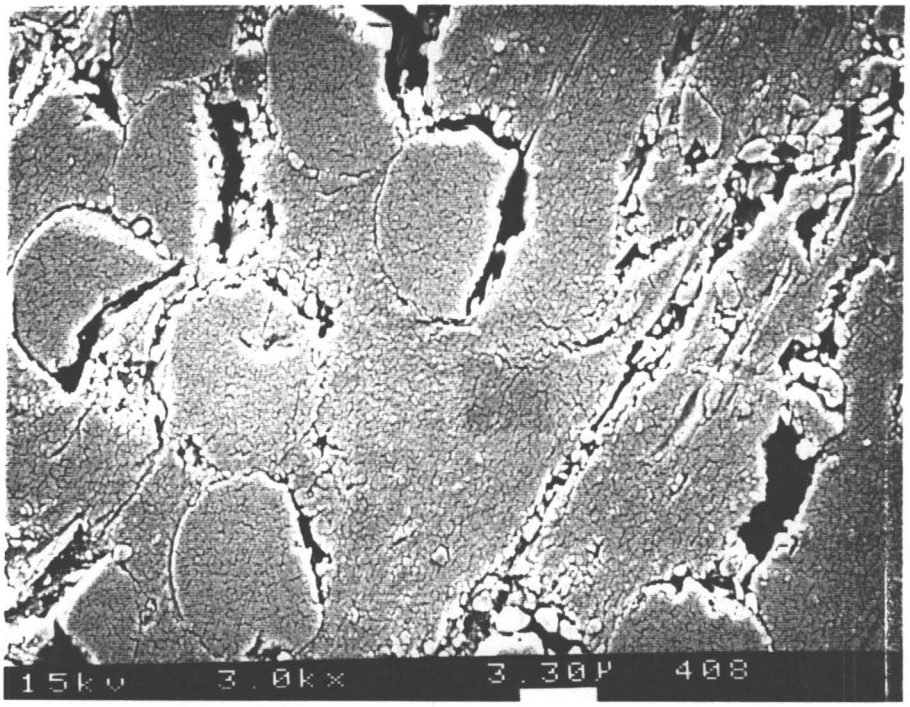

f)

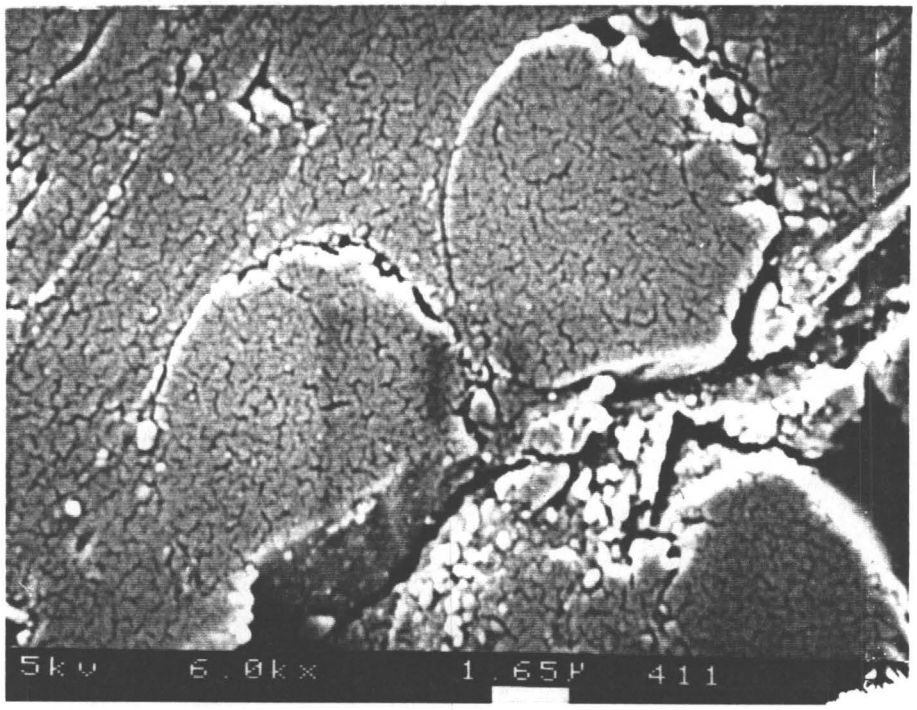

Fig. 62.(cont.) SEM's of wear scar in the normal orientation of carbon-PEEK. e) and f) fibers and matrix are removed uniformly.

a)

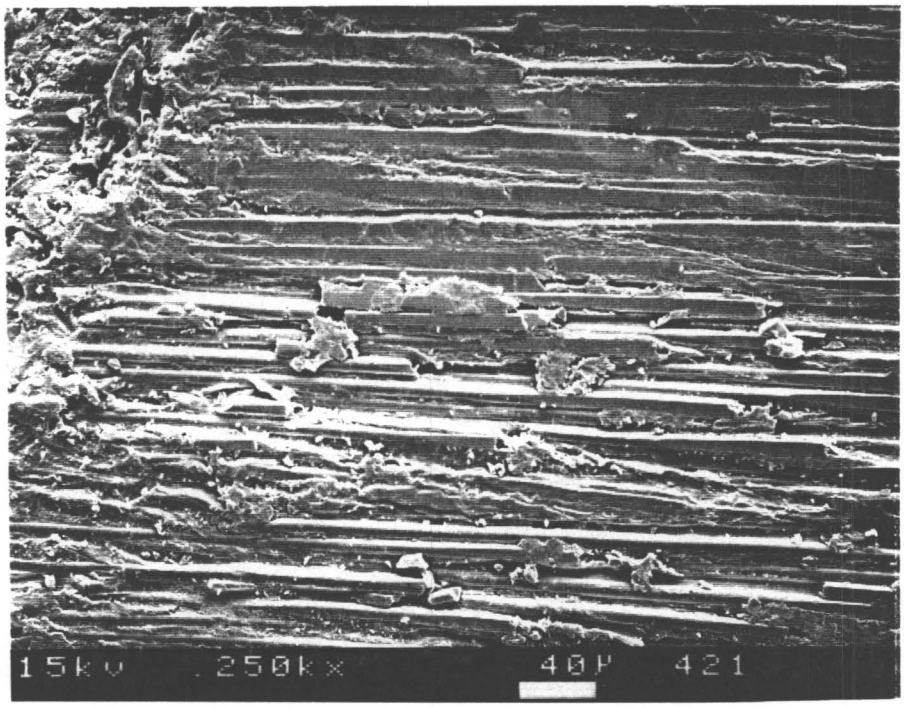

b)

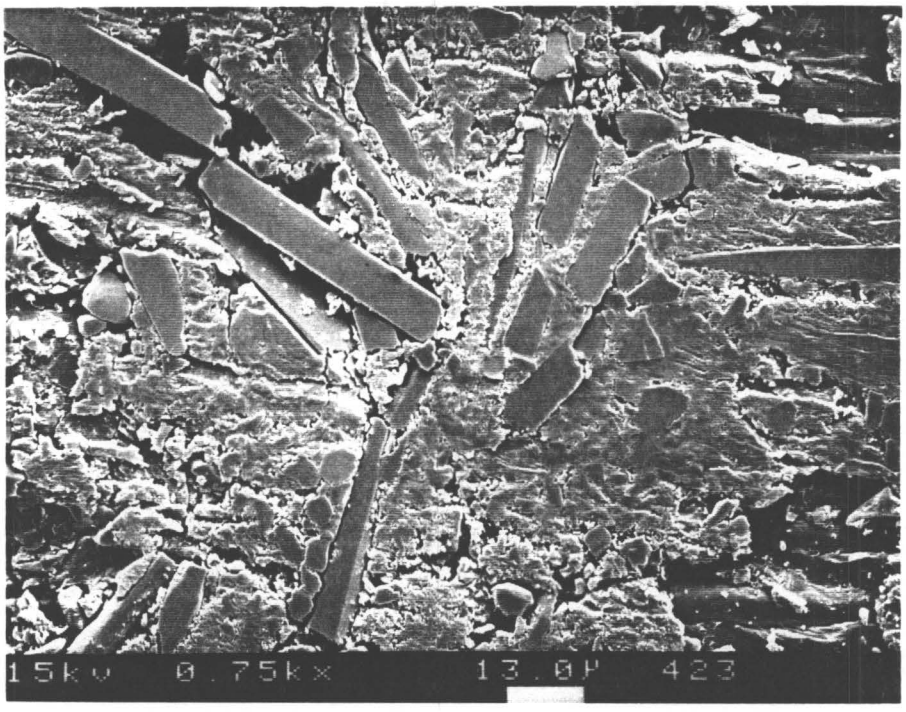

Fig. 63. SEM's of wear scar in the parallel orientation of carbon-PEEK. **a)** wear scar, **b)** fiber pieces in the wear debris.

c)

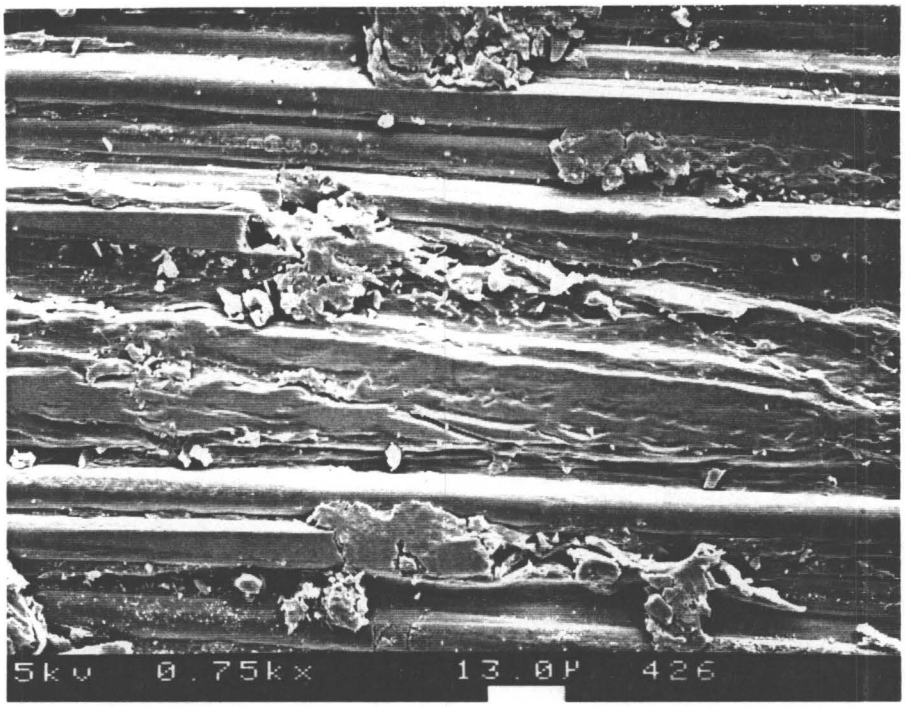

d)

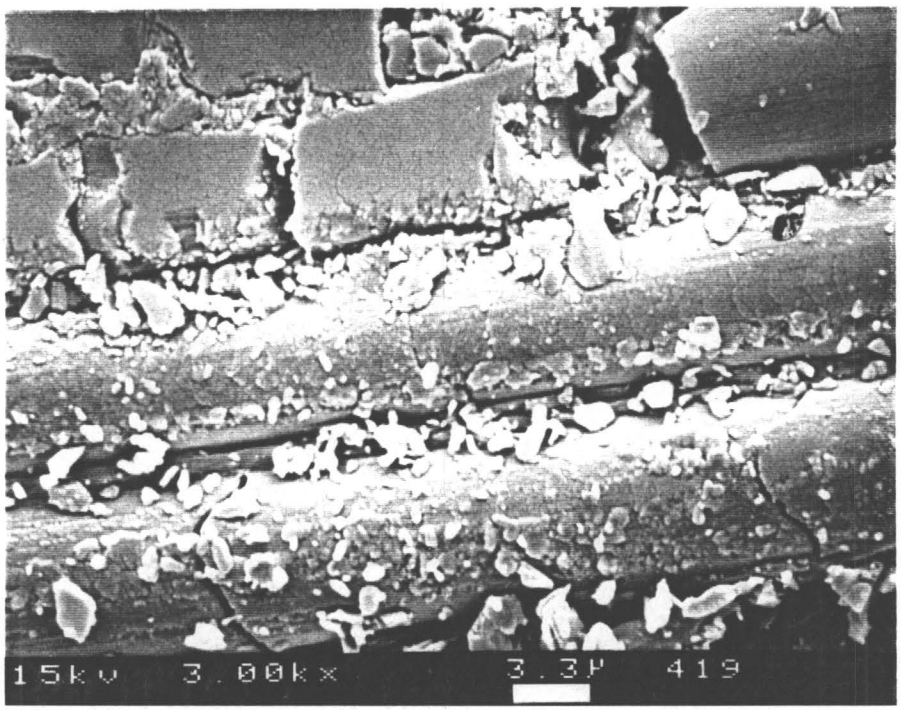

Fig. 63. (cont.) SEM's of wear scar in the parallel orientation of carbon-PEEK.
c) fiber removal through "pull out" from matrix as well as fiber wear,
d) transverse cracks in the fibers.

a)

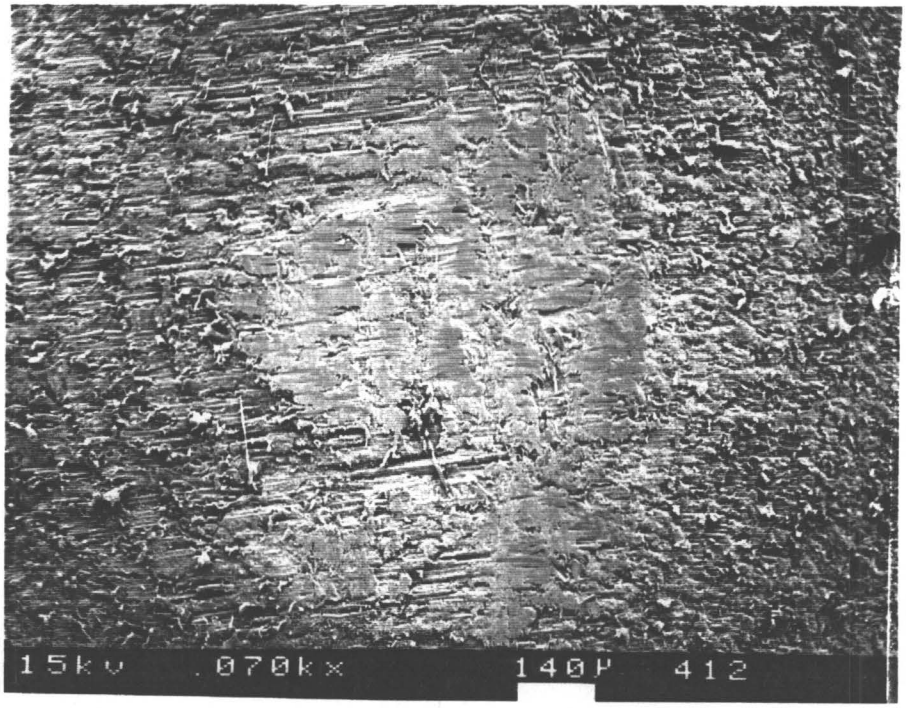

b)

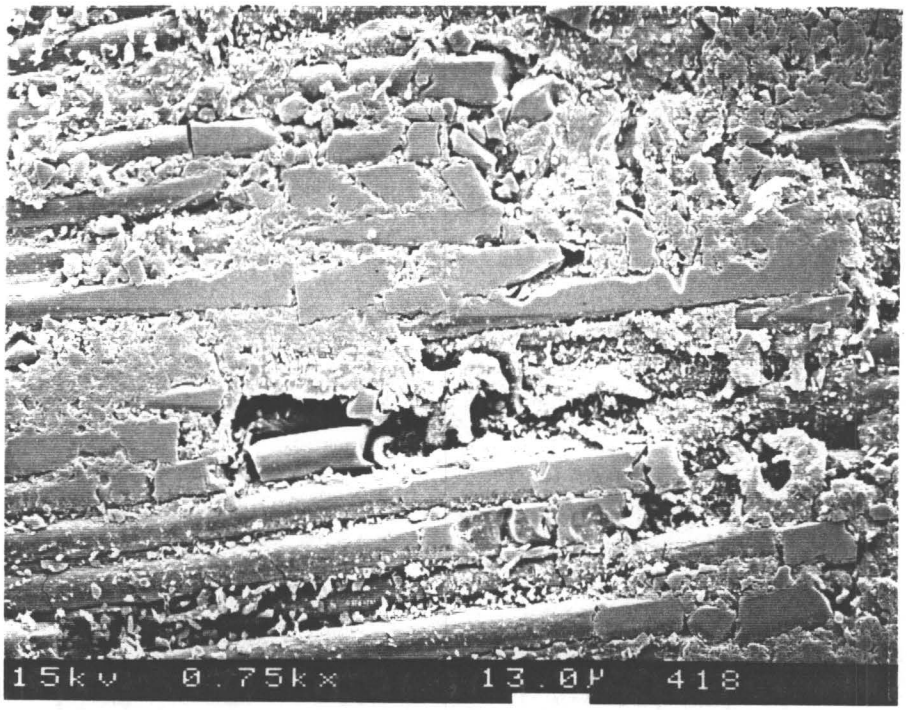

Fig. 64. SEM's of wear scar in the anti-parallel orientation of carbon-PEEK. **a)** complete wear scar, **b)** fiber breakage.

c)

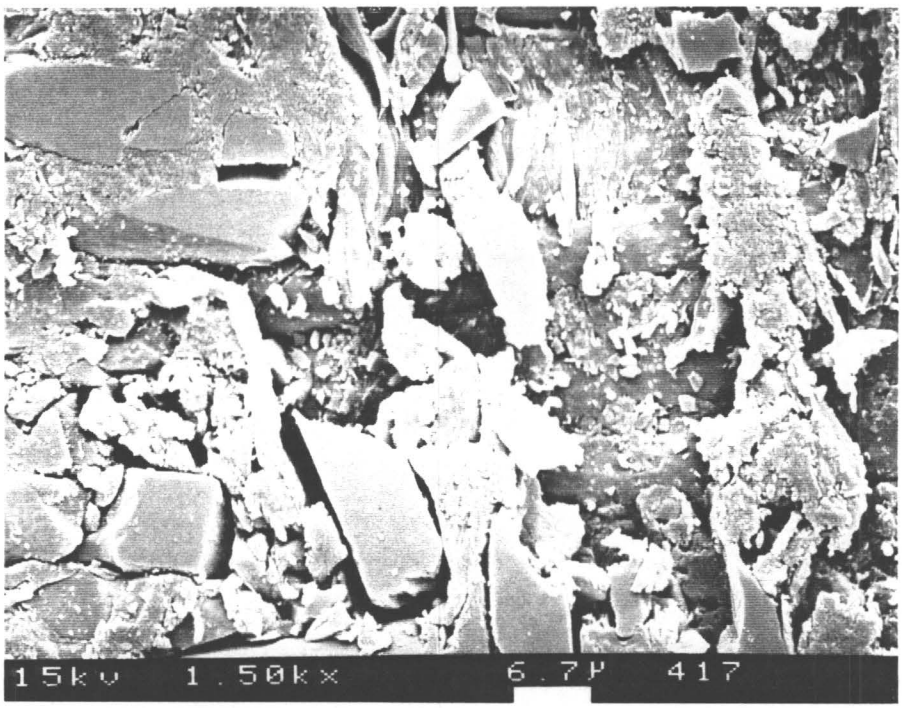

d)

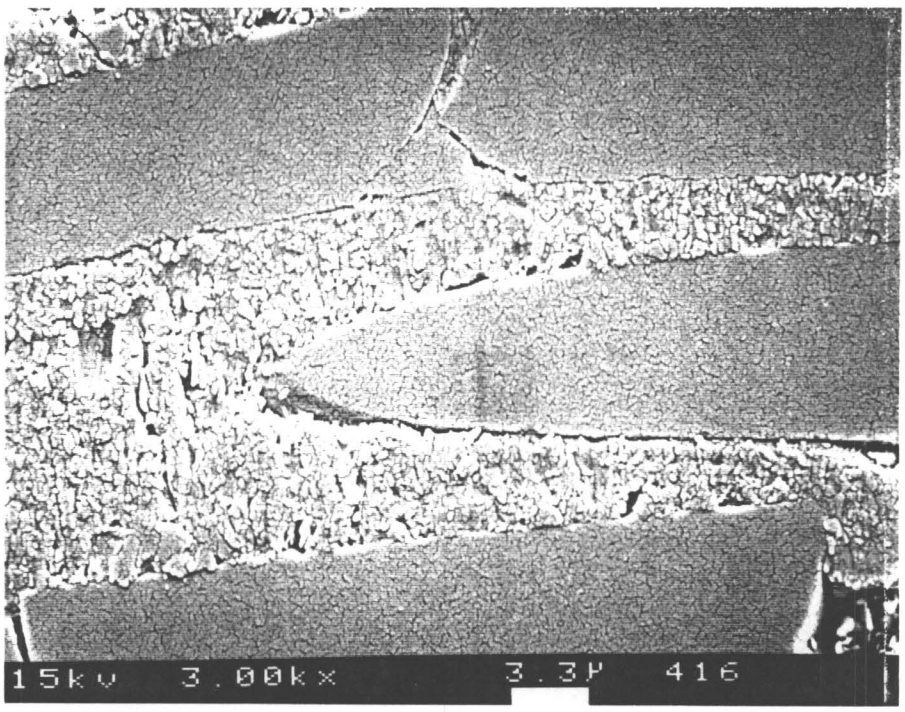

Fig. 64. (cont.) SEM's of wear scar in the anti-parallel orientation of carbon-PEEK.
c) pieces of fibers in the wear scar.
d) "transverse cracks" in the fibers and "microcracks" in the matrix.

oxidation of the sizing material. If so, then this could be one of the reasons for the debonding at the interface.

5. A number of microcracks can be seen on the fibers in the normal orientation. Some of these are shown in Fig. 62 f).

6. Unlike the graphite-epoxy wear scars, there are no gaps present between the fibers at the surface of the normal orientation.

7. In the parallel orientation, transverse cracks in the fibers are observed as shown in Fig. 63 d). Some grooves on the scar surface could also be observed (Fig. 63 c)). These could be grooves left after the fibers are pulled out of the matrix, or ploughing marks of "three-body" abrasive wear.

8. Transverse cracks on the fibers can also be observed in the anti-parallel orientation as shown in Figs 64 b) and 64 d).

9. Matrix cracks are observed in all three fiber orientations for carbon-PEEK.

CHAPTER 5

DISCUSSION

In the previous chapter, results of friction, wear, surface temperature rise, and observed surface damage of the two composites were presented. The two composites are seen to exhibit generally similar behavior, in spite of different types of matrix and fiber materials. In this chapter, an attempt is made to analyze the tribological behavior of these two polymer composites and propose possible causes. Possible connections between friction, surface temperature rise, and wear are also examined. The effect of material and fiber orientation on these parameters is also discussed.

The first section in this chapter includes a comparison between the experimental surface temperatures and the theoretically predicted temperatures using two theoretical techniques. The tribological behavior of graphite-epoxy and carbon-PEEK composites is discussed in subsequent sections. A generalized surface temperature model is also proposed. In the following section, the effect of fibre orientation is also discussed. Comparisons between friction, wear and surface temperatures of graphite-epoxy and carbon-PEEK composites are also included.

5.1 COMPARISON WITH THEORY

Measurement of surface temperature is one of the main objectives of this study. These experiments were carried out with sapphire as the counterface. Because of certain limitations, which are already discussed in chapter 3, measurements with this infrared system cannot be carried out with all types of counterfaces. Comparison with theory is therefore done to enable one to predict surface temperatures with all kinds of material systems. In the event of reasonable agreement of the theoretical temperature rise with the experimental value using sapphire as the counterface, the theory can be then used to predict temperatures in systems using other counterface materials. So far, no theoretical technique has been developed for these types of composite systems, which are anisotropic. The technique developed for isotropic materials by Vick, Foo and Golan (references [14,15,100]) has been found to successfully predict surface temperature rises in ceramics (reference [13,81]) and polymers (reference [16]). This technique is developed for isotropic materials only. An attempt is made here to find out how well the technique succeeds in predicting temperatures in anisotropic materials like the composites.

In this section, comparisons are made between the experimental surface temperature rise and the theoretically predicted temperature rise for a graphite epoxy-on-sapphire system, sliding under a load of 4N, and at velocity of 7 m/s. The techniques developed by Vick (references [14,15,100]) and Archard [89], have been used for this

purpose. Comparisons are made for each of the three fiber orientations.

For the computation of surface temperature rise, the size and distribution of the real area of contact is a necessary parameter. To simplify computations, Archard's theory assumes a single circular area of contact. Vick's theory on the other hand allows one to input the exact size and distribution of the contact area. However, no technique has been developed to compute the real area of contact exactly. Experimental attempts only result in an estimation of the contact area. Because of the unknown nature of the contact area, five different areas have been used for the computations. These are listed below.

1) Elastic Contact Area =

$$A_c = \pi \left[\frac{3WR}{4} \left(\frac{1-\nu_1^2}{E_1} + \frac{1-\nu_2^2}{E_2} \right) \right]^{2/3}$$

2) Plastic Contact Area =

$$A_p = \frac{W}{p_m}$$

3) Frictional Contact Area =

$$A_f = \frac{\mu W}{s}$$

The frictional contact area is based on the assumption that the friction force arises out of shearing of adhered junctions, and is equal to the product of the contact area and the shear strength of the junctions. Thus, contact area is obtained by dividing the measured friction force by the shear strength of the junctions. In these computations, the

shear strength of the junctions is assumed to be the bulk shear strength of the material.

4) Estimated Contact Area = E_s

Experimental techniques used to estimate the contact area have already been discussed in chapter 3.

5) Macroscopic Contact Area = E_m

This contact area represents the largest possible area, which is equal to the size of the wear scar.

where, W = normal load

R = effective radius of the contact geometry

ν_1, ν_2 = Poisson's ratio of the mating elements

E_1, E_2 = elastic modulus of the mating elements

p_m = flow pressure (hardness)

s = shear strength of the junctions

Figures 65 - 67 show the computed surface temperatures on a log-log scale for the normal, parallel, and anti-parallel orientations of graphite-epoxy respectively. The counterface used is sapphire, sliding at a velocity of 7 m/s and under a load of 4 N. The five different assumed contact areas are shown. In addition, the experimentally measured values are shown as horizontal lines. It can be seen from the plots that the variation of theoretical surface temperature with contact area on a log-log scale is linear, which implies that surface temperature and contact area are related through a power law relationship. The slope of the lines depends on the thermophysical properties of the

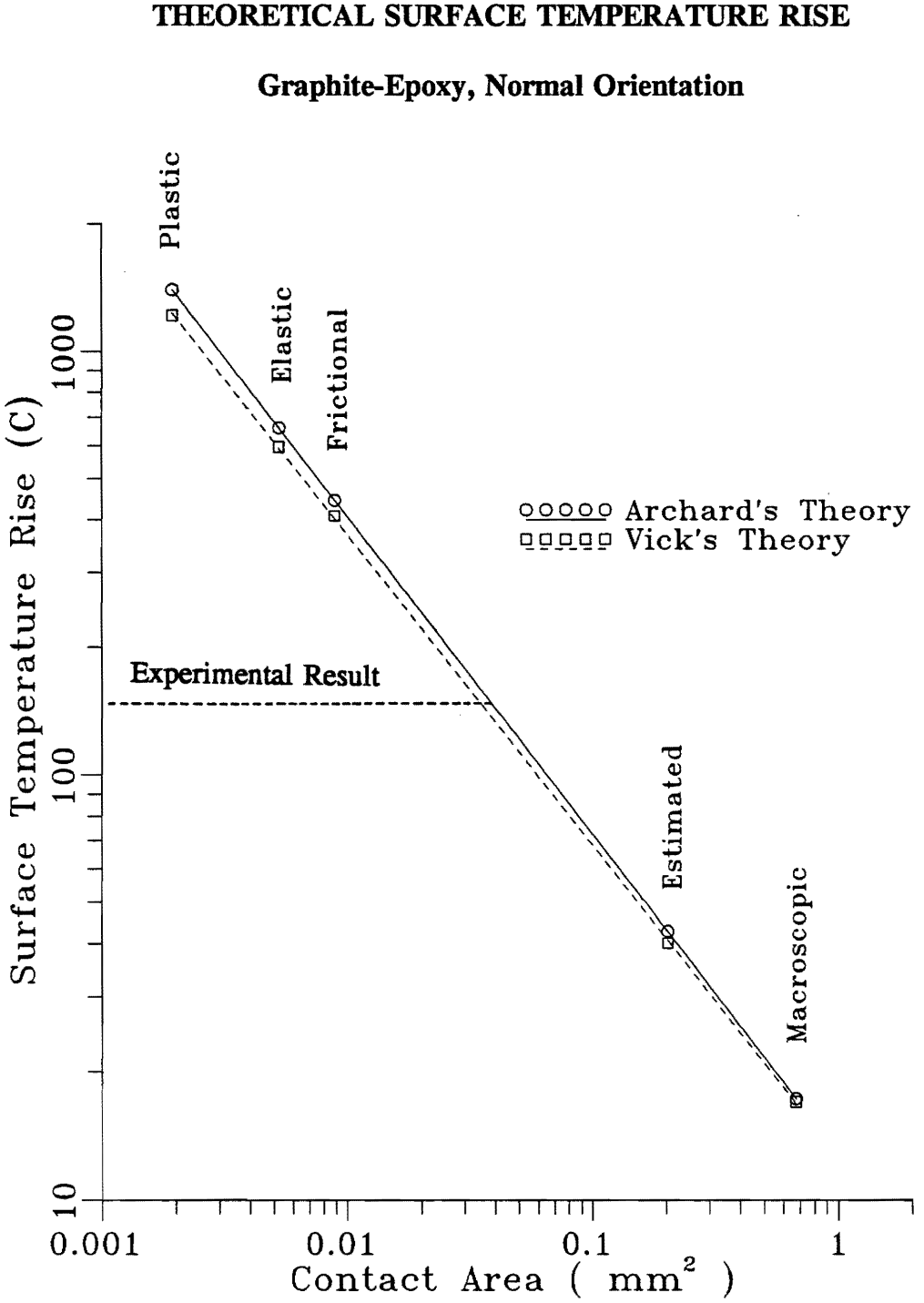

Fig. 65. Theoretical surface temperature rise per unit coefficient of friction for the normal orientation of graphite-epoxy sliding on sapphire using Vick's and Archard's theories. Load = 4 N, Sliding speed = 7 m/s.

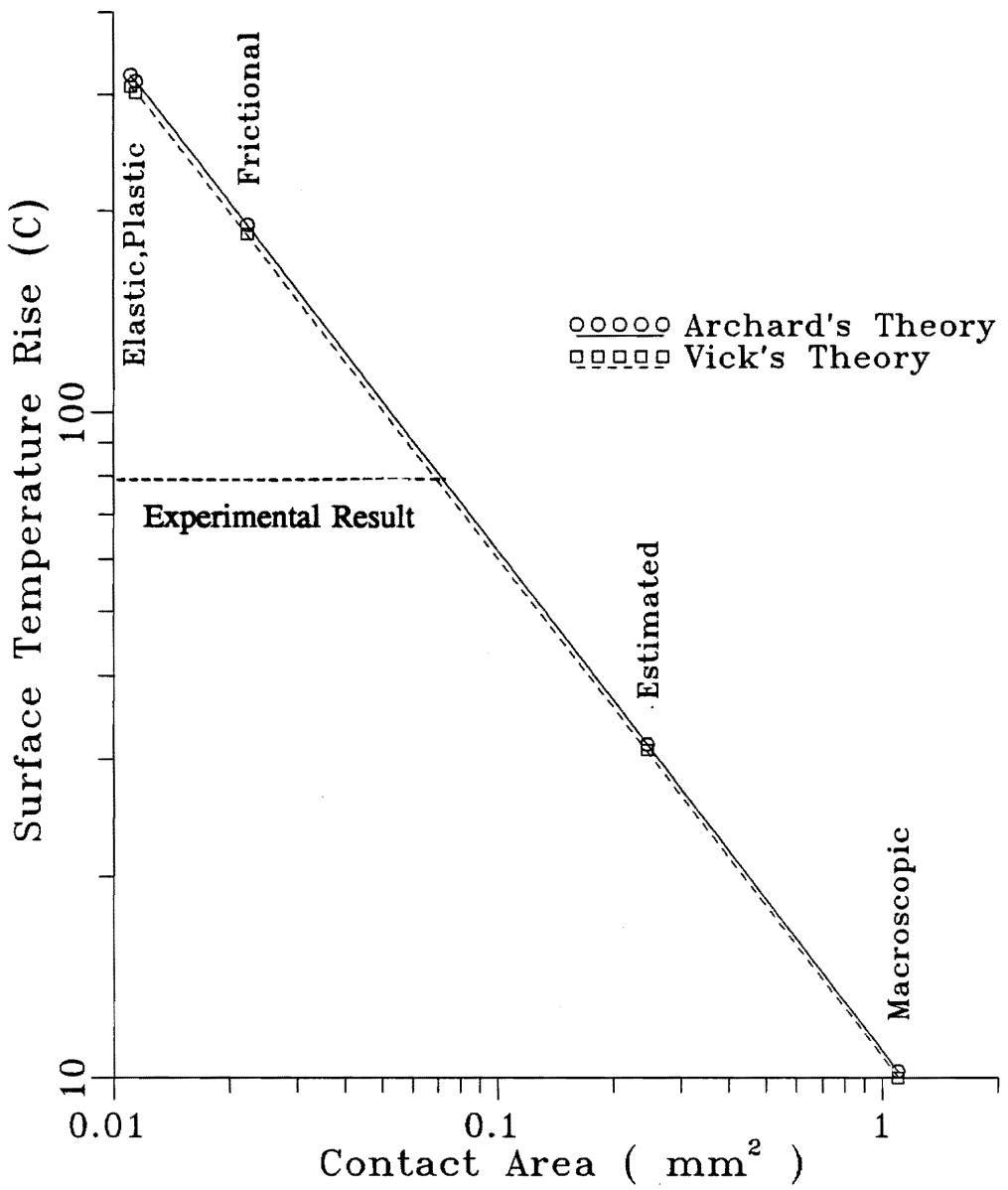

Fig. 66. Theoretical surface temperature rise per unit coefficient of friction for the parallel orientation of graphite-epoxy sliding on sapphire using Vick's and Archard's theories. Load = 4 N, Sliding speed = 7 m/s.

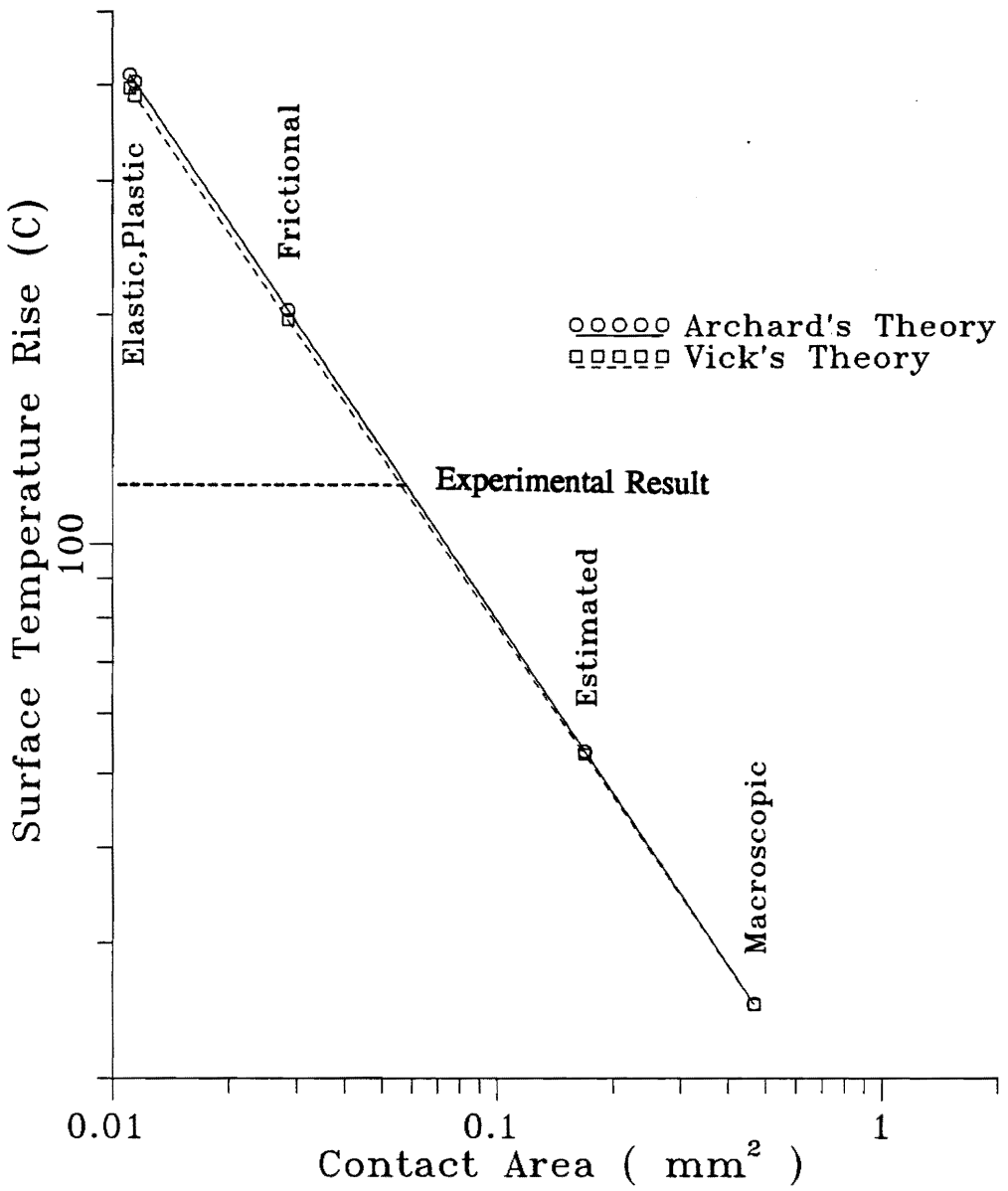

Fig. 67. Theoretical surface temperature rise per unit coefficient of friction for the anti-parallel orientation of graphite-epoxy sliding on sapphire using Vick's and Archard's theories. Load = 4 N, Sliding speed = 7 m/s.

mating elements and the sliding conditions.

The temperature values predicted by the two theories compare very well with each other. The actual temperature values and the percentage deviation of the values predicted by Archard's theory (from values predicted by Vick's theory) are listed in Table 12. Also, the surface temperature rises measured in the experiments are seen to lie between the temperatures predicted assuming the frictional and the estimated areas.

5.2 TRIBOLOGICAL BEHAVIOR OF THE COMPOSITES

Before getting into detailed discussion of the tribological behavior of these polymer composites, it is perhaps worthwhile to review the main results. With graphite-epoxy, the coefficient of friction is seen to decrease with increasing velocity in the normal and parallel orientations. In the anti-parallel orientation, the coefficient of friction is seen to increase initially and then decrease with increasing velocity. These results are shown in Fig. 31. Similar results are also observed in the case of carbon-PEEK and are shown in Fig. 58.

Mean surface temperature with graphite-epoxy is also seen to increase with increasing velocity or heat generation (Fig. 36 and 38) up to a certain velocity. Beyond this velocity, the surface temperature is seen to stay fairly constant. There is little difference in the maximum values of the mean surface temperatures attained by the three fiber orientations. This value is in the range of 125 - 135 °C for graphite-epoxy. In

Table 12. Comparison of Archard's and Vick's Theories. Temperatures are calculated for graphite-epoxy (normal, parallel and anti-parallel orientations) sliding on saphire at 7 m/s velocity and 4 N load.

GRAPHITE-EPOXY (NORMAL)

CONTACT AREA TYPE	CONTACT AREA (mm^2)	SURFACE TEMPERATURES (C)		PERCENTAGE DEVIATION†
		ARCHARD	VICK	
Elastic	.00529	660	595	10.9
Plastic	.00194	1394	1214	14.8
Frictional	.00889	445	408	9.1
Estimated	.202	42.7	40.	6.7
Macroscopic	.673	17.3	17.	1.8

† : Percentage deviation of Archard's computed results from Vick's results.

GRAPHITE-EPOXY (PARALLEL)

CONTACT AREA TYPE	CONTACT AREA (mm^2)	SURFACE TEMPERATURES (C)		PERCENTAGE DEVIATION†
		ARCHARD	VICK	
Elastic	.0111	322	309	4.2
Plastic	.01143	315	302	4.3
Frictional	.0223	191	185	3.2
Estimated	.245	31.6	31.	1.9
Macroscopic	1.100	10.24	10.	2.4

† : Percentage deviation of Archard's computed results from Vick's results.

Table 12 (cont). Comparison of Archard's and Vick's Theories. Temperatures are calculated for graphite-epoxy (normal, parallel and anti-parallel orientations) sliding on saphire at 7 m/s velocity and 4 N load.

GRAPHITE-EPOXY (ANTI-PARALLEL)

CONTACT AREA TYPE	CONTACT AREA (mm^2)	SURFACE TEMPERATURES (C)		PERCENTAGE DEVIATION†
		ARCHARD	VICK	
Elastic	.0111	413	396	4.3
Plastic	.01143	404	387	4.4
Frictional	.0286	203	197	3.0
Estimated	.169	53.5	53.	0.9
Macroscopic	.466	25.	25.	0.0

† : Percentage deviation of Archard's computed results from Vick's results.

the case of carbon-PEEK, the maximum temperature is seen to steady out after reaching a value of 150° - 170°C (Fig. 60).

The wear variation with velocity also shows some unusual trends. In the case of graphite-epoxy, the wear rate decreases initially with increasing velocity up to a certain minimum value and then increases (Fig. 39). This minimum wear rate is found to be independent of fiber orientation. Also, the velocity at which minimum wear occurs closely corresponds to the velocity for which the mean surface temperature is the maximum. A rather different kind of wear characteristic is seen in case of carbon-PEEK (Fig. 61). Here, in two of the fiber orientations (normal and anti-parallel), the wear rate is seen to increase initially and then decrease with an increase in velocity. In the parallel orientation, wear is found to remain unchanged with velocity.

In the discussion that follows, some of the possible causes for such behavior are analyzed. Finally, an attempt is also made to look at possible connections between the tribological parameters of these composites through a generalized model.

5.2.1 Surface Temperature

The maximum values of the mean temperatures attained in both the composites (refer to Figs. 36 and 60) are close to the glass transition temperature of the matrix materials. Glass transition is believed to be playing an important role in the behavior of these polymer composite systems. It is therefore felt appropriate to include a brief review on glass transition of polymeric materials.

Glass transition occurs in all amorphous polymers and the amorphous regions of semi-crystalline polymers when heated or cooled around a characteristic temperature. At the glass transition temperature, major changes in the mechanical properties are observed. On heating, as the glass transition temperature is traversed, the amorphous polymer changes from a hard, stiff and rigid phase to a soft rubbery phase. The decrease in the elastic modulus can even be up to three orders of magnitude. The transition typically occurs over a range of temperature; therefore the glass transition temperature is defined more precisely as the temperature at which maximum rate of change of properties is observed. Also, the glass transition temperature is dependent on the rate of testing, the lowest value being observed for very slow rates.

The glass transition is characterized as a second order phase transformation. As the material transforms from the glassy state to the rubbery state, the enthalpy of the system increases. This is therefore associated with dissipation of heat energy in the system.

In this study, attempts were made to measure the glass transition temperature of the materials. The value for carbon-PEEK was found to be around 139 °C. No results could be obtained for graphite-epoxy due to the high concentration of fibers in the sample. Hence this value for graphite-epoxy is obtained from literature, which is found to be in the range of 120 °C (reference [109]).

The present study shows that once the surface temperature approaches the glass transition temperature of the matrix material, higher velocities do not produce any further increase in temperature. Such a temperature plateau for graphite-epoxy is found to be

in the range of 125 - 135 °C. For carbon-PEEK, this temperature is in the range of 150 - 170 °C. This is contrary to theoretical predictions of a continuing increase in surface temperature with increasing velocity. Such a theoretical curve for graphite-epoxy in the normal orientation sliding on sapphire under 4 N load, based on Vick's theory, is shown in Fig. 68.

This suggests that the matrix material could be undergoing glass transition at the higher velocities. Initially, with an increase in velocity the surface temperature increases as expected until the temperature reaches the glass transition temperature of the matrix material. This transition occurs at the expense of energy. Thus some frictional energy generated during sliding gets dissipated in the process. Therefore the temperature is seen to stay fairly constant.

One would expect the temperature to rise further once all the matrix material present in the sample is completely transformed; in other words, at a particular velocity one would expect the temperature to go up after some time during the experiment. However, no such increase was observed in any of the experiments.

Although glass transition appears to be one reason for the friction-velocity trend, there are other reasons that could be responsible as well. Some of them are discussed here. Growth of the contact area could also be taking place with an increase in velocity. As velocity is increased, resulting in higher rates of frictional heat generation, the polymer matrix could be softening. Softening could also be occurring as a result of glass transition. It should be noted here that softening occurs only at the surface, with the bulk still hard enough to support load. Contact area, which depends strongly on the surface

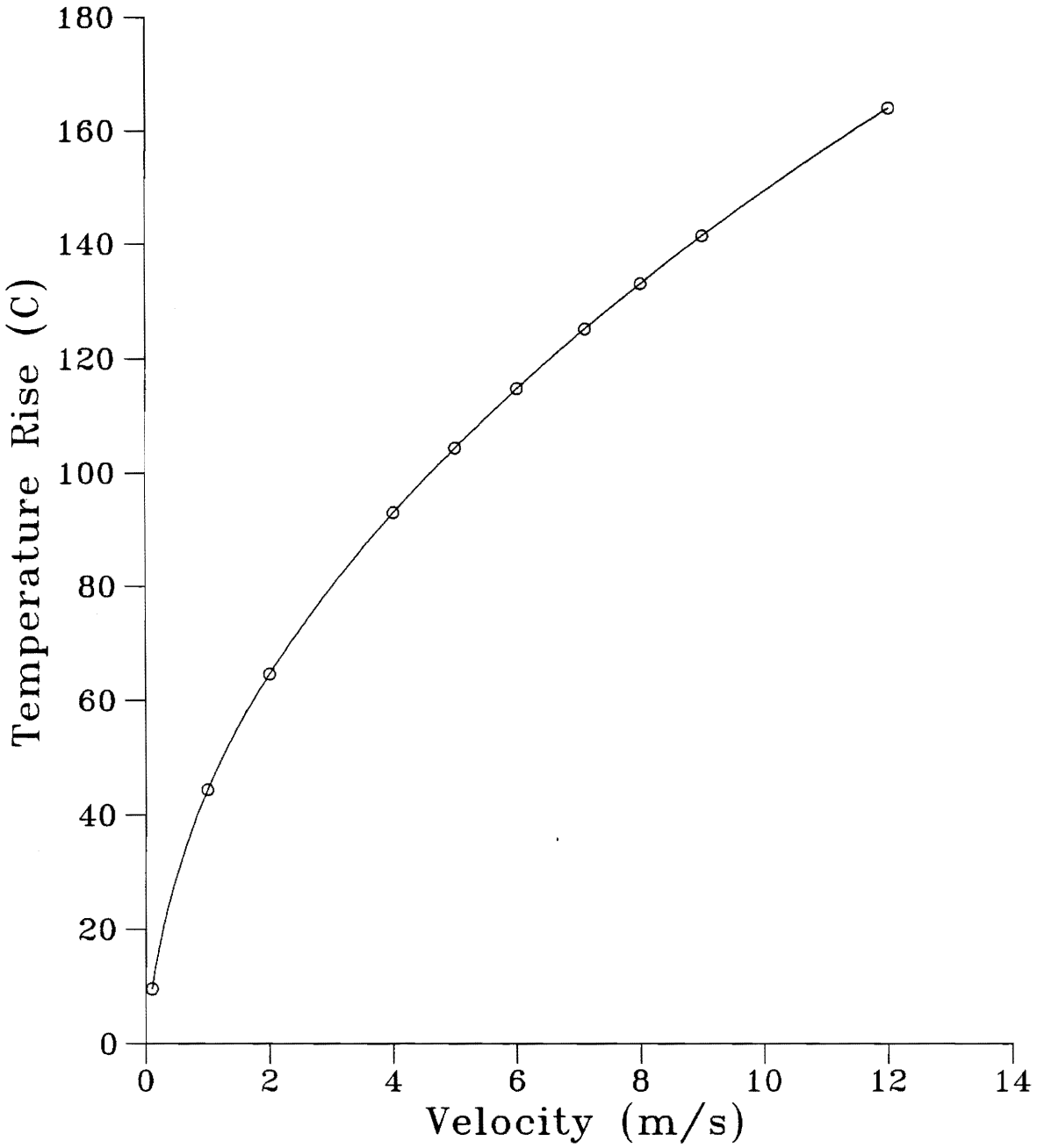

Fig. 68. Effect of velocity on theoretical surface temperature rise, computed using Vick's theory. Load = 4 N, Velocity = 7. m/s and Material system = Graphite-epoxy (normal) sliding on sapphire.

hardness of the material, is therefore expected to increase as the material softens. And since an increase in contact area lowers the surface temperature, this could be responsible for the lower values of the temperatures (when compared to theoretical values).

It appears that changes in the thermal properties of the mating surfaces could also be responsible for the reduction in temperature (from theory) at higher velocities. Theoretical predictions on the effect of thermal conductivity of the stationary body on surface temperature rise are shown in Fig. 69. It can be seen from this figure that any change in the thermal conductivity of the composite would not change the surface temperature significantly. Changes in specific heat of the composites also would not affect the temperature rise very much.

Changes in the thermal properties of the sapphire disk, on the other hand, could influence the surface temperature. A theoretical plot illustrating this effect is shown in Fig. 70. The plot shows the surface temperature variation with changing thermal conductivity of the moving body while sliding on the normal orientation of graphite-epoxy at a velocity of 7 m/s and a load of 4 N. The question that arises here is how much does the thermal conductivity of the sapphire disk change within the measured temperature range. Although no such measurements were done in this study, literature data have been collected and presented in Fig. 71 (reference [105]). The plot shows the change in thermal conductivity with temperature of a typical high purity synthetic sapphire single crystal. It can be observed from this figure that within the temperature range attained in these experiments (from room temperature to about 170°C), the thermal conductivity of sapphire decreases from 47 W/mK to 29 W/mK. Although the sapphire

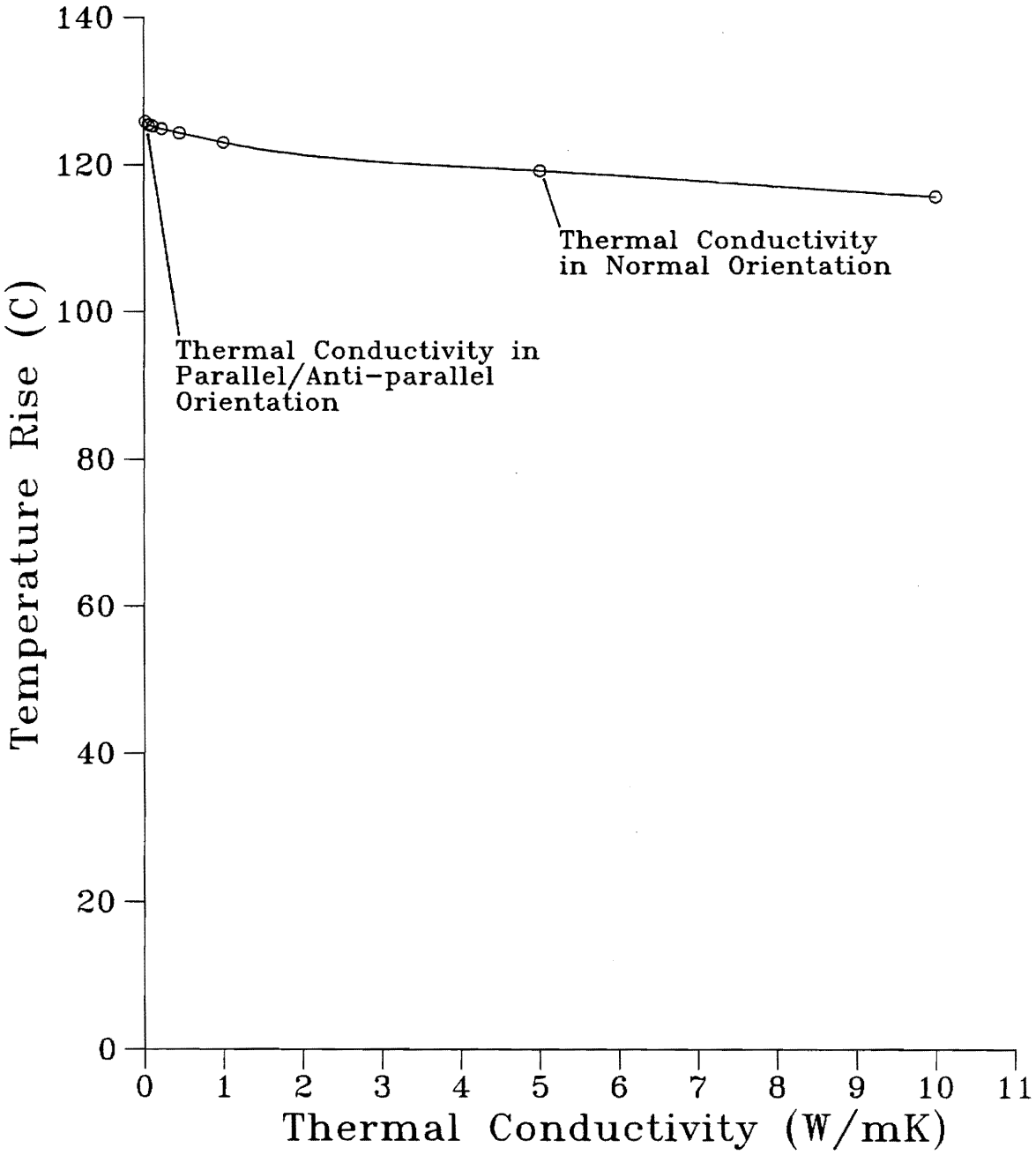

Fig. 69. Effect of thermal conductivity of the stationary body on theoretical surface temperature rise (computed using Vick's theory). Load = 4 N, Velocity = 7 m/s, Mating element = Sapphire.

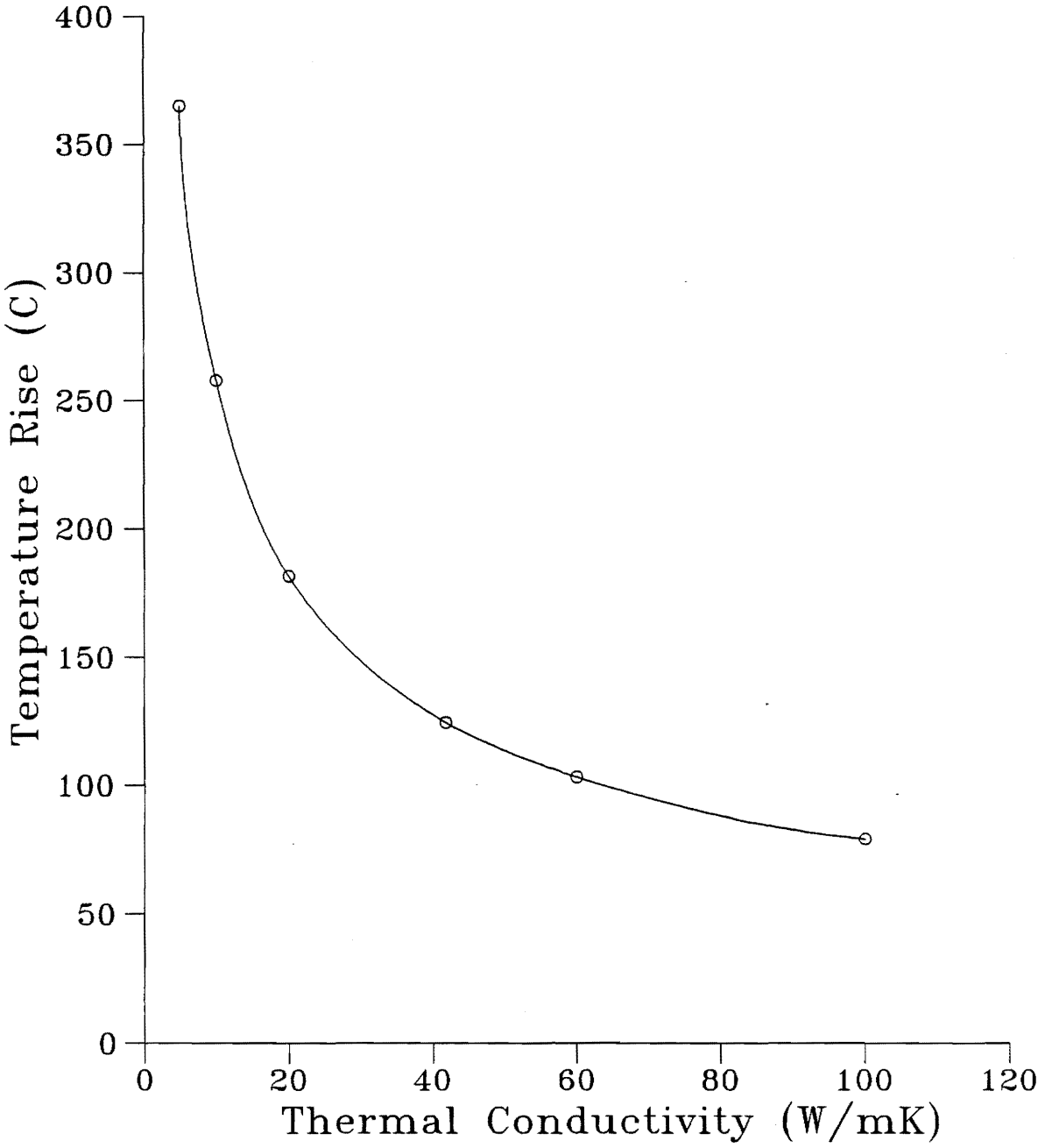

Fig. 70. Effect of thermal conductivity of the moving body on theoretical surface temperature rise (computed using Vick's theory). Load = 4 N, Velocity = 7 m/s, Mating element = Graphite-Epoxy (normal).

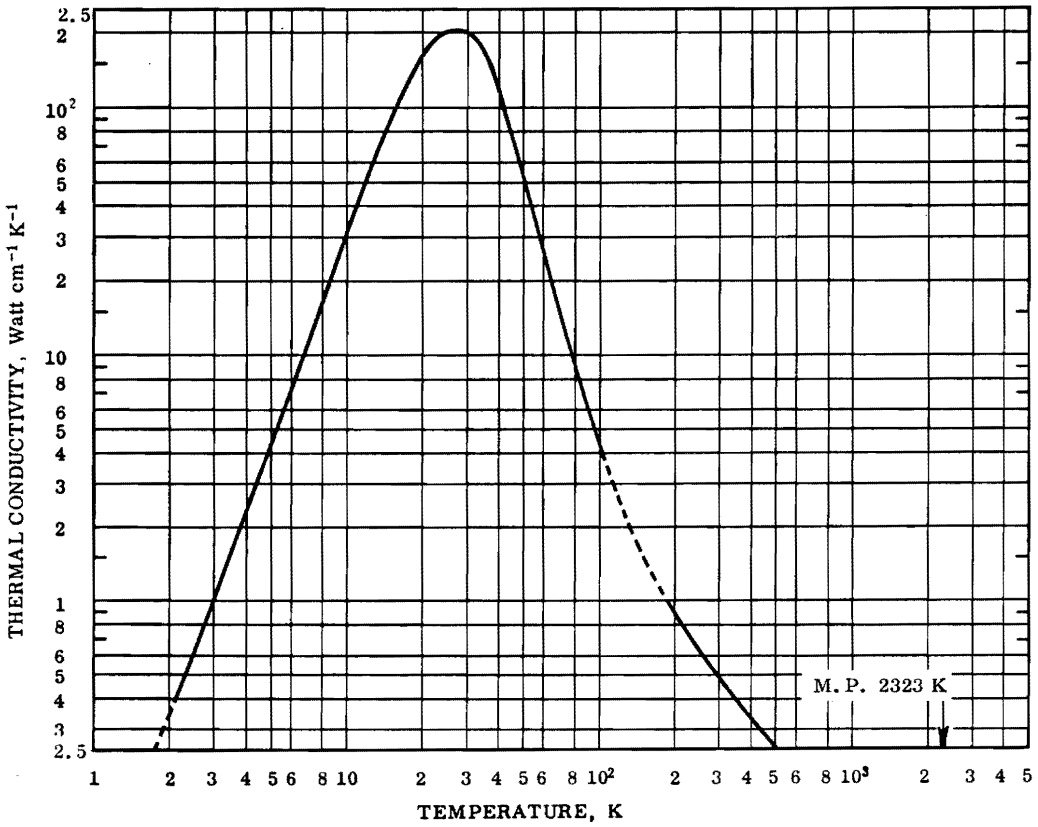

REMARKS

The recommended values are for high-purity synthetic sapphire single crystal with heat flow at 60 degrees to the hexagonal axis. The recommended values that are supported by experimental thermal conductivity data are thought to be accurate to within 10 to 15% of the true values at temperatures above 60 K. The thermal conductivity near and below the corresponding temperature of its maximum is highly sensitive to small physical and chemical variations of the specimens, and the recommended values below 60 K are intended as typical values for indicating the general trend.

Fig. 71. Changes in thermal conductivity of sapphire with temperature [105].

sample used in this study has a thermal conductivity of 41.8 W/mK, it is expected to show similar drops. The drop in thermal conductivity is expected to increase the temperature rise. But in the experiments, the temperatures are still seen to stay constant near the glass transition temperatures.

A plot of the change in specific heat of sapphire with temperature is shown in Fig. 72. (reference [105]). Within the temperature range of the experiment, the increase in specific heat of sapphire is very small. This, therefore, does not appear to be a significant factor.

5.2.2 Friction

It has been mentioned before that the coefficient of friction-velocity curve is seen to show a negative slope beyond a certain sliding velocity in both these composites. Since adhesive friction is believed to be the dominant friction mechanisms, the friction force is given by:

$$F = A\,s$$

The different slopes (+ve and -ve) of the coefficient of friction-velocity curve arise out of the difference in the rates at which (a) the contact area grows with rate of deformation (which corresponds to velocity) and temperature, and (b) the interfacial shear strength decreases with rate of deformation and temperature. This kind of friction-velocity behavior may be related to similar behavior observed in many polymers. In a study by Ludema and Tabor [106], the frictional properties of the polymers were related

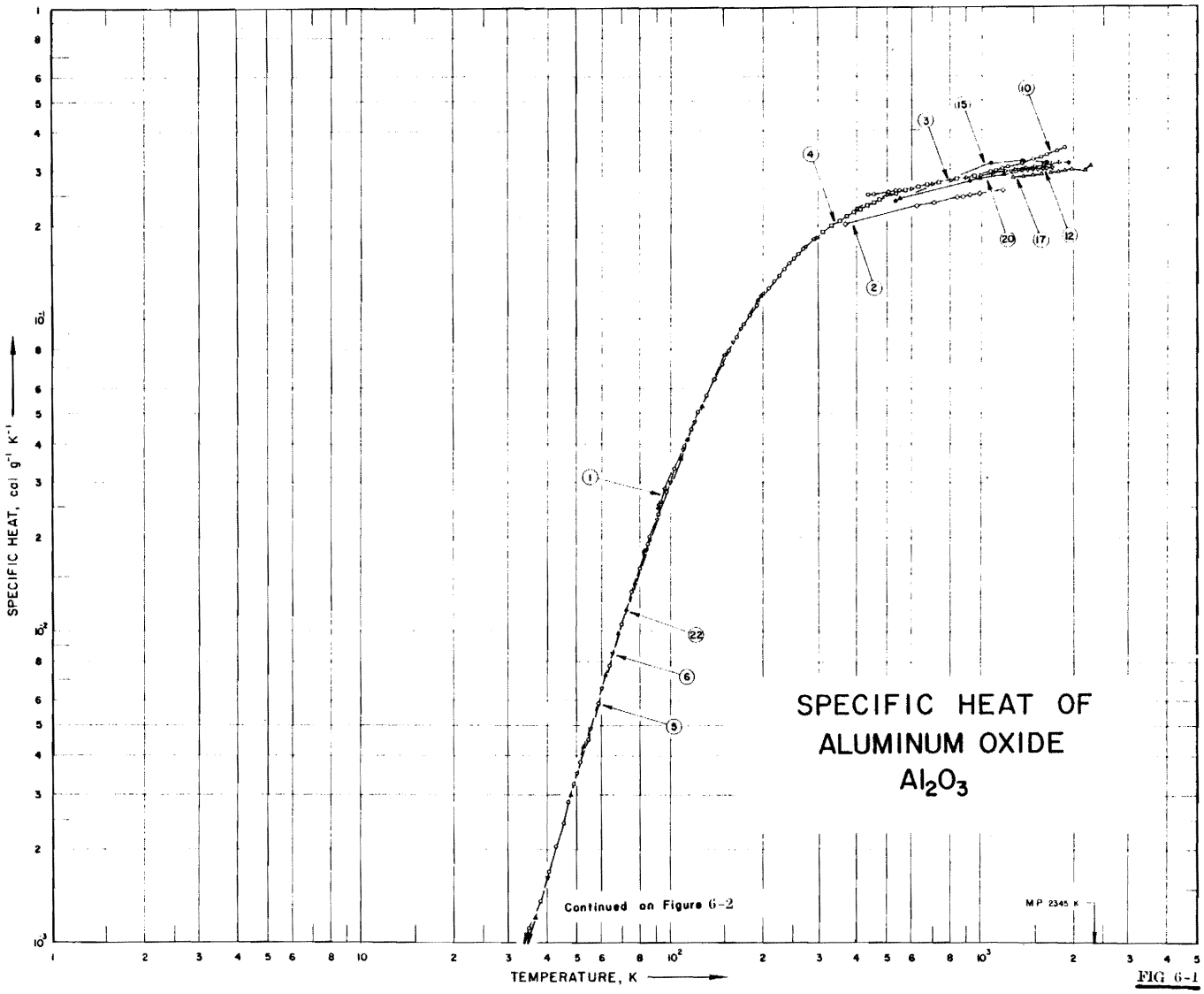

Fig. 72. Changes in the specific heat of sapphire with temperature [105]. Curve (2) represents values for sapphire.

to their viscoelastic characteristics. They used a simple model to explain the frictional properties in terms of the way in which the area of contact and the interfacial shear strength vary with rate of deformation and temperature. The model is shown qualitatively in Fig. 73. In their experiments, rubber was observed to show similar behavior. But rigid polymers below their glass transition temperature showed marked variation in coefficient of friction with speed, which did not seem to correlate directly with the visco-elastic properties of the polymers.

In the present study, composites in the anti-parallel orientation showed trends similar to the above model. But in the normal and parallel orientations, only the negative portions of the slope were observed within the velocity range tested. This could be due to differences in the viscoelastic characteristics of the composites in the three fiber orientations. The position and spread of the bell-shaped friction-velocity curve (in the model) depend on material properties and their response to rate of deformation and temperature. The material properties are known to be different for different fiber orientations. Further, for same velocity, the rates of deformation are not going to be the same for all the fiber orientations. As a result, different fiber orientations could exhibit such bell-shaped friction-velocity trends over different velocity ranges. Therefore, in the velocity range examined in this study, only the negative part of the curve was observed in the normal and parallel orientations.

The Ludema and Tabor model is a simplified representation of the viscoelastic behavior of composites. In a more detailed analysis of the viscoelastic characteristics of such composite systems, the anisotropy and non-homogeneity should be taken into

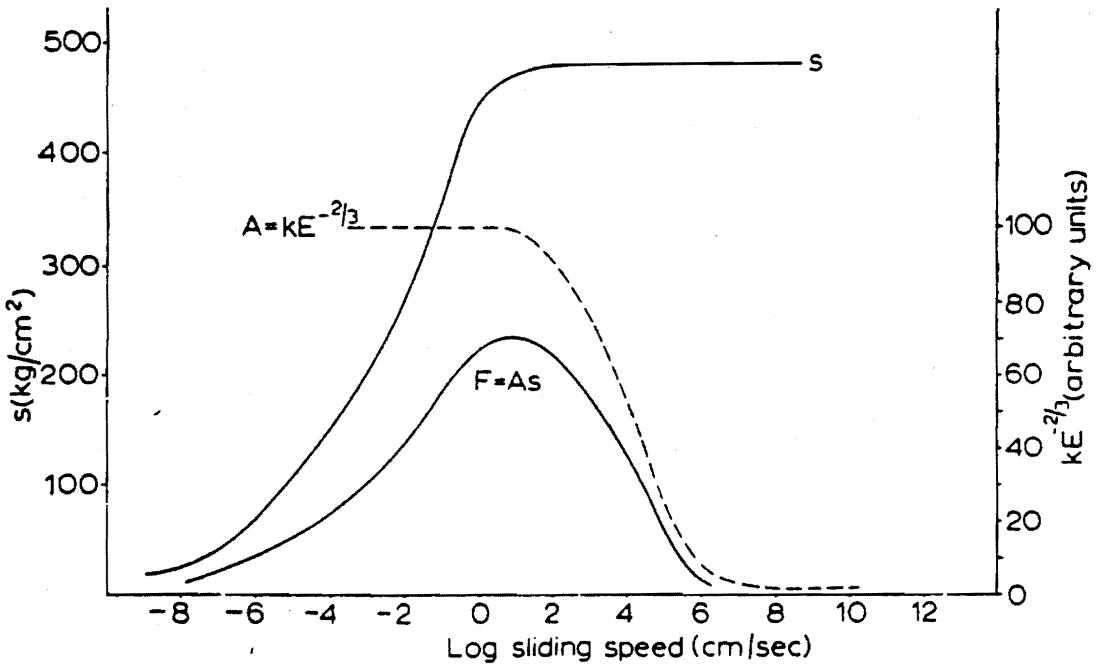

Fig. 73. Qualitative representation of the variation in coefficient of friction as a function of sliding velocity [106].

consideration. Moreover, the above model does not consider the effects of frictional heating. But in these systems, surface temperatures could be significantly high to influence the viscoelastic behavior, even under mild sliding conditions. Therefore, surface temperatures should also be considered in the model.

5.2.3 Wear

Wear is found to be maximum in the normal orientation and minimum in the anti-parallel orientation for both the materials examined. This is contrary to the observations in some other literature [18,24], where wear was found to be maximum in the anti-parallel orientation and minimum in the normal orientation. But in all those works, the counterfaces used were rough surfaces, where abrasive wear was believed to be the dominant wear mechanism. In this system with an optically smooth and very hard sapphire counterface, direct ploughing or abrasive wear is believed to be minimal. Therefore, some of the likely mechanisms of material removal in this system are adhesive wear, fatigue wear and three-body abrasive wear resulting from the wear debris. Furthermore, the commonly believed wear process in composites by debonding at the fiber-matrix interface and subsequent pull out of the fibers due to abrasive and/or adhesive action, is also possible. In the discussion that follows, the wear results of graphite-epoxy and carbon-PEEK are discussed separately as they are markedly different from each other.

Graphite-epoxy : It has already been mentioned that abrasive wear is less likely in all systems with optically smooth sapphire as the counterface. Adhesive wear typically leaves a layer of transfer film on the counterface. Investigation of the sapphire counterfaces after the experiment did not reveal any significant transfer at low sliding velocities. However, some amount of transfer was observed at high sliding velocities. This suggests that adhesive wear could be minimal at low sliding velocities but greater at higher velocities.

Another possible wear mechanism is fatigue wear. The fatigue wear process is normally associated with repeated stress cycling. In fatigue, failure in the material arises because of stress-reversal effects, i.e., fracture can develop under alternating stresses with a peak level, which should be safe if imposed only in tension or compression. Fatigue wear occurs as a result of surface fatigue, which is different from bulk fatigue in one important aspect. Bulk fatigue is usually associated with a "fatigue limit stress", below which the material enjoys an infinite life. But no such limit has been detected in surface fatigue. This means that surface fatigue can occur even at very low levels of cyclic stresses. More details about the surface fatigue wear mechanism can be found in references [107, 108]. A fundamental experimental study of the surface-fatigue process under cyclic variation of normal load has been done by Tyler, Burton, and Ku [108].

Experimental observation of surface fatigue wear indicates that wear proceeds by initiation of fatigue cracks, followed by propagation of the cracks until wear particles are formed. The mechanism of crack initiation and propagation has been discussed elsewhere (references [107, 108]).

In the present study, observation of Scanning Electron Micrographs of the wear scars reveals a large number of microcracks at the surface of the wear scar. Moreover, the normal and the tangential loads have been found to vary in a cyclic manner. This supports the belief that fatigue wear could be another wear mechanism contributing to the wear process in this system.

Three-body abrasive wear is also believed to be another likely wear mechanism in this system, particularly in the normal orientation. In the normal orientation, very fine wear debris is observed all over the wear scar. These debris from the harder fibers can abrade the soft matrix. In the normal orientation, the matrix is seen being removed from the surface, most likely due to abrasion by the fiber debris. No such debris is seen in the parallel and anti-parallel orientations. Also, preferential matrix removal from the surface is not observed in these two fiber orientations. The reason why the wear debris is found spread all over the wear scar only in the normal orientation and not in the other two orientations is not clear, but it points out that three-body abrasive wear is perhaps significant in the normal orientation only.

There is very little evidence of debonding at the fiber-matrix interface. The SEM photographs of the scar in the anti-parallel orientation -- where the fibers are seen transversely cracked, but still mostly attached to the matrix -- suggest that the bond at the fiber-matrix interface is probably very good. There is no evidence of fiber "pull out" either.

From the above discussions, it may be concluded that wear in the three fiber orientations occurs through a combination of adhesive and surface fatigue wear

mechanisms. Three-body abrasive wear also occurs in the normal orientation.

The wear is seen to decrease with increasing sliding velocity up to a certain velocity, beyond which it is seen to increase with velocity. This is observed in all the three fiber orientations of graphite-epoxy. Moreover, at this velocity corresponding to minimum wear, wear rates for all the three fiber orientations are found to be the same. Some possible reasons for this behavior are discussed in the next section based on an hypothesized model.

Carbon-PEEK : As in the case of graphite-epoxy, once again all possible wear mechanisms for carbon-PEEK are discussed. The possibility of direct abrasive wear has already been ruled out because of the smooth counterface. Adhesive wear could be a possibility as some amount of transfer of the material to the counterface was detected.

The presence of a large number of cracks in the fiber and matrix once again suggests that fatigue wear could also be another wear mechanism in carbon-PEEK. In carbon-PEEK, two types of cracks could be observed on the fibers. There were a large number of small cracks, typically an order of magnitude smaller than the diameter of the fibers. These cracks seem to be randomly oriented on the surface. Besides, transverse-cracks running across the cross section of the fibers could also be observed. The small cracks were mostly observed in the normal orientation and transverse cracks in the parallel and anti-parallel orientations. The causes of these cracks are believed to be due to the cyclic variation in the mechanical loading, both normal and tangential.

In certain cases, debonding at the fiber matrix interface could also be observed

in the parallel and anti-parallel orientations. At places, fibers are seen to have been removed, leaving grooves in the matrix.

It is therefore believed that wear in the normal orientation of carbon-PEEK proceeds by a combination of adhesive wear and fatigue cracking of the fibers and the matrix. In the parallel and anti-parallel orientations it is believed to be due a combination of adhesive wear and transverse cracking of the fibers and subsequent pull-out from the matrix.

5.2.4 Generalized Model

The tribological behavior exhibited by these polymer composites is markedly different from that shown by other materials. The inter-relationships between various parameters as friction, surface temperature rise and wear appear very complex. Nevertheless, an attempt is made here to explain the observations through a "2-regime" tribological model.

A qualitative representation of the variation of friction, surface temperature and wear of these composites with velocity is shown in Fig. 74. The trend of the curves suggests that the total velocity range could be broken down into two regimes -- a low velocity regime and a high velocity regime. The two regimes may be defined based on the surface temperature values attained in each of the regimes. It is known that surface temperature increases with velocity until it is equal to the glass transition temperature of the matrix material. So the low velocity regime may be defined as the velocity range

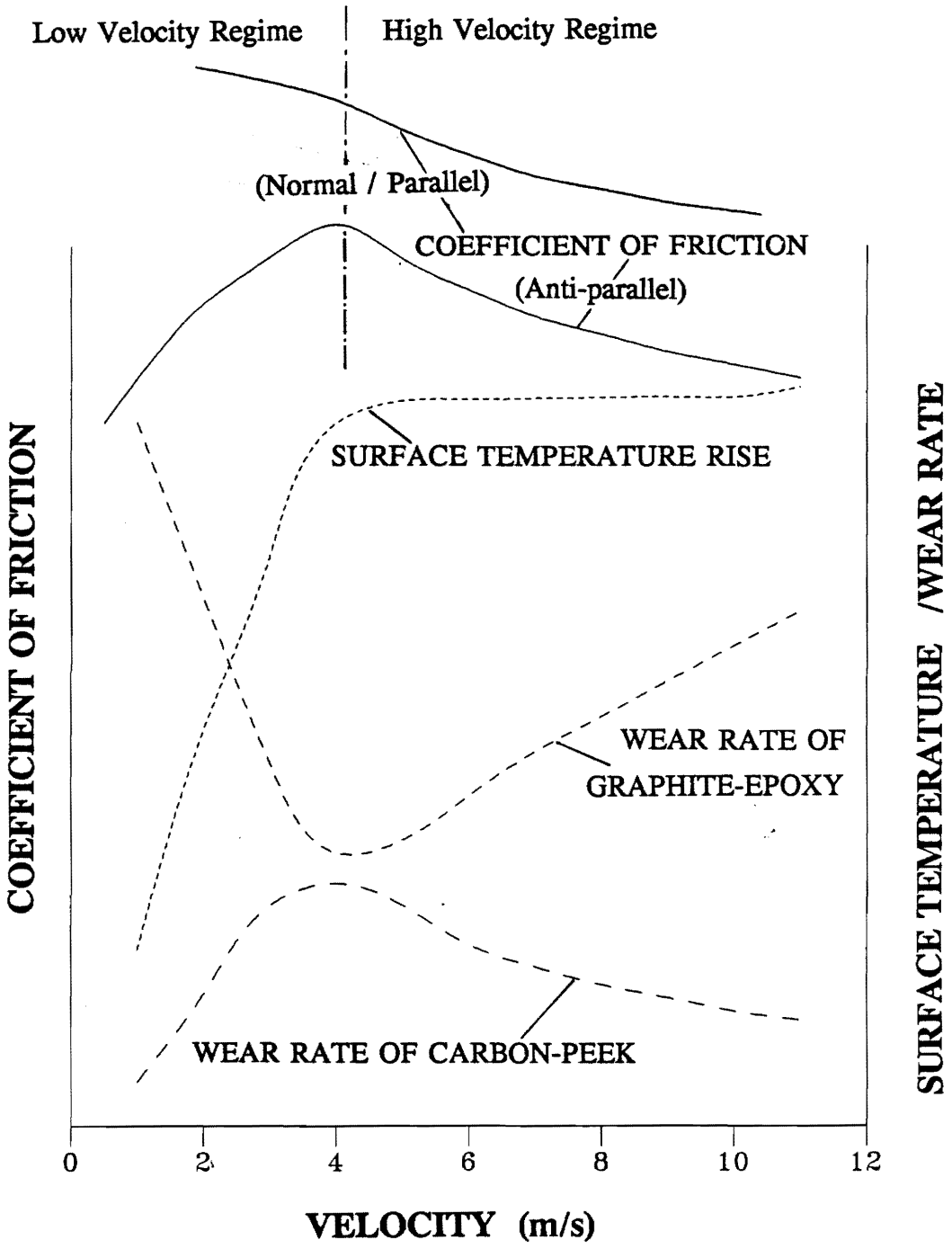

Fig. 74. Qualitative representation of the tribological processes in these polymer composites. The total velocity range may be divided into "Low Velocity Regime" and "High Velocity Regime".

for which the surface temperature is below the glass transition temperature of the matrix material; the high velocity regime is that for which the surface temperature is equal to the glass transition temperature of the matrix material. These velocity regimes are shown in Fig. 74. The demarkation between the two velocity regimes may not be very clearly defined. The transition from one regime to the other may actually take place over a velocity range.

Thus the low velocity regime may be characterized as follows: a) the surface temperature is below the glass transition temperature of the matrix material; typically surface temperature increases with increasing velocity in this regime; b) the coefficient of friction increases (anti-parallel fiber orientation) or decreases (normal and parallel fiber orientations) with increasing velocity, depending on the viscoelastic behavior of the composites in different fiber orientations; and c) wear rate varies differently with velocity depending on the material, i.e., in graphite-epoxy it decreases with velocity, but either increases or stays constant in carbon-PEEK. On the other hand, in the high velocity regime: a) surface temperature stays constant at the glass transition temperature with increasing velocity; b) coefficient of friction decreases with increase in velocity; and c) wear rate variation again depends on the material, i.e., in graphite-epoxy it increases with velocity, but decreases or stays constant with velocity in carbon-PEEK.

In the low velocity regime, surface temperature increases with an increase in velocity as the heat generation rate increases. The heat generation rate q is given by:

$$q = \mu W V$$

In the high velocity regime, surface temperature stays constant due to various reasons already outlined in this chapter. The variation of coefficient of friction with velocity has also been discussed in a previous section.

Before analyzing the variation of wear rate of these composites with velocity, a few ways by which wear rate could be influenced by velocity may be looked at.

I) Higher velocity may result in softening of the material through an increase in temperature. This may result in faster removal of material. The rate of softening is expected to be different in the two velocity regimes. It is expected to be small in the low velocity regime, but substantially large in the high velocity regime due to the temperature being equal to the glass transition temperature of the matrix material. Such a variation may be represented by curve (I) in Fig. 75.

II) In case of fatigue wear, which is believed to be one of the wear mechanisms in these material systems, the wear rate could decrease with an increase in velocity as a result of a decrease in the crack propagation velocity. Detailed analysis of this phenomenon is done by Lhymn [41 - 47]. Such a variation could be represented by curve (II) in Fig. 75. The exact nature of this curve is going to be dependent on the material properties. Two such variations are shown in the figure (Fig. 75) as II(a) and II(b). In carbon-PEEK which has a thermoplastic matrix, the curve is expected to be more like II(b). This is because as the temperature increases (resulting from an increase in velocity), thermoplastics are expected to undergo plastic flow more readily. In the event of crack propagation, plastic flow at the ends of the cracks tend to hinder the growth of the crack. Hence the decrease in the crack propagation velocity is expected

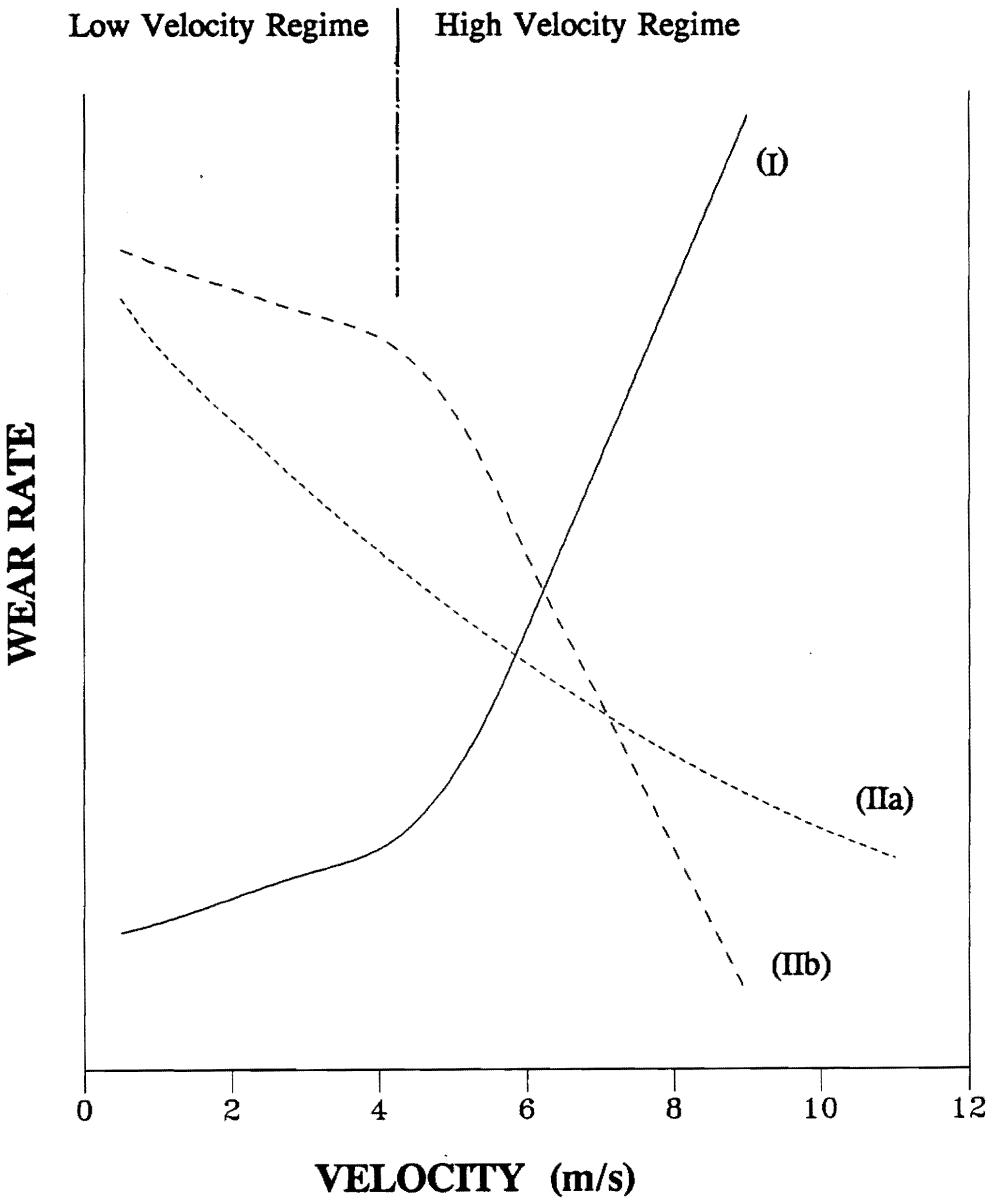

Fig. 75. Qualitative representation of the dependence of wear of polymer composites on sliding velocity. Curve (I) represents change in wear rate due to softening. Curve (IIa) and (IIb) represent fatigue wear. The exact nature of the curves will depend on the material properties. The behavior of graphite-epoxy is expected to be more like curve (IIa) and that of carbon-PEEK is expected to be more close to curve (IIb).

to be more drastic in case of carbon-PEEK. This may result in a much faster reduction in the wear rate in carbon-PEEK, which is represented by curve II(b).

Combinations of curves I and II are shown separately for the two materials in Figs. 76 and 77. Combination of curves I and II(a) represent the wear characteristic of graphite-epoxy which is shown in Fig. 76. The combination of curves I and II(b) represents the wear characteristics of carbon-PEEK, shown in Fig. 77.

5.2.5 Effect of Fiber Orientation

Surface temperature rise is observed to be the highest in the normal orientation for both graphite-epoxy and carbon-PEEK. This is observed in spite of the lower coefficient of friction. Moreover, this occurs in spite of the fact that the thermal conductivity of graphite-epoxy is approximately 50 times higher in the normal orientation than in the other two orientations, which apparently suggests that temperature should be lower in the normal orientation. But in this system of a very low conductive stationary composite sliding against a very high conductive sapphire, the thermal conductivity of the composite is of little consequence. Theoretical values of temperature rise with different thermal conductivities of the stationary material in contact with moving sapphire have already been shown in Fig. 69. Vick's theory has been used for this purpose. The thermal conductivities of the composites are marked on the figure. It is evident from this figure that in this system, the effect of any reasonable change in thermal conductivity of the stationary material on the surface temperature at the contact is negligible.

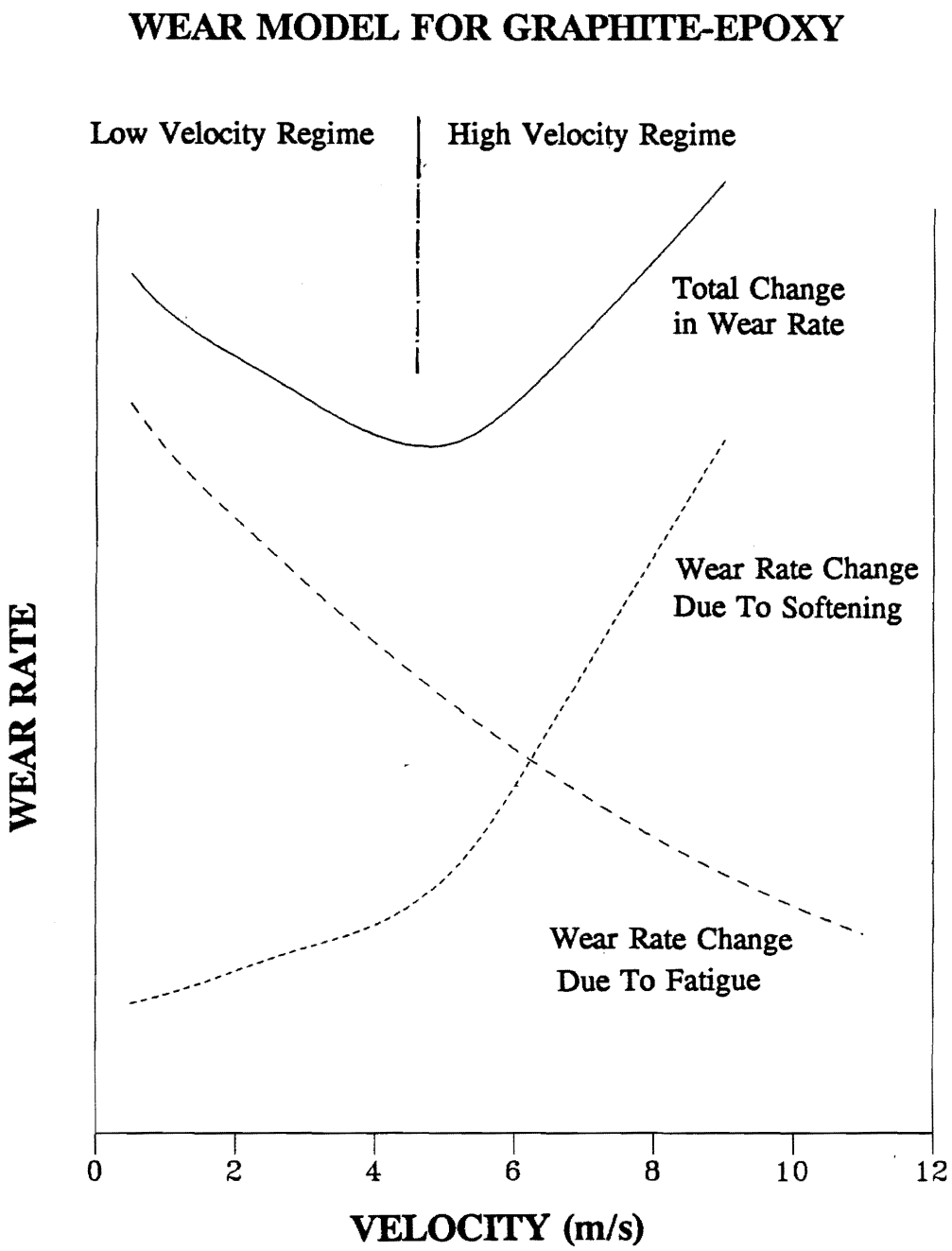

Fig. 76. Qualitative representation of the wear behavior of graphite-epoxy as the combination of curves (I) and (IIa).

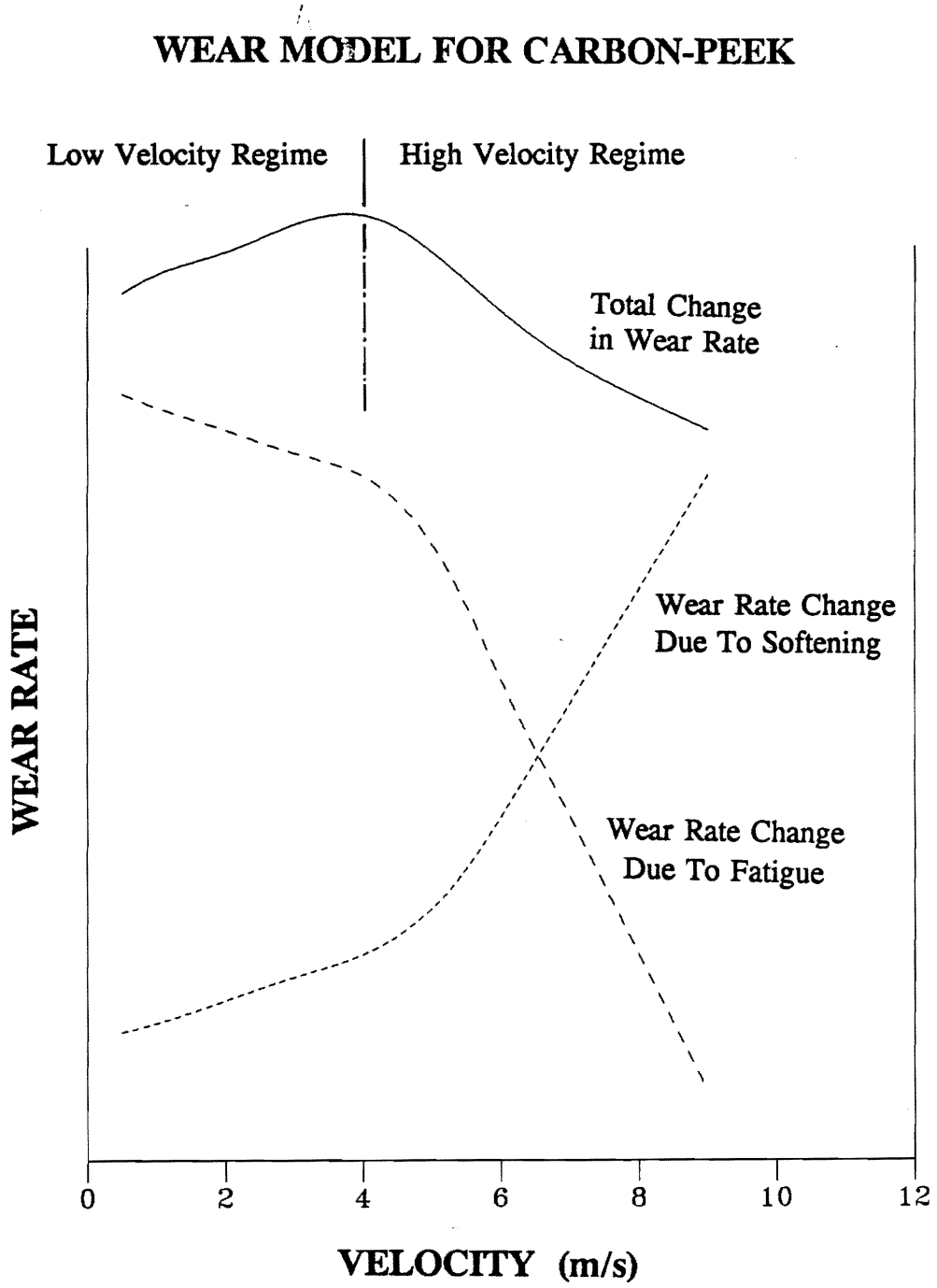

Fig. 77. Qualitative representation of the wear behavior of carbon-PEEK as a the combination of curves (I) and (IIb).

The only other important and controlling factor is once again the contact area. Graphite-epoxy is harder in the longitudinal direction compared to the other directions. The normal orientation referred to in this study corresponds to the longitudinal direction. Therefore, it is expected that the contact area in the normal orientation would be smaller compared to the other orientations. It can be seen from Table 12 that the elastic contact area in the parallel/anti-parallel orientation is more than twice that of the normal orientation. Similarly the plastic contact area in the parallel/anti-parallel orientation is about six times larger than that of the normal orientation. Therefore, even though the exact areas are unknown, it may be expected that the area is smaller in the normal orientation. As surface temperature increases exponentially with a decrease in contact area (as seen in Figs. 65-67), the smaller value in the normal orientation could be responsible for the higher temperature rise.

The difference in surface temperatures between the parallel and anti-parallel orientations is still not very clear. One possible reason could be the shape of the contact area. It has been shown [14,15] that for the same size of contact area, different shapes and orientations of the area result in different surface temperatures. But as no data are available on the shape of the contact area in the different fiber orientations, no conclusive statement can be made.

The coefficient of friction in unidirectional sliding of graphite-epoxy and carbon-PEEK is found to be the highest in the anti-parallel orientation and lowest in the normal orientation, except at low sliding velocities where it is the highest in the normal

orientation. Even in oscillating motion of graphite-epoxy, the coefficient of friction is found to be minimum in the normal orientation. As friction is believed to be predominantly due to adhesion, the shear strengths of the fibers and matrix could be playing an important role in determining the coefficient of friction. In the normal orientation, the fibers are subjected to transverse shear, whereas in the parallel orientation they are subjected to longitudinal shear. In the anti-parallel orientation, although the fibers are subjected to transverse shear, the shear area is more than twice (elastic area; six times in case of plastic area) that of the normal orientation. The difference in mechanical properties of the fibers in longitudinal and transverse directions could account for the difference in coefficients of friction in the various fiber orientations. Since the fibers are typically weaker in transverse shear, the coefficient of friction is lower in the normal orientation compared to the other two. The reasons for the difference between the coefficients of friction in the parallel and anti-parallel orientations is still unclear.

The difference in the wear rates among the three fiber orientations of graphite-epoxy can be explained based on the wear mechanisms already discussed. It should be mentioned here that the highest wear rates are observed in the normal orientation and the lowest in the anti-parallel orientation. The differences in wear rates are more pronounced at lower velocities. Wear in the normal orientation is the highest due to the combination of adhesive wear, fatigue wear and three-body abrasive wear. Three-body abrasion removes the matrix at the surface, leaving the fibers subjected to cantilever type

loading, and resulting in large deflections and stresses in the fibers. This facilitates in faster removal of material through fatigue. The difference in the wear rates between the parallel and anti-parallel orientations can be explained based on the direction of loading and propagation of cracks. In the parallel orientation, friction force produces tensile stresses along the length of the fibers, i.e., in the longitudinal direction, whereas in the anti-parallel orientation tensile stresses are produced in the transverse direction. Cracks propagate more easily in the direction perpendicular to the direction of tensile stresses. Therefore, cracks propagate transversely in the parallel orientation, and longitudinally in the anti-parallel orientation. As the fibers are stronger in the longitudinal direction, higher resistance to crack propagation is offered in the anti-parallel orientation. This causes lower wear of the fibers in the anti-parallel orientation. As the total wear rate strongly depends on the wear rates of the fibers, anti-parallel orientation is seen to show the minimum wear. At higher velocities, as adhesive wear dominates the wear process, such differences in wear rates among the three fiber orientations arising out of fatigue wear is very small.

Comparing the wear rates among the three fiber orientations of carbon-PEEK seems quite complex. The possible mechanisms of wear have already been discussed. The wear rate in the normal orientation is found to be the highest, but the reason why wear through micro-cracking should be higher than that through transverse cracking is still unclear. The wear in the anti-parallel orientation is found to be the lowest. The argument given for graphite-epoxy, based on the direction of crack propagation, also seems applicable to carbon-PEEK.

CHAPTER 6

CONCLUSIONS

1. The infrared microscope system was successfully used to carry out the first direct measurement of surface temperatures produced by friction with polymer composites.

2. Effects of fiber orientation and sliding velocity on friction, wear and surface temperature rise in unidirectional fiber reinforced graphite-epoxy and carbon-PEEK composites were investigated.

3. Surface temperatures on the order of 100 - 160°C were measured with graphite-epoxy and carbon-PEEK composites sliding on sapphire, at low rates of frictional heat generation. The corresponding coefficients of friction were on the order of 0.45 - 0.65.

4. There was very little effect of fiber orientation on the surface temperature rise in graphite-epoxy. In carbon-PEEK, normal orientation resulted in the highest temperature rise, and parallel orientation the lowest.

5. Fiber orientation was found to influence the coefficient of friction and wear. Normal orientation generally showed the lowest coefficient of friction, but the highest wear.

6. Surface temperatures in both the materials were found to increase with sliding velocity and reach a maximum value. Thereafter, the temperature stayed constant with further increase in velocity. The maximum temperature levels were found to be in the range of the glass transition temperatures of the matrix materials.

7. In unidirectional sliding, coefficients of friction were found to decrease with sliding velocity in the normal and parallel orientations within the velocity range examined. The coefficients of friction in the anti-parallel orientation were found to increase initially, and then decrease within the same velocity range.

8. Wear in graphite-epoxy wear was found to decrease with an increase in velocity at low sliding velocities. At higher velocities, it was seen to increase with velocity. The lowest values of wear rates for the three fiber orientations were found to be the same. On the contrary, with an increase in velocity, wear rate in carbon-PEEK showed an initial increase followed by a decrease.

9. Wear in graphite-epoxy is believed to be occurring due to a combination of adhesion and surface fatigue. Three-body abrasive wear is also believed to be occurring in the normal orientation.

10. Wear in the normal orientation of carbon-PEEK is also believed to be due to a combination of adhesion and surface fatigue. In the other two orientations, it is believed to be due to transverse cracking of the fibers.

11. Comparison of the experimental temperatures with the theory identifies the importance of contact area in surface temperatures. The experimental temperature values are found to lie between the values obtained using frictional and the estimated contact area. The two theories (Archard's and Vick's) are found to predict temperatures fairly close to each other.

12. A two-regime tribological model is proposed to explain the behavior of polymer composites. The "low velocity regime" is identified as the velocity range in which the surface temperature is below the glass transition temperature of the polymer matrix; the "high velocity regime" is that in which the surface temperature is equal to the glass transition temperature of the polymer matrix. The wear rate is believed to be controlled more by surface temperature in the high velocity regime.

13. No significant difference could be observed between the coefficients of friction of the two materials. Surface temperatures were found to be higher in carbon-PEEK compared to graphite-epoxy under similar sliding conditions. But wear was found to be higher with graphite-epoxy than with carbon-PEEK.

Significance of the Research

In addition to the above list of findings, it is perhaps important to mention the significance of this research. The significance may include the contributions of this work to the overall knowledge of composite tribology, including the design and processing of polymer composites for tribological applications. Although this work is not directly involved with the design and processing of polymer composites for tribological applications, certain inferences can be made, which could be important to such areas.

1. Knowledge of Composite Tribology - The study on surface temperatures including measurement and its effects on other tribological parameters is often neglected in the area of composite tribology. But this study points out the importance of surface temperatures in composite tribology. Even under mild sliding conditions, surface temperatures in such systems could be very high compared to other material systems; therefore they could be critical. They could conceivably be controlling or dominant factors in friction, wear, and lubrication of polymer composites.

2. Design of Tribological Components with Polymer Composites - Although this study does not directly involve the design of tribological components, certain results observed here could be important to design as well. It appears that for some composites, there exists a narrow velocity range in which the wear rate is a minimum. This optimum velocity range should be considered while designing with such composites. As an

example, graphite-epoxy shows least wear in the velocity range of 3-5 m/s. Thus, it may not therefore be a good choice for material in systems where the speed (or resultant surface temperature) exceeds this range.

Another aspect which should be given some thoughts is designing the right material for specific tribological applications. This may involve the designing of components out of composites consisting of more than two materials. A suitable combination of these materials could be investigated to widen the optimum operating range.

3. Processing of Polymer Composites for Tribological Applications - A few guidelines on processing techniques to be employed for manufacturing tribological components out of polymer composites can also be inferred from this study. Analysis of the mechanisms of wear in polymer composites indicates that fatigue wear is one of the mechanisms. Such wear is initiated by surface cracks. The presence of surface cracks induced during processing could therefore be extremely important. Presence of residual stresses could also be critical. As most of the polymer processing techniques involve some kind of thermal treatment, caution should be taken in designing processing techniques so that residual stresses and cracks are kept to a minimum.

Often, machining is employed to produce components out of composites. But this is expected to give rise to extensive surface cracking, which may result in severe wear in the component. It is therefore suggested to evaluate the process before using in the manufacture of tribological components.

CHAPTER 7

RECOMMENDATIONS

1. Experiments should be conducted to measure the variation of wear rate as a function of time. It is shown in this study that wear rate is influenced by surface temperature. Therefore, it would be of interest to know how wear rate changes as surface temperature builds up during an experiment. This could establish direct dependence of wear rate on surface temperature.

2. Chemical analysis of the worn surface should be done to find out if any chemical changes take place at the surface as a result of high surface temperatures. Possible changes include oxidation, thermal degradation and changes in crystallinity. Techniques as Electron Spectroscopy Chemical Analysis (ESCA) and Auger Electron Spectroscopy may be used for such analysis.

3. Experiments should be carried out to investigate the effects of bulk temperatures on tribological behavior of these composites. It should be verified if the maximum temperatures attained in tribological processes involving polymer composites is limited by the glass transition temperature of the matrix materials. This could be studied by

running experiments at increased bulk temperatures.

4. Further studies should be carried out to understand more thoroughly the mechanisms of friction and wear in these systems. Both physical and chemical analysis of the transfer film on the counterface should be done.

5. Experiments should be run over a much broader velocity range -- possibly up to 3 - 4 orders of magnitude. From this, viscoelastic effects of the polymer matrix on tribological behavior of the polymer composites would be more evident.

6. Viscoelastic modeling of polymer composites under tribological loading conditions should be studied.

7. Effects of atmosphere on tribological behavior of polymer composites should be investigated. This may include the effect of humidity, oxygen, and inert gases (e.g., N_2).

8. Thermophysical and mechanical properties of most currently used polymer composite materials are not readily available. Therefore, experiments to determine these values should be carried out.

9. Modifications in the test apparatus should be done to minimize normal load variation.

A low inertia loading arm (e. g., a pneumatic loading system) could be incorporated.

10. Better adhesives that would withstand high loads and temperatures may be investigated for mounting the sapphire disks on the shafts.

11. The possibility of using a video camera to record physical changes occurring at the contact area viewed through the optical channel of the infrared microscope may be investigated. This would enable one to record physical changes simultaneously with temperature variations at the contact area. Further, this would enable one to locate precisely the position of the infrared microscope during scanning.

12. Experiments should be carried out with composite-composite systems to demonstrate the severity of the effects of surface temperatures in tribological processes with polymer composites. The surface temperatures are expected to reach very high values in composite-composite systems under relatively mild sliding conditions compared to composite-sapphire systems. These experiments could be carried out in a pin-on-disk machine.

References

1. Furey, M. J., "Tribology," *Encyclopedia of Materials Science and Engineering*, Pergamon Press, Oxford, 1986, pp. 5154-5158.

2. Furey, M. J., "The 'in situ' Formation of Polymeric Films on Rubbing Surfaces, "*Proc. of International Conference on Polymers and Lubrication (Brest)*, publ. by Centre National de la Recherche Scientifique, Paris, 1975.

3. Furey, M. J., and C. Kajdas, "Models of Tribopolymerization as an Anti-Wear Mechanism," *Proc. of Japan Intl. Tribology Conf.*, Nagoya, Japan, Oct 29 - Nov 1, 1990.

4. Wiggins, J. M., *An Experimental Method for Measuring Surface Temperatures Generated by Friction*, Master of Science Thesis, Mechanical Engineering, Virginia Polytechnic Institute and State University, Blacksburg, VA., Dec. 1974.

5. Omori, D. I., *Infrared Measurement of Surface Temperatures Generated by Friction*, Master of Science Thesis, Mechanical Engineering, Virginia Polytechnic Institute and State University, Blacksburg, VA., Aug. 1975.

6. Li, S. H., *Experimental Investigation of Surface Temperatures of Some Polymers in Unlubricated Sliding*, Master of Science Thesis, Mechanical Engineering, Virginia Polytechnic Institute and State University, Blacksburg, VA., Aug. 1976.

7. Richardson, M. H., *Experimental Investigation of Surface Temperature of Graphite in a Sliding System Using an Infrared Microscope*, Master of Science Thesis, Mechanical Engineering, Virginia Polytechnic Institute and State University, Blacksburg,VA., Aug.1976.

8. Rogers, C. A., *An Experimental Investigation of the Effect of Subdivision of Contact Area on Surface Temperatures Generated by Friction*, Master of Science Thesis, Mechanical Engineering, Virginia Polytechnic Institute and State University, Blacksburg, VA.,Dec. 1982.

9. Moyer, S. C., *Infrared Radiometric Measurement of Surface Temperatures Generated by Friction of Iron-on-Sapphire*, Master of Science Thesis, Mechanical Engineering, Virginia Polytechnic Institute and State University, Blacksburg, VA., Feb. 1983.

10. Hollowell, E. L., *Infrared Measurements of Steady-State Temperatures and Average Surface Temperature Distributions for Silver Sliding on Sapphire,* Master of Science Thesis, Mechanical Engineering, Virginia Polytechnic Institute and State University, Blacksburg, VA., Nov.1983.

11. Sankar, J., *Data Acquisition Systems for Three-Dimensional Representation and Analysis of Surface Topography and Surface Temperatures in Tribological Processes,* Master of Science Thesis, Mechanical Engineering, Virginia Polytechnic Institute and State University, Blacksburg, VA., May 1986.

12. Furey, M. J., and H. M. Ghasemi, "Tribological Behavior of Thin Polymeric Coatings Under Conditions of Oscillating/Fretting Contact," *Proceedings of the Japan Intl. Tribology Conf.*, Nagoya, Japan, Oct. 29 - Nov. 1, 1990.

13. Weick, B. L., *Infrared Measurements of Surface Temperatures During Oscillating/Fretting Contact with Ceramics,* Master of Science Thesis, Mechanical Engineering, Virginia Polytechnic Institute and State University, Blacksburg, VA., May 1990.

14. Foo, S. J., *Theoretical Study of Heat Distribution and Surface Temperatures Generated in Oscillating Contact,* Master of Science Thesis, Mechanical Engineering, Virginia Polytechnic Institute and State University, Blacksburg, VA., Jan. 1990.

15. Golan, L. P., *Thermal Analysis of Sliding Contact Systems Using the Boundary Element Method,* Master of Science Thesis, Mechanical Engineering, Virginia Polytechnic Institute and State University, Blacksburg, VA., March 1991.

16. Ghasemi, H. M., *"Fundamental Studies on Tribological Behavior of Thin Polymer Coatings Under Fretting Contact Conditions Using Infrared and Photo/Video Techniques,"* Doctorate of Philosophy Dissertation, Materials Engineering and Science, Virginia Polytechnic Institute and State University, Blacksburg, VA., Anticipated Date: Nov. 1991.

17. Yoo, J. H., *Tribological Behavior of Unfilled and Carbon Fiber Reinforced Polyetheretherketone/Polyetherimide Composites,* Master of Science Thesis, Mechanical Engineering, Virginia Polytechnic Institute and State University, Blacksburg, VA., Sept. 1991.

18. Lancaster, J. K., "The Effect of Carbon Fiber Reinforcement on the Friction and Wear of Polymers," *Brit. J. Appl. Phys. (J. Phys. D.),* 1968, Ser. 2, Vol. 1, pp. 549-559.

19. Briscoe, B. J., A. K. Pogosian and D. Tabor, "The Friction and Wear of High Density Polythene: The Action of Lead Oxide and Copper Oxide Fillers," *Wear,* Vol. 27, 1974, pp. 19-34.

20. Bahadur, S., and D. Tabor, "The Wear of Filled Polytetrafluoroethylene," *Wear,* Vol. 98, 1984, pp. 1-13.

21. Tsukizoe, T., and N. Ohmae, "Wear Mechanism of Unidirectionally Oriented Fiber-Reinforced Plastics," *Trnsactions of the ASME Journal of Lubrication Technology*, Oct. 1977, pp. 401-407.

22. Fusaro, R. L., and H. E. Sliney, "Friction and Wear Behavior of Graphite Fiber Reinforced Polyimide Composites," *ASLE Transactions*, Vol. 21, 1978, pp. 337-343.

23. Tanaka, K., "Friction and Wear of Glass and Carbon Fiber-Filled Thermoplastic Polymers," *Transactions of the Journal of Lubrication Technology*, Oct. 1977, pp. 408-414.

24. Sung, N., and N. P. Suh, "Effect of Fiber Orientation on Friction and Wear of Fiber Reinforced Polymeric Composites," *Wear*, Vol. 53, 1979, pp. 129-141.

25. Clerino, M., and V. Patierno, "Sliding Wear of Polymeric Composites," *Wear*, Vol. 53, 1979, pp. 279-301.

26. Chang, H., "Wear Characteristics of Comosites: Effect of Fiber Orientation," *Wear*, Vol. 85, 1983, pp. 81-91.

27. Roberts, J. C., F. F. Ling, and W. R. Jones, Jr., "Fabrication and Wear Test of a Continuous Fiber/Particulate Composite Total Surface Hip Replacement," *ASLE Transactions*, Vol. 26, 3, 1983, pp. 367-375.

28. Roberts, J. C., "A Graphical Representation of Tribological Properties in Polymer-Graphite/Epoxy Sliding, *ASLE Transactions*, Vol. 27, 4, 1984, pp. 313-320.

29. Roberts, J. C., and J. G. Elliot, "An Analysis and Comparison of the Tribological Behavior of Two Polymers Sliding Against a Polymeric Composite," *ASLE Transactions*, Vol. 27, 2, 1984, pp. 138-145.

30. Roberts, J. C., "Surface Morphology Studies in Polymer-Graphite/Epoxy Sliding," *ASLE Reprint*, Reprint No. 84-LC-4A-2, 1984.

31. Fusaro,R.L.,"Counterface Effects on the Tribological Properties of Polyimide Composites," *ASLE Preprint*, Preprint No.85-TC-3A-1, 1985.

32. Abarou, S., D. Play, and F. E. Kennedy, "Wear Transition of Self-Lubricating Composites Used in Dry Oscillating Applications," *ASLE Transactions*, Vol. 30, 3, 1987, pp. 269-281.

33. Anderson, J. C., and A. Davis, "Polymer Composite Abrasiveness in Relation to Counterface Wear," *Lubrication Engineering*, Vol. 40, 1, 1984, pp. 41-46.

34. McGee, A. C., C. H. K. Dharan, and I. Finnie, "Abrasive Wear of Graphite Fiber-Reinforced Polymer Composite Materials, *Wear*, Vol. 114, 1987, pp. 97-107.

35. Voss, H., and K. Friedrich, "On the Wear Behavior of Short-Fiber-Reinforced PEEK Composites," *Wear,* Vol. 116, 1987, pp. 1-18.

36. Hanmin, Z., H. Guoren, and Y. Guicheng, "Friction and Wear of Poly(Phenylene Sulphide) and Its Carbon Fiber Composites:I Unlubricated," *Wear,* Vol. 116. 1987, pp. 59-68.

37. Friedrich, K., *Friction and Wear of Polymer Composites,* Fortschritt-Berichte Der VDI Zeitschriften, Reihe 18, No. 15, Dusseldorf: VDI-Verlag, 1984.

38. Kar, M. K. , and S. Bahadur, "The Wear Equation of Unfilled and Filled Polyoxymethylene," *Wear,* Vol. 30, 1974, pp. 337-348.

39. Bohner, J. J., and M. N. Gardos, "The Effect of Composition on the Load-Speed Time-Dependent Oscillatory Wear of Selected, Polymeric Self-Lubricating Composites," *Lubrication Engineering,* Vol. 43, 5, 1987, pp. 347-350.

40. Cirino, M., K. Friedrich, and R. B. Pipes, "Effect of Fiber Orientation on the Abrasive Wear Behavior of Polymer Composite Materials," *Wear,* Vol. 121, 1988, pp. 127-141.

41. Lhymn, C., "Analysis of Wear Statistics For Polymer Composites," *Wear,* Vol. 114, 1987, pp. 223-239.

42. Lhymn, C., and S. V. Pepper, "On the Specific Wear Rate of Polymer Composites," *Advances in Polymer Technology,* Vol. 9, No. 1.

43. Lhymn, C., "Tribological Properties of Unidirectional PolyPhenylene Sulfide-Carbon Fiber Laminate Composites," *Wear,* Vol. 117, 1987, pp. 147-159.

44. Lhymn, C., and R. Light, "Effect of Sliding Velocity on Wear Rate of Fibrous Polymer Composites," *Wear,* Vol. 166, 1987, pp. 343-359.

45. Lhymn, C., "Effect of Normal Load on the Specific Wear Rate of Fibrous Composites," *Wear,* Vol. 120, 1987, pp. 1-27.

46. Lhymn, C., "Effect of Environment on the Two-Body Abrasion of Polyether Etherketone (PEEK)/Carbon Fiber Composites," *ASLE Transactions,* Vol. 30, 3, 1987, pp. 324-327.

47. Lhymn, C., "Lubricated Wear of Fiber-Reinforced Polymer Composites," *Wear,* Vol. 122, 1988, pp. 13-31.

48. Tanaka, K., S. Ueda and N. Noguchi, "Fundamental Studies on the Brake Friction of Resin-based Friction Materials," *Wear,* Vol. 23, 1973, pp. 349-365.

49. Gong, D., Q. Xue, and H. Wang, "Study of the Wear of Filled Polytetrafluoroethelene," *Wear,* Vol. 134, 1989, pp. 283-295.

50. Evans, D. C., "The Friction and Wear Properties of PTFE Composites at Elevated Temperatures," Tribology 1978; Materials Performance and Conservation, *I Mech E Conference Publication 1978-6,* 1978, pp. 1-16.

51. Briscoe, B. J., and M. D. Steward, "The Effect of Carbon and Glass Fillers on the Transfer Film Behavior of PTFE Composites," Tribology 1978; Materials Performance and Conservation, *I Mech E Conference Publication 1978-6,* 1978, pp. 17-22.

52. West, G. H., and J. M. Senior, "High Temperature Plastics Bearing Compositions," *Tribology,* Dec. 1973, pp. 269-275.

53. Baranovskii, V. M., V. P. Dushchenko, E. M. Natanson, V. V. Levandovskii, V. M. Chegoryan, and B. P. Dem'yanyuk, "Temperature Dependence of the Thermophysical Properties of a Teflon-Bronze Antifriction Material," *Polymer Mechanics (Soviet),* Vol. 6, No. 6, Dec. 1973, pp. 269-273.

54. Ling, F. F., and C. F. Yang, "Surface Temperatures of Moving Layered Composites," *Surface Mechanics,* ASME, United Engineering Center, New York, 1969.

55. Roberts, J. C., and O. H. Griffin, Jr., "Analytical Experimental Heat Transfer in Dry Sliding of Polymeric Composites, *ASLE Transactions,* Vol. 26, 4, 1983, pp. 493-500.

56. Day, A. J., "An Analysis of Speed, Temperature, and Performance Characteristics of Automotive Drum Brakes," *Transactions of the ASME Journal of Tribology,* Vol. 110, Apr. 1988, pp. 298-305.

57. McLaren, K. G., and D. Tabor, "Friction of Polymers at Engineering Speeds: Influence of Speed, Temperature and Lubricants," *Paper presented for discussion during the Lubrication and Wear Convention,* Bournemouth, May 23-25, 1963.

58. Vinogradov, G. V., G. M. Bartenev, A. I. El'kin, and V. K. Mikhaylov, "Effect of Temperature on Friction and Adhesion of Crystalline Polymers," *Wear,* Vol. 16, 1970, pp. 213-219.

59. Price, H. L., and H. D. Burks, "Friction and Friction-Generated Temperature at a Polymer-Metal Interface," *Polymer Engineering and Science,* Vol. 14, No. 4, Apr. 1974.

60. Kar, M. K., and S. Bahadur, "An Investigation of the Temperature Rise in Polymer-Metal Sliding," *Wear,* Vol. 82, 1982, pp. 81-92.

61. Ettles, C. M. M., "Polymer and Elastomer Friction in the Thermal Control Regime," *ASLE Transactions,* Vol. 30, 2, 1987, pp. 149-159.

62. Ettles, C. M. M., and J. H. Shen, "The Influence of Frictional Heating on the Sliding Friction of Elastomers and Polymers," *Presented at a meeting of the Rubber Division, American Chemical Society,* Montreal, Quebec, Canada, May 26-29, 1987.

63. Tanaka, K., and Y. Yamada, "Effect of Temperature on the Friction and Wear of Some Heat-Resistant Polymers," Conference: Polymer Wear and Its Control, *American Chemical Society Symposium*, Series 287, 1984, pp. 103-128.

64. Vroegop, P. H., H. H. Vermeulen, and R. Bosma, "The Infuence of Temperature, Speed and Roughness on the Dry Sliding Friction and Wear of Nylon 6.6 Against Steel," *Friction and Traction, Proceedings of the 7th Leeds-Lyon Symposium on Tribology*, Leeds, England, Sept. 9-12, 1980.

65. Anderson, J. C., and E. J. Robbins, "The Influence of Temperature Generation on the Wear of Some Polymers", Wear of Non-Metallic Materials, *Proceedings of the Leeds-Lyon Symposium on Tribology, 3rd Meeting*, England, 1978, pp. 94-98.

66. Santini, J. J., and F. E. Kennedy, "An Experimental Investigation of Surface Temperatures and Wear in Disk Brakes", *ASLE Preprint*, No. 74, LC-IB-3, 1974, pp. 1-7.

67. Spurr, R. T., "Temperatures Reached During Sliding", *Wear*, Vol. 55, 1979, pp. 289-293.

68. Ling, F.F., and T. E. Simkins, "Measurement of Pointwise Juncture Condition of Temperature at the Interface of Two Bodies of Sliding Contact," *ASME Transactions, Journal of Basic Engineering*, No. 62, 1962, pp. 1-5.

69. Shore, H., "Thermoelctric Measurement of Cutting Tool Temperature," *Journal Washington Academy of Science*, Vol. 15, 1925, pp. 85-88.

70. Furey, M. J., "Surface Temperatures in Sliding Contact," *ASLE Transactions*, Vol. 7, 1964, pp. 133-146.

71. Kannel, J. W., F. F. Augaro, and T. A. Dow, "A Method for Measuring Surface Temperatures Between Rolling/Sliding Steel Cylinders," *ASME Transactions, Journal of Lubrication Technlogy*, Vol. 100, Jan. 1978, pp. 110-114.

72. Quinn, T. F., and W. O. Winer, "An Experimental Study of the 'Hot-Spots' Occurring During the Oxidational Wear of Tool Steel on Sapphire," *Transactions of the ASME, Journal of Tribology*, Vol. 109, April 1987, pp. 315-511.

73. Quinn, T. F., "The Dry Wear of Steel as Revealed by Electron Microscopy and X-Ray Diffraction," *Proc. Institute of Mechanical Engineers*, Vol. 182, 1968.

74. Parker, R. C., and P. R. Thomas, "The Measurement of the Temperature of Sliding Surfaces with Particular Reference to Railway Brake Blocks," *Proc. Institute of Mechanical Engineers*, Vol. 158, 1948, pp. 209-229.

75. Bowden, P. F., and P. H. Thomas, "The Surface Temperature of Sliding Solids," *Royal*

Society of London Proceedings, A223, 1954, pp. 29-40.

76. Chao, B. T., H. L. Li, and K. J. Trigger, "An Experimental Investigation of Temperature Distribution at Tool Flank Surface," *ASME Transactions, Journal of Engineering for Industry,* Nov. 1961, pp. 496-504.

77. Turchina, V., D. M. Sanborn, W. O. Winer, "Temperature Measurements in Sliding Elastohydrodynamic Point Contacts," *ASME Transactions, Journal of Lubrication Technology,* July 1974, pp. 464-471.

78. Ausherman, V. K., H. S. Nagraj, D. M. Sanborn, and W. O. Winer, "Infrared Temperature Mapping in Elastohydrodynamic Lubrication," *ASME Transactions, Journal of Lubrication Technology,* Apr. 1976, pp.236-243.

79. Nagraj, H. S., D. M. Sanborn, and W. O. Winer, "Effects of Load, Speed and Surface Roughness on Sliding EHD Contact Temperatures, *ASME Transactions, Journal of Lubrication Technology,* Apr. 1976, pp. 254-263.

80. Winer, W. O., D. M. Sanborn, and H. S. Nagraj, "Direct Surface Temperature Measurements by Infrared Radiation in Elastohydrodynamic Contacts and the Correlation with the Blok Flash Temperature Theory," *Wear,* Vol. 49, 1978, pp. 43-59.

81. Griffioen, J. A., S. Bair, and W. O. Winer, "Infrared Surface Temperature Measurements in a Sliding Ceramic-Ceramic Contact," *Mechanisms and Surface Distress,* Dowson et al., eds., Butterworths, 1986, pp. 238-245.

82. Furey, M. J., "Infrared Measurement of Surface Temperatures Produced in Tribological Processes," *Proceedings, 3rd International Tribology Congress ("EUROTRIB-81"), Warsaw, 21-24 September 1981, Vol. I (Tribological Processes in Solid Body Contact Areas),* pp. 118-139.

83. Furey, M. J. and C. A. Rogers, "Infrared Measurements of Surface Temperatures Generated in Friction in Dry Sliding Contact," *National Science Foundation Workshop on Tribology,* Atlanta, GA, 10-11 Aug. 1987.

84. Furey, M. J., B. Vick, S. J. Foo and B. L. Weick, "A Theoretical and Experimental Study of Surface Temperatures Generated During Fretting, "*Proceedings of the Japan Intl. Tribology Conf.*, Nagoya, Japan, Oct 29-Nov 1, 1990.

85. Blok, H., "Theoretical Study of Temperature Rise at Surfaces of Actual Contact Under Oiliness Lubricating Conditions, "*Proc. Inst. of Mechanical Engineers General Discussion on Lubrication,* of Mechanical Engineers, London, Vol.2, 1937, pp. 222-235.

86. Blok, H., "The Flash Temperature Concept," *Wear,* Vol.6, 1963, pp. 483-494.

87. Blok, H., "Thermo-tribology - Fifty Years On," *Proceedings of the International*

Conference on Tribology Fifty Years On, The Institution of Mechanical Engineers, London, Vol.1, 1987, pp. C248-C251.

88. Jaeger, J. C., "Moving Sources of Heat and the Temperature at Sliding Contacts," *J. Royal Society of N. S. Wales,* Vol.76, 1942, pp. 203-224.

89. Archard, J. F., "The Temperature of Rubbing Surfaces," *Wear,* Vol.2, 1958/1959, pp. 438-455.

90. Archard, J. F., and R. A. Rowntree, "Temperature of Rubbing Bodies: Part 2, The Distribution of Temperatures," *Wear,* Vol. 128, 1988, pp. 1-17.

91. Ling, F. F., "A Quasi-Interactive Method for Computing Interface Temperature Distributions," *ZAMP,* Vol. 10, 1959, pp. 461-474.

92. Ling, F. F., and C. W. Ng, "On Temperatures at the Interfaces of Bodies in Sliding Contact," *Proc. 4th U. S. Natl. Congr. of Applied Mechanics, ASME,* New York, 1962, pp. 1343-1349.

93. Ling, F. F., and S. L. Pu, "Probable Interface Temperatures of Solids in Sliding Contact," *Wear,* Vol. 7, 1964, pp. 13-34.

94. Ling, F. F., "On Temperature Transients at Sliding Surfaces," *Journal of Lubrication Technology,* Vol. 91, 1969, pp. 397-405.

95. Lai, W. T., and H. C. Cheng, "Temperature Analysis in Lubricated Simple Sliding Rough Contacts," *ASLE Transactions,* Vol. 28, 1984, pp. 303-312.

96. Kennedy, F. E., "Surface Temperatures in Sliding Systems -- A Finite Element Analysis," *Journal of Lubrication Technology,* Vol. 103, 1981, pp. 90-96.

97. Kennedy, F. E., F. Colin, A. Floquet, and R. Glovsky, "Improved Techniques for Finite Element Analysis of Sliding Surface Temperatures," *Proceedings, 10th Leeds-Lyon Symposium on Tribology,* Butterworths, London, 1983.

98. Colin, F., and A. Floquet, "A Combination of Finite Element and Integral Transform Techniques in a Heat Conduction Quasi-Steady State Problem," *Int. J. Num. Meth. Eng.,* Vol. 23, 1986, pp. 13-23.

99. Rizzo, F. J., and D. J. Shippy, "A Method of Solution for Certain Problems of Transient Heat Conduction," *AIAA J.,* Vol. 8(11), 1970, pp. 2004-2009.

100. Vick, B., M. J. Furey, and S. J. Foo, "A Boundary Element Thermal Analysis of Sliding Contact," *Numerical Heat Transfer Part A: Applications,* Vol. 20, 1991, pp. 19-40.

101. Furey, M. J., and B. Vick, *Surface Temperatures Generated in Oscillating Contact,*

Research Proposal, National Science Foundation, 1988.

102. Furey, M. J., and S. Jayaram, "Advanced Techniques in Infrared Measurements of Surface Temperatures Produced By Friction," *Proceedings of the Japan International Tribology Conference,* Nagoya, Japan, Oct. 29 - Nov. 1, 1990.

103. Instruction Manual, Infrared Radiometric Microscope, Model RM-2A, BEC 06 200970, Barnes Engineering Company, Stamford, Conn.

104. Composites and Laminates, Ed. 1, D. A. T. A. Inc., and The International Plastics Selector, 1978, San Diego, California.

105. Thermophysical Properties of Matter, Vol. 2, 5, 8, 10, Series Editor - Y. S. Touloukian, IFI/Plenum Data, Plenum Publishing, 1970-1973.

106. Ludema, K. C., and D. Tabor, "The Friction and Visco-elastic Properties of Polymeric Solids", *Wear,* Vol. 9, 1966, pp. 329-348.

107. Czichos, H., *Tribology, a Systems Approach to the Science and Technology of Friction, Lubrication and Wear,* Elsevier Scientific Pub. Co., New York, 1978.

108. Tyler, J. C., R. A. Burton, and P. M. Ku, "Contact Fatigue Under Oscillating Normal Load," *ASLE Transactions,* Vol. 6, 1963, pp. 225-269.

109. Gillham, J. K., "The Time-Temperature-Transformation (TTT) State Diagram and its Role in Determining Structure/Property Relationships in Thermosetting Systems", *Proceedings of the 55th Meeting of the American Chemical Society,* Atlanta, Georgia, March 1981, pp. 215-225.

APPENDICES

Appendix A. Calibration of the Infrared Microscope

Three different radiance scales (X1, X10 and X100) are available on the Barnes RM-2A infrared microscope. Since all the three settings were used in this study, each was calibrated separately. The calibration of the microscope is done using a heated blackbody source and control unit as shown in Fig. A1.

The infrared microscope is turned on and allowed to warm up for approximately 30 minutes. Proper settings corresponding to the objective (15X or 36X), bandwidth (narrow or wide) and the radiance scale are chosen. The microscope is focused on the center of the blackbody source at ambient temperature and zeroed using the zero-set knob. It is then positioned away from the blackbody source and the temperature of the source is increased. After equilibrium temperature is reached (after approximately 10 minutes) the microscope is focused back on to the source and the AC/DC and DC outputs are recorded using a multimeter. This procedure is repeated at different temperatures of the source. These data are listed in Tables A1 - A3 for the three settings.

The output voltage is plotted against radiance corresponding to the various temperatures of the blackbody source, and the regression equations are obtained. These curves and the regression equations for the three settings are shown in Figs. A2 - A4.

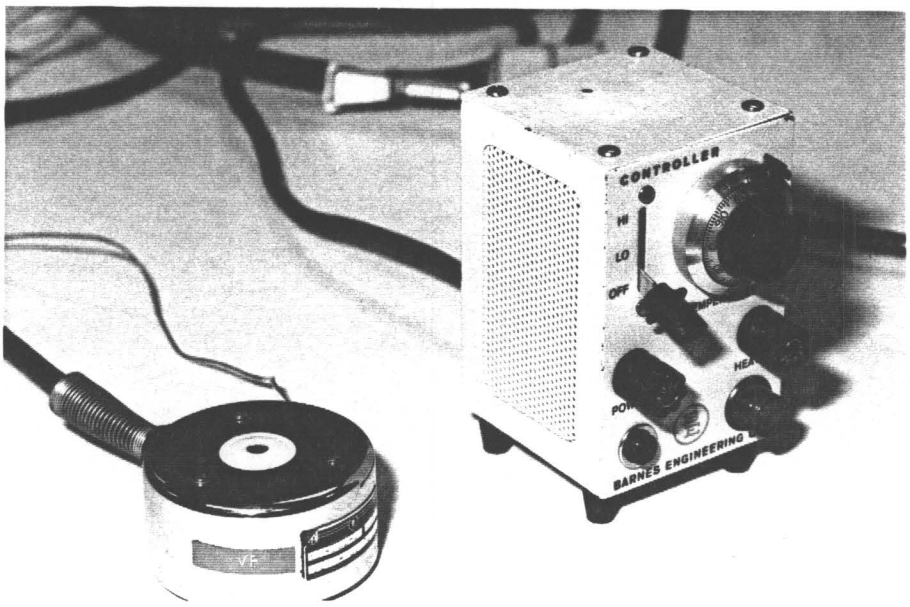

Fig. A1. Blackbody calibration source and control unit.

Table A1. Infrared microscope calibration data at X1 setting.

Temperature of blackbody (°C)	Radiance from blackbody (10^{-2} W/cm^{2}sr)	Output voltage from AC/DC channel (Volts)	Output voltage from DC channel (Volts)
57.5	.98	.81	.42
70.4	1.40	1.36	.76
87.9	2.17	2.46	1.29
93.0	2.44	2.98	1.57
106.1	3.28	3.60	1.89
112.7	3.77	4.22	2.22
119.1	4.30	4.86	2.56
119.5	4.35	5.51	2.90
125.7	4.93	6.14	3.23
133.3	5.71	6.75	3.55

Table A2. Infrared microscope calibration data at X10 setting.

Temperature of blackbody (°C)	Radiance from blackbody (10^{-2} W/cm^{2}sr)	Output voltage from AC/DC channel (Volts)	Output voltage from DC channel (Volts)
59.0	1.05	.065	.033
72.7	1.55	.116	.061
83.5	2.05	.168	.088
99.8	2.95	.273	.143
113.7	4.00	.389	.204
126.5	5.20	.521	.273
139.0	6.70	.681	.357
150.0	8.20	.846	.444
164.0	10.50	1.107	.580
181.5	14.00	1.490	.782
202.5	19.50	2.138	1.122
228.5	27.50	3.085	1.620

Table A3. Infrared microscope calibration data at X100 setting.

Temperature of blackbody (°C)	Radiance from blackbody (10^{-2} W/cm^{2}sr)	Output voltage from AC/DC channel (Volts)	Output voltage from DC channel (Volts)
59.0	1.05	-.008	-.004
88.0	2.30	.005	.0024
107.0	3.60	.018	.0095
123.0	4.90	.033	.017
139.0	6.70	.051	.027
153.5	8.70	.071	.037
172.3	12.20	.105	.055
196.0	17.60	.165	.0865
228.5	27.50	.270	.142

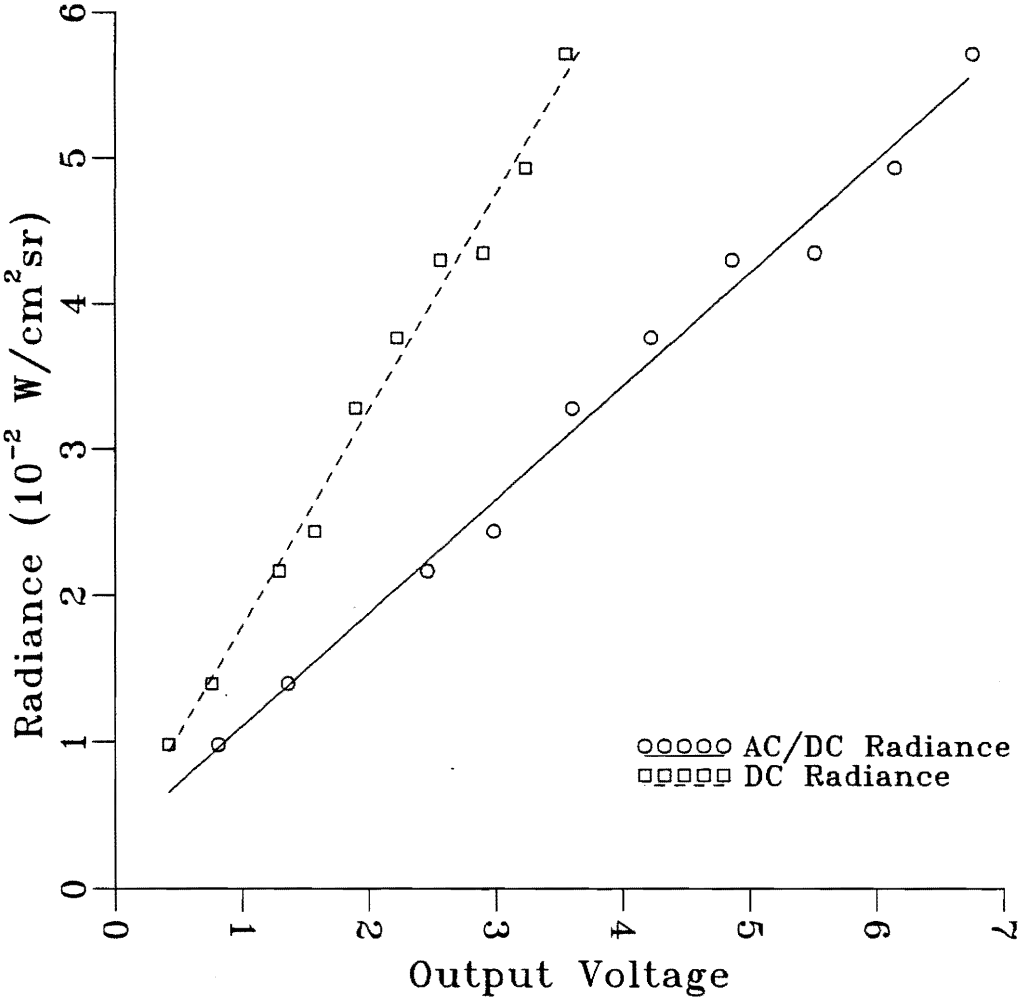

Regression Equations :
Radiance = 0.776 (AC/DC VOLTS) + 0.330
Radiance = 1.482 (DC VOLTS) + 0.312

Fig. A2. Infrared microscope calibration curve for X1 setting.

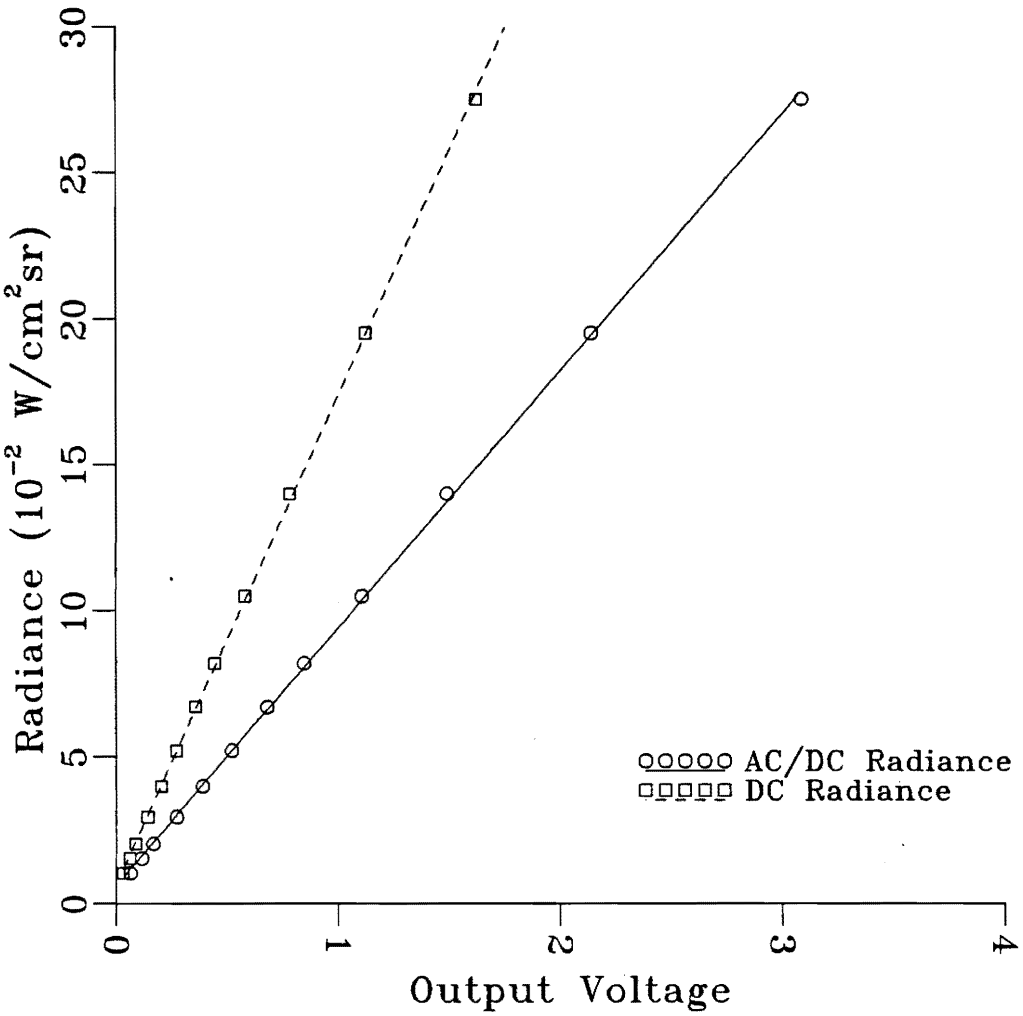

Regression Equations :
Radiance = 8.765 (AC/DC VOLTS) + 0.627
Radiance = 16.746 (DC VOLTS) + 0.636

Fig. A3. Infrared microscope calibration curve for X10 setting.

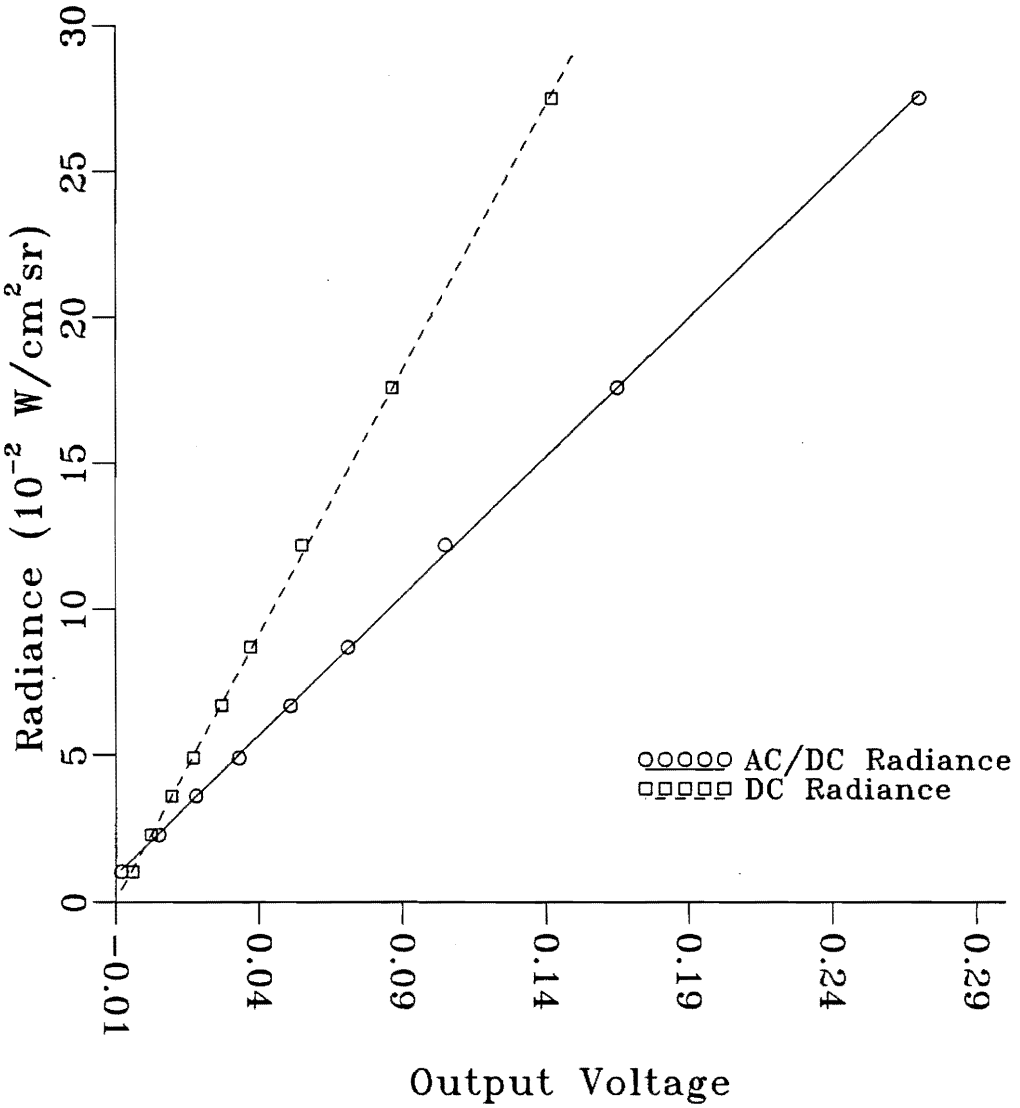

Regression Equations :
Radiance = 95.343 (AC/DC VOLTS) + 1.873
Radiance = 181.380 (DC VOLTS) + 1.889

Fig. A4. Infrared microscope calibration curve for X100 setting.

Appendix B. Calibration of the Strain Ring

The strain ring is comprised of two channels -- the tangential or friction channel and the normal load channel. In this study, only the friction channel was used to measure the friction force. The calibration of the friction channel of the strain ring is done with the help of a calibration arm attached to the set-up as shown in Fig. B1. Through a cable, supported by a miniature cable pulley, known loads are imposed on the strain ring. Voltage outputs from the strain gages are measured using a multimeter.

The data taken at 21°C is presented in Table B1. The calibration curve along with the regression equation is shown in Fig. B2.

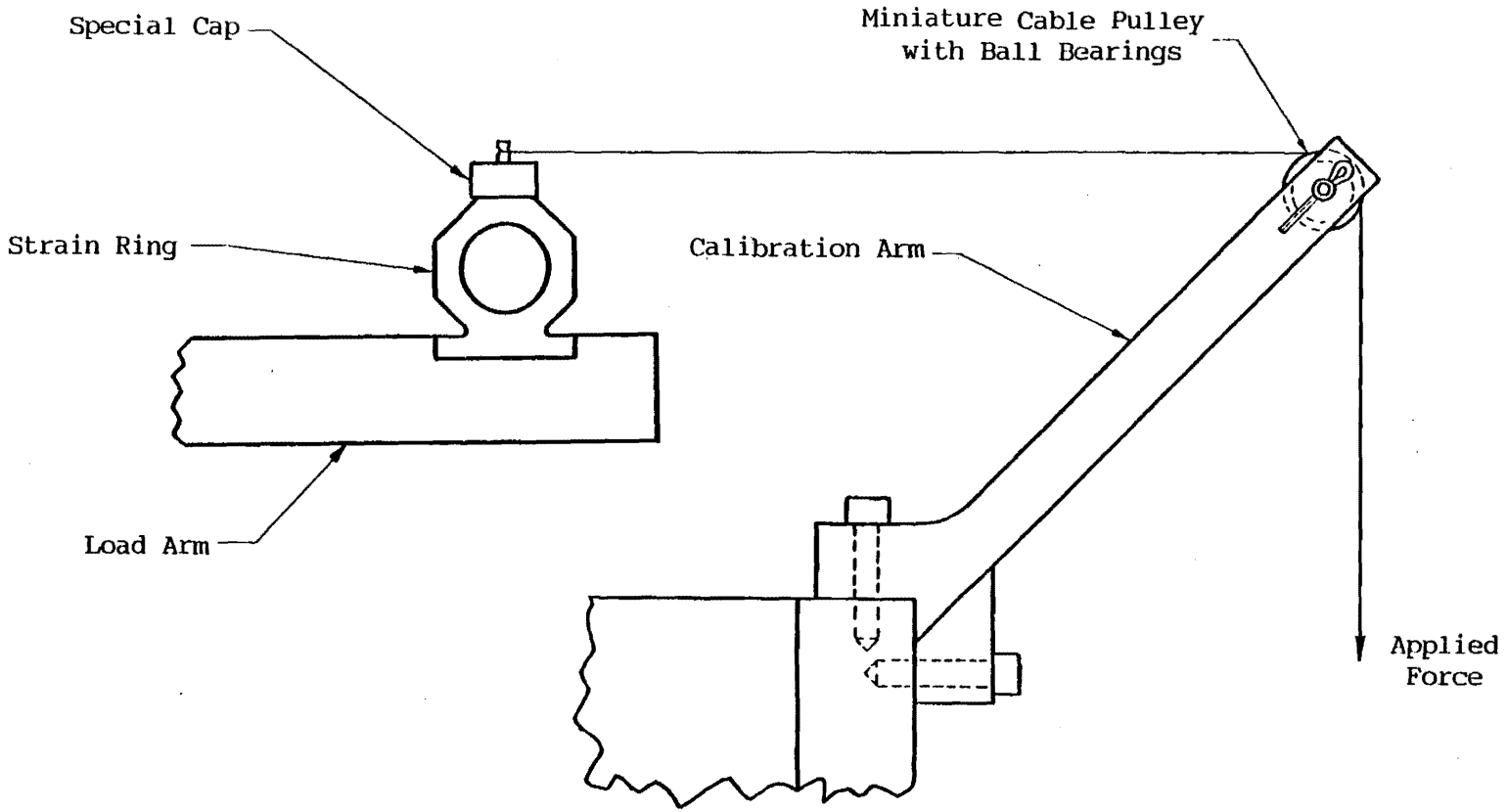

Fig. B1. Set-up for the calibration of the friction channel of the strain ring [13].

Table B1. Calibration data for the friction channel of the strain ring.

TANGENTIAL FORCE (N)	VOLTAGE OUTPUT (milivolts)
1.96	3.
3.88	5.
5.85	7.
7.81	9.
9.74	10.
11.70	12.
13.72	13.
15.69	15.
17.59	17.
19.62	20.
21.58	22.
23.50	24.
25.47	25.
27.43	27.
28.90	31.
33.24	34.
35.20	36.
38.14	38.

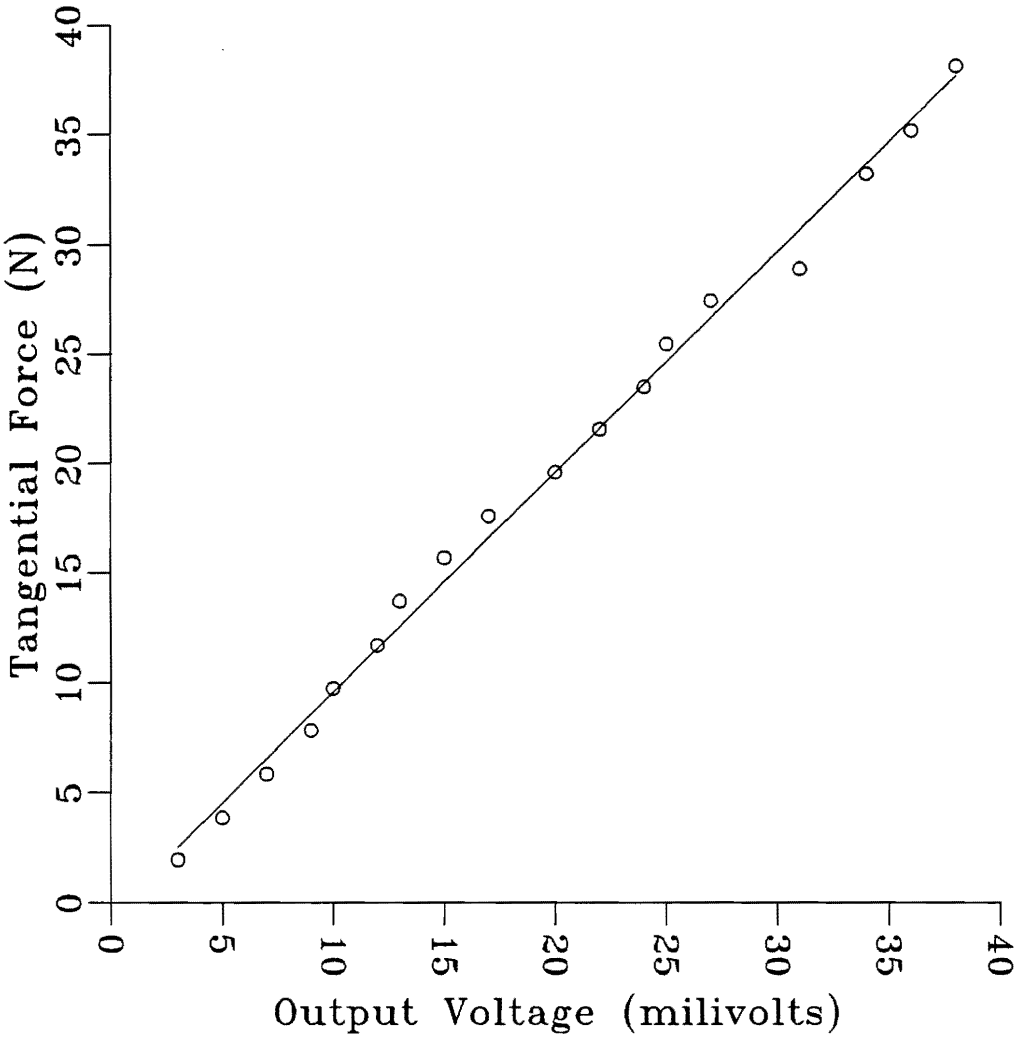

Regression Equation :
Tangential Force (N) = 1.0055 (OUTPUT milivolts) + (−0.4933)

Fig. B2. Calibration curve for the friction channel of the strain ring.

Appendix C. Calibration of the Torque Transducer

The Lebow miniature torque transducer is calibrated using two sets of pulley blocks installed on the experimental set up as shown in Fig. C1. A rigid clamp is used to arrest any movement of the lower end of the torque transducer shaft. An aluminum disk is fixed to the other end of the torque transducer shaft. A length of nylon monofilament is attached to the screw positioned edgewise on the aluminum disk. A pan is attached at one end of the monofilament while a counterweight to balance the weight of the pan is attached at the other end. The torque transducer is powered through a 10 V power supply. Weights are placed on the pan to produce known torques on the transducer. The output voltage is recorded for each torque value.

The calibration data are listed in Table C1. Figure C2 shows the calibration curve along with the regression equation.

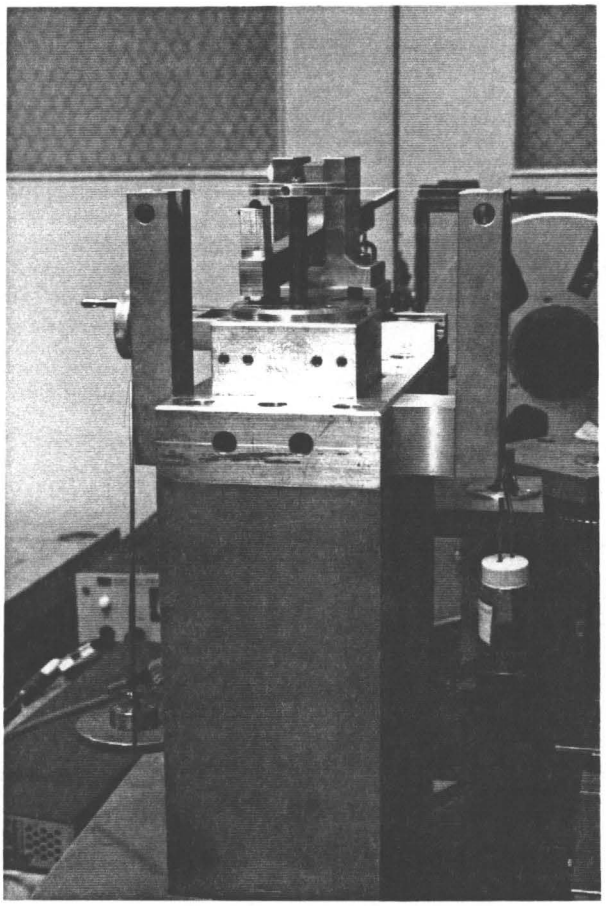

Fig. C1. Set-up for calibration of the torque transducer.

Table C1. Calibration data for the Lebow torque transducer.

APPLIED TORQUE (N cm)	VOLTAGE OUTPUT (milivolts)
0.00	-.33
1.25	.49
2.49	1.33
3.74	2.17
4.98	3.04
6.23	3.95
7.48	4.82
8.72	5.72
9.97	6.59
11.21	7.43
12.46	8.20
13.70	9.07
14.95	9.90
16.19	10.76
17.44	11.63
18.69	12.50
19.93	13.31
21.18	14.18
22.43	15.05
23.67	15.92
24.92	16.75

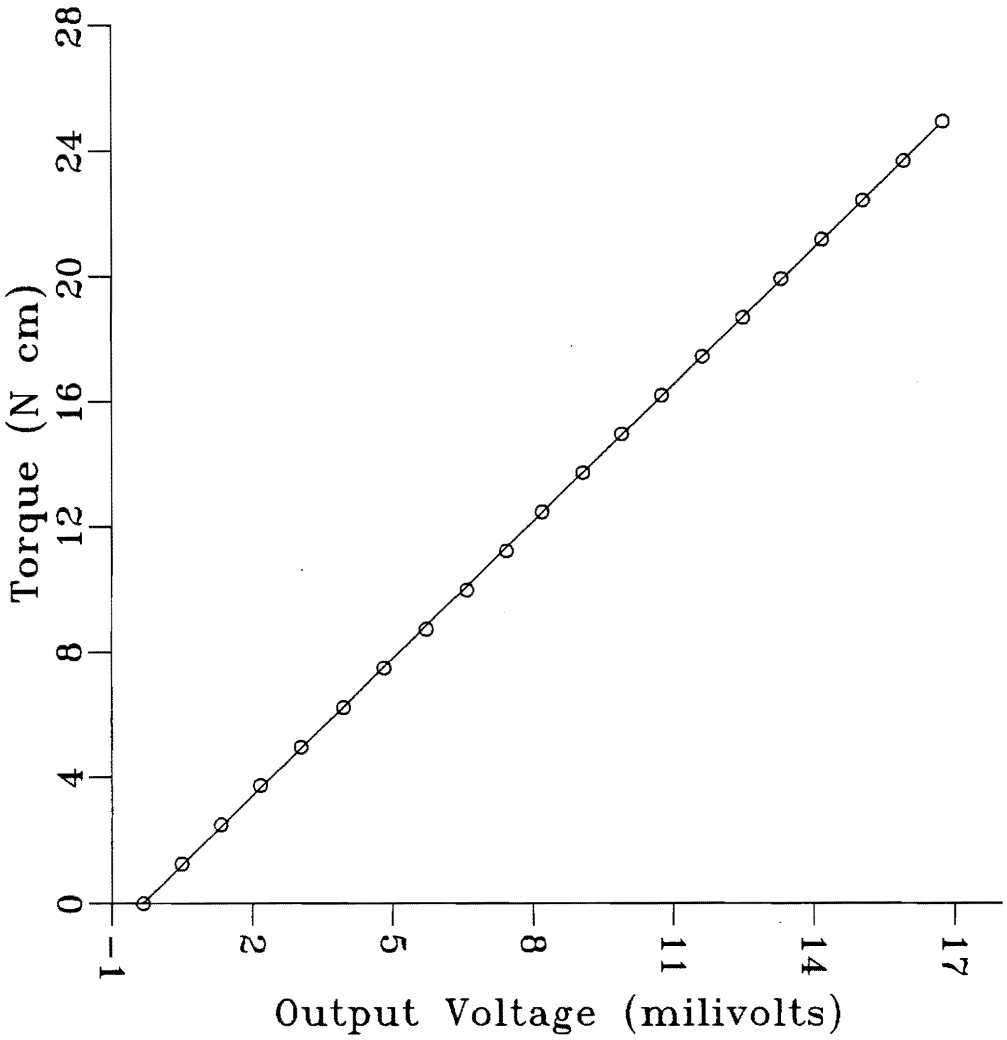

Regression Equation :
Torque (N cm) = 1.457 (OUTPUT milivolts) + 0.4904

Fig. C2. Calibration curve for the Lebow torque transducer.

Appendix D. Calibration of the LVDTs

There are two Linear Variable Differential Transducers (LVDT) used to monitor the position of the microscope. These are named the X-LVDT and the Y-LVDT. Calibration of the LVDTs is done by applying a known displacement to the microscope and recording the voltage output from the LVDTs. The vernier micrometers attached to the X-Y table of the microscope are used to measure the applied displacement. Calibration data for the LVDTs are listed in Table D1. Figure D1 and D2 show the calibration curves for the X-LVDT and Y-LVDT respectively. Regression equations are also shown.

Table D1. Calibration data for the X and Y LVDTs.

X - LVDT

POSITION (micrometers)	VOLTAGE OUTPUT (milivolts)
0.	13.5
127.	193.5
254.	357.6
381.	521.7
508.	688.7
635.	858.7
762.	1042.0
889.	1211.0

Y - LVDT

POSITION (micrometers)	VOLTAGE OUTPUT (milivolts)
0.	44.3
127.	248.7
254.	446.9
381.	648.8
508.	844.1
635.	1043.3
762.	1241.1
889.	1429.6

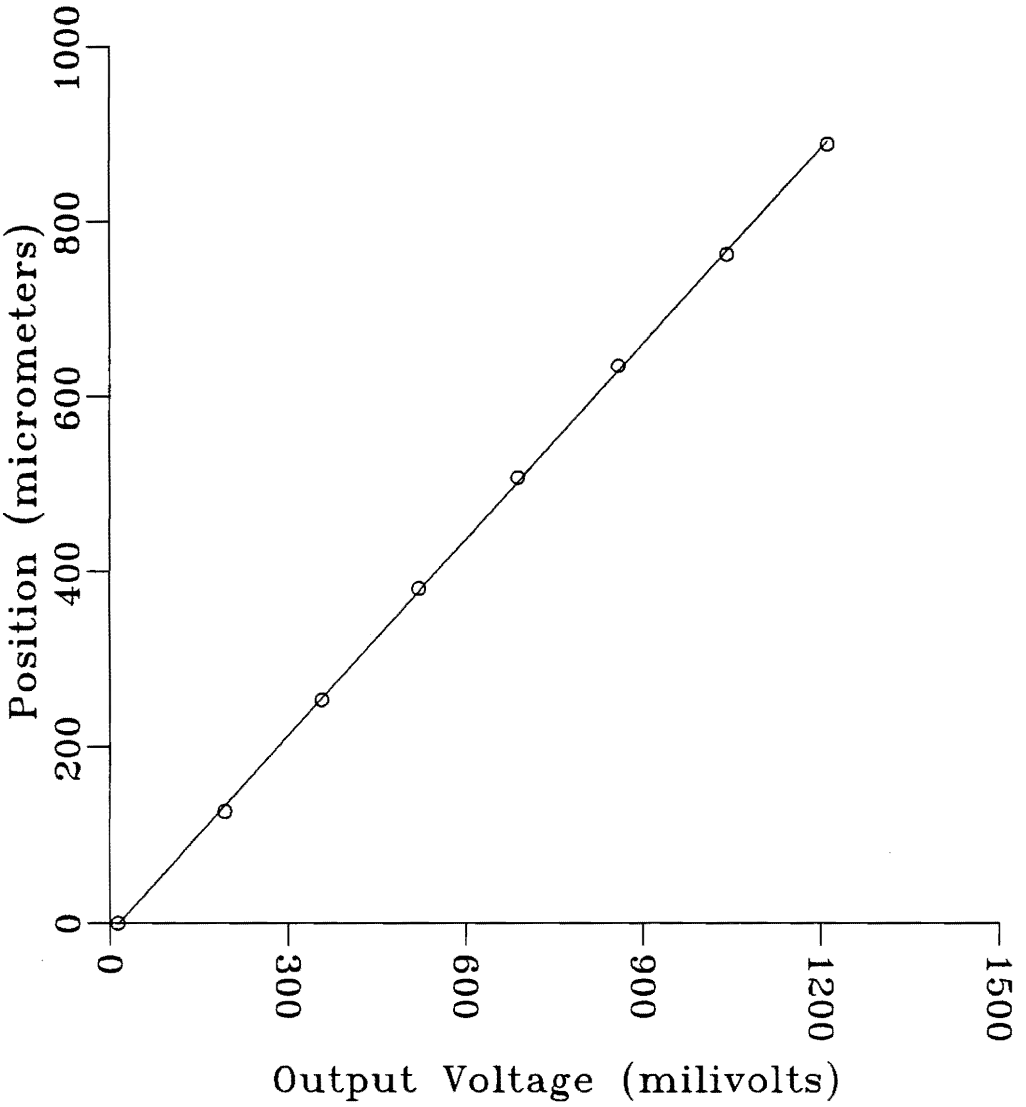

Regression Equation :
Position (micrometers) = 0.746 (OUTPUT milivolts) + (−11.23)

Fig. D1. Calibration curve for the X - LVDT.

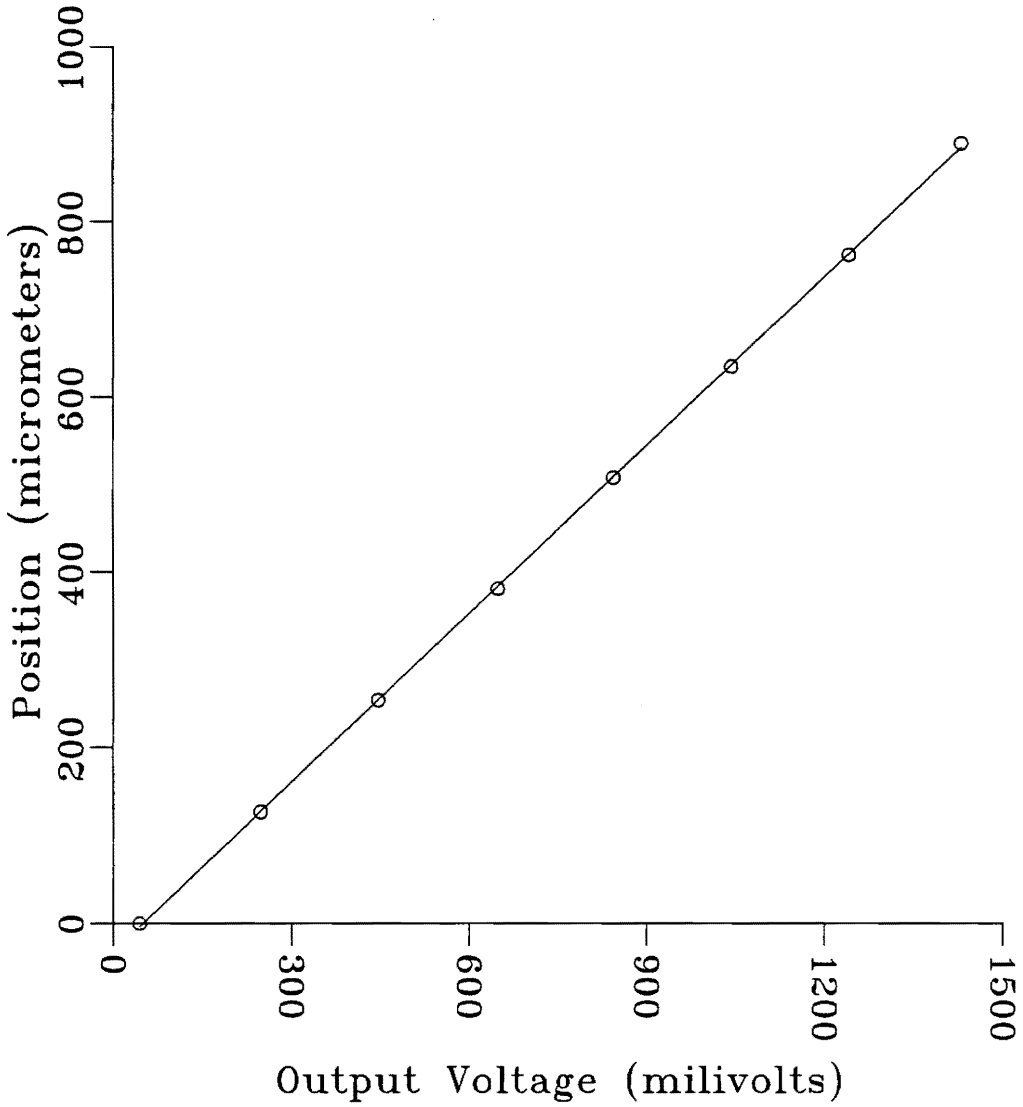

Regression Equation :
Position (micrometers) = 0.641 (OUTPUT milivolts) + (−31.93)

Fig. D2. Calibration curve for the Y - LVDT.

Appendix E. Calculation of Coefficient of Friction

Coefficient of friction in any sliding system is given by :

$$\mu = \frac{F}{W}$$

For constant normal loads, the expression for coefficient of friction is a simple ratio of the friction force to the constant normal load. In situations where normal load varies significantly, the variation should be taken into consideration to get a more appropriate value for the coefficient of friction. In the unidirectional sliding experiments, the variation in normal load appears to be appreciably high, particularly at high sliding speeds. Therefore, the equation for normal load derived here is used in these cases.

The variation in normal load in unidirectional sliding experiments is primarily due to the small wobble of the disk, a highly exaggerated schematic view of which is shown in Fig. E1. This results in a non-horizontal disk surface. The typical height variation as a result of the wobble is on the order of 25 μm (0.001 in.) at 12 mm from the center of rotation. As the disk rotates, the specimen along with the loading arm and the dead load, reciprocates with a frequency equal to the rotational frequency of the disk, and with a peak-to-peak amplitude equal to the wobble of the disk. A simple analysis of the dynamics of the system gives the actual value of the normal load. This analysis is done

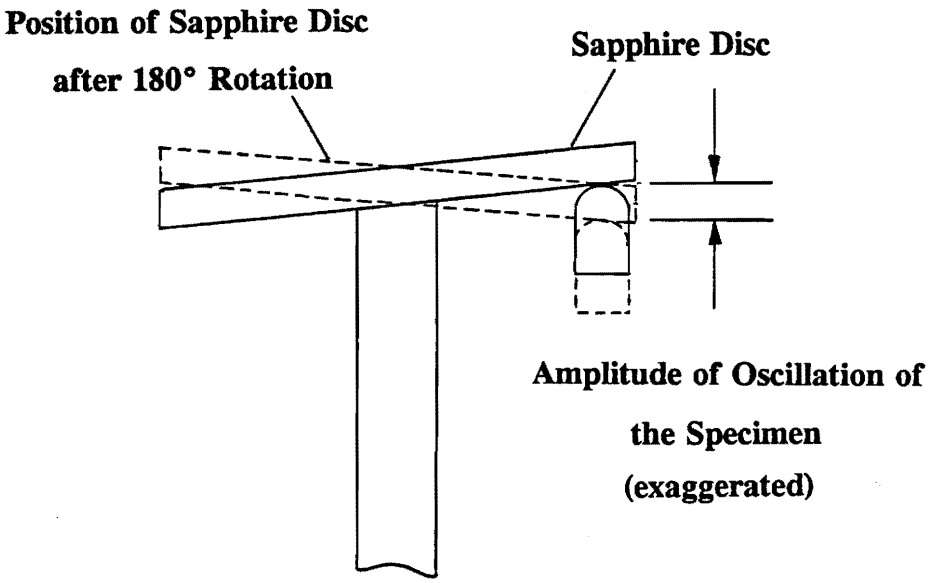

Fig. E1. An exaggerated schematic view of the disk wobble and the resulting normal load variation.

below.

Figure E2 shows the acceleration of the loading arm and the dead load. It is

---

Nomenclature and Some Physical Parameters

a_{load} = Acceleration of Dead Load

A = Amplitude of Oscillation of Load Arm at Point A. (Fig. E2)

= 0.025 mm

b = Width of Arm = 12.5 mm

F = Friction Force

g = Acceleration Due to Gravity

L = Length of Load Arm = 0.318 m

m_{arm} = Mass of the Load Arm = 0.240 kg

t = Time

w = Angular Velocity of the Disk

W = Normal Load

W_{arm} = Dynamic Normal Load Due to Rotational Oscillation of Load Arm

W_{load} = Dynamic Normal Load Due to Translational Oscillation of Dead Load

W_s = Applied Static Load (Dead Load) = 4 N.

x, x = Displacement and Acceleration of Point A (Fig. E2)

α_{arm} = Angular Acceleration of the Arm

μ = Coefficient of Friction

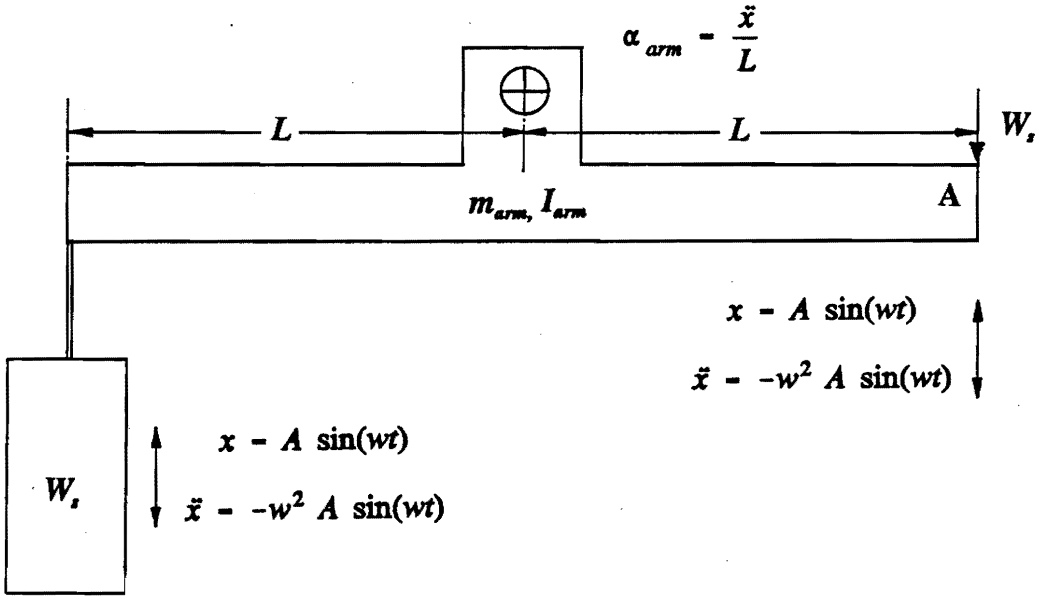

Fig. E2. Motions of the load arm and the dead load.

assumed that the load arm and the dead load are rigid bodies. The normal load W is given by :

$$W = W_s + W_{load} + W_{arm}$$

Since acceleration of the dead load is equal in magnitude and frequency to the acceleration of point A (because of the rigid arm),

$$W_{load} = \left(\frac{W_s}{g}\right) a_{load} = \left(\frac{W_s}{g}\right) \ddot{x}$$

$$W_{arm} = I_{arm}\, \alpha_{arm} = \frac{m_{arm}}{12} (b^2 + 4L^2) \frac{\ddot{x}}{L}$$

Also,

$$x = A \sin(wt)$$

$$\ddot{x} = -w^2 A \sin(wt)$$

Therefore,

$$W = W_s + \left(\frac{W_s}{g}\right) \ddot{x} + \frac{m_{arm}}{12} (b^2 + 4L^2) \frac{\ddot{x}}{L}$$

$$= W_s + \left(\frac{W_s}{g} + \frac{m_{arm}}{12L} (b^2 + 4L^2)\right) \ddot{x}$$

$$= W_s - w^2 A \sin(wt) \left(\frac{W_s}{g} + \frac{m_{arm}}{12L} (b^2 + 4L^2)\right)$$

On substituting the physical parameters in the above equation, it can be rewritten as :

$$W\ (N) = [\ 4. - 6.77E\text{-}06\ w^2\ \sin(wt)\ ]$$

This expression shows the sinusoidal variation of the normal load. Table E1 lists the maximum and minimum values of the normal load at the three velocities used. In the present study, coefficients of friction are calculated corresponding to the maximum and the minimum normal loads. The reported values of coefficients of friction are the averages of these two values.

Table E1. The maximum and minimum values of normal load at various velocities, for a vertical displacement of 0.025 mm (0.001 in).

Velocity (m/s)	Maximum Normal Load (N)	Minimum Normal Load (N)
2.17	4.24	3.76
3.5	4.63	3.38
7.0	6.58	1.42

Appendix F. Emissivity Results

The emissivity values measured in the two directions (normal and parallel/anti-parallel fiber orientations) of graphite-epoxy and carbon-PEEK composites are listed in Tables F1 and F2, respectively. The values listed represent emissivities of both worn and unworn surfaces as there was no difference in these values between the two surfaces.

Table F1. Emissivity of graphite-epoxy (worn and unworn surfaces).

Temperature (°C)	Emissivity	
	Normal	Parallel / Anti-parallel
30.	.60	.56
37.	.64	.64
46.	.69	.80
54.	.74	.83
61.	.77	.83
65.	.80	.82
75.	.80	.82

Table F2. Emissivity of carbon-PEEK.

Temperature (°C)	Emissivity	
	Normal	Parallel / Anti-parallel
30.	.60	.60
41.	.70	.72
51.	.73	.74
60.	.72	.74
75.	.72	.74
86.	.73	.73
98.	.72	.73
110.	.72	.74

Appendix G. Analysis of Variance Tables

In this section, the tables of the Two-way Analysis Of Variance (ANOVA) of the test results are presented.

Table G1. ANOVA of friction data of graphite-epoxy. Fiber orientation (TYPE), velocity (VEL) and the orientation-velocity interaction terms are present in the model.

ANOVA OF GRAPHITE-EPOXY FRICTION 1

ANALYSIS OF VARIANCE PROCEDURE

CLASS LEVEL INFORMATION

CLASS	LEVELS	VALUES
TYPE	3	1 2 3
VEL	3	7 3.5 2.17

NUMBER OF OBSERVATIONS IN DATA SET = 18

ANOVA OF GRAPHITE-EPOXY FRICTION 2

14:27 TUESDAY, OCTOBER 1, 1991

ANALYSIS OF VARIANCE PROCEDURE

DEPENDENT VARIABLE: FRIC

SOURCE	DF	SUM OF SQUARES	MEAN SQUARE	F VALUE

GEFRI OUTPUT A1 10/01/91 14:28 F 132 72 RECS 10/01/91 14:50 PAGE 2

MODEL	8	0.04301111	0.00537639	2.02
ERROR	9	0.02390000	0.00265556	PR > F
CORRECTED TOTAL	17	0.06691111		0.1569

R-SQUARE	C.V.	ROOT MSE	FRIC MEAN
0.642810	9.5824	0.05153208	0.53777778

SOURCE	DF	ANOVA SS	F VALUE	PR > F
TYPE	2	0.00181111	0.34	0.7199
VEL	2	0.00857778	1.62	0.2516
TYPE*VEL	4	0.03262222	3.07	0.0748

Table G2. ANOVA of mean surface temperature data of graphite-epoxy. Fiber orientation (TYPE), velocity (VEL) and the orientation-velocity interaction terms are present in the model.

```
                    ANOVA OF GRAPHITE-EPOXY TEMPERATURE                    1
                       ANALYSIS OF VARIANCE PROCEDURE
                          CLASS LEVEL INFORMATION
                       CLASS      LEVELS    VALUES
                       TYPE            3    1 2 3
                       VEL             3    7 3.5 2.17

                  NUMBER OF OBSERVATIONS IN DATA SET = 16
                    ANOVA OF GRAPHITE-EPOXY TEMPERATURE                    2
                                          13:58 TUESDAY, OCTOBER 1, 1991
                       ANALYSIS OF VARIANCE PROCEDURE

 DEPENDENT VARIABLE: TEMP

 SOURCE                    DF      SUM OF SQUARES         MEAN SQUARE      F VALUE


 GETEM    OUTPUT1  A1 10/01/91 14:14   F 132    72 RECS 10/01/91 14:50 PAGE      2

 MODEL                      8       9983.50937500       1247.93867188         1.39
 ERROR                      7       6302.56000000        900.36571429       PR > F
 CORRECTED TOTAL           15      16286.06937500                            0.3400

 R-SQUARE                C.V.           ROOT MSE           TEMP MEAN
 0.613009           33.0486         30.00609462         90.79375000

 SOURCE                     DF           ANOVA SS    F VALUE    PR > F
 TYPE                        2         68.93520833       0.04    0.9626
 VEL                         2       9506.59304167       5.28    0.0400
 TYPE*VEL                    4        407.98112500       0.11    0.9737
```

Table G3. ANOVA of mean surface temperature data of graphite-epoxy. Fiber orientation (TYPE) and velocity (VEL) are present in the model. The orientation-velocity interaction term has been removed as it is clearly insignificant, as evident from Table G2.

ANOVA OF GRAPHITE-EPOXY TEMPERATURE 1

ANALYSIS OF VARIANCE PROCEDURE

CLASS LEVEL INFORMATION

CLASS	LEVELS	VALUES
TYPE	3	1 2 3
VEL	3	7 3.5 2.17

NUMBER OF OBSERVATIONS IN DATA SET = 16

ANOVA OF GRAPHITE-EPOXY TEMPERATURE 2

14:11 TUESDAY, OCTOBER 1, 1991

ANALYSIS OF VARIANCE PROCEDURE

DEPENDENT VARIABLE: TEMP

SOURCE	DF	SUM OF SQUARES	MEAN SQUARE	F VALUE
MODEL	4	9575.52825000	2393.88206250	3.92
ERROR	11	6710.54112500	610.04919318	PR > F
CORRECTED TOTAL	15	16286.06937500		0.0323

R-SQUARE	C.V.	ROOT MSE	TEMP MEAN
0.587958	27.2036	24.69917394	90.79375000

SOURCE	DF	ANOVA SS	F VALUE	PR > F
TYPE	2	68.93520833	0.06	0.9453
VEL	2	9506.59304167	7.79	0.0078

GETEM OUTPUT A1 10/01/91 14:16 F 132 71 RECS 10/01/91 14:16 PAGE 2

Table G4. ANOVA of wear data of graphite-epoxy. Fiber orientation (TYPE), velocity (VEL) and the orientation-velocity interaction terms are present in the model.

ANOVA OF GRAPHITE-EPOXY WEAR 1

ANALYSIS OF VARIANCE PROCEDURE

CLASS LEVEL INFORMATION

CLASS	LEVELS	VALUES
TYPE	3	1 2 3
VEL	3	7 3.5 2.17

NUMBER OF OBSERVATIONS IN DATA SET = 18

ANOVA OF GRAPHITE-EPOXY WEAR 2
14:35 TUESDAY, OCTOBER 1, 1991

ANALYSIS OF VARIANCE PROCEDURE

DEPENDENT VARIABLE: WEAR

SOURCE	DF	SUM OF SQUARES	MEAN SQUARE	F VALUE
MODEL	8	345.46744444	43.18343056	1.21
ERROR	9	321.65520000	35.73946667	PR > F
CORRECTED TOTAL	17	667.12264444		0.3892

R-SQUARE	C.V.	ROOT MSE	WEAR MEAN
0.517847	113.3198	5.97824947	5.27555556

SOURCE	DF	ANOVA SS	F VALUE	PR > F
TYPE	2	95.26631111	1.33	0.3112
VEL	2	176.47204444	2.47	0.1397
TYPE*VEL	4	73.72908889	0.52	0.7266

GEWEAR OUTPUT1 A1 10/01/91 14:47 F 132 72 RECS 10/01/91 14:50 PAGE 2

Table G5. ANOVA of wear data of graphite-epoxy. Fiber orientation (TYPE) and velocity (VEL) are the only terms present in the model. The orientation-velocity interaction term has been removed as it is clearly insignificant (Table G4).

ANOVA OF GRAPHITE-EPOXY WEAR 1

ANALYSIS OF VARIANCE PROCEDURE

CLASS LEVEL INFORMATION

CLASS	LEVELS	VALUES
TYPE	3	1 2 3
VEL	3	7 3.5 2.17

NUMBER OF OBSERVATIONS IN DATA SET = 18

ANOVA OF GRAPHITE-EPOXY WEAR 2
14:49 TUESDAY, OCTOBER 1, 1991

ANALYSIS OF VARIANCE PROCEDURE

DEPENDENT VARIABLE: WEAR

SOURCE	DF	SUM OF SQUARES	MEAN SQUARE	F VALUE
MODEL	4	271.73835556	67.93458889	2.23
ERROR	13	395.38428889	30.41417607	PR > F
CORRECTED TOTAL	17	667.12264444		0.1217

R-SQUARE	C.V.	ROOT MSE	WEAR MEAN
0.407329	104.5370	5.51490490	5.27555556

SOURCE	DF	ANOVA SS	F VALUE	PR > F
TYPE	2	95.26631111	1.57	0.2458
VEL	2	176.47204444	2.90	0.0908

GEWEAR OUTPUT A1 10/01/91 14:49 F 132 71 RECS 10/01/91 14:50 PAGE 2

Table G6. ANOVA of friction data of carbon-PEEK. Fiber orientation (TYPE), velocity (VEL) and the orientation-velocity interaction terms are present in the model.

ANOVA OF CARBON-PEEK FRICTION 1

ANALYSIS OF VARIANCE PROCEDURE

CLASS LEVEL INFORMATION

CLASS	LEVELS	VALUES
TYPE	3	1 2 3
VEL	3	7 3.5 2.17

NUMBER OF OBSERVATIONS IN DATA SET = 20

ANOVA OF CARBON-PEEK FRICTION 2

10:03 WEDNESDAY, OCTOBER 2, 1991

ANALYSIS OF VARIANCE PROCEDURE

DEPENDENT VARIABLE: FRIC

SOURCE	DF	SUM OF SQUARES	MEAN SQUARE	F VALUE
MODEL	8	0.16883833	0.02110479	4.35
ERROR	11	0.05341667	0.00485606	PR > F
CORRECTED TOTAL	19	0.22225500		0.0138

R-SQUARE	C.V.	ROOT MSE	FRIC MEAN
0.759660	13.0619	0.06968544	0.53350000

SOURCE	DF	ANOVA SS	F VALUE	PR > F
TYPE	2	0.01957881	2.02	0.1795
VEL	2	0.08608833	8.86	0.0051
TYPE*VEL	4	0.06317119	3.25	0.0544

CPFRI OUTPUT A1 10/02/91 10:04 F 132 73 RECS 10/02/91 10:04 PAGE 2

Table G7. ANOVA of mean surface temperature data of carbon-PEEK. Fiber orientation (TYPE), velocity (VEL) and the orientation-velocity interaction terms are present in the model.

ANOVA OF CARBON-PEEK TEMPERATURE 1

ANALYSIS OF VARIANCE PROCEDURE

CLASS LEVEL INFORMATION

CLASS	LEVELS	VALUES
TYPE	3	1 2 3
VEL	3	7 3.5 2.17

NUMBER OF OBSERVATIONS IN DATA SET = 20

ANOVA OF CARBON-PEEK TEMPERATURE 2

9:45 WEDNESDAY, OCTOBER 2, 1991

ANALYSIS OF VARIANCE PROCEDURE

DEPENDENT VARIABLE: TEMP

SOURCE	DF	SUM OF SQUARES	MEAN SQUARE	F VALUE
MODEL	8	25275.81950000	3159.47743750	8.65
ERROR	11	4016.43000000	365.13000000	PR > F
CORRECTED TOTAL	19	29292.24950000		0.0009

R-SQUARE	C.V.	ROOT MSE	TEMP MEAN
0.862884	15.3907	19.10837513	124.15500000

SOURCE	DF	ANOVA SS	F VALUE	PR > F
TYPE	2	3139.15545238	4.30	0.0417
VEL	2	20369.91741667	27.89	0.0001
TYPE*VEL	4	1766.74663095	1.21	0.3609

CPTEM OUTPUT A1 10/02/91 9:46 F 132 73 RECS 10/02/91 10:01 PAGE 2

Table G8. ANOVA of wear data of carbon-PEEK. Fiber orientation (TYPE), velocity (VEL) and the orientation-velocity interaction terms are present in the model.

ANOVA OF CARBON-PEEK WEAR 1

ANALYSIS OF VARIANCE PROCEDURE

CLASS LEVEL INFORMATION

CLASS	LEVELS	VALUES
TYPE	3	1 2 3
VEL	3	7 3.5 2.17

NUMBER OF OBSERVATIONS IN DATA SET = 20

ANOVA OF CARBON-PEEK WEAR 2

9:58 WEDNESDAY, OCTOBER 2, 1991

ANALYSIS OF VARIANCE PROCEDURE

DEPENDENT VARIABLE: WEAR

SOURCE	DF	SUM OF SQUARES	MEAN SQUARE	F VALUE

CPWER OUTPUT A1 10/02/91 10:00 F 132 73 RECS 10/02/91 10:01 PAGE 2

MODEL	8	27.56966667	3.44620833	5.10
ERROR	11	7.43083333	0.67553030	PR > F
CORRECTED TOTAL	19	35.00050000		0.0076

R-SQUARE	C.V.	ROOT MSE	WEAR MEAN
0.787694	31.4305	0.82190651	2.61500000

SOURCE	DF	ANOVA SS	F VALUE	PR > F
TYPE	2	21.45621429	15.88	0.0006
VEL	2	1.99800000	1.48	0.2699
TYPE*VEL	4	4.11545238	1.52	0.2622

Vita

The author was born on July 25, 1964 in Bhubaneswar, India to Ratna and Kanduri C. Tripathy. He recieved his Bachelor of Technology degree with Honors in Mechanical Engineering from Indian Institute of Technology, Kharagpur, in 1987. After graduation he was employed as a Design Engineer in Tata Engineering and Locomotive Company, India. He began his work towards Master of Science degree in Mechanical Engineering at Virginia Polytechnic Institute and State University in August 1989. Upon completion of his M.S. requirements, he will pursue his Doctorate degree in Mechanical Engineering.

Bhawani S Tripathy

(Bhawani S. Tripathy)